THESIS

ON

RELIABILITY BASED FRAGILITY ANALYSIS OF RC FRAME BUILDINGS UNDER NEAR-FIELD AND FAR-FIELD EARTHQUAKES CONSIDERING SOIL-STRUCTURE INTERACTION

Submitted by

DEBAPRIYA DAS

Master of Civil Engineering
(Structural Engineering)
Year-2nd
Class Roll No.- 001710402022
Examination Roll No.- M4CIV19024
University Registration No.- 140648 of 2017-2018
Session-2018-2019

in partial fulfilment of the requirement for the degree of

M.E.

in

CIVIL ENGINEERING
(Specialisation- STRUCTURAL ENGINEERING)

under the guidance of

Dr. AMIT SHIULY

FACULTY OF ENGINEERING AND TECHNOLOGY
DEPARTMENT OF CIVIL ENGINEERING
(STRUCTURAL ENGINEERING)
JADAVPUR UNIVERSITY
KOLKATA – 700032

MAY 2019

DECLARATION

This thesis titled **'RELIABILITY BASED FRAGILITY ANALYSIS OF RC FRAME BUILDINGS UNDER NEAR-FIELD AND FAR-FIELD EARTHQUAKES CONSIDERING SOIL-STRUCTURE INTERACTION'** is prepared and submitted in the partial fulfilment of the requirements for the degree of Master of Civil Engineering (with specialisation in Structural Engineering) at Jadavpur University for the academic session 2018-2019.

Date: 30.05.2019

Place: Civil Engineering Department,
Jadavpur University,
Kolkata.

DEBAPRIYA DAS
Master of Civil Engineering
(Structural Engineering)
2nd Year
Class Roll No.- 001710402022
Examination Roll No.- M4CIV19024
University Registration No.- 140648 of 2017-2018

JADAVPUR UNIVERSITY,
DEPARTMENT OF CIVIL ENGINEERING,
KOLKATA – 700032

RECOMMENDATION CERTIFICATE

It is hereby certified that this thesis titled **'RELIABILITY BASED FRAGILITY ANALYSIS OF RC FRAME BUILDINGS UNDER NEAR-FIELD AND FAR-FIELD EARTHQUAKES CONSIDERING SOIL-STRUCTURE INTERACTION'** is prepared and submitted in the partial fulfilment of the requirements for the degree of **Master of Civil Engineering (with specialisation in Structural Engineering)** at **Jadavpur University** by **Debapriya Das**, a student of 2nd year of the said course for the session 2018-2019, under my supervision and guidance. It is also declared that no part of this thesis mentioned above has been presented or published elsewhere.

Dr. AMIT SHIULY
(Thesis Guide)
Assistant Professor
Department of Civil Engineering,
Jadavpur University

Countersigned by:

Head of the Department
Department of Civil Engineering,
Jadavpur University

Dean
Faculty of Engineering and Technology,
Jadavpur University

JADAVPUR UNIVERSITY,
DEPARTMENT OF CIVIL ENGINEERING,
KOLKATA – 700032

CERTIFICATE OF APPROVAL*

This is to certify that this thesis is hereby approved as an original work conducted and presented satisfactorily to warrant its acceptance as a prerequisite to the degree for which it has been submitted. It is implied that by this approval the undersigned do not necessarily endorse or approve any statement made, opinion expressed or conclusion drawn therein, but approve the thesis only for the purpose for which it is submitted.

Final Examination for evaluation of thesis:

1. _____

2. _____

3. _____

(Signature of Examiners)

*Only in case the thesis is approved.

ACKNOWLEDGEMENT

I am taking the opportunity of this precious and auspicious moment to acknowledge the individuals who have helped me lot in completing this thesis. At first, I express sincere gratitude to my thesis guide **Dr. AMIT SHIULY**, Assistant Professor, Department of Civil Engineering, Jadavpur University, for his constant inspiration and guidance; without which it would have been difficult for me to complete this thesis. I am also deeply indebted to all the professors of Civil Engineering Department of Jadavpur University who helped me a lot. It is only for their constant suggestions that I have been able to finish my thesis.

I am grateful to my family members for always standing by my side. Their blessings, motivation and inspiration have always provided me high mental support. I am also thankful to my classmates for their assistance and cooperation during the course. Last but not the least; I am thankful to the Almighty and all those who helped me directly or indirectly at various stages of this work.

Date: 30.05.2019

Place: Civil Engineering Department,
Jadavpur University,
Kolkata.

DEBAPRIYA DAS
Master of Civil Engineering
(Structural Engineering)
2nd Year
Class Roll No.- 001710402022
Examination Roll No.- M4CIV19024
University Registration No.- 140648 of 2017-2018

Research is
to see what everybody else has seen,
and
to think what nobody else has thought.

- Albert Szent-Gyorgyi

ABSTRACT

It is a well-established fact that under seismic excitation, the response of a structure is greatly influenced by the underlying soil layers. However, while performing the dynamic analysis of structures, the soil under the foundation of the superstructure is considered as rigid and its flexibility is ignored. However, previous researches clearly demonstrate that during seismic excitation, soft soil layers not only amplify the seismic waves but soil-structure interaction (SSI) greatly affects the seismic response of a structure.

In this thesis, an attempt has been made to study the SSI behaviour of frame buildings constructed over both uniform and layered soils by nonlinear dynamic analysis using three-dimensional finite element modelling (FEM) by Abaqus (Version 14.5) software. In case of uniform soil, three types of soils (Hard, Medium and Soft) have been used. On the other hand, seven types of layered soils (Soil 1 to Soil 7), each of which has six different layers, have been considered for analysis. For all the soil layers fundamental frequency and amplification at fundamental frequency have been determined. In order to find out the response of structure due to these soil condition, three types of buildings (G+1, G+4 and G+9) have been considered in the present study. The whole soil-structure system is subjected to Loma Prieta (1989) earthquake motion as near-field and Denali (2002) earthquake as far-field seismic excitation. Due to the prescribed input motions, the horizontal displacements and percentage drifts of all the storeys are computed. Thereafter, fragility curves for each storey are developed. In addition to that based on the developed fragility curves, reliability index plots for Saltlake area have been generated in case of different soil-structure combinations. The result clearly shows that for any type of soil and under a specific seismic excitation, the probability of exceedance of a certain limit state in case of a G+1 building is always minimum and that of a G+9 building is always maximum among all the cases. In addition to that, building is subjected to an earthquake motion situated on hard soil, it has the least probability of exceeding a limit state. However, it has the largest probability of exceeding a limit state when located on soft soil. Further, under the action of a near-field earthquake, the limit state exceedance probability is more compared to the far-field earthquake.

CONTENTS

LIST OF FIGURES

LIST OF TABLES

LIST OF SYMBOLS USED

% =Percentage

2-D = Two-dimensional

3-D = Three-dimensional

a, b = Regression Coefficients of PSDM

ATC = Applied Technology Council

C = Drift Capacity at the Chosen Limit State

CP = Collapse Prevention

D = Ground Storey Drift

DL = Damage Limitation

DOF = Degree of Freedom

E = Modulus of Elasticity

e.g. = exempli gratia (means "for example")

E_0 *=Initial or Undamaged Elastic Stiffness of Material*

EDP = Engineering Damage Parameter

ETABS = Extended Three-dimensional Analysis of Building System

FEM =Finite Element Method

FEMA = Federal Emergency Management Association

FFT = Fast Fourier Transform

$F_R(x)$ *= Probability of Exceedance*

G = Mohr-Coulomb Yield Function

$G_A(x)$ *= Annual Rate of Exceedance*

I_1 *= First Invariant of Stress*

IIEES = International Institute of Earthquake Engineering and Seismology

IM = Intensity Measure

IO = Immediate Occupancy

IS = Indian Standard

J_2 = Second Invariant of Stress Deviator

LHS = Latin Hypercube Sampling

LRC = Lightly Reinforced Concrete

LS = Life Safety

LSF = Limit State Function

N/A = Not Applicable

NTHA = Non-linear Time History Analysis

OGS = Open Ground Storey

P(D≥C|IM) = Probability of Exceedance of Ground Storey Drift for Particular Limit State Capacities

P[LS] = Probability of Failure Corresponding to Limit State

PGA = Peak Ground Acceleration

PGD = Peak Ground Displacement

PGV = Peak Ground Velocity

PSDM = Probabilistic Seismic Demand Model

RC = Reinforced Concrete

RHS = Right Hand Side

RI = Reliability Index

RSA = Response Spectrum Analysis

SD = Significant Damage

SDOF = Single Degree of Freedom

SRSS = Square Root of Sum of Squares

SSI = Soil-Structure Interaction

USA = United States of America

V_S *= Shear Wave Velocity*

vs. = versus

α , β *= Rayleigh Damping Coefficients*

β_C *=Dispersion in Capacities*

β_M *=Dispersion in Modelling*

β_{pf} *= Reliability Index*

θ *= Polar Angle through which Third Invariant Enters the Deviatoric Plane*

ν *= Poisson's Ratio*

ξ *= Damping Ratio*

ρ *= Density*

ψ *= Angle of Dilatancy*

ω *= Frequency*

LIST OF UNITS USED

cm = Centimetre

cps = Cycles per second

g = Acceleration due to gravity

Hz = Hertz

kg =Kilogram

km = Kilometre

m = Metre

mm = Millimetre

MPa = Mega Pascal

N = Newton

s = Second

Chapter-1: INTRODUCTION

1.1. GENERAL

Earthquake is one of the most destructive natural disaster, which occurs due to sudden energy release in the earth's crust. The unpredictability of place and time of earthquake occurrence has made it more catastrophic. Some of the seismic events are very small and they are not even felt. However, some of them are so large in magnitude that they can cause major damage to the infrastructures and cost thousands of lives over a large area. The socio-economic damages caused by earthquakes depend largely on the characteristics of the strong ground motion. It is to be mentioned that characteristics of the ground motions primarily depend upon three factors, namely, source characteristics, propagation path of waves, and local site conditions. The local site condition plays an important role in ground motion characteristics and damage distribution. The large amplification of bedrock motion by the soil deposit may occur due to resonance and further amplification of motion in structure may occur if fundamental frequency of soil column is close to the structure. This phenomenon is called double resonance. The disastrous earthquake like 1985 Mexico earthquake[1]–[3], 1985 Chille earthquake[4], 1989 San Francisco earthquake, 1994 Northridge earthquake[5], 1995 Kobe earthquake[6], 1995 Los Angeles earthquake, 2003 Bam Iran earthquake[7] etc. demonstrated that large concentrated damage and consequent loss of life and property in specific pockets occur due to local site effect. In India, the effects of local site condition on ground motion were reported during 2001 Bhuj earthquake[8], [9]. Further, the ground motion characteristics in the vicinity of a seismic event are ominously dissimilar from the far-field seismic events. Therefore, the damage potential significantly varies due to these two type of seismic events[10]. In case of near-field earthquake, the ground motions consist both high and low frequency component of seismic event and may be eminent by short period impulsive motions with permanent ground deformation. However, for far- field earthquake, the seismic wave consists mainly long period seismic wave and prominent by long period impulsive motion. Moreover, it is to be mentioned that low frequency seismic wave largely amplifies while travelling in soft soil medium. These are very important for analysis and design of any structure[11]–[13].

Therefore, under seismic excitations, more attention should be paid to Soil-Structure Interaction (SSI) phenomenon, which is a major problem in the field of Structural Engineering. It is to be mentioned that most of the civil engineering structures involve some type of structural element with direct contact with ground. However, when the external forces, such as earthquakes, act on these systems, neither the structural displacements nor the ground displacements, are independent of each other. The process in which the response of the soil influences the motion of the structure and the motion of the structure influences the response of the soil is termed as soil-structure interaction (SSI)[14]. Neglecting SSI is reasonable for light structures in relatively stiff soil such as low-rise buildings and simple rigid retaining walls. The effect of SSI, however, becomes prominent for heavy structures resting on relatively soft soils for example nuclear power plants, high-rise buildings and elevated-highways on soft soil[15].

The dimensions of a structure are finite and its dynamic model can be constructed with a finite number of degrees of freedom. As the structure interacts with the surrounding soil, analysing only the structure is not feasible. In many important cases (e.g. earthquake excitation), the loading is applied to the soil region around the structure. Thus it is important to model the soil, as a semi-infinite unbounded domain. It is to be noted that in case of static loading, a fictitious boundary where the response is expected to be died out practically, is introduced at a sufficient distance from the structure. This results in a finite domain for the soil, which can be modelled similarly to the structure. Finally, with the discretised structure and the soil system static loading problem can be analysed easily. However, this procedure cannot be followed in case of dynamic loading. In this case, the fictitious boundary will reflect the waves originating from the vibrating structure back into the discretised soil region instead of letting them pass through and propagate toward infinity. Thus, under dynamic loading, the unbounded subsoil should be modelled in a proper way.

1.2. NEED FOR PRESENT STUDY

Ground motions close to an earthquake source can be ominously dissimilar than the far source seismic event. It is to be mentioned that far source earthquake consists low frequency seismic wave. However, near source earthquake contain both high frequency and low frequency seismic wave with discrete forward directivity pulse. Thus, the response of a structure largely varies due to these two types of earthquakes. These specifications of near-fault earthquake records make structural responses to be different from those expected in far-fault earthquakes.

Further, conventional structural design methods neglect the SSI effects. This SSI may be neglected for a lightweight flexible structure built on a very stiff rock site. This is due to the input motion at the base of the structure is nearly same as the free-field seismic excitation. However, when the structure is massive and stiff and the soil is relatively soft, the motion at the base of the structure may be significantly changed from the free- field surface motion. Moreover, due to SSI, depending on the type of soil and structure, the free-field response of a site may be amplified significantly. It is to be noted that, the damage occurred in Kobe Earthquake (1995) revealed that the response of a structure under seismic excitation is highly influenced by superstructure, foundation and the subsoil.

The Indian code for seismic design suggests that Soil-Structure Interaction (SSI) may not be considered in the seismic analysis of structures supported on rock or rock-like material at shallow depth[16]. But, the code is silent about whether SSI is to be taken account of or not for soft, medium and hard soil. Again, the soil under the foundation is not always uniform throughout. It exists in layers. The code does not provide any guideline how to deal with the layered soil under earthquake and does not tell us whether SSI should be considered or ignored in this case. Depending on the epicentre distance from the affected area, time history profile of an earthquake is altered. It is also not mentioned in the code, for which kind of earthquake (near-field or far-field) SSI phenomenon has more contribution towards structural response and to be taken into account for design purposes. Here lies the necessity of performing dynamic soil-structure interaction analysis of structures constructed on uniform soil (hard, medium and soft soil) as well as on layered soil under the effect of near-field and far-field earthquakes. It is also necessary to develop the fragility curves and to check the seismic amplification capacity of different types of soils.

1.3. OBJECTIVE AND SCOPE OE WORK

The fundamental objective of this research work is to analyse the effects of dynamic soil-structure interaction on frame buildings constructed over different types of soils under near-field and far-field seismic excitations using direct method.

The scopes of the present study are as follows:

1. Sensitivity analysis of response of the structure due to variation of soil properties.
2. Sensitivity analysis of response of the structure due to variation of thickness of soil layers.

3. Sensitivity analysis of response of the structure due to variation of height or storeys of frame buildings.
4. Sensitivity analysis of response of the structure due to near-field and a far-field earthquakes.
5. To generate the fragility curves for different soil-structure combinations.
6. To collect the seismic hazard curve for a particular area and to develop the reliability index curves for different soil-structure combinations.

1.4. ORGANISATION OF THE REPORT

This thesis is an assembly of six chapters. The table and figures have been presented sequentially as they appear in the text.

In **Chapter 1**, the SSI concept and its significance have been described in brief. Besides that, an attempt has been made to point out the problems, which emphasise the need for the present research. The objective and scopes of this work are then clarified. At the end of the chapter, the organisation of thesis has been discussed briefly.

Chapter 2 furnishes a detailed discussion on various topics relevant to the present thesis work, such as different parts of dynamic SSI, different methods of solving dynamic SSI problems, probabilistic seismic demand model, fragility curves with different plotting methods and reliability analysis. A state of the art literature review on relevant topics has also been done to understand the present scenario.

Chapter 3 discusses the influence of SSI on frame buildings constructed on uniform soil. Three types of soils (Hard Soil, Medium Soil and Soft Soil) are combined with three types of buildings (G+1, G+4 and G+9) to develop nine analytical models. Each model is subjected to a near-field and a far-field earthquake. In case of every model, fragility curves are developed for all the floors under the influence of aforesaid two earthquakes. Besides these, amplification factors for each type of soil under each type of seismic excitation are calculated separately and compared.

Chapter 4 deals with the effect of SSI on frame buildings resting on layered soil. Seven types of soils (Soil 1 to Soil 7) are combined with three types of buildings (G+1, G+4 and G+9) for the development of twenty-one models used for analysis. Each type of soil has six different layers and each model is subjected to a near-field and a far-field earthquake. For every model, fragility curves are developed for all the floors under the effect of two earthquakes. In addition to that,

amplification factor of seismic excitation in each soil layer is also worked out for the aforementioned earthquakes.

Chapter 5 has been devoted to the reliability-based assessment of different soil-structure combinations. In this chapter, a brief description about seismic hazard curves and reliability curves is provided along with the procedure for developing reliability curves from fragility curves. Finally, the reliability indices for different soil-structure combinations under different seismic excitations have been presented in graphical form.

Chapter 6 summarises all the results obtained from the overall thesis work and significant remarks have been drawn out after analysing the results. The limitations of the present study and future scopes in this regard have also been discussed in this chapter.

The Books, Codes and Standards, Journals, Conference Papers and other articles used for preparing this thesis are listed in the section **'References'** at the end.

Chapter-2: LITERATURE REVIEW

2.1. GENERAL

The numbers of casualties during earthquakes around the world have been increasing every year and calls for serious thinking for the scientist, urban planner, engineers to strengthen their efforts to mitigate the disastrous effect of earthquakes. These earthquakes have left many lessons, like the requirement of mitigation strategy including seismic hazard assessment, proper planning and design of buildings and structures. Thus, minimization of earthquake risk and taking earthquake mitigation strategy is a global concern today. In past it has been observed that soil–structure interaction (SSI) plays an important role on response of a building during a seismic event. Further, due to characteristics difference of near field and far field earthquake, the response of a structure varies significantly. Thus, reliability based fragility analysis of R.C. frame buildings under near-field and far-field earthquakes considering soil-structure interaction are very important. Therefore in the present study a brief literature review of dynamic SSI has been carried out. Further, literature review of fragility analysis and reliability analysis has also carried out. Further, a critical appraisal has been made based on these reviews.

2.2. DYNAMIC SOIL-SRUCTURE INTERACTION

The effects of dynamic SSI depends upon mass and stiffness of the structure, stiffness of the soil, and the damping properties of both the structure and the soil. Dynamic SSI is actually a combination of two interactions- Kinematic Interaction and Inertial Interaction. The stiffness of the structure is responsible for the kinematic interaction. On the other hand, the inertial interaction is caused due to the mass of the structure.

2.2.1. KINEMATIC INTERACTION

Kinematic interaction takes place when the development of the free-field motion is obstructed by the stiffness of the foundation system. When foundation is subjected to vertically propagating S waves having wavelength equal to the embedment depth, rocking and torsion modes of vibration, which are absent in case of the free-field motion, are induced in the structure because of kinematic

interaction. The deformation occurred only due to kinematic interaction can be calculated assuming that the structure and the foundation have stiffness but they are massless. This is shown in Figure 2.2.1.

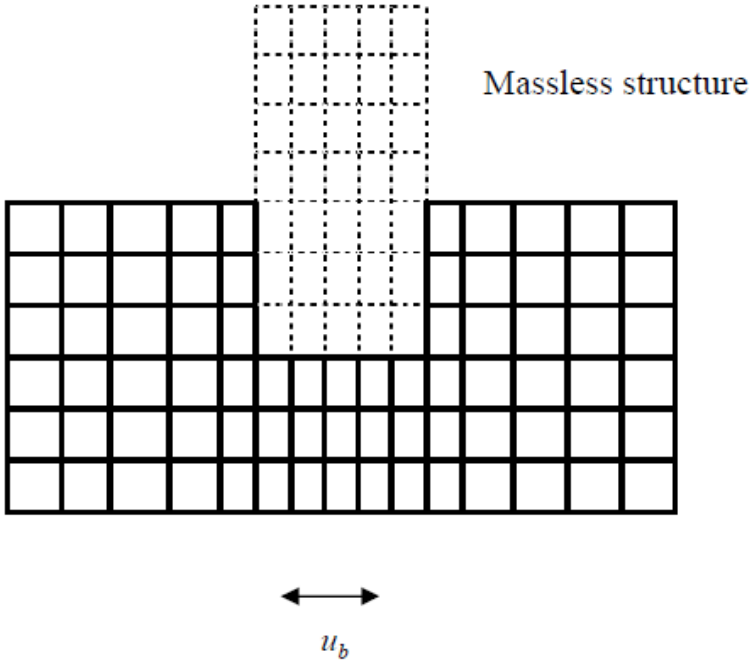

Figure 2.2.1. Kinematic interaction analysis (Kramer, 1996)[6]

For this case, the equation of motion will be[6]:

$$[\boldsymbol{M_{soil}}]\{\ddot{\boldsymbol{u}}_{\boldsymbol{KI}}\} + [\boldsymbol{K}^*]\{\boldsymbol{u_{KI}}\} = -[\boldsymbol{M_{soil}}]\{\ddot{\boldsymbol{u}}_{\boldsymbol{b}}(\boldsymbol{t})\} \qquad \textbf{...2.2.1.}$$

where,

$[M_{soil}]$ = Mass matrix assuming structure and foundation massless,

$\{u_{KI}\}$ = Foundation input motion,

$[K^*]$ = Stiffness matrix,

$\{\ddot{u}_b(t)\}$ = Acceleration at the boundary.

The kinematic interaction can be described with the help of Figure 2.2.2.(a–d).

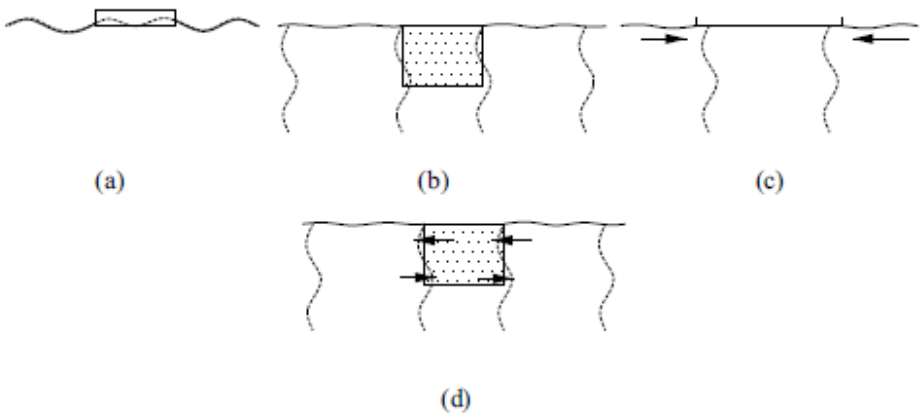

Figure 2.2.2. Kinematic interaction: (a) vertical motion modified; (b) horizontal motion modified; (c) incoherent ground motion prevented; and (d) rocking motion introduced (Datta,2010)[17]

In Figure 2.2.2.(a), the vertical movement of the ground motion is restrained due to the flexural stiffness the massless mat foundation. As a result of this, the movement of the mat foundation differs from the free-field ground motion. In addition to that, because of this action, the characteristics of the ground motion in the close vicinity and below the foundation get changed from that of the free-field ground motion. This interaction of the foundation with the ground motion is known as kinematic interaction. Similar examples of kinematic interaction have been presented in Figure 2.2.2.(b) and Figure 2.2.2.(c). In Figure 2.2.2.(b), the vertically propagating shear waves have been restrained by the embedded foundation. Figure 2.2.2.(c) shows the incoherent ground motion, which is generated below the foundation due to the vertically propagating shear waves, is prevented due to the axial stiffness of the slab. In Figure 2.2.2.(d), it is shown that the kinematic interaction can also be responsible for inducing rotational movement in a foundation because of the vertically propagating purely S waves.

Clough and Penzien[18] have explained the tau (τ) effect, which is another example of kinematic interaction. In Figure 2.2.3., a ground motion is generated in the x-direction, which varies with y, due to the horizontally propagating shear wave in the y-direction.

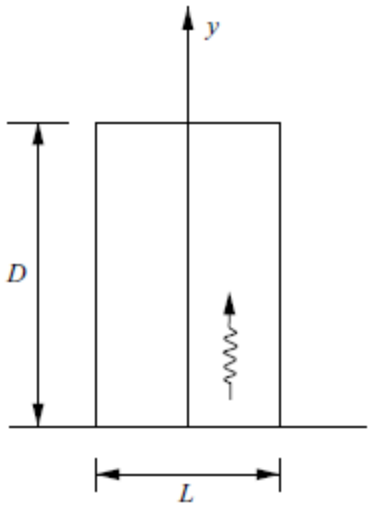

Figure 2.2.3. Horizontally propagating shear wave in the y-direction beneath the rigid slabs (Clough and Penzien,1993)[18]

This varying motion is restrained because of rigidity of the slab, and the motion of the slab, in the x-direction, differs from that of the free-field ground motion. If τ is defined as the ratio of the amplitudes of translational motion of the rigid base and the free-field motion for a certain harmonic component, it is shown that[18]

$$\boldsymbol{\tau = \frac{1}{\alpha}\sqrt{2(1-\cos\alpha)}} \qquad \textbf{...2.2.2.}$$

$$\boldsymbol{\alpha = \frac{\omega D}{V_a} = \frac{2\pi D}{\lambda(\omega)}} \qquad \textbf{...2.2.3.}$$

where,

$\lambda(\omega) = \frac{2\pi V_a}{\omega}$ = Wavelength,

D = Dimension of the base in y-direction,

V_a = The apparent wave velocity.

From the equations 2.2.2. and 2.2.3., it can be shown that the values of τ decrease from unity (at $\alpha = 0$ and $\lambda \to \infty$) to zero (at $\alpha = 2\pi$ and $\lambda \to D$).

This signifies that if the dimension of the base of the foundation is very small compared to the wavelength of the ground motion, the τ effect becomes negligible. On the other hand, when the dimension of the base of the foundation is comparable with the wavelength of the ground motion,

the τ effect has to be considered, and in this case, the base motion could be much smaller than the free-field ground motion.

2.2.2. INERTIAL INTERACTION

The mass of the foundation and the structure causes them to respond dynamically. Inertial interaction is that part of the SSI effect, which is related to the mass of the structure. It is caused only due to the inertia forces developed in the structure because of the movement of masses of the structure in the time of vibration. The inertial loads applied to the structure generate an overturning moment and a transverse shear. When the supporting soil is flexible, the inertial force transmits dynamic forces to the foundation resulting in its dynamic displacement, which would not occur for a fixed-base structure. The deformations occurred due to the inertial interaction can be calculated from the equation of motion[6] for this case.

$$[\boldsymbol{M}]\{\ddot{\boldsymbol{u}}_{\boldsymbol{II}}\} + [\boldsymbol{K}^{*}]\{\boldsymbol{u}_{\boldsymbol{II}}\} = -[\boldsymbol{M}_{\boldsymbol{structure}}]\{\ddot{\boldsymbol{u}}_{\boldsymbol{KI}}(\boldsymbol{t}) + \ddot{\boldsymbol{u}}_{\boldsymbol{b}}(\boldsymbol{t})\} \qquad \textbf{...2.2.4.}$$

where,

$[M_{structure}]$ = Mass matrix assuming the soil massless (shown in Figure 2.2.4.).

The inertial loading on the structure-foundation system is represented by the R.H.S. of equation 2.2.4. It can be clearly understood that this loading is dependent upon the base motion as well as on the foundation input motion including the kinematic interaction effect.

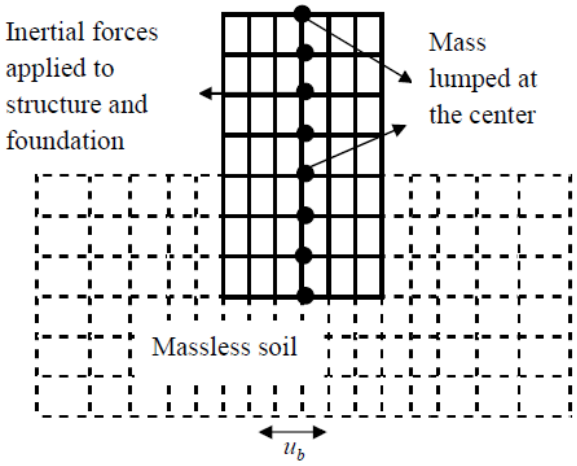

Figure 2.2.4. Inertial interaction analysis (NPTEL)[19]

Dynamic SSI phenomenon can be analysed using two different methods. The first method is called Direct Method, which is comparatively easier between the two methods but has some limitations.

To eliminate these limitations, a second method known as Substructure Method is introduced, where a multi-step analysis has to be performed. In the present study, as the direct method of analysis is employed, it is described in detail. However, a brief discussion about the substructure method has also been presented.

2.2.3. DIRECT MEHOD

In this method of analysis, the structure, foundation and soil are modelled together using FEM and the whole model is analysed in a single step. The ground motion is considered as the free-field motion and this motion is applied to all the boundaries. The soil domain, with some material damping, is restricted using a fictitious exterior boundary. This boundary has to be placed far away from the structure so that during earthquake, the waves produced along the soil-structure interface cannot reach there. Nodes present along the soil-structure interface are indicated by subscript *f* (foundation). On the other hand, the nodes of the structure have been denoted using subscript *st* (structure) and the nodes present along the interior foundation medium/soil are represented by subscript *s* (soil).

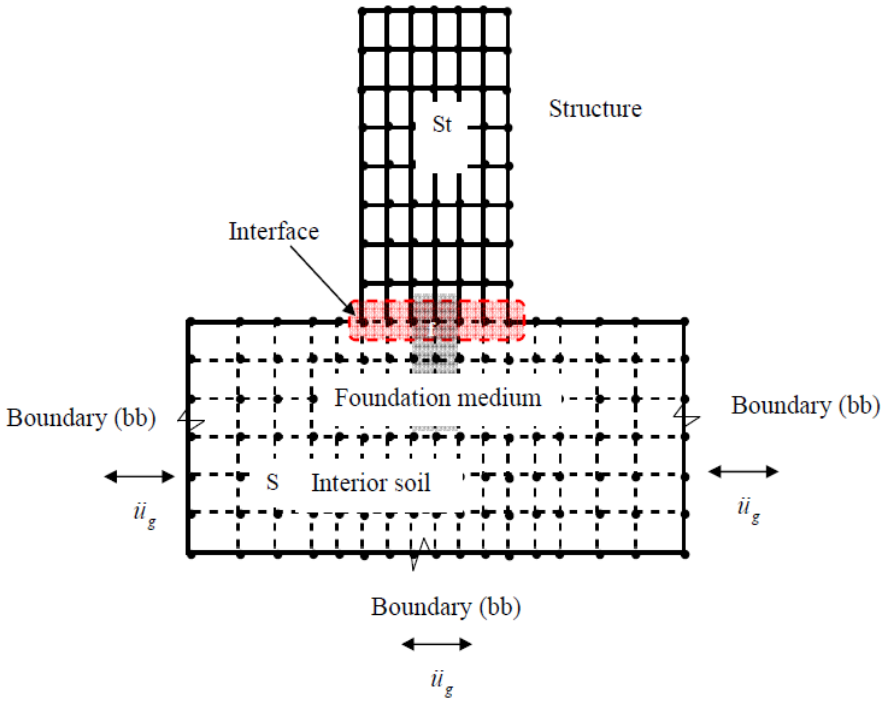

Figure 2.2.5. Finite element model of soil-structure system for direct method of analysis (NPTEL)[19]

In Figure 2.2.5., the soil domain is modelled as an assembly of rectangular plane-strain elements. At each node of these elements, two translational DOFs are considered. On the other hand, the

structure is modelled as an assembly of beam elements. The kinematic interaction has been neglected and it is assumed that the foundation block will move with free-field ground motion. The inertia forces, which act on the structure, result in the vibration of the structure, foundation, underlying soil and the soil at the soil-structure interface.

The equation of motion (in time domain) for the whole system shown in Figure 2.2.5. can be written as

$$\boldsymbol{M\ddot{u} + C\dot{u} + ku = -M_{st}I\ddot{u}_g} \qquad \textbf{...2.2.5.}$$

where,

M = Mass matrix of the whole system containing entire structure, foundation and soil

$$= \begin{bmatrix} [M_{st\,st}] & [M_{st\,f}] & 0 \\ [M_{f\,st}] & \left[M_{ff}^{st}\right] + [\overline{M_{ff}^{s}}] & [\overline{M_{f\,s}}] \\ 0 & [\overline{M_{s\,f}}] & [\overline{M_{s\,s}}] \end{bmatrix}$$

C = Damping matrix (Material) of the soil and the structure

$$= \begin{bmatrix} [C_{st\,st}] & [C_{st\,f}] & 0 \\ [C_{f\,st}] & \left[C_{ff}^{st}\right] + [\overline{C_{ff}^{s}}] & [\overline{C_{f\,s}}] \\ 0 & [\overline{C_{s\,f}}] & [\overline{C_{s\,s}}] \end{bmatrix}$$

K = Stiffness matrix of the whole system, which can be generated using standard assembling procedure

$$= \begin{bmatrix} [K_{st\,st}] & [K_{st\,f}] & 0 \\ [K_{f\,st}] & \left[K_{ff}^{st}\right] + [\overline{K_{ff}^{s}}] & [\overline{K_{f\,s}}] \\ 0 & [\overline{K_{s\,f}}] & [\overline{K_{s\,s}}] \end{bmatrix}$$

M_{st} = Mass matrix consisting of non-zero masses for the structural degree of freedom

$$= \begin{bmatrix} [M_{st\,st}] & [M_{st\,f}] & 0 \\ [M_{f\,st}] & \left[M_{ff}^{st}\right] & 0 \\ 0 & 0 & 0 \end{bmatrix}$$

I = Influence coefficient vector,

$\ddot{u_g}$= Free-field ground acceleration,

u = Relative displacement vector with respect to the base.

Here the damping matrix C has been formed by generating damping matrix of the soil and the structure separately from their modal damping ratio using Rayleigh damping and then combining them together. The coupling terms between the structure and the soil are taken as zero, while at the interface of the structure and the soil, they as considered as non-zero.

The RHS of equation 2.2.5. represents the inertia force, which is responsible for the deformation of the soil at the soil-structure interface when transferred to the foundation (base) in the form of shear force and moment. The contribution of material damping towards the response reduction of the soil-structure system is very less and can be ignored. The deformation of the soil occurred because of the inertia forces acting at the interface propagates in the form of radiation waves. These radiation waves result in radiation damping, which mostly affects the response of the whole structure-soil-foundation system. If the radiation damping does not die out at the boundary and reflects back from there, some error may be introduced in the solution and also the problem becomes very large. In order to decrease the problem size, the concept of absorbing boundary condition is introduced in FEM.

Using the direct method, problems in time domain can also be solved in frequency domain using Fourier transform function for a certain free-field ground motion. If the time histories of the ground motion differs at different supports, the problem can be solved by adjusting the influence coefficient vector I used in equation 2.2.5.

The main advantage of direct method is that in this method, non-linear behaviour of the soil can be taken into account. To solve dynamic SSI problem using direct method, several computer programs and softwares (e.g. Abaqus, ANSYS, OpenSEES, SAP 2000) are used. However, there are many drawbacks of direct method of SSI analysis. Some of them are listed below:

- Perfect representation of the damping matrix is difficult.
- If a 3D system has to be modelled, the size of the problem turns into a very large one and modelling of the soil-structure interface becomes very complex.

2.2.4. SUBSTRUCTURE METHOD

This method of dynamic SSI analysis is computationally more efficient than the direct method because using this method, most of the drawbacks of the direct method can be eliminated. In this method of analysis, the effective input motion is initially represented in terms of the free-field

motion of the soil layer. Thereafter the soil (foundation) medium and the structure are expressed as two independent mathematical models (substructures) as shown in Figure 2.2.6.

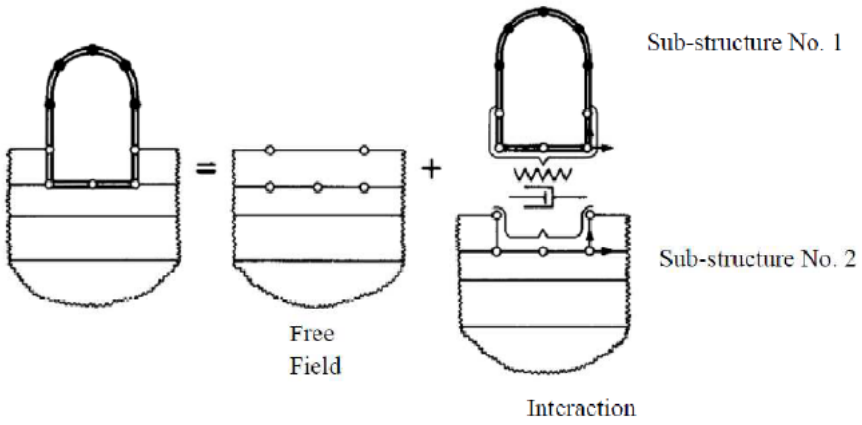

Figure 2.2.6. Seismic soil-structure interaction with substructure method (Wolf, 1985)[15]

The substructures are connected using interaction forces having equal amplitude. These interaction forces act in opposite directions for the two substructures. The total motions developed at the interface are obtained by adding the free-field motions at the interface of the soil without considering the structure to the additional motions generated from the interaction. The substructure method is said to be advantageous because this method permits the breaking down of complicated soil-structure system into more manageable parts. These parts can be analysed, solved and checked very easily. As the damping and stiffness properties of the soil are dependent on frequency, it is more convenient to perform seismic response analysis in the frequency domain to get the response history. After that, the obtained response history is converted in the time domain. It should be noted that for modelling some soil-structure interaction phenomenon, it is necessary to include some portion of the soil in the superstructure. This type of modelling is shown in Figure 2.2.7.(c). For these cases, two interfaces exist – one is at the free ground surface while the other one is at the surface between the superstructure and the soil medium.

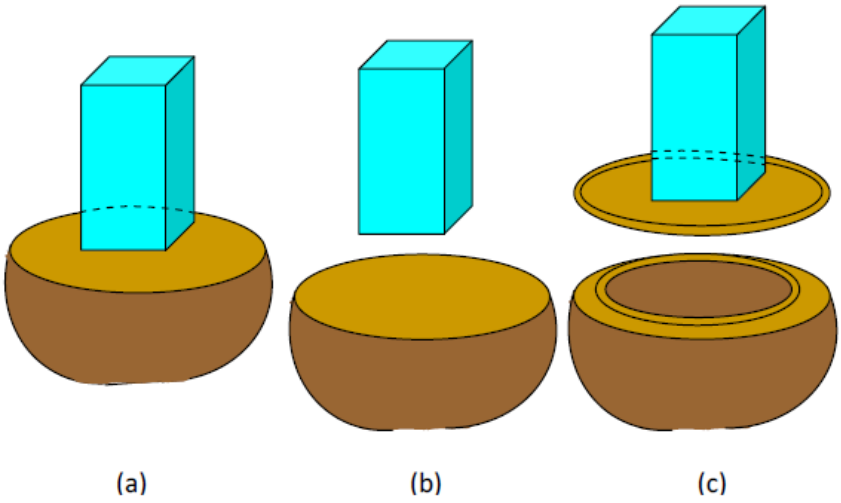

Figure 2.2.7. Seismic soil-structure interaction with substructure method: (a) SDOF system resting on a half space; (b) modeling superstructure and soil medium separately; (c) some portion of the soil is included in the superstructure model (NPTEL)[19]

2.2.5. PREVIOUS RESEARCHES ON DYNAMIC SOIL-STRUCTURE INTERACTION

Stewart et al. (1999)[20] demonstrated the procedure for evaluating the effects of inertial soil-structure interaction on seismic structural response. The data used for analysis are according to the provisions provided in the standard building codes considering the influence of site conditions, foundation embedment, flexibility and shape of foundation. Implementation of analysis techniques and system identification methods are exemplified using a time-history of Northridge earthquake (1994). A companion paper uses these analyses to evaluate the SSI effects empirically using available strong motion data from a broad range of sites and then comes with general conclusions. García (2008)[21] observed the impact of soil-structure interaction during the analysis and design of a RC frame building having six storeys and basement. The models are created with different support conditions including soil-structure interaction (flexible base and fixed-base) behaviour. Considering the soil-structure interaction effect influences the dynamic behaviour of the building resulting increase in vibration period along with increase in the system damping in comparison with the fixed-base model. The impact of the soil-structure interaction in the earthquake resistant design of the structure is reflected in a reduction of the horizontal spectral acceleration values. The results (stresses and displacements) obtained after introducing artificial flexibility in the structural analysis are closer to the actual behaviour of the structure in comparison with those obtained from the analysis of a fixed-base structure.

Mylonakis et al. (2010)[22] investigated the effect of SSI on the response of structures subjected to seismic excitation. At first, a brief discussion is done about the way of treating the present seismic provisions along with SSI effect. Response spectrum specified in code along with amplified fundamental period and effective damping due to SSI lead invariably to decrease the base shear of the structure. In certain seismic and soil environments, an increase in the fundamental natural period of a moderately flexible structure due to SSI may have a detrimental effect on the imposed seismic demand. In addition to that, an inelastic bridge pier, a widely used structural model for assessing SSI effects, is also analysed. Comparing the theoretical values with the values obtained from numerical analysis, it is shown that inappropriate use of ductility concepts and geometric relations may lead to erroneous conclusions in the calculation of seismic performance. Numerical examples are presented which highlight various critical issues of the problem.

Anand et al (2010)[23] described the seismic behaviour of RC buildings with and without shear wall under different soil conditions. One to fifteen storeyed space frames with and without shear wall have been analysed using ETABS software for different soil conditions (hard, medium, soft). The Base Shear, Axial Force and Lateral Displacement values for the two frames are compared. It is observed that when soil type gets changed from hard to medium and medium to soft, the values of Lateral Displacement, Base Shear, Axial Force and Moment in the column increases in case of all the building frames. Therefore, SSI effect must be included for designing frames under seismic excitations.

Matinmanesh et al. (2011)[24] performed the idealised 2-D finite element analysis of dynamic SSI assuming plane strain condition using Abaqus (v.6.8) software. The recording the ground motion is done for low, intermediate and high frequency content earthquakes. If SSI effect is taken into consideration, results show that the sandy soil amplifies the seismic waves on the soil-structure interface. During earthquakes, seismic waves propagate from the bedrock through different soil layers beneath and cause damages to the superstructure. Special attention has to be paid towards the effects of strong ground motion for the mitigation of earthquake disasters as well as for the earthquake resistant design of local buildings.

Pandey et al. (2011)[25] studied the static Pushover Analysis and Response Spectrum Analysis (RSA) of five buildings having different configuration (three step back buildings and two step back-set back buildings) with varying support conditions. These buildings are analysed for different soil conditions (hard, medium and soft soils) idealised by equivalent springs. The

response spectra parameters including total base shear, displacement from pushover analysis, displacement from response spectrum method and response correction factor have been studied with respect to the fixed base analysis for comparing the effect of flexibility of soil springs. It is found that response reduction factor decreases with the increment of time period, but becomes constant beyond a specific value of time period.

Priyanka et al. (2012)[26] analysed the effect of SSI on multi-storeyed buildings having different foundation systems. Dynamic properties of soil can influence the seismic waves while they pass through a soil layer. When a structure is subjected to a seismic excitation, it interacts with the foundation as well as with the soil, and thus alters the motion of the ground. Therefore, the type of soil and the type of structure both affect the response of the whole soil-structure system. The responses of buildings, with rigid and flexible foundations, subjected to seismic forces are computed in this study. Multi-storeyed buildings constructed on different soils (hard, medium and soft) with fixed and flexible support conditions are subjected to seismic forces and the analysis is performed. The buildings are analysed as per Response Spectrum Method using software STAAD.Pro. The values of response, such as Lateral Deflection, Storey Drift, Base Shear, Axial Force and Column Moment, are determined for all the building frames used for analysis.

Mahadeva et al. (2014)[22] presented the criteria for earthquake resistance design of structures. It gives the spectrum analysis for different types of soil, such as hard, medium and soft, and also for SSI with various foundation systems. In this paper, analysis of the 3-D frame is done using SAP 2000 (v.14) software. The structure and the soil are considered as a single continuum model. It also gives the idea about the response of a building having raft foundation under the action of seismic forces. The structure is analysed according to the response spectrum method using software SAP 2000 (v.14). The focus of the work is the analysis of energy transfer mechanism from the substructure to the superstructure during earthquakes, which is a critical criteria for designing earthquake resistant structures and for the renovation of the existing structures.

Kuladeepu et al. (2015)[27] investigated the dynamic behaviour of building frames on raft footing under seismic excitations considering the SSI effect. The analysis has been carried out using SAP 2000 (v.14) software. For SSI analysis of building frames, the soil and the foundation and are considered as the parts of a single compatible unit and the soil is idealised using the soil models for analysis. The soil under the raft slab is substituted by providing a true soil model (continuum model). For developing the elastic continuum model, soil is assumed as homogeneous and

isotropic. Dynamic Shear Modulus and Poisson's Ratio of the soil are given as inputs. In this study, influence of number of storeys, soil types and height ratio on SSI are observed for seismic zone-V. For bare frame, building responses are computed with and without considering the soil flexibility. Result parameters, such as natural time period (lateral), seismic base shear and lateral displacements, have also been evaluated.

Gaikwad et al. (2015)[28] inspected the behaviour of bare frames and in-filled frames having soil beneath. In this paper, three types of soils (soft, medium and hard) are considered. The in-filled panels are of brick masonry only. For seismic analysis of building frames, the columns are assumed to be fixed at the foundation level. But, the real condition is not like that. Incorporating the properties of the soil does not ensure 100% fixity of the building columns. The superstructure gets altered due to settlement and rotation of the foundation, shear force and bending moment. This effect is known as "Soil-Structure Interaction". Various cases are studied, such as bare frame with and without soil, in-filled frame with and without soil, using ANSYS (v.14.5) software. The results obtained considering the effect of SSI are compared to those obtained neglecting the SSI.

Kumar et al. (2016)[22] analysed the seismic performance of frame structures considering the influence of the SSI phenomenon. The dynamic responses of a fixed base structure are compared with that of flexible base structure. FEM is used to model the SSI effect of frame structures resting on raft foundation. The problems have been solved with the help of SAP 2000 (v.14) software. The time period, lateral displacement, storey drift and bending moment in X-X and Y-Y directions are extracted as results. After carrying out the time-history analysis, various parameters such as base shear and roof top displacement of the building frames have been studied along with the effect of soil media. It is observed that SSI effect plays a significant role to increase the time period and lateral displacement as well as the bending moment in X-X and Y-Y directions. The reason behind this is due to SSI, flexibility of soil gets increased significantly.

Magade et al. (2016)[22] illustrated the common design practices for dynamic loading with the assumption that the building is fixed at base. In reality, the supporting soil always allow some sort of movement due to its property to deform. The flexibility of the foundation may reduce the stiffness of the structural system resulting in an increase of the natural periods of the whole system. Such an interdependent behaviour of the soil and the structure influencing the overall response is referred to as SSI. This SSI effect is suggested to be accounted considering springs of specified

stiffness. The change in natural period of the system due to the SSI effect is an important issue from the perspective of design considerations.

Hosseinzadeh et al. (2017)[22] observed the response of embedded buildings under seismic excitation using experimental tests (with the help of shaking table) and finite element analysis. According to this paper, SSI is caused by the flexibility of the foundation soil as well as by the change in the free-field response of soil media due to the presence of structures. The effects of SSI phenomenon on the dynamic behaviour of buildings can be altered by embedding the foundations. In this work, scaled models are designed as per four different steel buildings with 5, 10, 15 and 20 storeys representing common buildings in urban area. The geometric scale of the models is kept as 1:100. Both soft and relatively soft soil media have been considered for this study. The developed models have been subjected to earthquake records of El Centro, USA (1940) and Tabas, Iran (1981) using International Institute of Earthquake Engineering and Seismology (IIEES) shaking table. The results, such as building aspect ratio, shear wave velocity, frequency content, damping ratio, and acceleration of structural models, found from finite element analysis of the entire soil-structure system are compared with those obtained from the shaking table experiment. Finally, it is concluded that the SSI effect can be reduced by increasing the depth of embedment of the foundation.

Ghannad et al.[29] investigated the seismic response with SSI on the basis of , the concept of Cone models, subjected to near fault ground motions. In this investigation, moving average filtering is used to disintegrate near fault ground motions long period and short period component. The study signifies that considering SSI, peak acceleration response for the original near fault ground motion and their disintegrated parts become nearer as compared to the fixed base systems.

Zhang and Tang[30] studied numerically the dynamic SSI by a lumped two degree of freedom system which was exposed to pulse like near fault ground motions. Their simulations corroborates that the SSI effects largely governed by the pulse to structure frequency ratio, the foundation-structure stiffness ratio, the rocking of foundation and the nonlinearity in structure system.

A parametric study has been performed by Azarhoosh and Ghodrati Amiri[31] using the elastic response of different SSI systems having shallow foundations which were exposed to synthetic pulses and near fault motions. The study revealed that SSI has negligible effects on the dynamic responses of structures which have very low or very large period ratios. Further, considering SSI effects, synthetic pulses and near fault motions generates similar type of seismic demand.

Minasidis et al.[32] investigated SSI effect of the response of 2D steel frames exposed to near fault earthquake ground motions. They used springs and dashpots to simulate flexibility of soil at the soil foundation contact surface. In this study they found that considering SSI effect, larger inter story drift ratios and lesser floor accelerations as compare to stiff soil.

Gelagoti et al.[33] examined the seismic performance of rocking isolated frame structures considering SSI by employing nonlinear FEM. In this study near source ground motion has been used to determine factor of safety against toppling collapse of the structure. Their results signified in addition to PGA, impact pulse velocity and the number of strong motion cycle plays an important role on toppling of the structure.

Davoodi and Sajadi [34] investigated response of single degree of freedom (SDOF) system with considering SSI subjected to 71 ground motian which consists both near field and far field earthquakes. The findings from the study revealed that near field ground motion record generally yield greater seismic responses than far field ground motions. Further, parametric study between Peak Ground Velocity to Peak Ground Acceleration ratio (PGV/PGA) of near field ground motion record signifies that with increase in structure to soil stiffness ratios, earthquakes with higher PGV/PGA ratio produce greater responses.

2.3. FRAGILITY CURVE AND PROBABILISTIC SEISMIC DEMAND MODELS

Fragility analysis is an effective statistical tool used for the assessment of vulnerability of a structure. By performing fragility analysis fragility curves can be developed, which are nothing but a graphical representation of change in probability of exceedance of Engineering Damage Parameter (EDP) at particular limit capacities (IO, LS and CP) with the variation of certain specific demand. The EDPs may be roof drift, percentage storey drift, energy dissipation etc. On the other hand, the demands may be Peak Ground Acceleration (PGA), Peak Ground Displacement (PGD), Spectral Acceleration for a specific time period etc.

Probabilistic Seismic Demand Model (PSDM) defines EDP as a function of Intensity Measure. Usually, it is represented by a curve indicating the alteration of percentage storey drift with respect to the change of PGA. Fragility curves and PSDMs can be developed by LHS-Monte Carlo method and 2000 SAC/FEMA[35] method.

2.3.1. LHS-MONTE CARLO METHOD

In this method, a selected frame is analysed under all ground motions to obtain PSDMs and fragility curves. Each ground motion is scaled to several PGA level for Non-linear Time History Analysis (NTHA). This procedure is followed for all the selected ground motions. As per this method, the total number for analysis required is equal to 'selected ground motions × 20'.

The maximum ground storey drifts are recorded with respect to PGA. The probability of exceedance of ground storey drift at a certain PGA level for a particular limit state capacity can be calculated using the equation 2.3.1.

$$\textbf{Probability of exceedance at a PGA level} = \frac{\textbf{Number of analysis cases where ground storey drift exceeds the limit}}{\textbf{Total number of analysis cases at that PGA level}} \quad \textbf{...2.3.1.}$$

2.3.2. 2000 SAC/FEMA METHOD

Cornell et al. (2002)[36] has studied the probabilistic exceedance for seismic design along with limit capacity addressing the uncertainties in hazard, structural damage, and loss analysis. The relationship between probabilistic exceedance limit and seismic intensity is determined using non-linear time-history analysis (NTHA). The equations for the EDP function and probabilistic exceedance limit are also developed. The framework, which provides the probabilistic basis for design recommendations, is obtained from the 2000 SAC/FEMA project[35].

In this method, a closed form expression is used which contains formula for developing fragility curves. A fragility curve is expressed using a lot of discrete functions due to the involvement of various uncertainties like uncertainties in modelling, material properties, rebar locations etc.

Celik and Ellingwood (2010)[37] have expressed the seismic fragility function by the equation 2.3.2.

$$\mathrm{P(D \geq C \mid IM)} = 1 - \emptyset\left(\frac{ln\frac{S_C}{S_D}}{\sqrt{\beta_{D|IM}^2 + \beta_C^2 + \beta_M^2}}\right) \quad \textbf{...2.3.2.}$$

where,

$\mathrm{P(D \geq C \mid IM)}$ = Probability of exceedance of ground storey drift for particular limit state capacities,

D = Ground storey drift,

C = Drift capacity at the chosen limit state,

$\beta_{D|IM}$ = Dispersion in the Intensity Measure (IM) like ground storey drifts at different PGA levels,

β_C = Dispersion in capacities,

β_M = Dispersion in modelling.

S_C is expressed in terms of IM at particular limit state capacities such as IO, LS and CP.

S_D is also known as EDP and can be expressed in a generalised form in terms of IM, which is shown in equation 2.3.3.

$$\boldsymbol{EDP = a(IM)^b} \qquad \textbf{...2.3.3.}$$

where, a and b are the regression coefficients of the PSDM.

Therefore using equation 2.3.3., equation 2.3.2. can be rewritten as:

$$\mathbf{P(D \geq C \mid IM) = 1 - \emptyset}\left(\frac{\ln S_c - ln(a.IM^b)}{\sqrt{\beta_{D|IM}^2 + \beta_C^2 + \beta_M^2}}\right) \qquad \textbf{...2.3.4.}$$

From NTHA, dispersion in the ground storey drifts at different PGA levels, $\beta_{D|IM}$, is calculated using equation 2.3.5.

$$\boldsymbol{\beta_{D|IM} = \sqrt{\frac{\sum[\ln(d_i) - \ln(a.IM^b)]^2}{N-2}}} \qquad \textbf{...2.3.5.}$$

Now, uncertainty value for β_C depends upon strength and other properties of the materials used, construction quality etc. For existing buildings, β_C depends on field investigation and the documents (drawings) which are available for the verification of accuracy. In case of new buildings, it depends on how well the assumptions for designing the structure match with the actual construction process in the field. The values of β_C with representative conditions have been recommended in ATC-58 (2012)[38]. In the present study, the value of β_C is taken as 0.25 according to the paper of Pragalath (2016)[39], where the building design is completed to a level design development, construction quality is assured and limited quality inspection is anticipated. As per ATC-58 (2012)[38], the total dispersion in modelling, β_M, can be calculated as:

$$\boldsymbol{\beta_M = \sqrt{\beta_C^2 + \beta_q^2}} \qquad \textbf{...2.3.6.}$$

β_q indicates that the hysteretic models may not accurately represent the behaviour of the structural components, even if the details of construction are precisely known. In this paper, the value of β_q is considered as 0.25 from the paper of Pragalath (2016)[39]. The limiting value of ground storey drift in terms of intensity measure (IM) at a particular limit state capacity (IO, LS, CP) can be obtained from FEMA 356 (2000)[35] and IS-1893 (Part-1):2016[16]. As mentioned in FEMA 356 (2000)[35], the different performance objectives with their corresponding inter-storey drift limits for concrete frame structures are presented in Table 2.3.1. However, according to IS-1893 (Part-1): 2016[16], the maximum limit for inter-storey drift is 0.004 means 0.4%.

Table 2.3.1. DAMAGE CONTROL AND BUILDING PERFORMANCE LEVELS

Building Type	Member Type	Immediate Occupancy (IO)	Life Safety (LS)	Collapse Prevention (CP)
Concrete Frame	Primary	• Minor hairline crack. • Limited yielding at few locations. • No crushing. • Strain < 0.003.	• Extensive damage to beams. • Spalling of cover and shear cracking ($< \frac{1}{8}"$ wide) for ductile columns. • Minor spalling in non-ductile columns. • Joint cracks $< \frac{1}{8}"$ wide.	• Extensive cracking and hinge formation in ductile element. • Limited cracking and/or splice failure in some non-ductile columns. • Severe damage in short column.
	Secondary	• Minor spalling in a few places in ductile columns and beams. • Flexural cracking in beams and columns. • Shear cracking ($< \frac{1}{8}"$ wide) in joints.	• Extensive cracking and hinge formation in ductile elements. • Limited cracking and/or splice failure in some non-ductile columns. • Severe damage in short columns.	• Extensive spalling in columns (limited shortening) and beams. • Severe joint damage. • Buckling of some reinforcements.
	Drift	• 1% transient drift. • Negligible permanent drift.	• 2% transient drift. • 1% permanent drift.	• 4% transient drift. • 4% permanent drift.

2.3.3. PREVIOUS RESEARCHES ON FRAGILITY CURVE

Singhal and Kiremidjian (1996)[40] have described the method for probabilistic evaluation of seismic structural damage. In this paper, fragility curves are developed for low, mid and high-rise RC buildings using LHS-Monte Carlo method. The entire Non-linear Time History Analysis (NTHA) has been carried out by using the observed building damage data from the Northridge earthquake (1994).

Mosalam et al. (1997)[41] performed push over analysis on seismic fragility of Lightly Reinforced Concrete (LRC) frames with and without masonry infill walls. In this paper, fragility curves have been generated by using LHS-Monte Carlo method. The developed fragility curves indicate that the effect is comparatively lower in case of LRC with infill walls.

Guneyisi and Altay (2008)[42] have developed fragility curves for a high-rise RC office building retrofitted with fluid viscous dampers in Istanbul region. In this study, a suit of 240 artificially generated ground motions compatible with the design spectrum has been used for representing the variability in ground motions. NTHA responses of the structure before and after retrofit are also studied. The fragility curves have been represented by lognormal distribution functions with two parameters - spectral acceleration and spectral displacement, which are developed in terms of PGA.

Investigation carried out by Suraj V. Borele (2015)[43] demonstrates the methodology for generating a fragility curve, which is the graphical representation of the seismic risk of a structure. In this study, fragility curves have been developed based on the guidelines given by Hazus technical manual. Two and four storeyed RC frame buildings are selected for case study and their seismic behaviour with and without infill walls are observed. The infill walls have been modelled as equivalent diagonal struts and for each infill panel the width of the struts are evaluated following the guidelines given in FEMA 356[35]. The RC buildings are modelled and analysed using SAP 2000 (v.14) software and the design methods are based on IS 456:2000[44] and IS 1893(Part 1):2002[45]. Static non-linear analysis or push over analysis of the building models has been performed to develop the capacity curves. The values obtained from the capacity curves are used to plot the fragility curves. Based on these fragility curves, seismic performance of all the buildings are compared.

Reliability based seismic analysis of OGS frame buildings have been carried out by Pragalath (2016)[39]. In this paper, fragility curves and PSDMs are developed by using both push over

analysis and NTHA. The capacity limits, such as Damage Limitation (DL), Significant Damage (SD), Collapse Prevention (CP) or near collapse level of buildings, have been studied for two storeyed, four storeyed, six storeyed and eight storeyed buildings using push over analysis.

Vazurkar and Chaudhari (2016)[46] have done the vulnerability assessment of RC buildings with the help of fragility curves. Fragility curves describe the probability of damage being exceeded a particular damage state. In this work, the fragility curves are developed according to the guidelines given by Hazus technical manual. The RC buildings have been modelled and analysed using SAP 2000 (v.14) software. For analysing the buildings, non-linear static analysis procedure is followed. Pushover analysis has been carried out following the guidelines given in ATC-40 (1996)[47]. In addition to that, capacity curves are also plotted. The results obtained from the pushover analysis are used to plot the fragility curves. For plotting the fragility curves, spectral displacements are taken as ground motion parameter. The damage states have been described as per Hazus technical manual. Finally, the spectral displacement values satisfying the predefined performance level requirements are estimated based on the fragility curves. Thus, the fragility curves are used to study the seismic performance of building models.

2.4. RELIABILITY ANALYSIS

Reliability of a structure is its ability to meet the specific requirements within a stipulated time period. While designing a structure, this factor plays an important role as it quantifies the probability that the structure will fulfil its design requirements. Reliability analysis is a tool that assists the structural engineer to take into account all possible uncertainties during the design, construction and life of a structure in order to calculate its probability of failure and to estimate the level of risk against a local or a global structural failure.

2.4.1. RELIABILITY INDEX AND RELIABILITY CURVES

Reliability Index (RI) is a statistical parameter, which helps to determine the reliability of a structure. It is computed by subtracting the probability of failure of a structure from unity. If the value of RI for a system is more, it indicates that the system is more reliable and has less probability of failure. Plotting the RI values against the intensity of seismic excitation gives the reliability curves. The detailed procedure for calculating RI values and plotting reliability curves has been demonstrated in Chapter 5 of this thesis.

2.4.2. PREVOIUS RESEARCHES ON RELIABILITY ANALYSIS

Collins et al. (1996)[48] discussed about dual-level seismic design which is a reliability-based methodology. In that paper, an equivalent system methodology and uniform hazard spectra have been used to determine the performance of a structure. The performance criteria are expressed using probabilistic terms, and from these criteria, deterministic design-checking equations are developed.

Ellingwood (2001)[49] showed the significance of reliability analysis of building responses to understand the behaviour of buildings. This paper highlighted the procedure for developing seismic hazard curve and fragility curve to evaluate the earthquake risk in case of buildings. This study also revealed the importance of inherent properties and modelling uncertainties of buildings through fragility curves.

Wen (2001)[50] described the concept of reliability and performance-based design. In this paper, the minimum lifecycle cost criteria was proposed to arrive at an optimal target reliability for the performance-based design under the action of multiple natural hazards.

Pragalath (2016)[39] carried out the reliability based seismic design of open ground storey frame buildings. The main objective of this paper is to determine the multiplication factors (MF) for different reliability curves. For this purpose, reliability curves for two storey, four storey, six storey and eight storey buildings at different floor levels have been generated to obtain various multiplication factors. At the end, all the results are summarised draw the conclusion.

2.5. CRITICAL APPRAISAL OF LITERATURE

On the basis of above literature survey following observations may be made.

i) The variation of response of structure due to soft, medium and hard soil using fragility analysis has not been performed.

ii) The variation of response of structure due to different soil under near-field and far-field earthquake is essential.

iii) The effect of different soil layer in the response of different story building using fragility analysis is missing in the literature and it should be carried out.

iv) The response of different type of buildings under different soil layers during near and far-field earthquakes should be focussed.

iv) Reliability based fragility analysis using hazard curve for a particular region for different kinds of soil and soil layers are absent in the existing literature and should be conducted.

v) Reliability based fragility analysis for various type of soil and buildings during far and near field earthquake has not been conducted yet.

Chapter-3: FRAME STRUCTURES ON UNIFORM SOIL

3.1. GENERAL

The damage pattern during several past earthquakes like Mexico earthquake (1985), San Francisco earthquake (1989), Los Angeles earthquake (1995) have shown that local soil plays significant role in the amplification of ground motion especially in those areas, that are located on unconsolidated young sedimentary deposits[51]. In India during Bhuj earthquake of 2001, Ahmedabad city, situated on younger alluvial deposits, experienced a heavy damage in spite of relatively larger distance from epicentre. Further, during seismic excitations, more attention should be paid to Soil-Structure Interaction (SSI) phenomenon, which is a major problem in the field of Structural Engineering. This chapter presents the behaviour of various parameters under the influence of dynamic soil-structure interaction when frame structures constructed on uniform soil are subjected to near-field and far-field earthquakes. In this chapter, three types of soils (Hard Soil, Medium Soil and Soft Soil) are combined with three types of buildings (G+1, G+4 and G+9) to develop analytical models. Each model is subjected to both near-field and far-field earthquake. It is to be mentioned that, in case of every model, fragility curves has been developed for all the floors under the influence of aforesaid two earthquakes. Moreover, amplification factors at fundamental frequency for each type of soil under each type of seismic excitation are computed separately and compared. To simulate the non-linear properties of concrete, concrete damaged plasticity model has been used. This model is briefly described in the next section followed by the all the analysis results.

3.2. CONCRETE DAMAGED PLASTICITY MODEL

Concrete damaged plasticity model provides a general capability for analysing concrete structures under the action of cyclic and dynamic loading. The main failure mechanisms of concrete are- (i) cracking under tension, and (ii) crushing under compression. Concrete behaves in a brittle manner when subjected to low confining pressures. If this confining pressure becomes sufficiently large to prevent crack propagation, the brittle behaviour of concrete vanishes. In this situation, failure

of concrete is driven by the consolidation and collapse of its microporous microstructure, which leads to a macroscopic response like a ductile material with work hardening.

The constitutive theory of the model aims to incorporate the effects of irreversible damage related to the failure mechanisms occur in concrete under quite low confining pressures. These effects result in the following macroscopic properties:

- Variation in yield strengths under tension and compression (The initial yield stress under compression is 10 times or more higher than the initial yield stress in tension).
- Only softening under tension, while initial hardening followed by softening under compression.
- Unlike elastic stiffness degradation under tension and compression.
- Stiffness recovery effect during cyclic loading.
- Rate sensitivity, particularly an increase in the peak strength with the increment of strain rate.

The main limitations of the model are that it cannot consider anisotropicity of the material and shear strength of the cracked section. An overview of this model has been presented below.

(A) Damage and Stiffness Degradation

Damaged states under tension and compression can be characterised independently using two hardening variables, namely equivalent plastic strains in tension ($\tilde{\varepsilon}_t^{pl}$) and equivalent plastic strains in compression ($\tilde{\varepsilon}_c^{pl}$). The equations of these hardening variables, $\tilde{\varepsilon}_t^{pl}$and $\tilde{\varepsilon}_c^{pl}$, are developed considering uniaxial loading conditions first and thereafter extended to multi-axial conditions.

(B) Uniaxial Conditions

It is assumed that the uniaxial stress versus strain curves can be converted into stress-plastic strain curves having the following form,

$$\boldsymbol{\sigma_t = \sigma_t(\tilde{\varepsilon}_t^{pl}, \dot{\tilde{\varepsilon}}_t^{pl}, \theta, f_i)}$$
$$\boldsymbol{\sigma_c = \sigma_c(\tilde{\varepsilon}_c^{pl}, \dot{\tilde{\varepsilon}}_c^{pl}, \theta, f_i)} \qquad \textbf{…3.2.1.}$$

In equation 3.2.1., the subscripts *t* and *c* denote tension and compression respectively.

$\dot{\tilde{\varepsilon}}_t^{pl}$= Equivalent plastic strain rate under tension,

$\dot{\tilde{\varepsilon}}_c^{pl}$= Equivalent plastic strain rate under compression,

$\tilde{\varepsilon}_t^{pl} = \int_0^1 \dot{\tilde{\varepsilon}}_t^{pl} dt$ = Equivalent plastic strain under tension,

$\tilde{\varepsilon}_c^{pl} = \int_0^1 \dot{\tilde{\varepsilon}}_c^{pl} dt$ = Equivalent plastic strain under compression,

θ = Temperature, and

f_i (i = 1, 2,...) = Other predefined field variables.

If the rate of strain is denoted as $\dot{\varepsilon}_{11}^{pl}$, the effective plastic strain rates under the action of uniaxial loading conditions are given as

$$\dot{\tilde{\varepsilon}}_t^{pl} = \dot{\varepsilon}_{11}^{pl} \text{ (in uniaxial tension)}$$
$$\dot{\tilde{\varepsilon}}_c^{pl} = -\dot{\varepsilon}_{11}^{pl} \text{ (in uniaxial compression)} \qquad \text{…3.2.2.}$$

When a concrete specimen is unloaded from any point located on the strain-softening region of the stress-strain curve, the elastic stiffness of the material appears to be degraded (or damaged), which has been shown in Figure 3.2.1. This degradation of elastic stiffness significantly differs in case of tension and compression. The degraded response of concrete can be characterised using two independent uniaxial damage variables. These variables, denoted as d_t and d_c, are assumed to be functions of the plastic strains, temperature, and field variables (as shown in equation 3.2.3.).

$$d_t = d_t\left(\tilde{\varepsilon}_t^{pl}, \theta, f_i\right), \quad 0 \le d_t \le 1$$
$$d_c = d_c\left(\tilde{\varepsilon}_c^{pl}, \theta, f_i\right), 0 \le d_c \le 1 \qquad \text{…3.2.3.}$$

The uniaxial degradation variables are increasing functions of equivalent plastic strains. They can take values from zero (for undamaged material) to unity (for the fully damaged material).

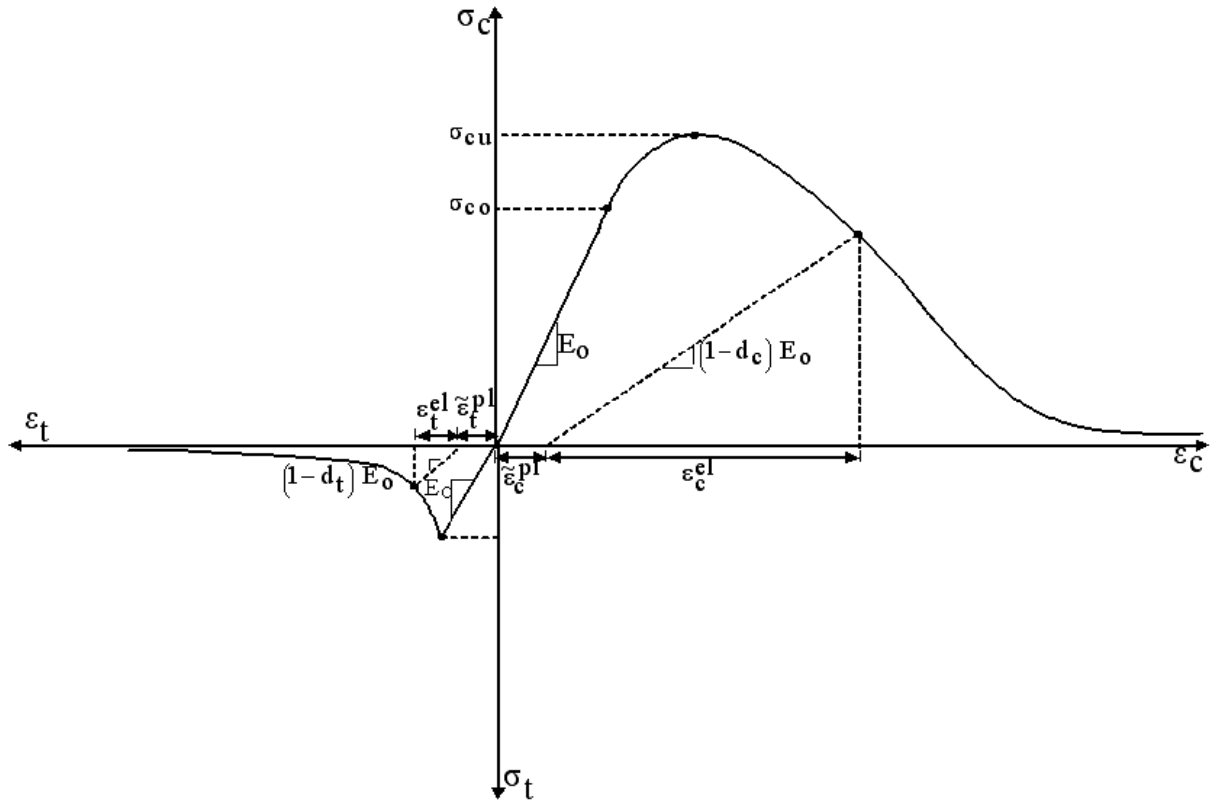

Figure 3.2.1. Response of concrete to uniaxial loading in compression and tension (Sarkar et al, 2007)[52]

If E_0 is the initial or undamaged elastic stiffness of the material, the stress-strain relations under uniaxial tension and compression loading are expressed as,

$$\boldsymbol{\sigma_t = (1 - d_t) E_0 (\varepsilon_t - \tilde{\varepsilon}_t^{pl})}$$
$$\boldsymbol{\sigma_c = (1 - d_c) E_0 (\varepsilon_c - \tilde{\varepsilon}_c^{pl})} \qquad \textbf{…3.2.4.}$$

Under the action of uniaxial tensile loading, damage propagates in a direction perpendicular to the direction of the stress. As a result of this, the nucleation and propagation of damage causes a reduction in the available load-carrying area, which in turn increases the effective stress. This effect is quite less under the action of compressive loading; as in this case, damage runs parallel to the direction of loading. However, after a significant amount of crushing, the effective load-carrying area is largely reduced. The effective uniaxial stresses $\bar{\sigma}_t$ and $\bar{\sigma}_c$ are given by Equation 3.2.5.

$$\overline{\sigma_t} = \frac{\sigma_t}{(1-d_t)} = E_0(\varepsilon_t - \tilde{\varepsilon}_t^{pl})$$

$$\overline{\sigma_c} = \frac{\sigma_c}{(1-d_c)} = E_0(\varepsilon_c - \tilde{\varepsilon}_c^{pl}) \qquad \text{...3.2.5.}$$

For avoiding the unreasonable mesh-sensitive results because of lack of reinforcements in the structure, the post-failure behaviour under tension has been expressed using a fracture energy cracking criterion by specifying a stress-displacement curve in place of a stress-strain curve, as presented in Figure 3.2.2. The values of $\overline{\sigma_t}$ and $\overline{\sigma_c}$ are computed following the experimental and numerical results presented by Lee and Fenves (1998)[53].

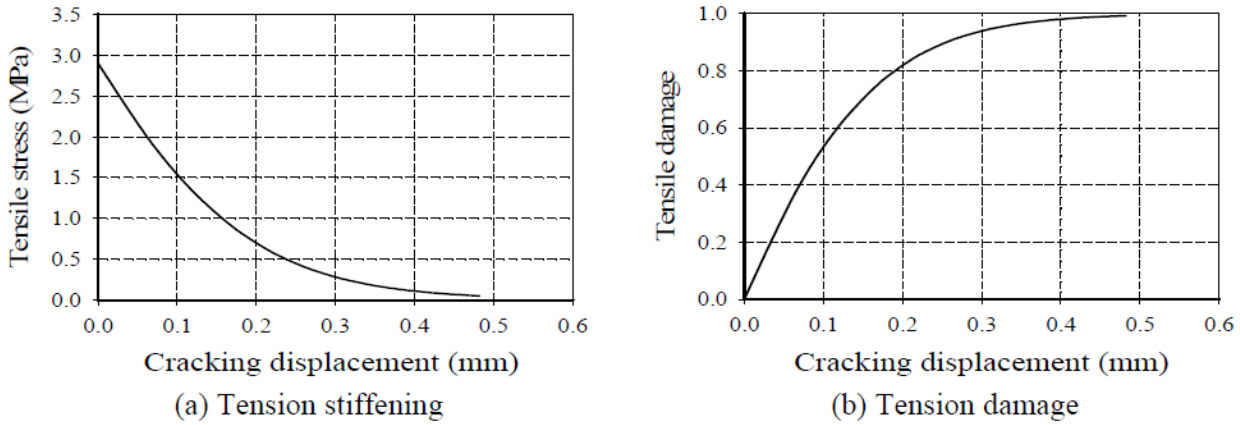

Figure 3.2.2. Tensile material properties of concrete (Sarkar et al, 2007)[52]

It is a well-known fact that the materials like concrete exhibits a significant change in volume when subjected to severe inelastic states. This volume change, caused due to the plastic distortion, can be represented well using an adequate plastic potential function G in the definition of plastic-flow rule[54]. For G, the classical Mohr-Coulomb yield function with the angle of dilatancy ψ is

$$G(\sigma, \psi) = \frac{I_1}{3}\sin\psi + \sqrt{J_2}\left(\cos\theta - \frac{\sin\theta \sin\psi}{\sqrt{3}}\right) \qquad \text{...3.2.6.}$$

where,

J_2 = Second invariant of stress deviator,

I_1 = First invariant of stress, and

θ = Polar angle through which the third invariant enters the deviatoric plane.

Under the action of multiaxial cyclic loading, the degradation mechanism becomes quite complex, as it involves opening and closing of the previously formed micro-cracks along with their interaction. However, the fundamentals of the model are the similar to the uniaxial conditions. Experimentally, some recovery of the elastic stiffness is observed as the load changes its sign during a uniaxial cyclic test. The stiffness recovery effect, which is also known as unilateral effect, is an important feature of the behaviour of concrete under cyclic loading. This effect is generally more prominent when the load is changed from tension to compression causing tensile cracks to close, which in turn results in recovery of the compressive stiffness. This behaviour has also been incorporated in the model[53].

3.3. PROBLEM FORMULATION

To detect the effect of soil properties on SSI, three types of soils namely- Hard Soil, Medium Soil and Soft Soil have been considered. It is assumed that all the soils are homogenous in nature. The mass density, Young's modulus and shear wave velocity in the soil medium are maximum for the hard soil and minimum for the soft soil. On the other hand, Poisson's ratio is minimum for the hard soil and maximum for the soft one. All the values for the medium soil lie between the hard and soft soil. However, the properties of all the soils used for analysis are mentioned in Table 3.3.1.

Table 3.3.1. PROPERTIES OF THE SOILS

Type of Soil	**Mass Density (ρ) in kg/m^3**	**Young's Modulus (E) in N/m^2**	**Poisson's Ratio (ν)**	**Shear Wave Velocity (V_S) in m/s**
Hard Soil	2300	1.99×10^9	0.2	600
Medium Soil	2000	6.5×10^8	0.32	350
Soft Soil	1500	9.7×10^7	0.43	150

It is to be mentioned that, SSI effects also depend on various properties of the structure like stiffness of the structure, height of the structure, type of foundation used etc. To study the contribution to the structures for the SSI effect, three frame buildings (G+1, G+4 and G+9) have been taken for analysis. All the buildings are square in shape having plan dimension 15 m × 15 m. Each building has three bays of equal length in both the directions. The heights of the buildings

are taken as 6 m, 15 m and 30 m respectively. Floor to floor height of all the buildings is considered as 3 m. Raft footings are used as the foundation of the buildings. Various properties of the constituents of the buildings are shown in Table 3.3.2.

Table 3.3.2. PROPERTIES OF THE CONSTITUENTS OF THE BUILDINGS

1.	**Grade of Concrete**		M 25
2.	**Mass Density (ρ) of Concrete**		2500 kg/m^3
3.	**Young's Modulus (E) of Concrete**		2.5×10^{10} N/m^2
4.	**Poisson's Ratio (ν) of Concrete**		0.15
6.	**Floor to Floor Height of the Building**		3 m
7.	**Depth of Footing**		2.5 m
8.	**Cross-sectional Area of the Columns**	**G+1 Building**	300 mm × 300 mm
		G+4 Building	400 mm × 400 mm
		G+9 Building	500 mm × 500 mm
9.	**Cross-sectional Area of the Beams**	**G+1 Building**	250 mm × 300 mm
		G+4 Building	250 mm × 400 mm
		G+9 Building	300 mm × 500 mm

3.4. MODELLING THE PROBLEM

There are numerous methods to model and analyse the dynamic SSI phenomenon. Among them, finite element method (FEM) is one of the easiest numerical techniques which can accurately simulate SSI effect and most commonly used. Nowadays, many software packages are available in the market to solve different problems using FEM. In the present work, a software named Abaqus (v.14.5) has been used for modelling and solving the above stated problem.

To solve a SSI problem using Abaqus software, generally, the steps mentioned below are sequentially followed:

1. Forming the geometries of different parts of the soil-structure model in the PART module.

2. Creating the materials and sections with desired properties and assigning them to the parts created before in the PROPERTIES module.
3. Generating the whole soil-structure model combining all the parts suitably in the ASSEMBLY module.
4. Mentioning the type of analysis required in the STEP module.
5. Choosing the sizes and properties of the elements of individual parts as per requirement in the MESH module.
6. Defining appropriate boundary conditions of the model in the LOAD module.
7. Indicating the type of interaction (or, constraints) between the different components of the model in the INTERACTION module.
8. Creating the job and submitting it for analysis in the JOB module.
9. Viewing the outputs and obtaining the desired results in the VISUALIZATON module.

In this study, six parts, such as Infinite Soil, Soil Base, Soil Tetrahedron, Footing, Column and Beam, have been used to model the above stated soil-structure interaction problem. The plan dimensions of the soil base part (32.5 m × 32.5 m) is kept almost double compared to the plan dimensions of the structure (15 m × 15 m) so that its boundaries cannot disturb the response of the structure. Its depth (30 m) is also kept higher than the depth of footing (2.5 m) due to the same reason. A 22.5 m × 22.5 m × 5 m rectangular groove is created at the centre of the soil base in order to fit the soil tetrahedron into it. The soil tetrahedron part actually works as a bridge between the footing and the soil base. This part also has a square shaped groove where the dimensions of the groove are same as that of the footing. The depth of the footing is 2.5 m. The footing is positioned in its respective groove. The beams of length 5 m are positioned on top of each two adjacent columns.

Homogeneous materials are created as per the predefined properties. The required sections for all the parts are generated and have been assigned accordingly. Proper orientations are also provided to the beams and the columns.

After forming all the parts and assigning all the material properties and section properties to them, they are assembled in the correct pattern to get the complete soil-structure model.

Two steps are created for two different types of analysis. The first step named Frequency is generated to carry out modal analysis of the whole model. The other step has been named as

Seismic, which performs the seismic analysis. From this step, all the stress and displacement components under the action of the input seismic motion can be easily obtained.

Meshing is the most vital part of the finite element method. The size of mesh plays an important role in the calculation process. If the mesh size is reduced gradually, the solution becomes more accurate. But, the problem is that with the reduction in mesh size, the number of nodes and elements increases which leads to more computer memory consumption and more computation time requirement. Therefore, an optimum mesh size has to be selected so that neither problem in accuracy of solution nor problem in computer memory and computation time arises. Keeping this in mind, the soil base and the infinite soil are meshed using eight-noded linear brick elements of size 2.5 m × 2.5 m × 2.5 m, while the footing is meshed using eight-noded linear brick elements of size 0.625 m × 0.625 m × 0.625 m. The soil tetrahedron is suitably meshed using four-noded linear tetrahedron elements so that it can be connected to the soil base as well as to the footing. The beams and the columns are meshed using two-noded linear elements of 1 m and 0.6 m length respectively. The properties and meshing details of all the elements used for analysis are summarised below in Table 3.4.1.

For modal analysis, the whole model is considered fixed at the base. To incorporate this property, all the displacement and rotation components of the nodes present at the bottom of the model are restricted to zero. On the other hand, to perform seismic analysis, only the displacement component of the bottom nodes along the direction of earthquake force is released.

At last, all the duplicate nodes are merged to fix all the parts with one another and to get the complete model. Different views (Plan, Elevation and Isometric view) of the prepared models for the G+1, G+4 and G+9 buildings are shown in Figure 3.4.1. to Figure 3.4.9.

Table 3.4.1. PROPERTIES AND MESHING DETAILS OF THE ELEMENTS USED IN ABAQUS

Name of the Part		Cross-sectional Area	Depth or Length of the Part	Element Size for Meshing	No. of Nodes in Each Element	Type of Element
Infinite Soil		2.5 m × 2.5 m	N/A	2.5 m × 2.5 m × Infinite Length	8	Linear Hexahedron (Type CIN3D8)
Soil Base (Surrounded by the Infinite Soil)		32.5 m × 32.5 m	30 m	2.5 m × 2.5 m × 2.5 m	8	Linear Hexahedron (Type C3D8)
Soil Tetrahedron (Embedded in the Soil Base)		22.5 m × 22.5 m	5 m	N/A	4	Linear Tetrahedron (Type C3D4)
Footing (Embedded in the Soil Tetrahedron)		17.5 m × 17.5 m	2.5 m	0.625 m × 0.625 m × 0.625 m	8	Linear Hexahedron (Type C3D8)
Column (Each column is placed on a Footing)	For G+1 Building	300 mm × 300 mm	3 m	0.6 m	2	Linear Line (Type B31)
	For G+4 Building	400 mm × 400 mm				
	For G+9 Building	500 mm × 500 mm				
Beam (Each beam is placed on two Columns)	For G+1 Building	250 mm × 300 mm	5 m	1 m	2	Linear Line (Type B31)
	For G+4 Building	250 mm × 400 mm				
	For G+9 Building	300 mm × 500 mm				

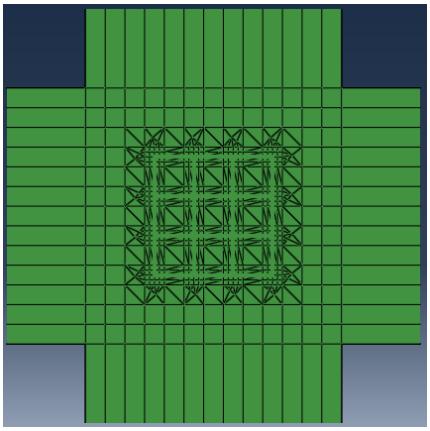

Figure 3.4.1. . Plan of the model used for G+1 building

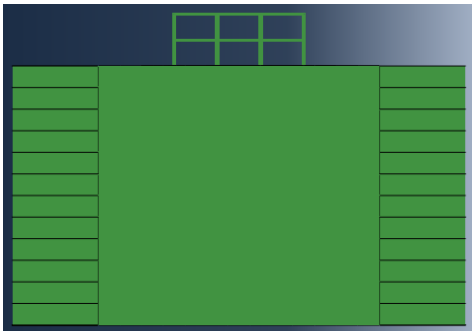

Figure 3.4.2. Elevation of the model used for G+1 building

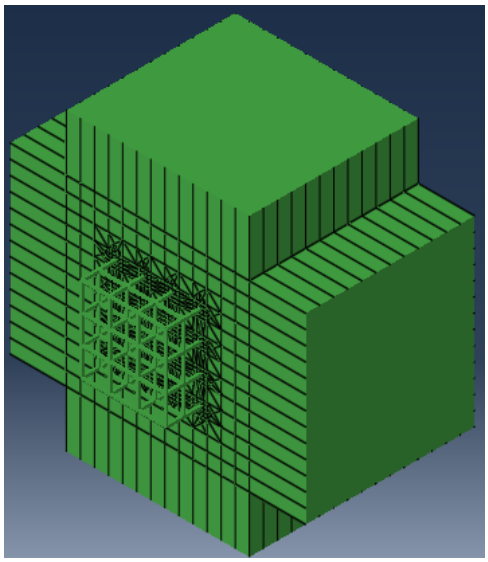

Figure 3.4.3. Isometric view of the model used for G+1 building

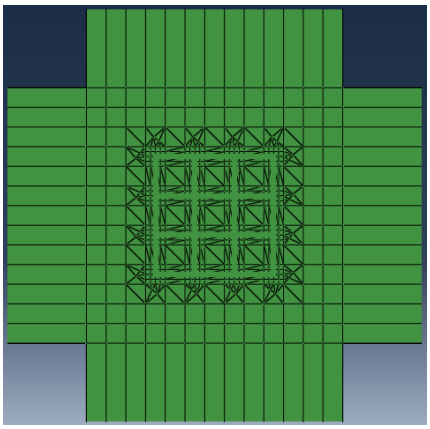

Figure 3.4.4. Plan of the model used for G+4 building

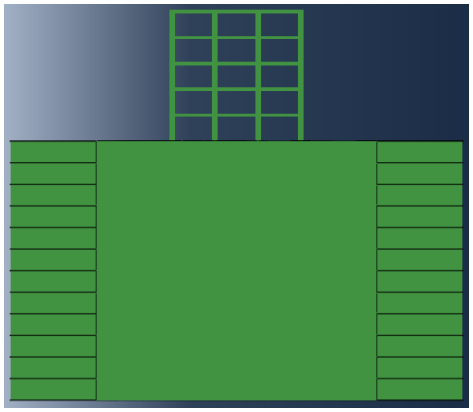

Figure 3.4.5. Elevation of the model used for G+4 building

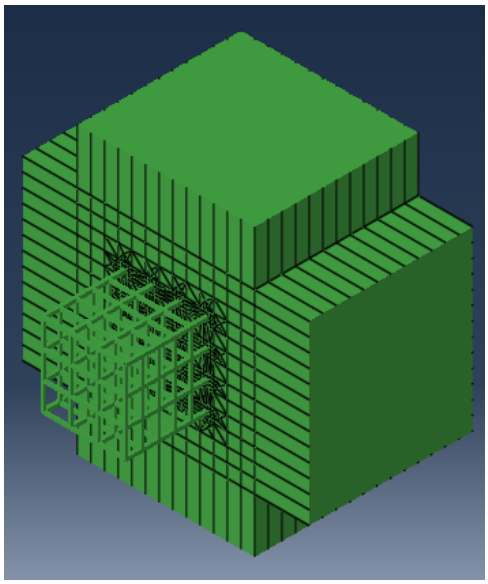

Figure 3.4.6. Isometric view of the model used for G+4 building

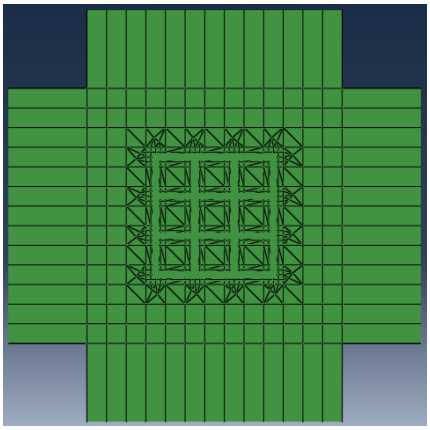

Figure 3.4.7. Plan of the model used for G+9 building

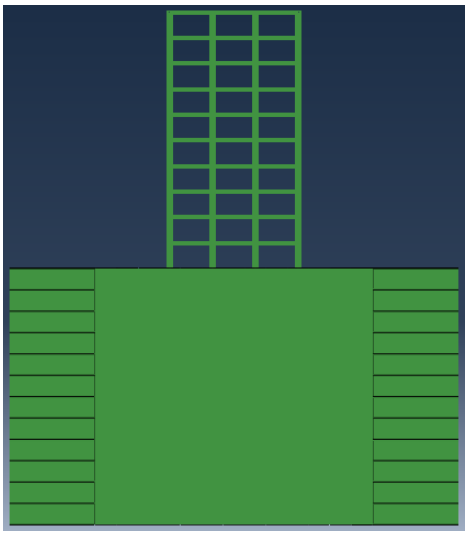

Figure 3.4.8. Elevation of the model used for G+9 building

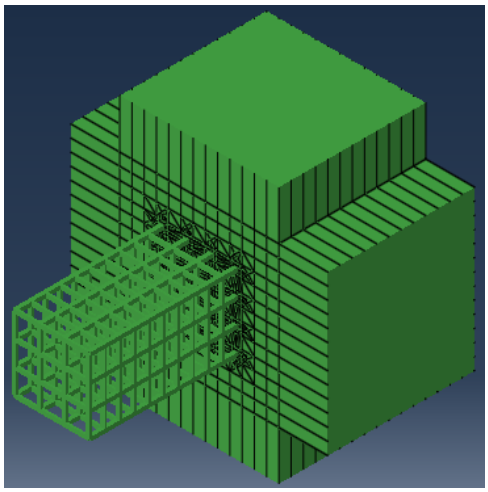

Figure 3.4.9. Isometric view of the model used for G+9 building

After preparing all the models, jobs are created. The first step of each job are submitted for analysis to obtain the first mode and fifth mode frequencies. Considering a damping ratio of 0.05, Rayleigh Damping Coefficients α and β are determined for every model using the equations 3.4.1. and 3.4.2.[55].

$$\boldsymbol{\beta = \frac{2\xi_1\omega_1 - 2\xi_m\omega_m}{{\omega_1}^2 - {\omega_m}^2}} \qquad \textbf{...3.4.1.}$$

$$\boldsymbol{2\xi\omega_1 = \alpha + \beta{\omega_1}^2} \qquad \textbf{...3.4.2.}$$

where,

m = Number of significant modes considered (Here, m=5),

ξ_1 = Damping Ratio of the first mode,

ξ_m = Damping Ratio of the m-th mode,

(In this problem, $\xi_1 = \xi_m = \xi$)

ω_1 = Frequency of the first mode,

ω_m = Frequency of the m-th mode.

Table 3.4.2. shows the first mode frequency, fifth mode frequency and Rayleigh damping coefficients for each possible soil-structure combination.

Table 3.4.2. RAYLEIGH DAMPING COEFFICIENTS OF MATERIALS FOR DIFFERENT SOIL-STRUCTURE COMBINATIONS

SOIL TYPE	STRUCTURE TYPE	FREQUENCY OF 1ST MODE (cps)	FREQUENCY OF 5TH MODE (cps)	DAMPING RATIO (ξ)	RAYLEIGH DAMPING COEFFICIENTS	
					α	β
Hard	G+1	3.0795	3.4903	0.05	1.02794691	0.002422523
	G+4	1.3906	3.4402	0.05	0.622223955	0.003294588
	G+9	0.73763	2.4122	0.05	0.354931576	0.005052811
Medium	G+1	2.0733	3.1321	0.05	0.783832971	0.003057497
	G+4	1.3799	2.1019	0.05	0.523402403	0.004571054
	G+9	0.73422	2.0865	0.05	0.34124358	0.005642352
Soft	G+1	0.92271	2.2938	0.05	0.41344309	0.004948063
	G+4	0.90515	1.4058	0.05	0.345965995	0.006886992
	G+9	0.69189	0.97079	0.05	0.253824502	0.009572193

These Rayleigh damping coefficient values are added to all the materials of the respective models in order to get the correct models.

3.5. INPUT MOTIONS AND THEIR PROPERTIES

In order to observe the effect of epicentre distance on dynamic SSI phenomenon, all the models are subjected to a near-field and a far-field earthquake. Loma prieta earthquake, which occurred in 1989, has been taken as a sample from the near-field earthquakes. On the other hand, Denali earthquake (2002) is considered a representative of the far-field earthquakes. Some general properties of Loma prieta and Denali earthquakes are tabulated in Table 3.5.1.

The acceleration time-histories of the above two earthquakes are displayed in Figure 3.5.1 and 3.5.2. respectively. Further, for better understanding of the properties of Loma prieta and Denali earthquakes, acceleration response spectra and Fast Fourier Transform (FFT) have been developed for both the earthquakes, which are shown in Figure 3.5.3 to Figure 3.5.6.

Table 3.5.1. GENERAL PROPERTIES OF THE EARTHQUAKES

Earthquake Name	**Loma Prieta**	**Denali**
Year	1989	2002
Station Name	UCSC	Valdez - Valdez Dock Company
Earthquake Type	Near-Field	Far-Field
Epicentre Distance (R_{rup})	18.51 km	239.52 km
Mechanism	Reverse Oblique	Strike Slip
Magnitude	6.93	7.9
V_{s30}	713.59 m/s	708.02 m/s
Spectral Ordinate	SRSS	SRSS
Scale Factor	1	1
Peak Ground Acceleration	0.311 g	0.009 g
Peak Ground Velocity	10.208 cm/s	1.77 cm/s
Peak Ground Displacement	4.054 cm	1.296 cm

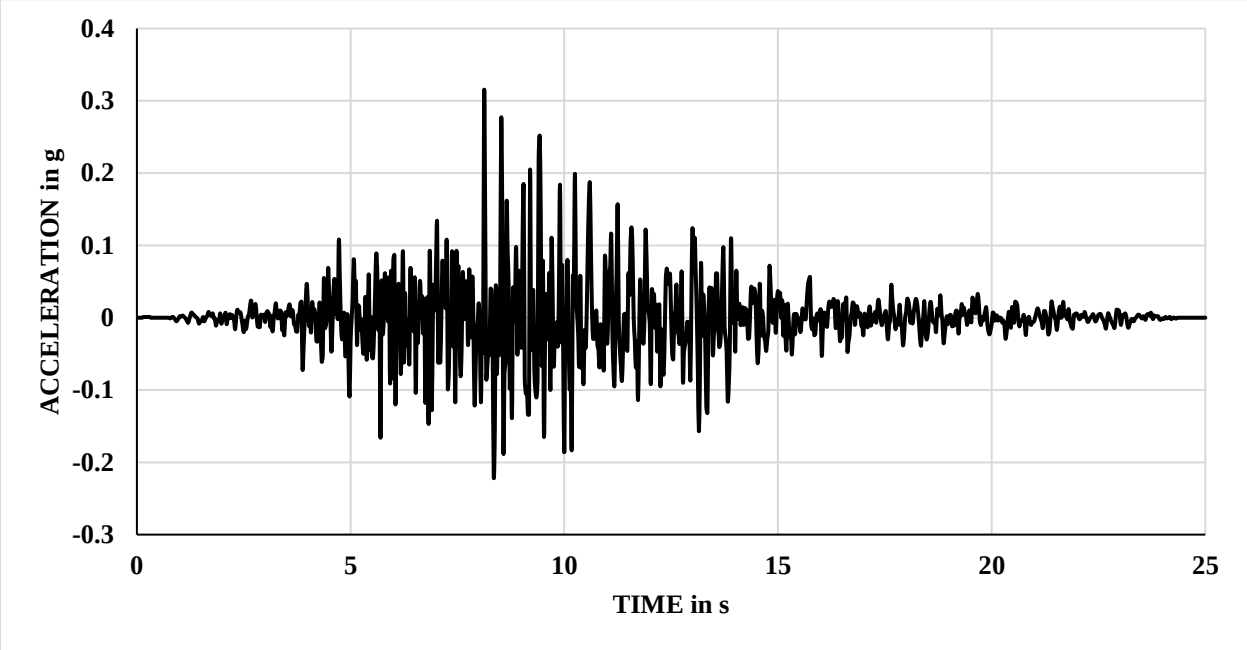

Figure 3.5.1. Acceleration time-history of Loma prieta earthquake

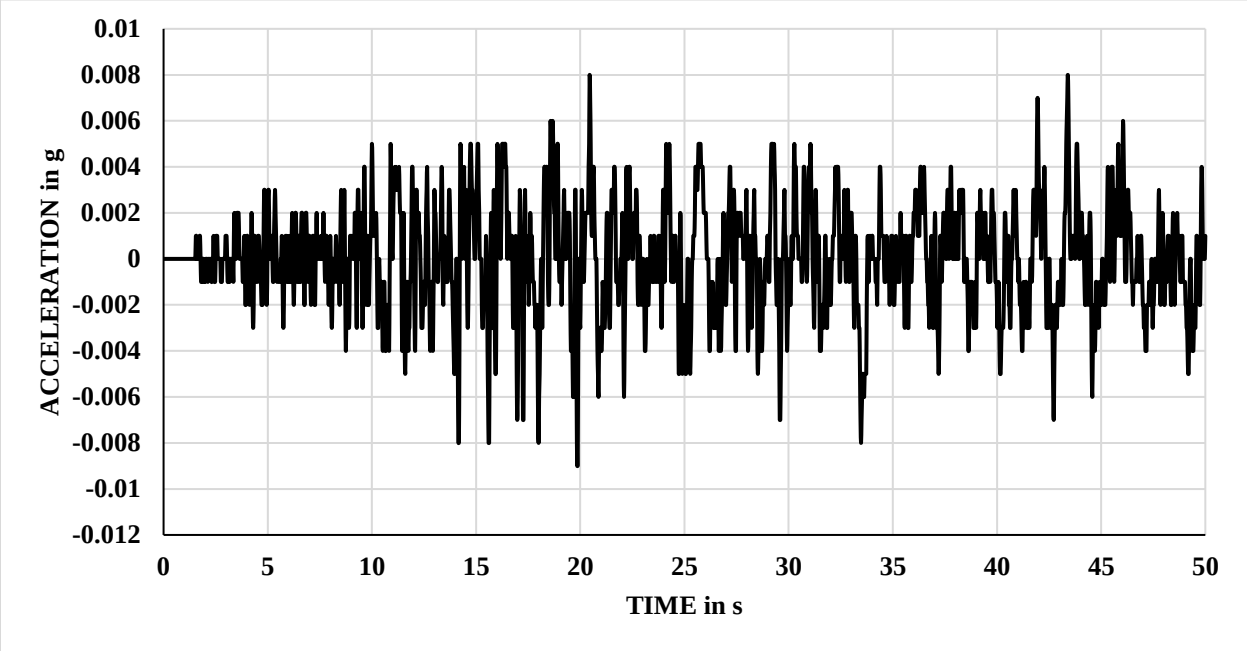

Figure 3.5.2. Acceleration time-history of Denali earthquake

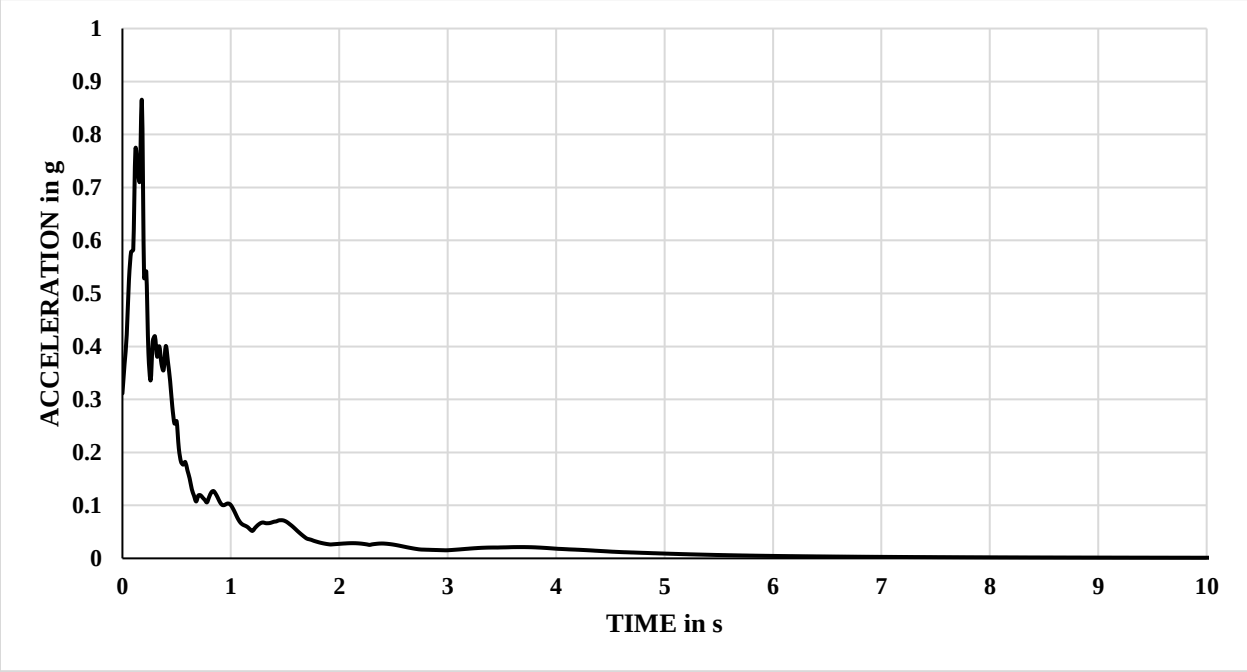

Figure 3.5.3. Acceleration response spectra of Loma prieta earthquake

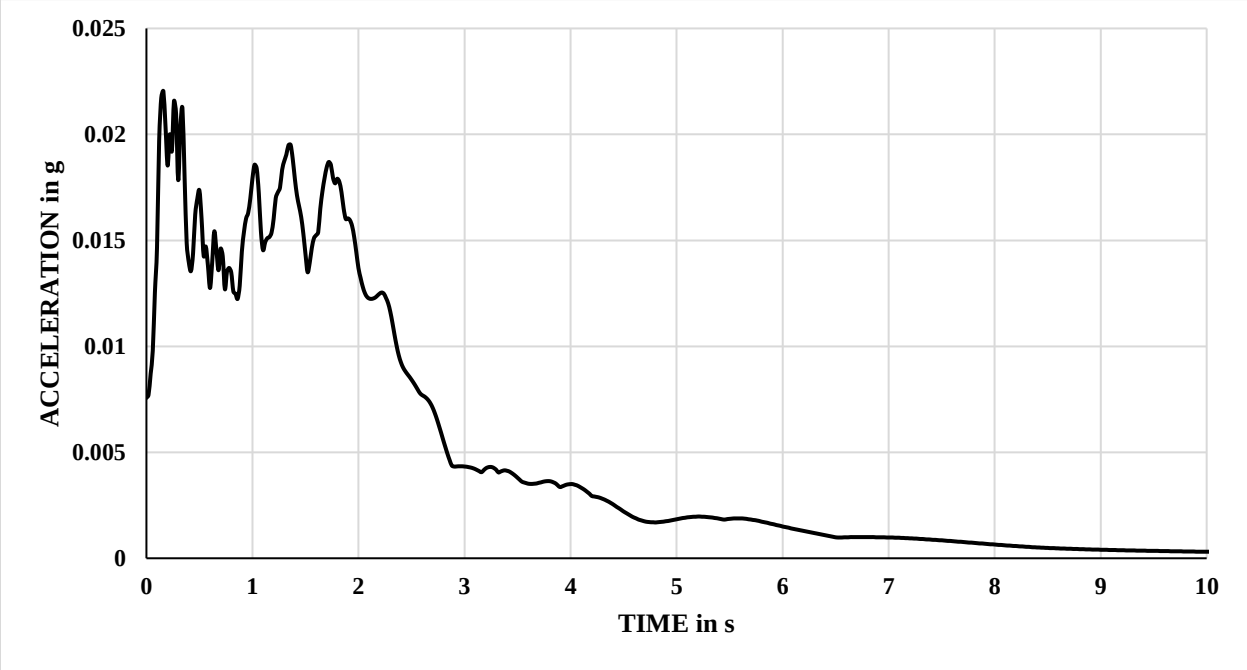

Figure 3.5.4. Acceleration response spectra of Denali earthquake

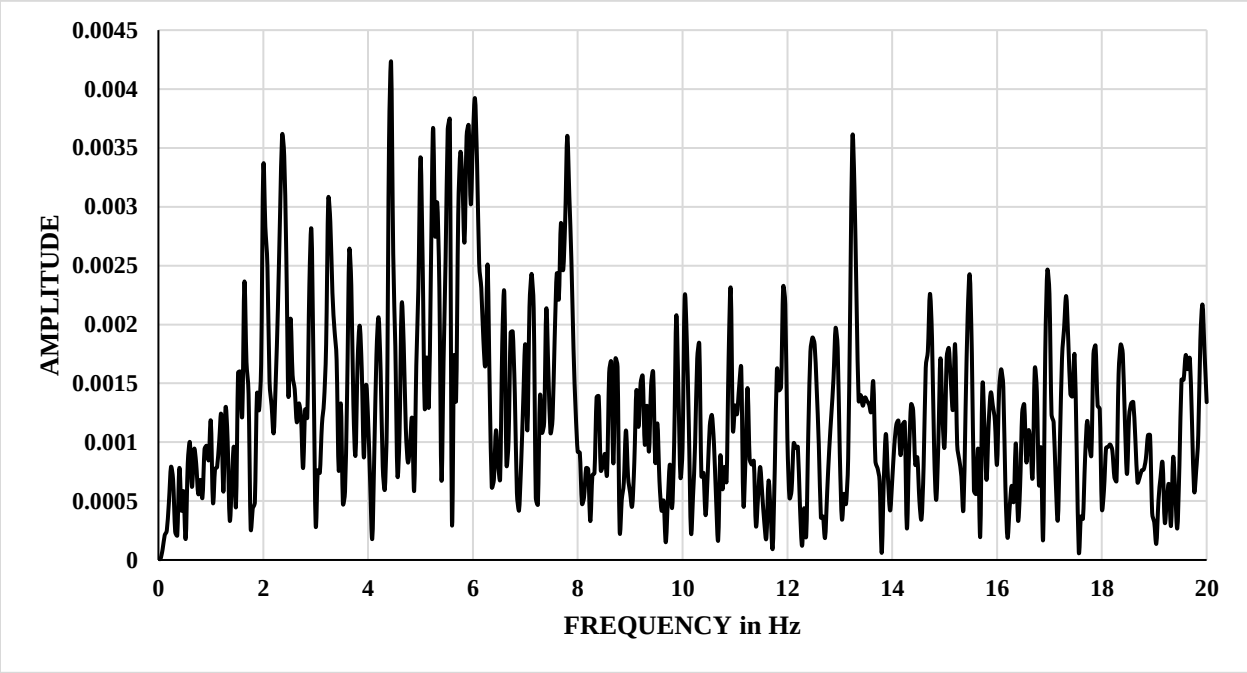

Figure 3.5.5. FFT of Loma prieta earthquake

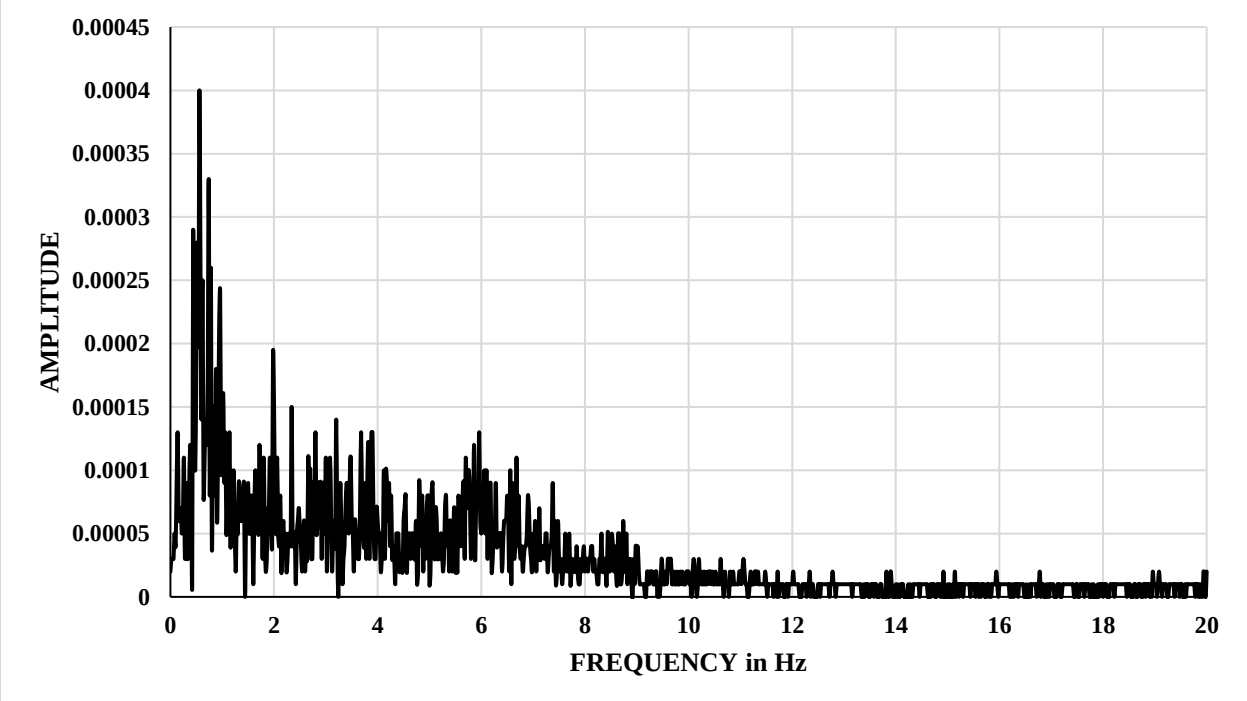

Figure 3.5.6. FFT of Denali earthquake

3.6. FUNDAMENTAL FREQUENCIES OF SOIL MEDIA

In order to obtain fundamental frequency and amplification at fundamental frequency, Loma prieta and Denali Earthquake time history motions have been applied at the base of the soil column and response time histories have been recorded at the surface of the soil. After that, Fourier transformation has been conducted of both these two time histories. Fourier transformation of surface motion to Fourier transfer of base motion gives amplification due to the soil in frequency domain. The first highest amplification indicates the amplification at fundamental frequency and corresponding frequency signifies the fundamental frequency of soil column. The fundamental frequencies and amplification at fundamental frequency of different uniform soils used for analysis have been tabulated in Table 3.6.1. The values in that table show that soft soil has the highest fundamental frequency value, while hard soil has the lowest. From this table, it can be observed that the value of amplification factor is maximum for soft soil and minimum for hard soil. It should also be noted that the amplification factor value of a soil is independent of the type of earthquake it experienced.

Table 3.6.1. AMPLIFICTION FACTORS OF VARIOUS SOILS UNDER DIFFERENT EARTHQUAKES

Type of Soil	Amplification Factor	Fundamental Frequency (cps)
Hard Soil	1.29	20.50
Medium Soil	1.45	23.50
Soft Soil	2.77	24.88

3.7. DISPLACEMENT TIME-HISTORIES OF ROOF AND BASE RESPONSES

After performing the entire analysis in Abaqus, displacement time-histories of the roof and the base have been plotted in case of every model. These plots are presented in Figure 3.7.1. to 3.7.36. The base response under the action of a particular earthquake differs mainly due to the variation in soil properties. When the input motion and soil type are kept unchanged, no significant alteration in the base response is observed with the change in building height. It is to be mentioned that for most cases, when a particular building is subjected to a certain earthquake, roof drift is the highest

when the building is located on hard soil. On the contrary, when the building rests on soft soil, roof displacement is the least. This may be due to higher flexibility effect of soft soil. However, when a G+9 building is subjected to a near-field earthquake, maximum roof displacement has been observed for medium soil. This may be due to this building is subjected higher value of spectral acceleration for medium type soil. If all other parameters are kept identical, the roof drift of a G+9 building is the maximum and roof drift of G+1 building is minimum. Further, the response of roof due to a far-field earthquake is more than the response of roof due to a near-field earthquake. This may be due to presence of low frequency wave in the far field ground motion.

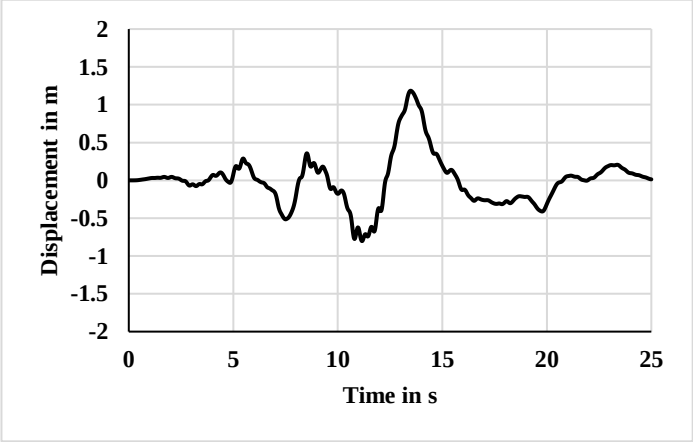

Figure 3.7.1. Displacement time-history for Roof of G+1 building on hard soil under Loma prieta earthquake

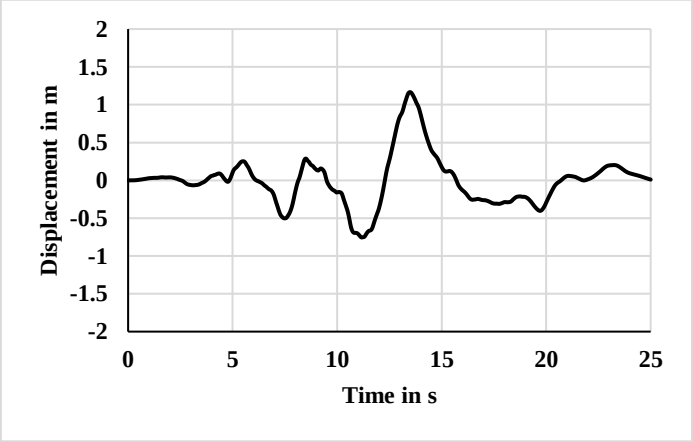

Figure 3.7.2. Displacement time-history for Base of G+1 building on hard soil under Loma prieta earthquake

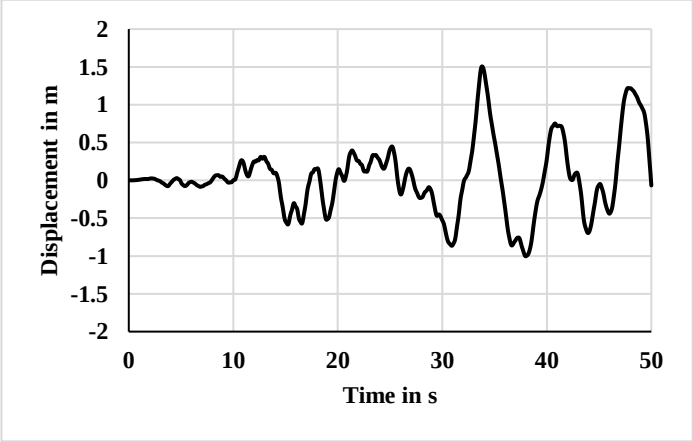

Figure 3.7.3. Displacement time-history for Roof of G+1 building on hard soil under Denali earthquake

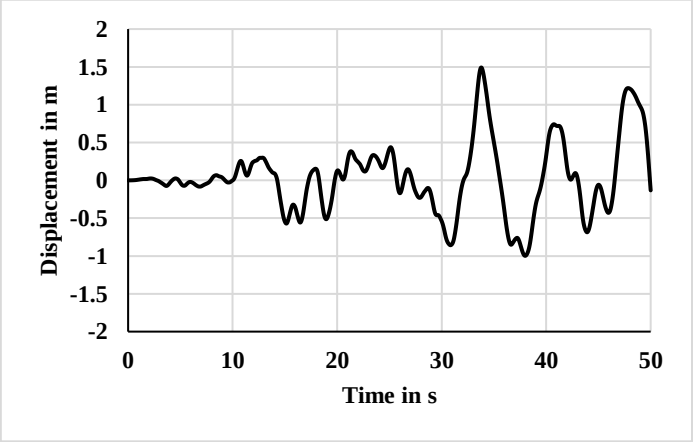

Figure 3.7.4. Displacement time-history for Base of G+1 building on hard soil under Denali earthquake

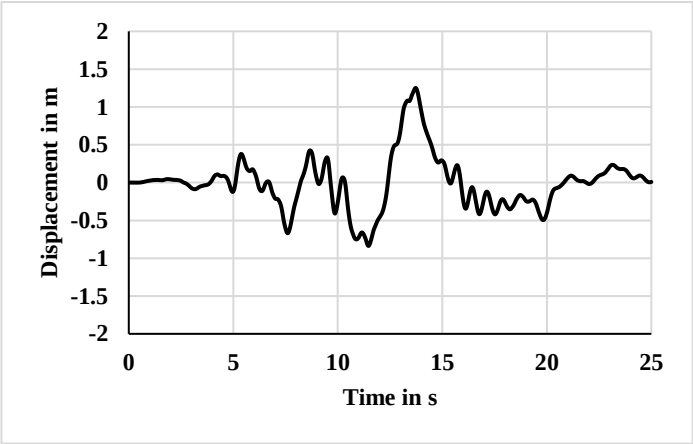

Figure 3.7.5. Displacement time-history for Roof of G+4 building on hard soil under Loma prieta earthquake

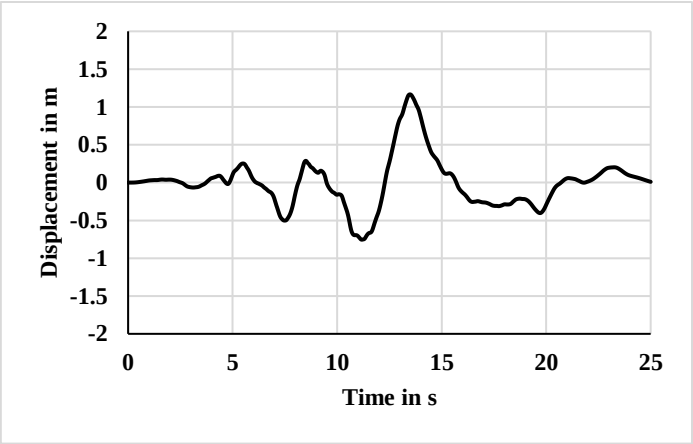

Figure 3.7.6. Displacement time-history for Base of G+4 building on hard soil under Loma prieta earthquake

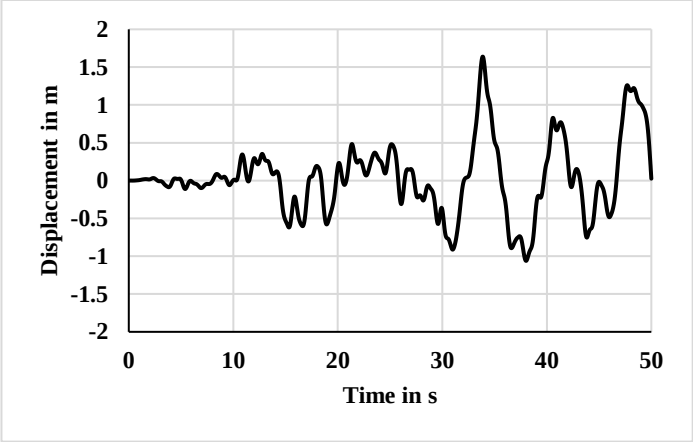

Figure 3.7.7. Displacement time-history for Roof of G+4 building on hard soil under Denali earthquake

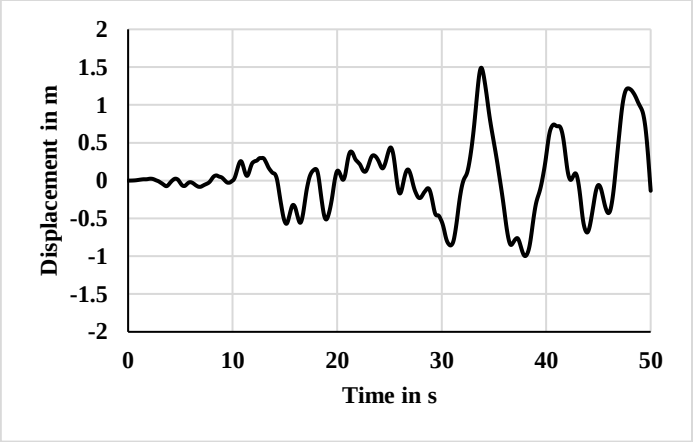

Figure 3.7.8. Displacement time-history for Base of G+4 building on hard soil under Denali earthquake

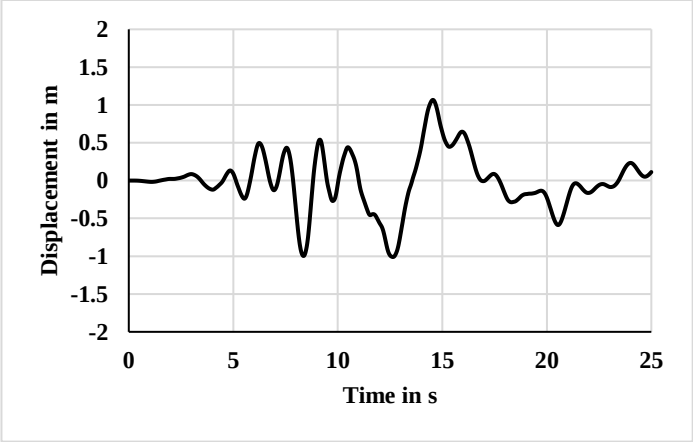

Figure 3.7.9. Displacement time-history for Roof of G+9 building on hard soil under Loma prieta earthquake

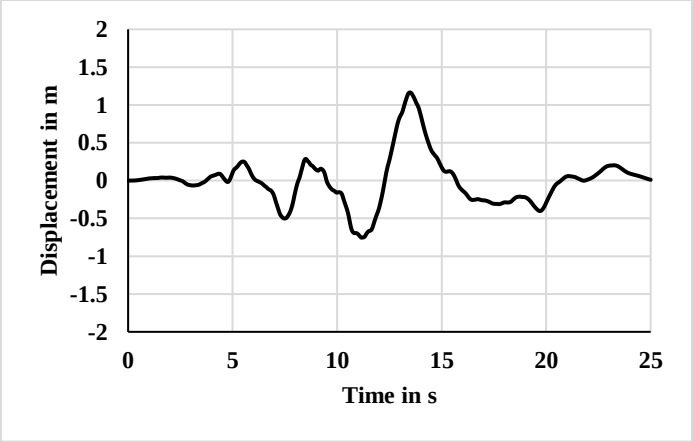

Figure 3.7.10. Displacement time-history for Base of G+9 building on hard soil under Loma prieta earthquake

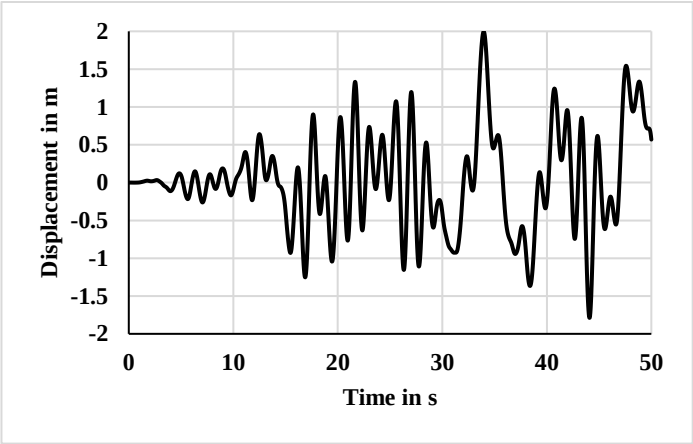

Figure 3.7.11. Displacement time-history for Roof of G+9 building on hard soil under Denali earthquake

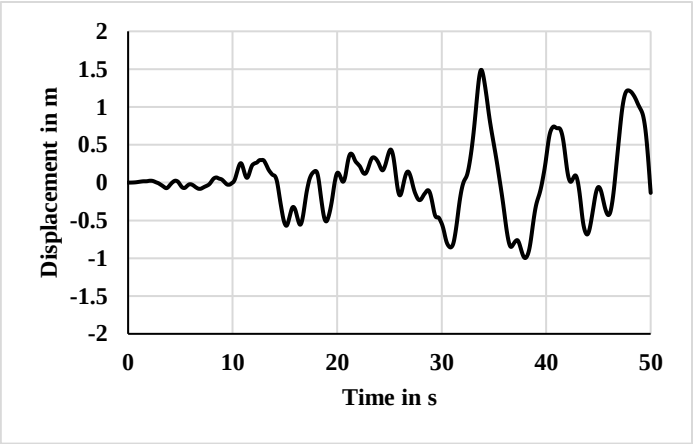

Figure 3.7.12. Displacement time-history for Base of G+9 building on hard soil under Denali earthquake

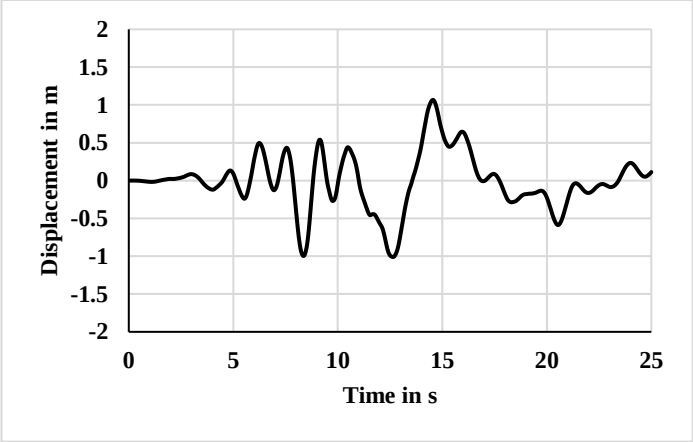

Figure 3.7.13. Displacement time-history for Roof of G+1 building on medium soil under Loma prieta earthquake

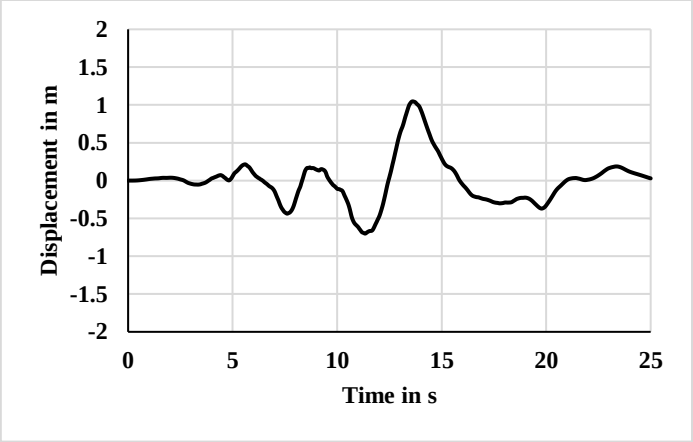

Figure 3.7.14. Displacement time-history for Base of G+1 building on medium soil under Loma prieta earthquake

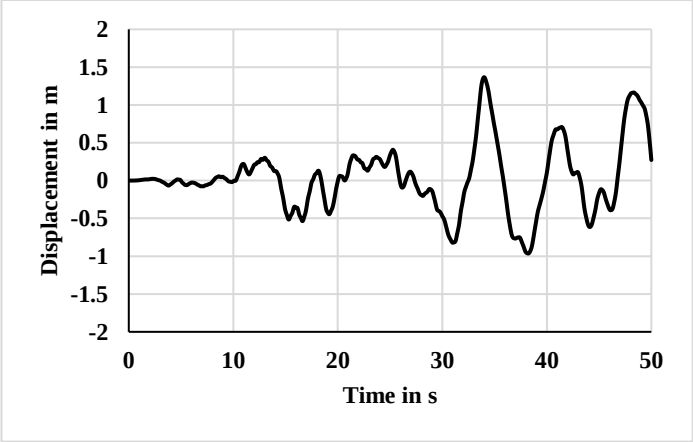

Figure 3.7.15. Displacement time-history for Roof of G+1 building on medium soil under Denali earthquake

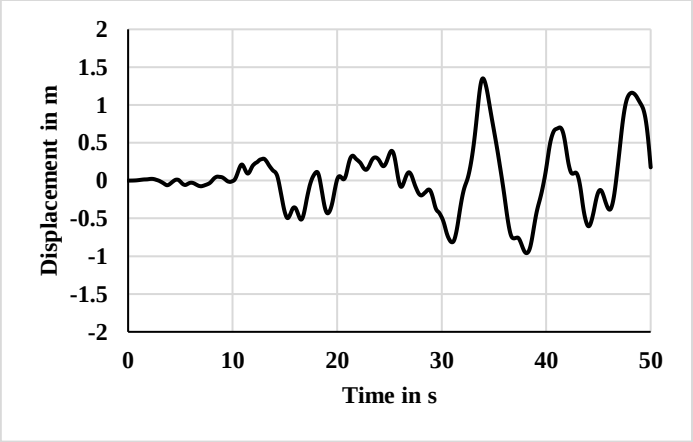

Figure 3.7.16. Displacement time-history for Base of G+1 building on medium soil under Denali earthquake

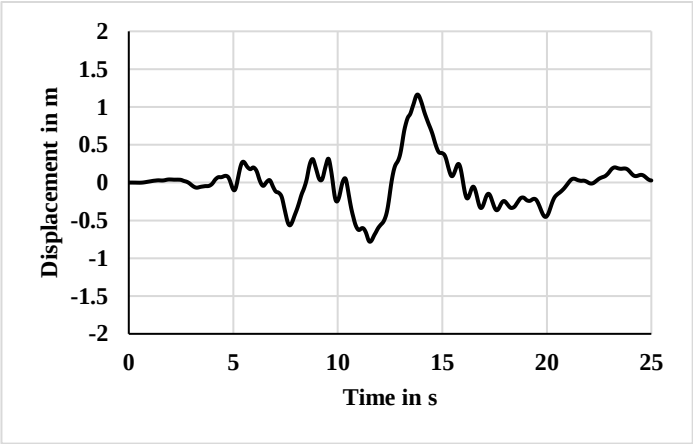

Figure 3.7.17. Displacement time-history for Roof of G+4 building on medium soil under Loma prieta earthquake

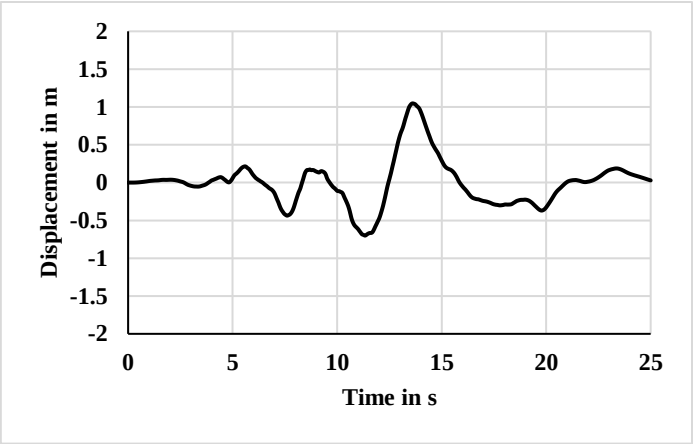

Figure 3.7.18. Displacement time-history for Base of G+4 building on medium soil under Loma prieta earthquake

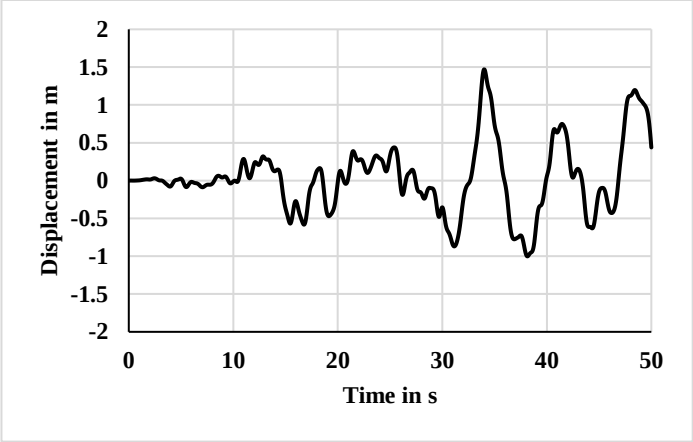

Figure 3.7.19. Displacement time-history for Roof of G+4 building on medium soil under Denali earthquake

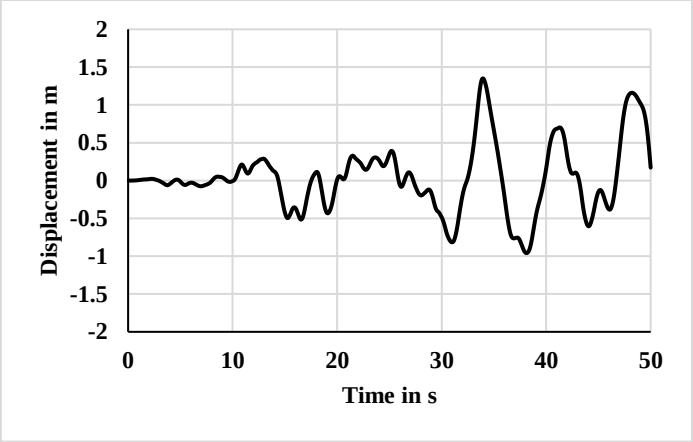

Figure 3.7.20. Displacement time-history for Base of G+4 building on medium soil under Denali earthquake

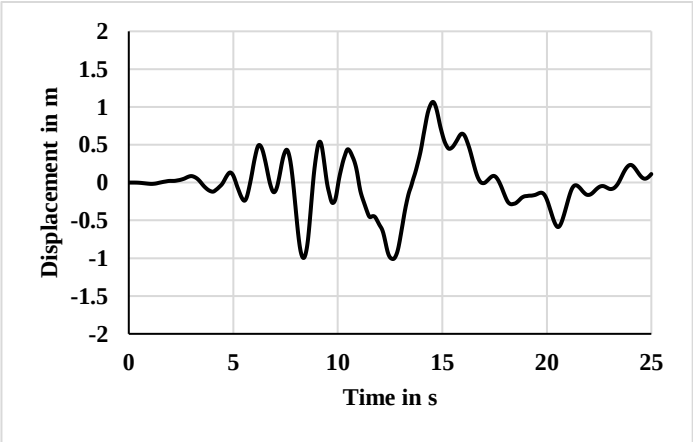

Figure 3.7.21. Displacement time-history for Roof of G+9 building on medium soil under Loma prieta earthquake

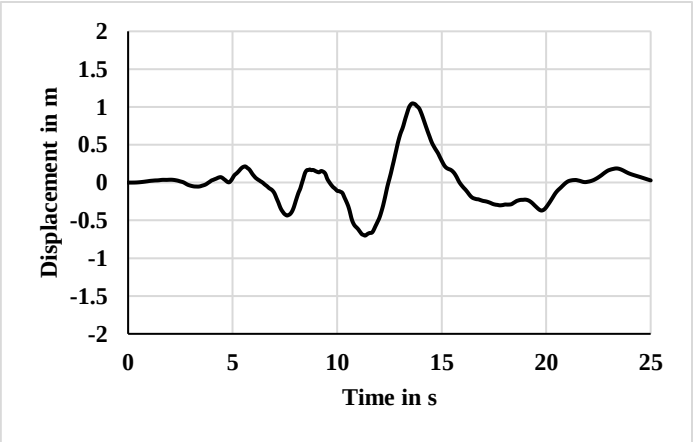

Figure 3.7.22. Displacement time-history for Base of G+9 building on medium soil under Loma prieta earthquake

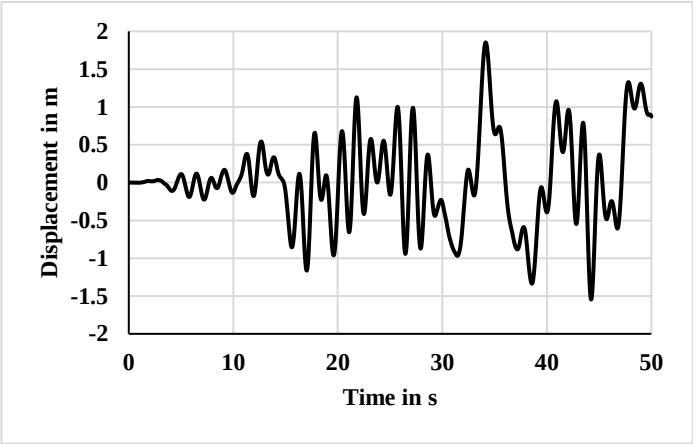

Figure 3.7.23. Displacement time-history for Roof of G+9 building on medium soil under Denali earthquake

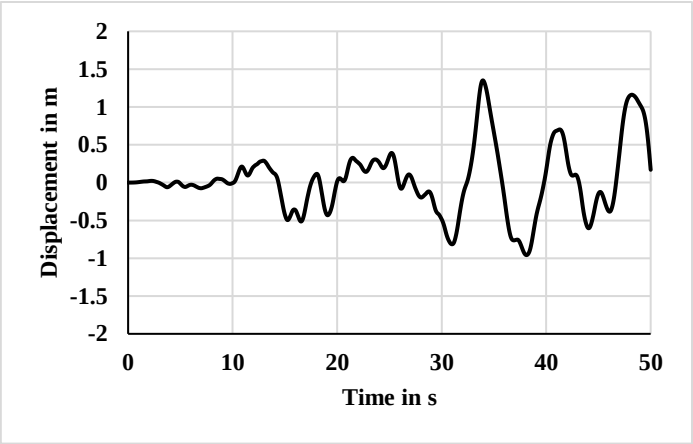

Figure 3.7.24. Displacement time-history for Base of G+9 building on medium soil under Denali earthquake

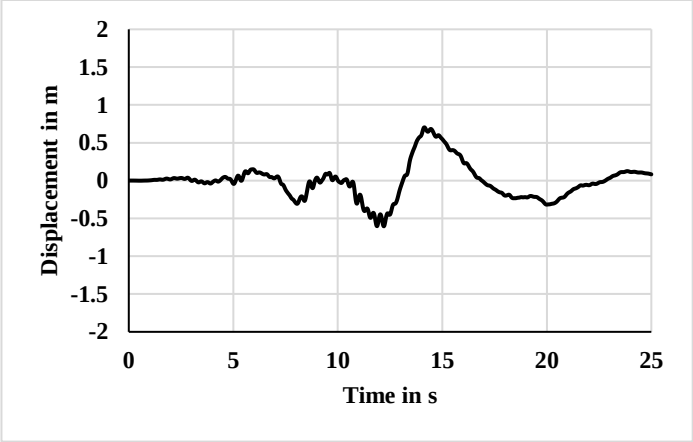

Figure 3.7.25. Displacement time-history for Roof of G+1 building on soft soil under Loma prieta earthquake

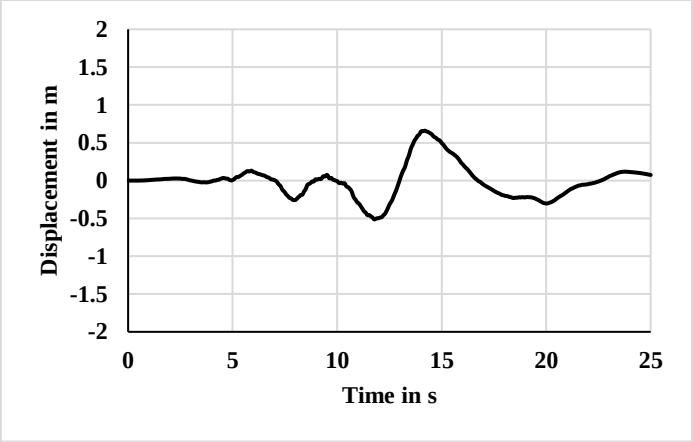

Figure 3.7.26. Displacement time-history for Base of G+1 building on soft soil under Loma prieta earthquake

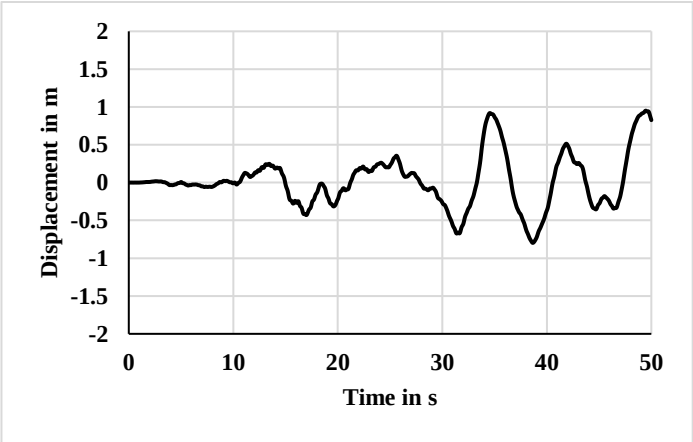

Figure 3.7.27. Displacement time-history for Roof of G+1 building on soft soil under Denali earthquake

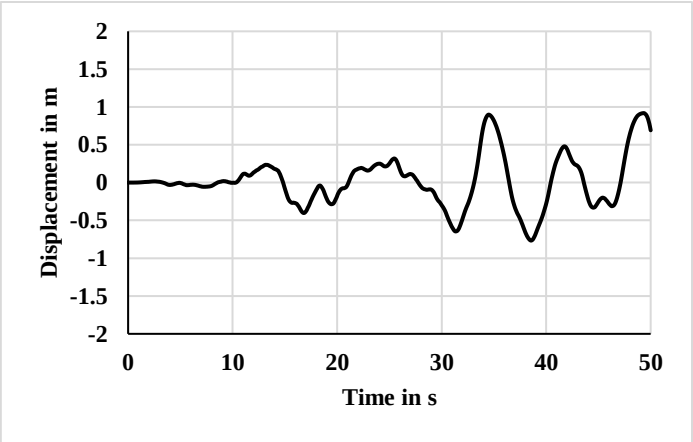

Figure 3.7.28. Displacement time-history for Base of G+1 building on soft soil under Denali earthquake

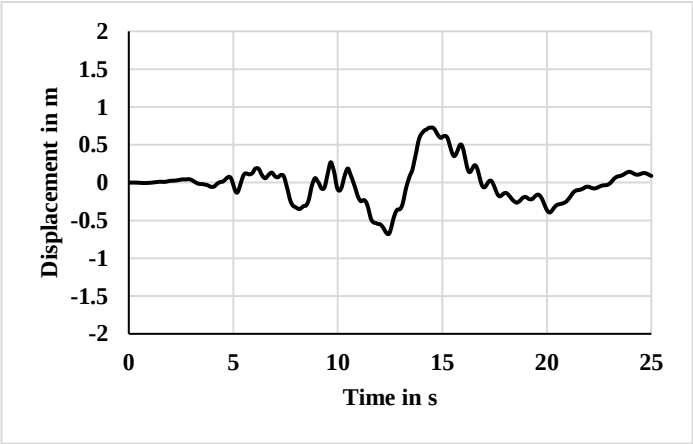

Figure 3.7.29. Displacement time-history for Roof of G+4 building on soft soil under Loma prieta earthquake

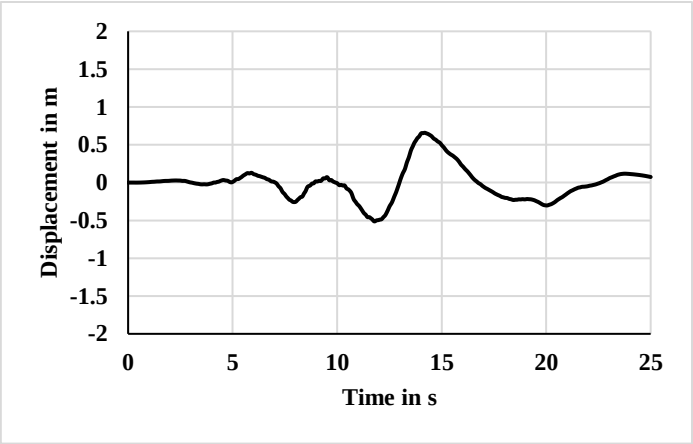

Figure 3.7.30. Displacement time-history for Base of G+4 building on soft soil under Loma prieta earthquake

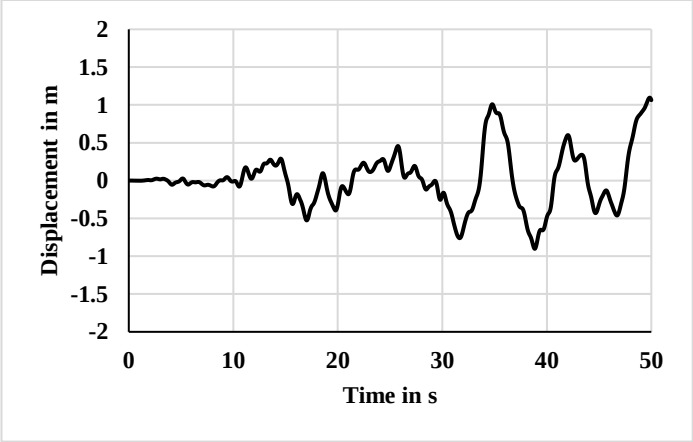

Figure 3.7.31. Displacement time-history for Roof of G+4 building on soft soil under Denali earthquake

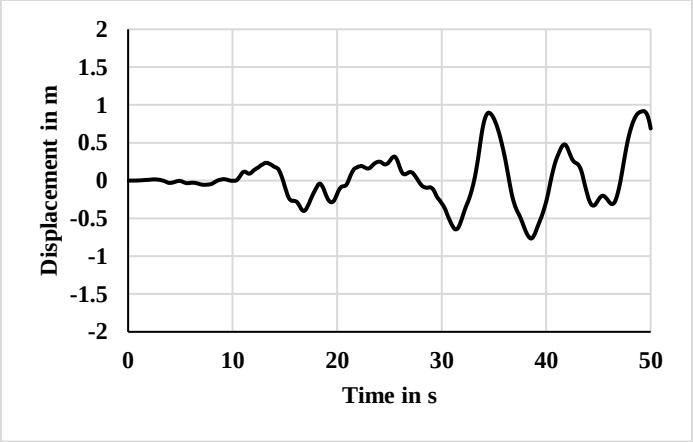

Figure 3.7.32. Displacement time-history for Base of G+4 building on soft soil under Denali earthquake

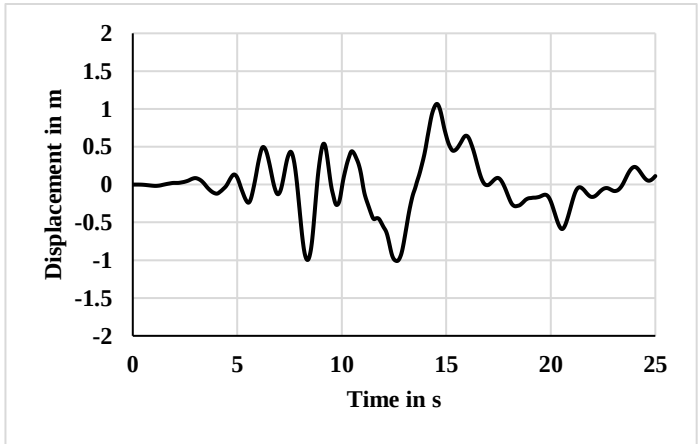

Figure 3.7.33. Displacement time-history for Roof of G+9 building on soft soil under Loma prieta earthquake

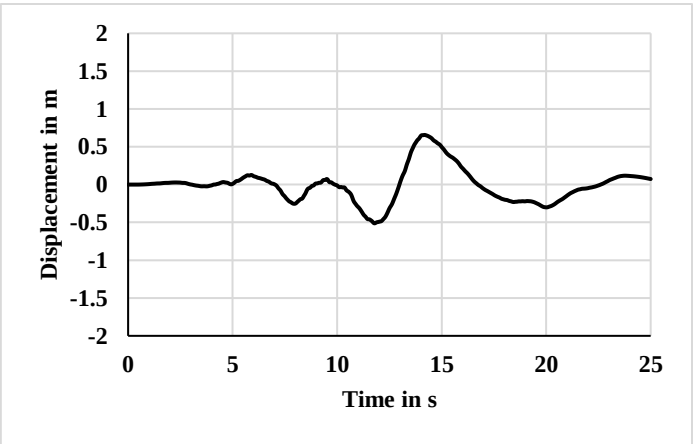

Figure 3.7.34. Displacement time-history for Base of G+9 building on soft soil under Loma prieta earthquake

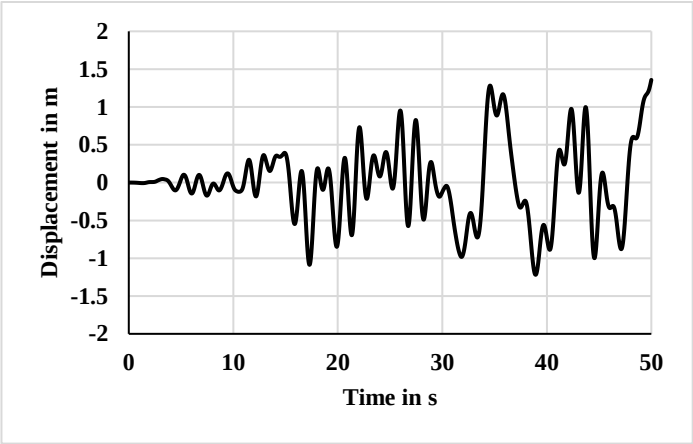

Figure 3.7.35. Displacement time-history for Roof of G+9 building on soft soil under Denali earthquake

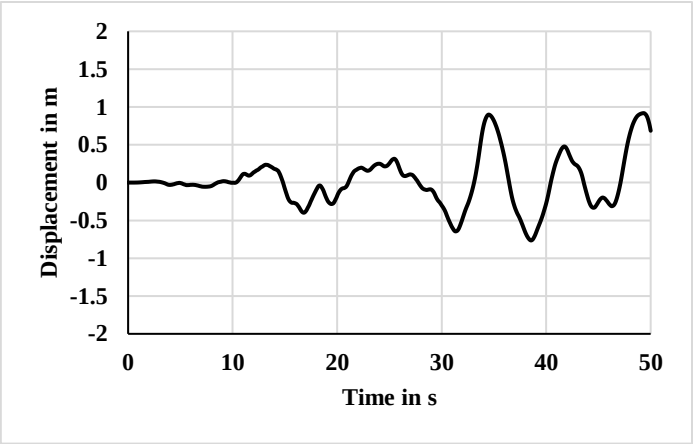

Figure 3.7.36. Displacement time-history for Base of G+9 building on soft soil under Denali earthquake

3.8. MAXIMUM DISPLACEMENT PROFILES

The maximum displacements of all the floors of each model are determined from the displacement time-history data of the respective floor. These values are plotted accordingly to obtain the maximum displacement profile of every building. These plots are shown in Figure 3.8.1. to 3.8.18. The figures clearly depicts that, a building resting on hard or medium soil is subjected to a far-field earthquake like Denali earthquake, its maximum displacement profile is concave upward. However, in case the building is located on soft soil and subjected to a far-field earthquake, its maximum displacement profile becomes convex upward. It is to be noted that under a far-field earthquake, the maximum displacements of the floors always increase with the increase of height. However, when a near-field earthquake like Loma prieta earthquake motion is subjected to G+4 or G+9 building situated on hard or medium soil, the maximum displacements of the floors first decreases and then increases with the increase in height. In all other cases, the shape of the maximum displacement profile strictly depends on the type of structure and soil.

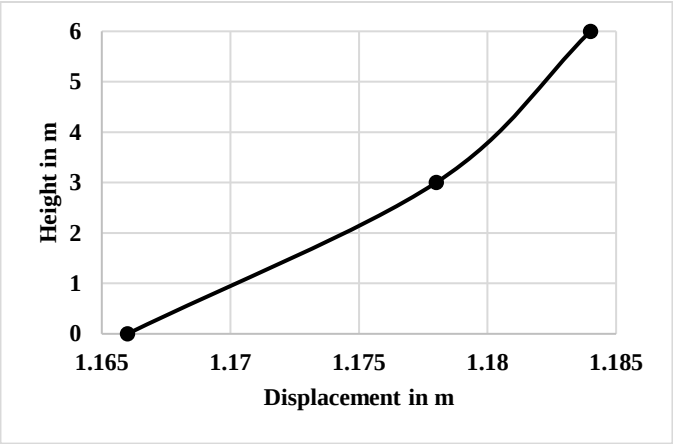

Figure 3.8.1. Maximum displacements of different floors of G+1 building on hard soil under Loma prieta earthquake

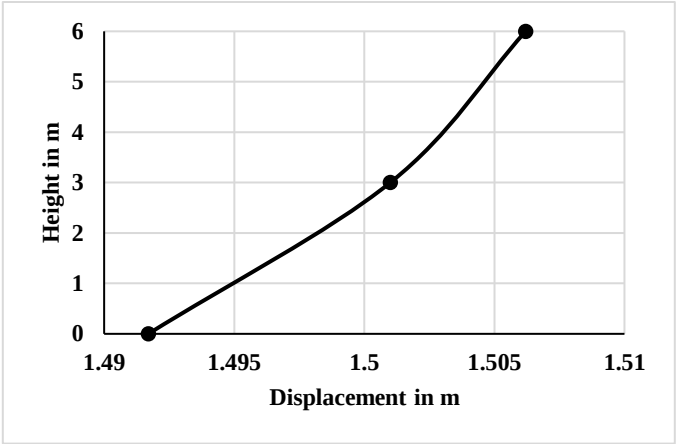

Figure 3.8.2. Maximum displacements of different floors of G+1 building on hard soil under Denali earthquake

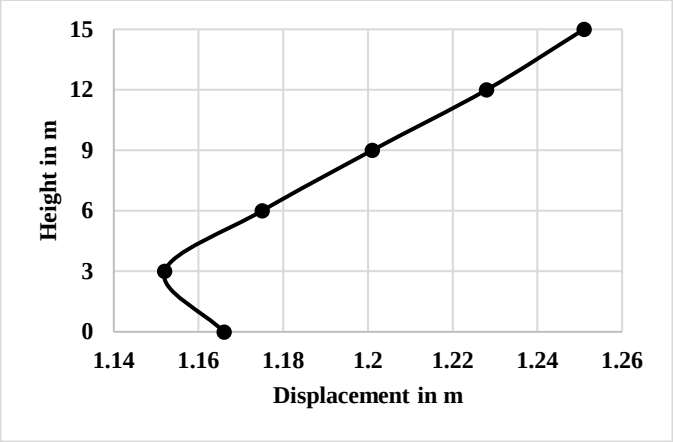

Figure 3.8.3. Maximum displacements of different floors of G+4 building on hard soil under Loma prieta earthquake

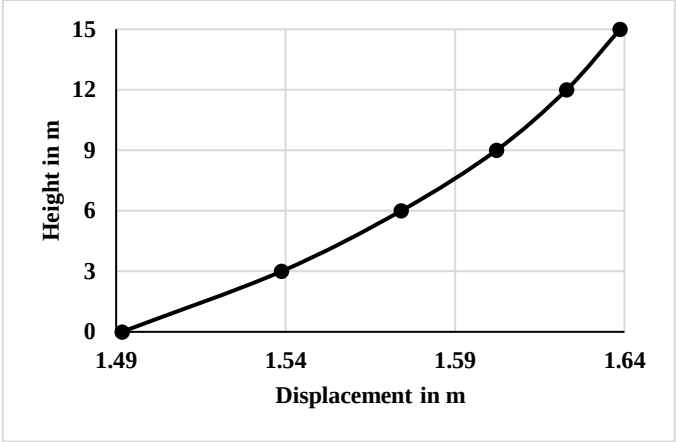

Figure 3.8.4. Maximum displacements of different floors of G+4 building on hard soil under Denali earthquake

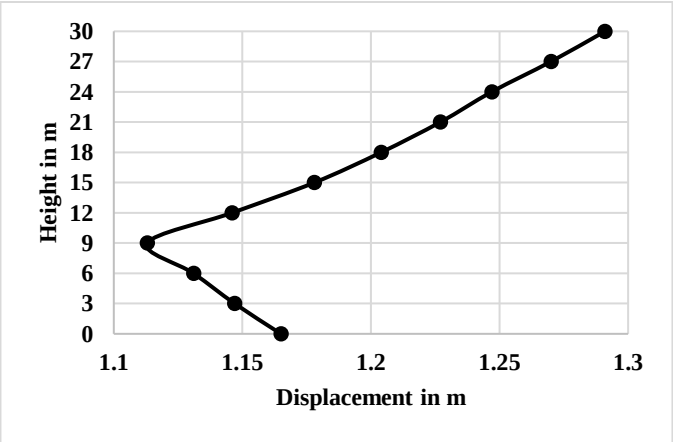

Figure 3.8.5. Maximum displacements of different floors of G+9 building on hard soil under Loma prieta earthquake

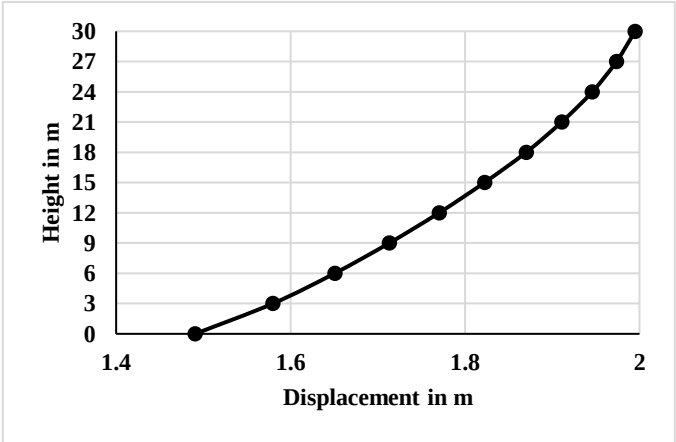

Figure 3.8.6. Maximum displacements of different floors of G+9 building on hard soil under Denali earthquake

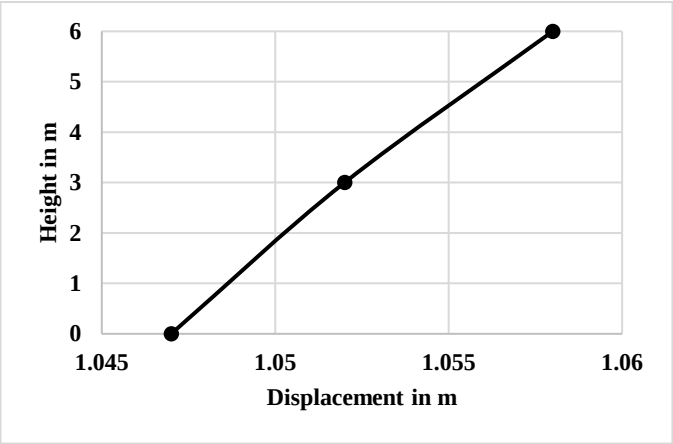

Figure 3.8.7. Maximum displacements of different floors of G+1 building on medium soil under Loma prieta earthquake

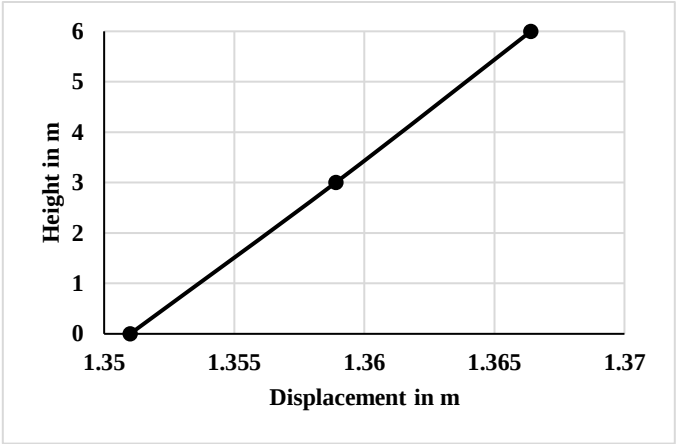

Figure 3.8.8. Maximum displacements of different floors of G+1 building on medium soil under Denali earthquake

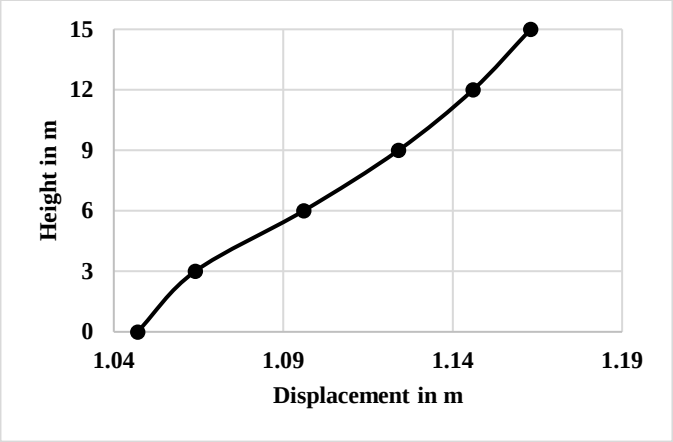

Figure 3.8.9. Maximum displacements of different floors of G+4 building on medium soil under Loma prieta earthquake

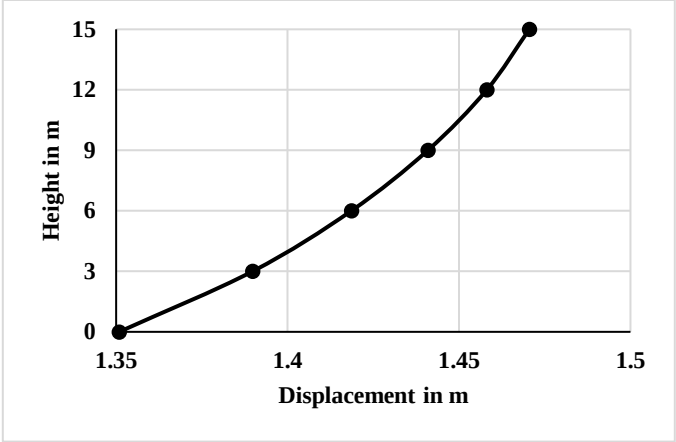

Figure 3.8.10. Maximum displacements of different floors of G+4 building on medium soil under Denali earthquake

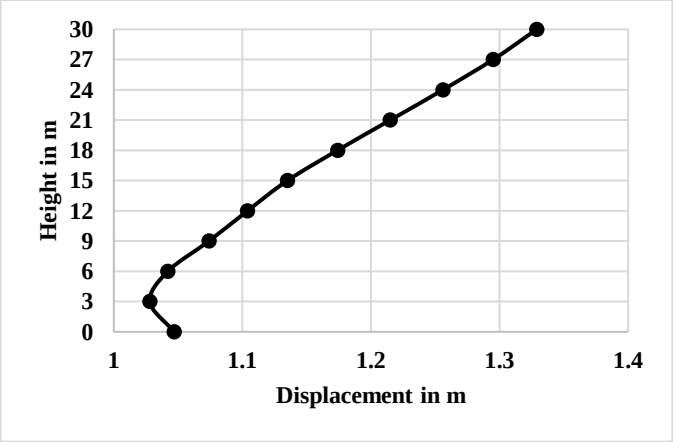

Figure 3.8.11. Maximum displacements of different floors of G+9 building on medium soil under Loma prieta earthquake

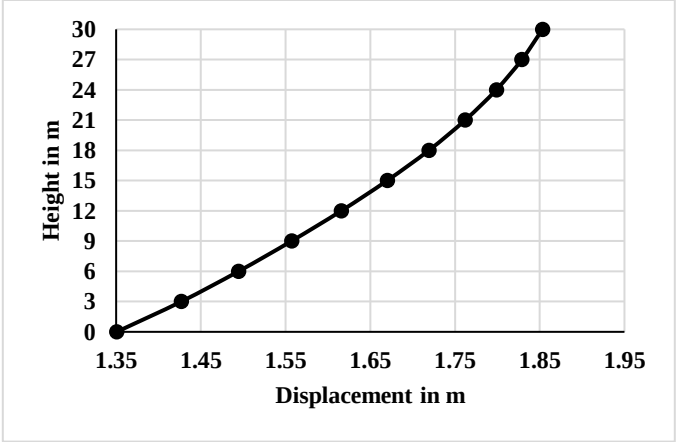

Figure 3.8.12. Maximum displacements of different floors of G+9 building on medium soil under Denali earthquake

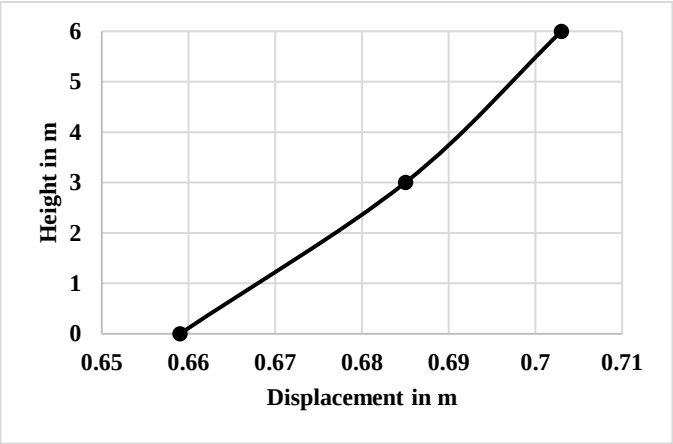

Figure 3.8.13. Maximum displacements of different floors of G+1 building on soft soil under Loma prieta earthquake

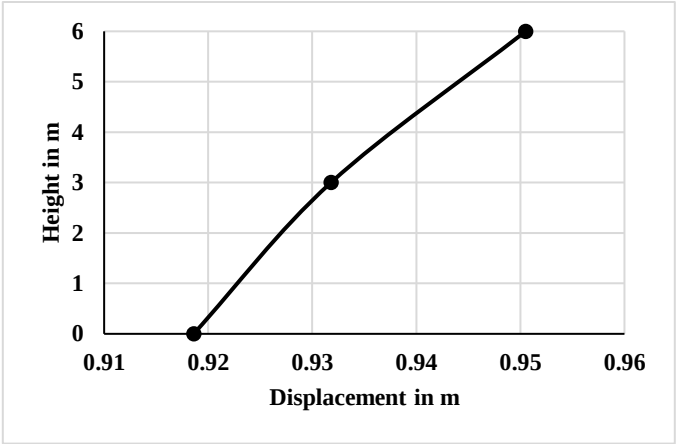

Figure 3.8.14. Maximum displacements of different floors of G+1 building on soft soil under Denali earthquake

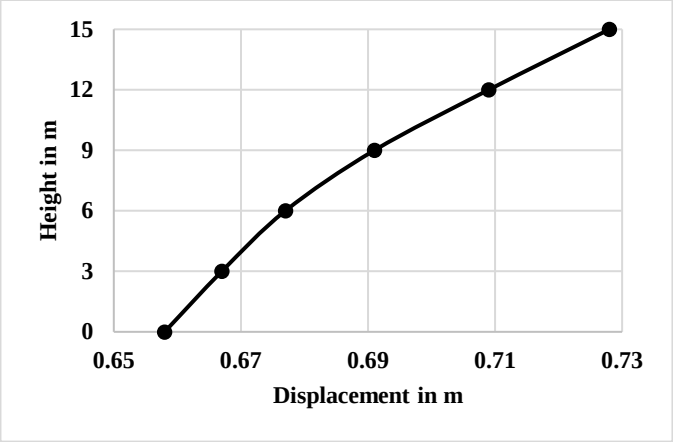

Figure 3.8.15. Maximum displacements of different floors of G+4 building on soft soil under Loma prieta earthquake

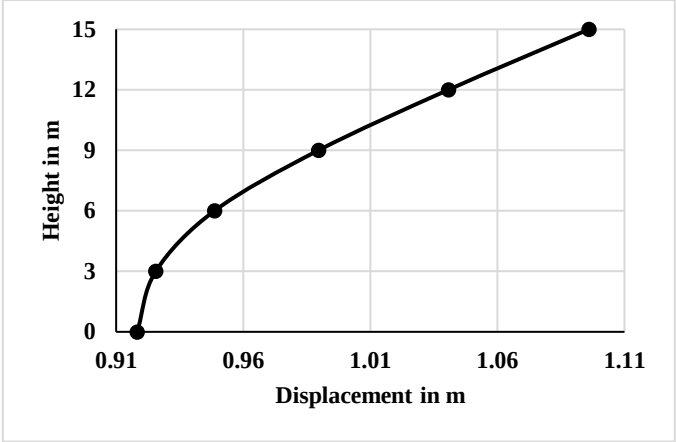

Figure 3.8.16. Maximum displacements of different floors of G+4 building on soft soil under Denali earthquake

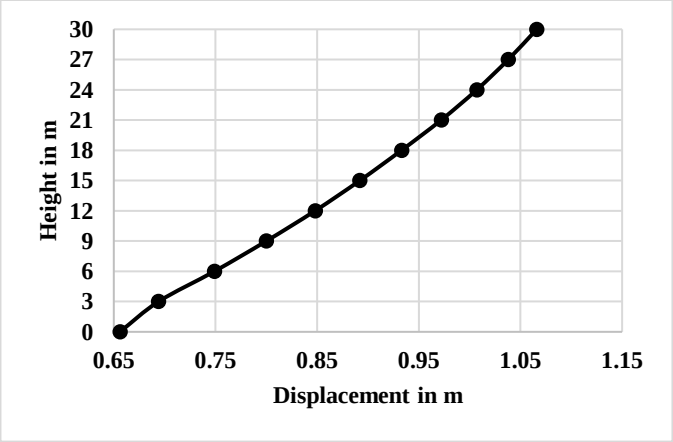

Figure 3.8.17. Maximum displacements of different floors of G+9 building on soft soil under Loma prieta earthquake

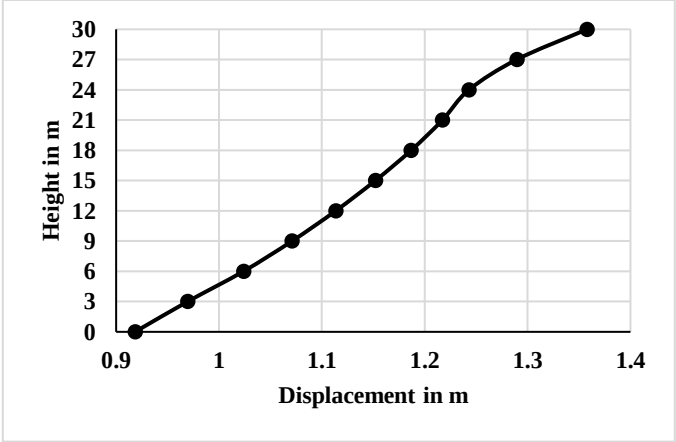

Figure 3.8.18. Maximum displacements of different floors of G+9 building on soft soil under Denali earthquake

3.9. FRAGILITY CURVES

A detailed overview about the fragility curves along with different methods of plotting them has already been presented in Chapter 2 of this thesis. In this chapter at first PSDMs, for all the models, are developed from the percentage roof drifts. Thereafter, 2000 SAC/FEMA method[35] has been used for plotting the fragility curves considering IO, LS, CP and Indian Codal Limit. The PSDMs and fragility curves for all the models are shown in Figure 3.9.1. to 3.9.36.

After analysing the PSDMs and fragility curves of frame buildings resting on uniform soil, several important remarks has been made. All the PSDMs are straight line in nature, which passes through the origin. The steep slope of the PSDM curve indicates the probability of exceeding the prescribed limit state (IO, LS, CP or Indian Codal Limit) under a specific earthquake intensity (in terms of PGA). Further, it is obvious that under a particular earthquake, the probability of exceeding Indian Codal Limit is the maximum and that of Collapse Prevention is the minimum. It is to be mentioned that, for any type of soil and under a specific seismic excitation, the probability of exceedance of a certain limit state in case of a G+1 building is always minimum and that of a G+9 building is always maximum among all the cases. In addition to that, when a G+1 building is subjected to a particular earthquake, it has the least probability of exceeding a limit state when it is situated on hard soil. On the contrary, it has the largest probability of exceeding a limit state when located on soft soil. Moreover, under the action of a particular seismic excitation, a G+4 building has the lowest probability of exceeding any limit state when it rests on the medium soil. However, it should also be noted that in case a building is located on hard or medium soil, the probability of exceedance of a specific limit state for that soil-structure system is more when it is subjected to a near-field earthquake. On the other hand, if the building rests on soft soil, the probability of exceedance value of the soil-structure system will be greater under the influence of far-field earthquake.

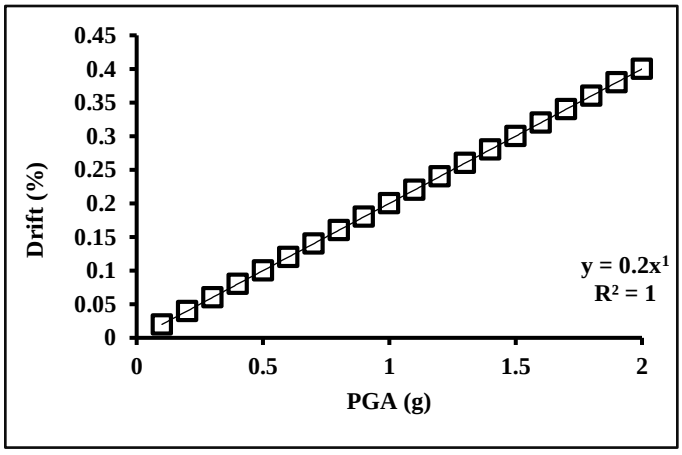

Figure 3.9.1. PSDM for roof of G+1 building on hard soil under Loma prieta earthquake

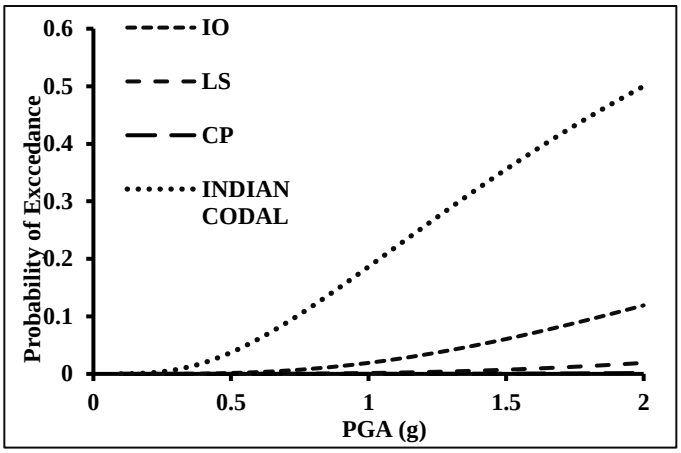

Figure 3.9.2. Fragility curves for roof of G+1 building on hard soil under Loma prieta earthquake

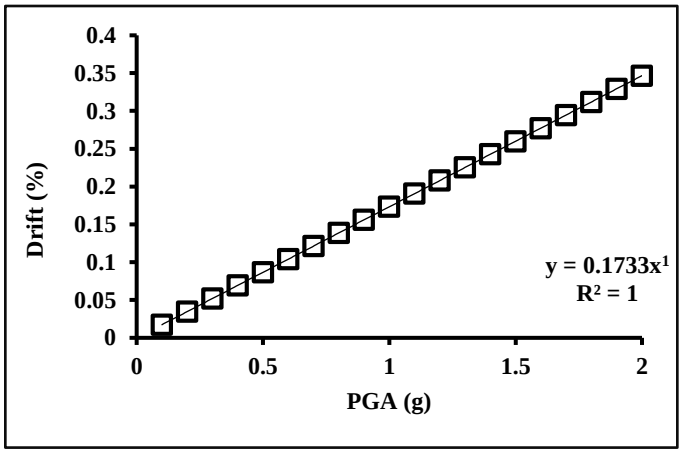

Figure 3.9.3. PSDM for roof of G+1 building on hard soil under Denali earthquake

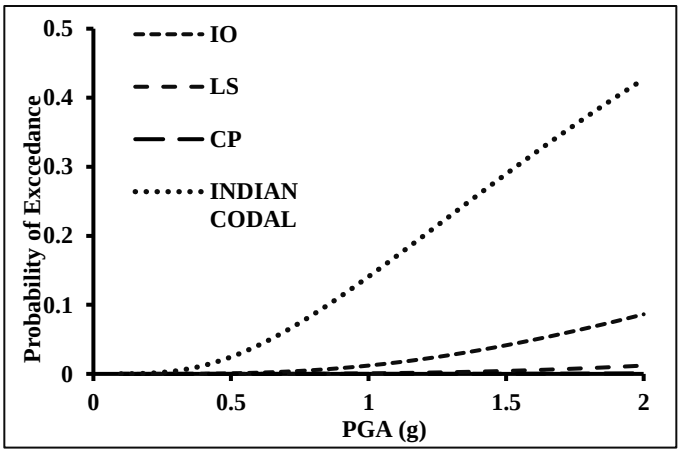

Figure 3.9.4. Fragility curves for roof of G+1 building on hard soil under Denali earthquake

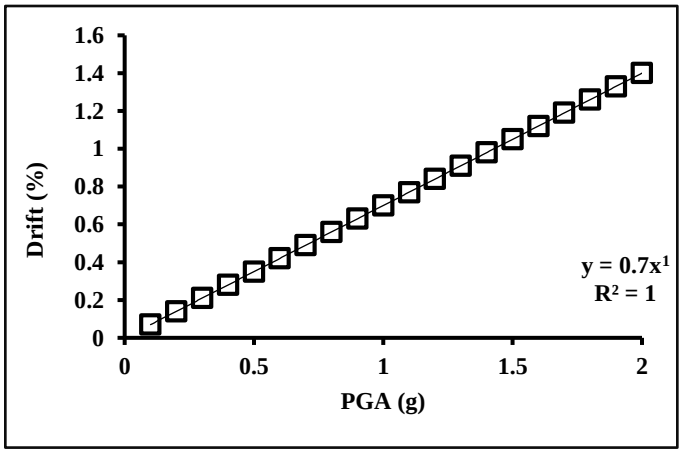

Figure 3.9.5. PSDM for roof of G+4 building on hard soil under Loma prieta earthquake

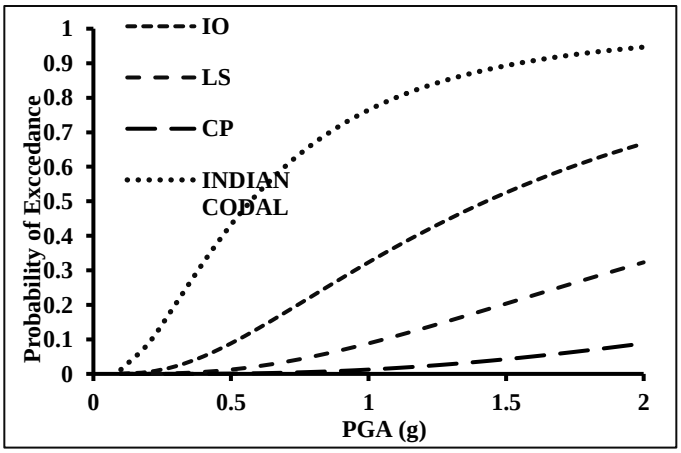

Figure 3.9.6. Fragility curves for roof of G+4 building on hard soil under Loma prieta earthquake

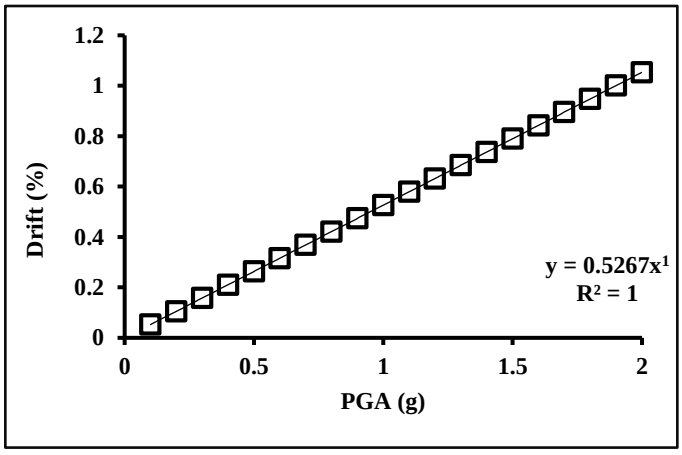

Figure 3.9.7. PSDM for roof of G+4 building on hard soil under Denali earthquake

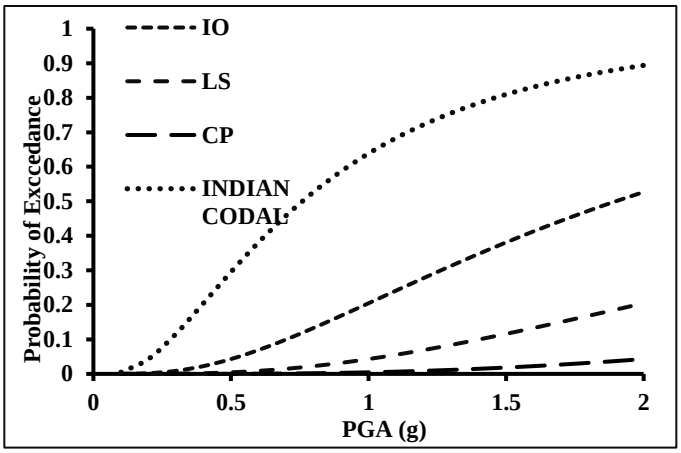

Figure 3.9.8. Fragility curves for roof of G+4 building on hard soil under Denali earthquake

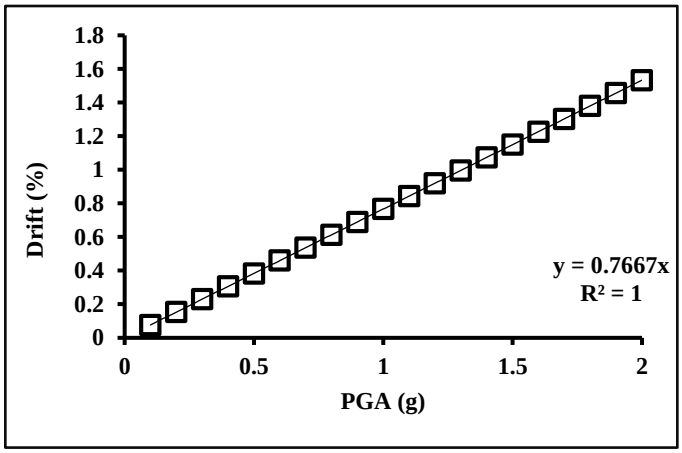

Figure 3.9.9. PSDM for roof of G+9 building on hard soil under Loma prieta earthquake

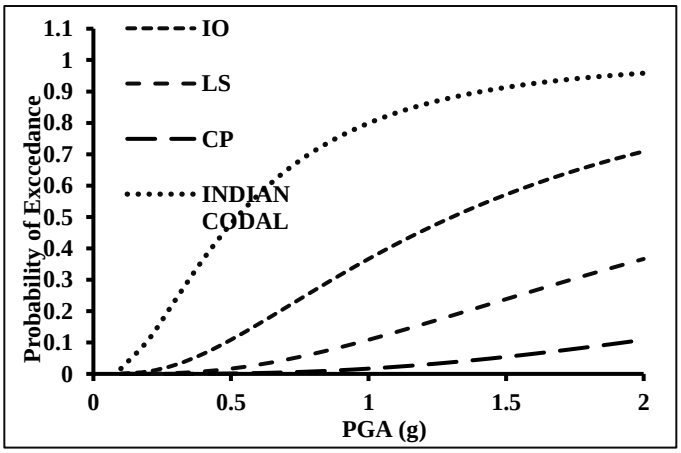

Figure 3.9.10. Fragility curves for roof of G+9 building on hard soil under Loma prieta earthquake

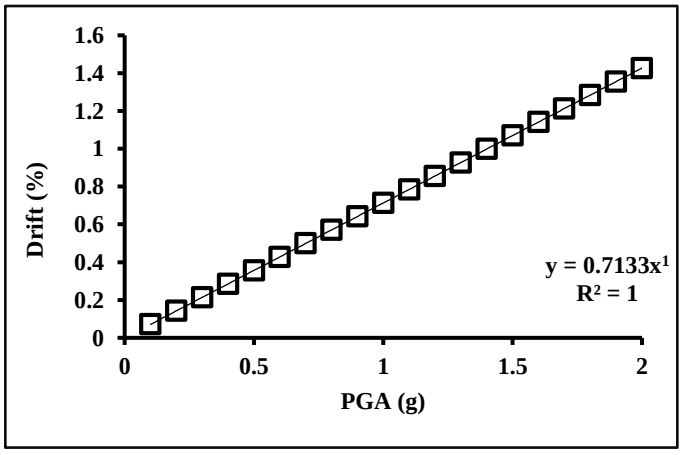

Figure 3.9.11. PSDM for roof of G+9 building on hard soil under Denali earthquake

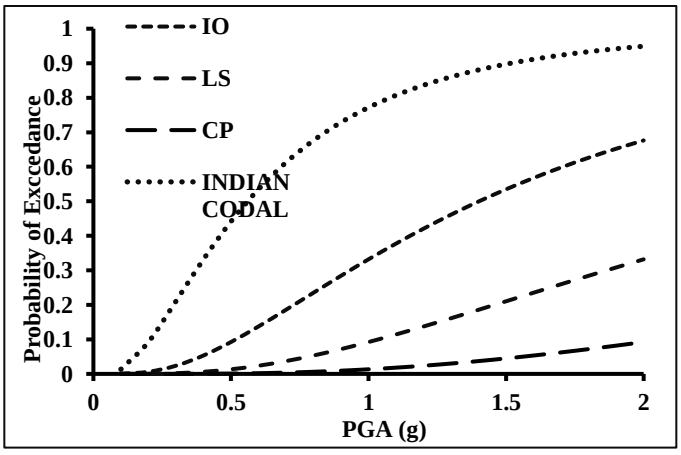

Figure 3.9.12. Fragility curves for roof of G+9 building on hard soil under Denali earthquake

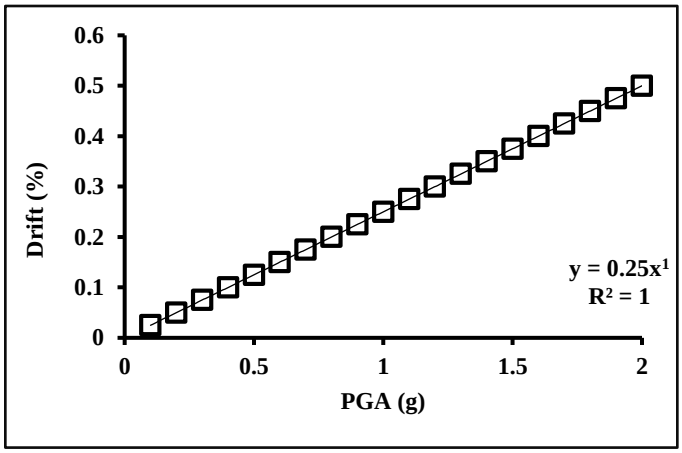

Figure 3.9.13. PSDM for roof of G+1 building on medium soil under Loma prieta earthquake

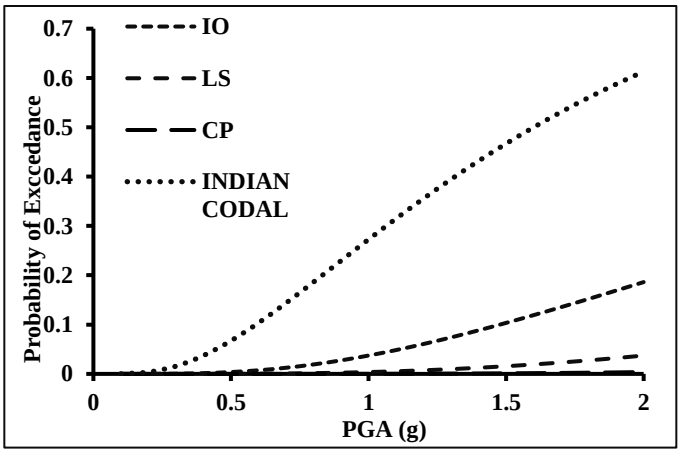

Figure 3.9.14. Fragility curves for roof of G+1 building on medium soil under Loma prieta earthquake

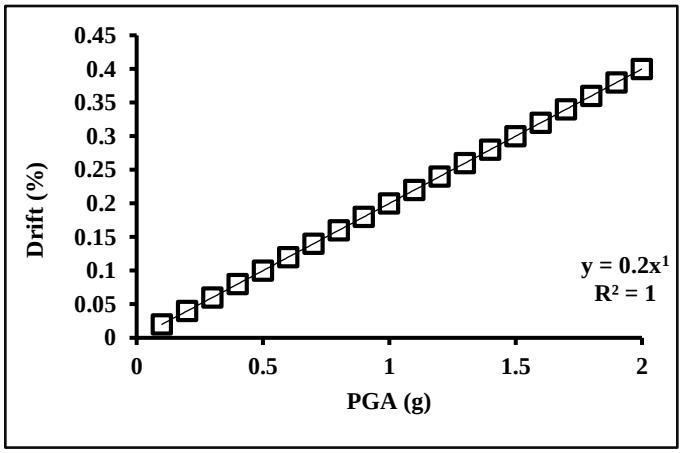

Figure 3.9.15. PSDM for roof of G+1 building on medium soil under Denali earthquake

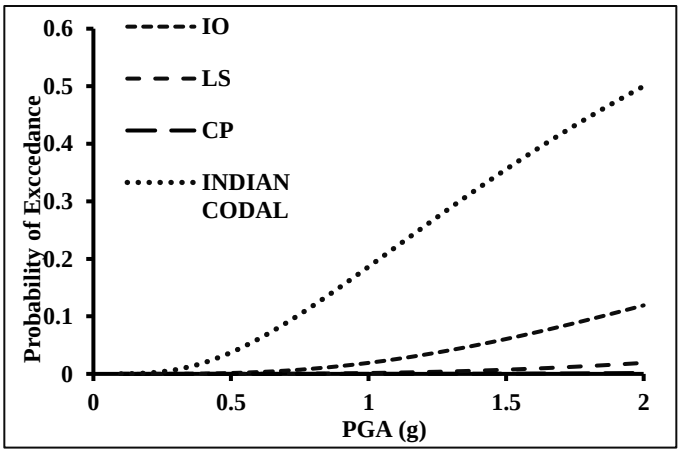

Figure 3.9.16. Fragility curves for roof of G+1 building on medium soil under Denali earthquake

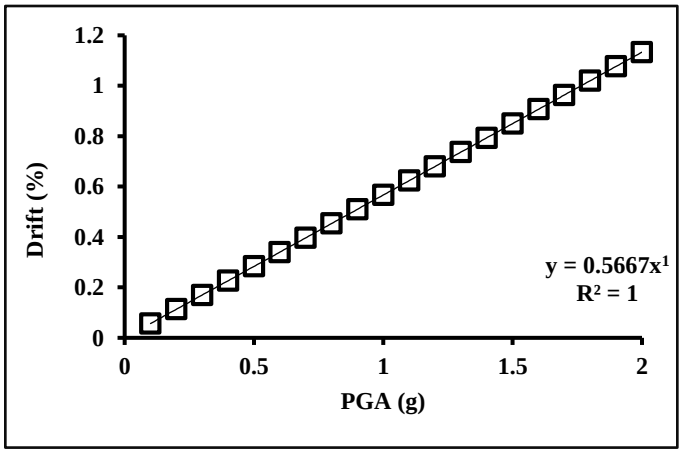

Figure 3.9.17. PSDM for roof of G+4 building on medium soil under Loma prieta earthquake

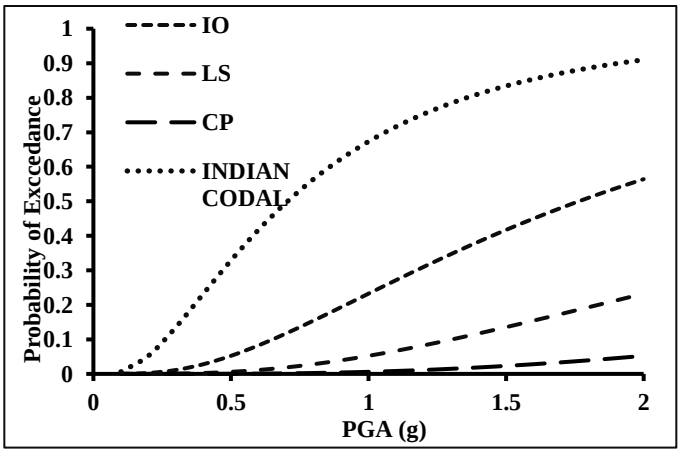

Figure 3.9.18. Fragility curves for roof of G+4 building on medium soil under Loma prieta earthquake

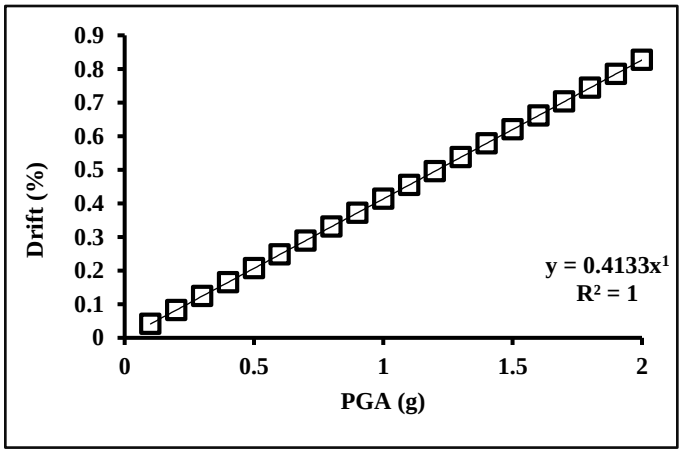

Figure 3.9.19. PSDM for roof of G+4 building on medium soil under Denali earthquake

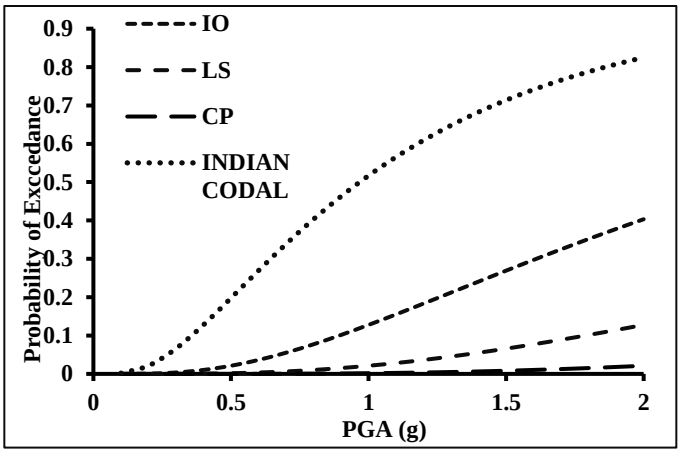

Figure 3.9.20. Fragility curves for roof of G+4 building on medium soil under Denali earthquake

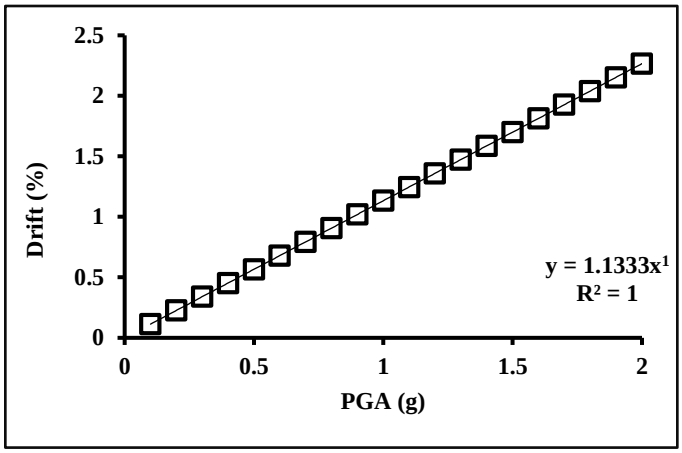

Figure 3.9.21. PSDM for roof of G+9 building on medium soil under Loma prieta earthquake

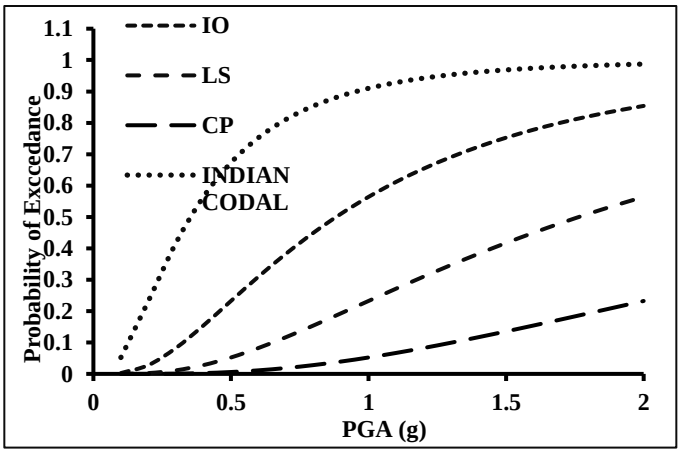

Figure 3.9.22. Fragility curves for roof of G+9 building on medium soil under Loma prieta earthquake

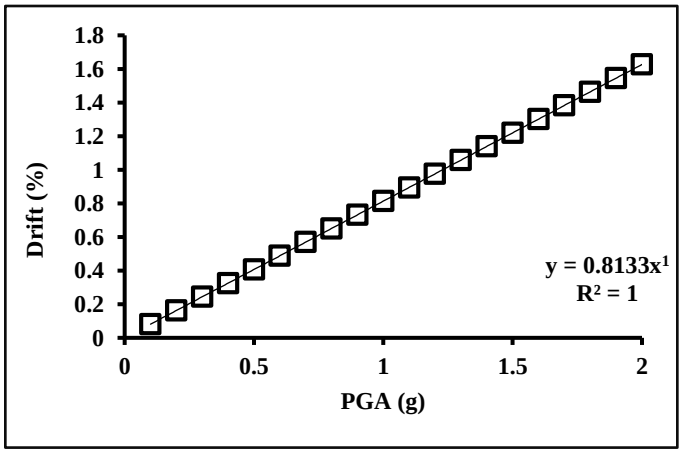

Figure 3.9.23. PSDM for roof of G+9 building on medium soil under Denali earthquake

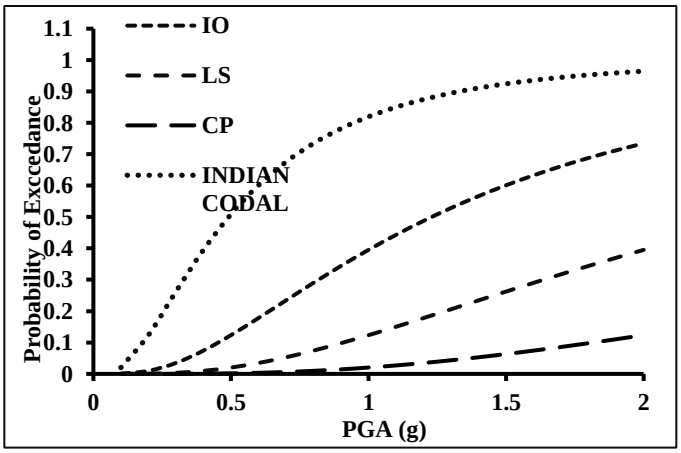

Figure 3.9.24. Fragility curves for roof of G+9 building on medium soil under Denali earthquake

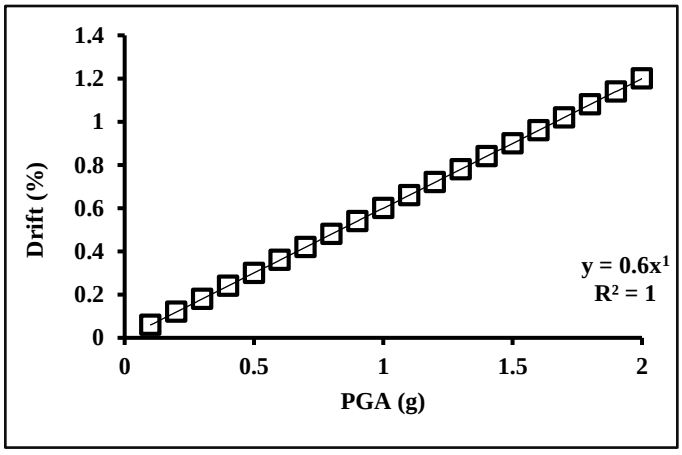

Figure 3.9.25. PSDM for roof of G+1 building on soft soil under Loma prieta earthquake

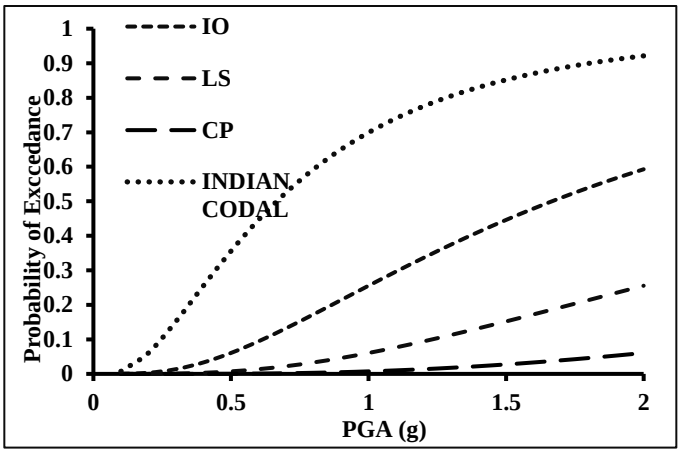

Figure 3.9.26. Fragility curves for roof of G+1 building on soft soil under Loma prieta earthquake

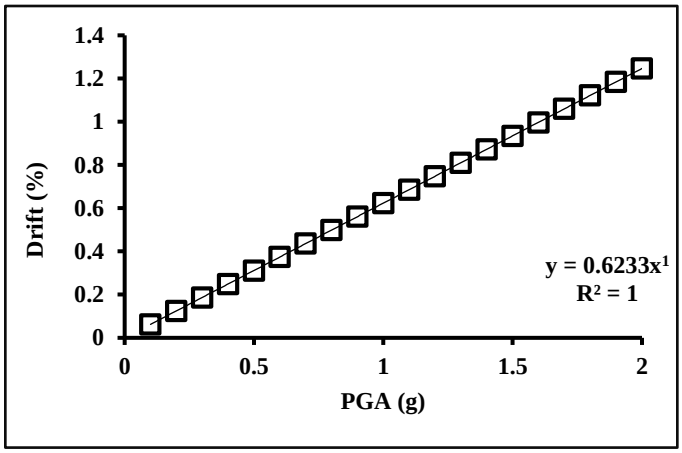

Figure 3.9.27. PSDM for roof of G+1 building on soft soil under Denali earthquake

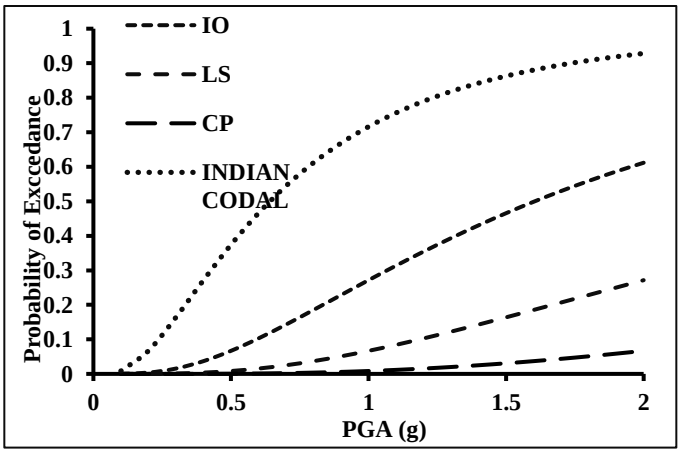

Figure 3.9.28. Fragility curves for roof of G+1 building on soft soil under Denali earthquake

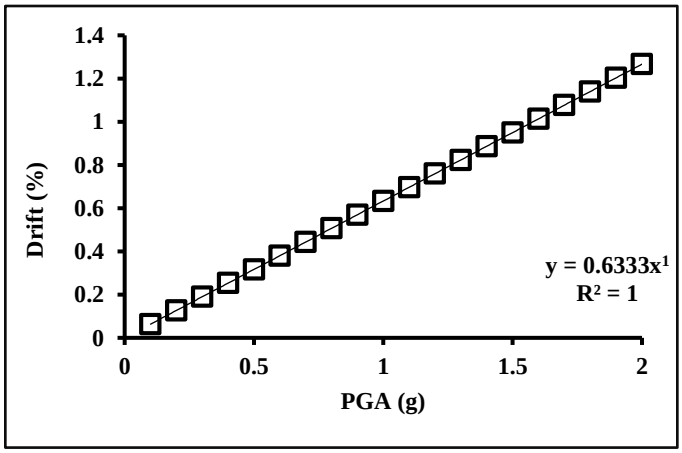

Figure 3.9.29. PSDM for roof of G+4 building on soft soil under Loma prieta earthquake

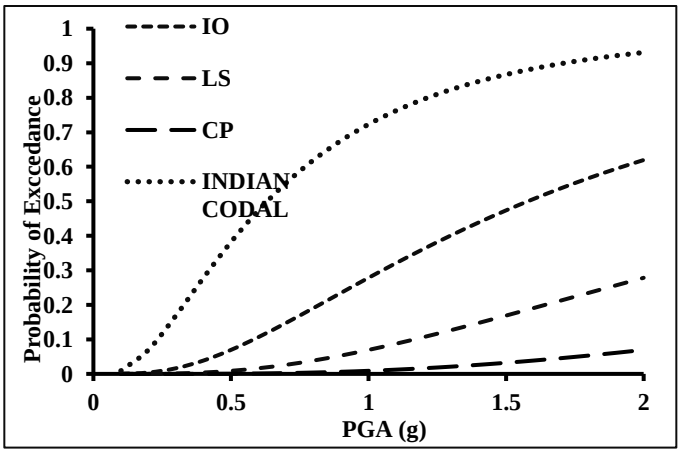

Figure 3.9.30. Fragility curves for roof of G+4 building on soft soil under Loma prieta earthquake

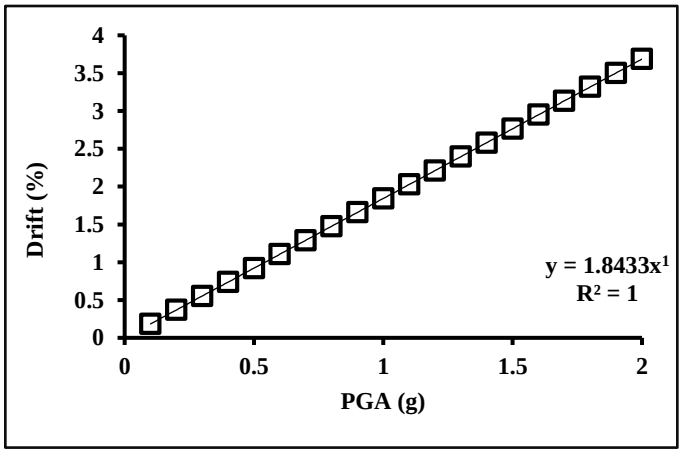

Figure 3.9.31. PSDM for roof of G+4 building on soft soil under Denali earthquake

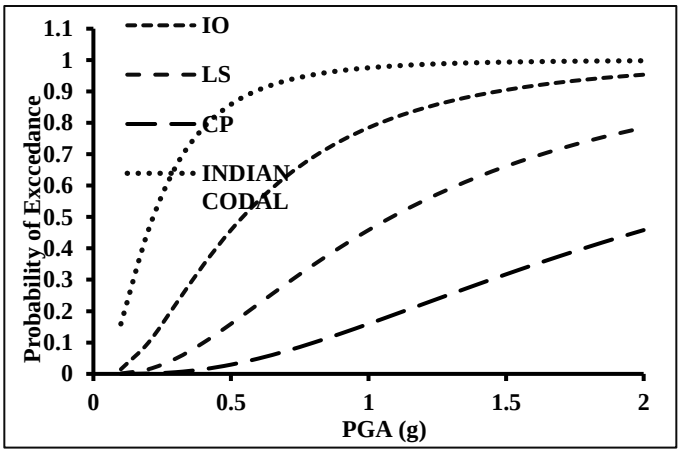

Figure 3.9.32. Fragility curves for roof of G+4 building on soft soil under Denali earthquake

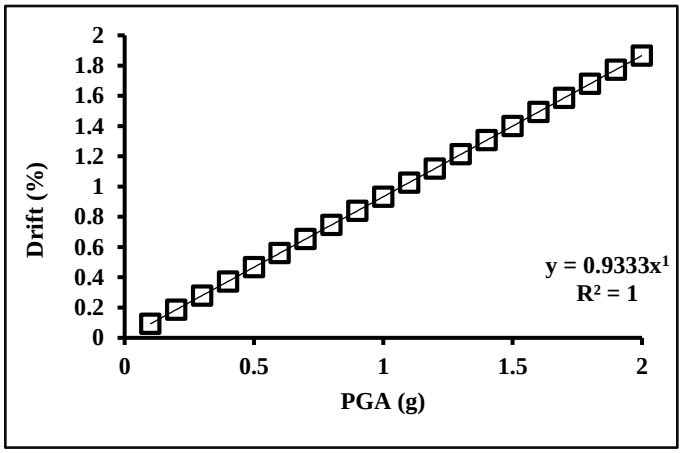

Figure 3.9.33. PSDM for roof of G+9 building on soft soil under Loma prieta earthquake

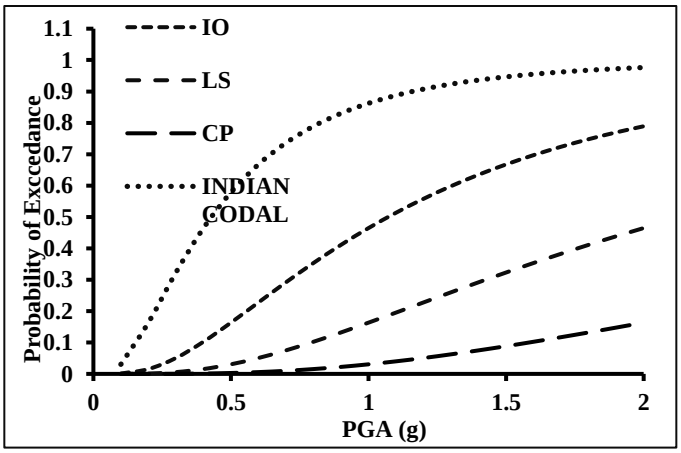

Figure 3.9.34. Fragility curves for roof of G+9 building on soft soil under Loma prieta earthquake

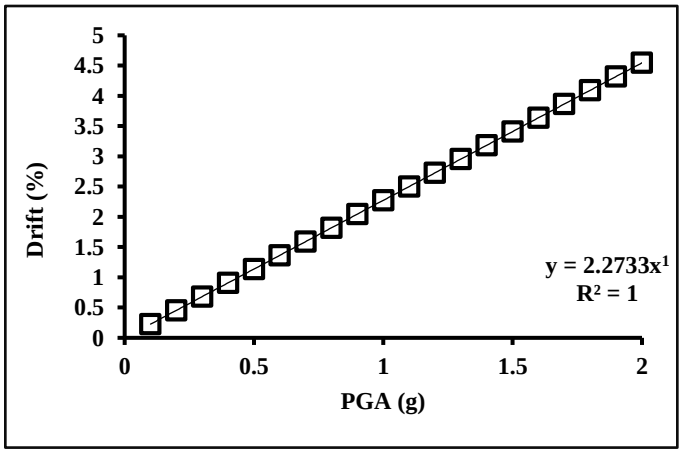

Figure 3.9.35. PSDM for roof of G+9 building on soft soil under Denali earthquake

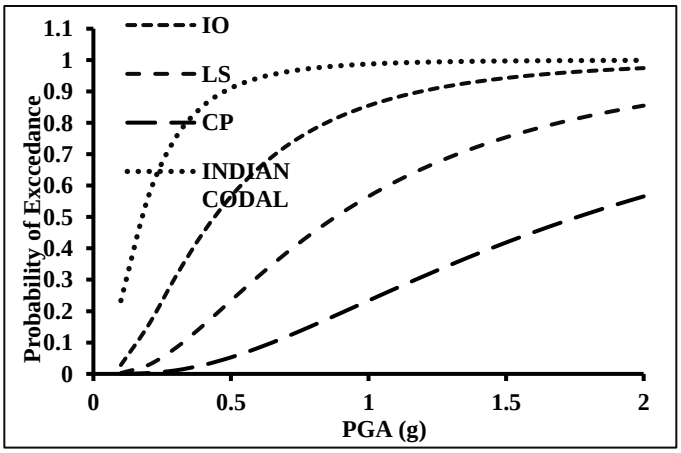

Figure 3.9.36. Fragility curves for roof of G+9 building on soft soil under Denali earthquake

Chapter-4: FRAME STRUCTURES ON LAYERED SOIL

4.1. GENERAL

Local soil largely affects the ground motion characteristics and plays an important role in damage distribution during an earthquake[56]–[59]. Significant differences in structural damage in basin on soft soil as compared with the surrounding exposed rocks or even in the basin itself from place to place have been reported during the past earthquakes. When there are sharp changes in soil properties like impendence contrasts many things can happen. By the principle of conservation of energy, amplitude increases in low velocity soil deposits. There may be trapping of seismic waves due to large impedance contrast between soft sediment and underline bedrock and this lead resonance pattern. When the peak acceleration is small, acceleration at soil surface is slightly greater than rock surface. This is what happened in Mexico City and San Francisco Bay area. But at moderate or high acceleration level acceleration level at rock surface is greater than soil surface. At higher acceleration levels, due to low stiffness and non-linearity prevent to develop peak acceleration.

In this chapter, response of buildings due to variation of different soil layers under the action of near-field and far-field earthquakes ground motion has been observed. In the present study, seven types of layered soils (Soil 1 to Soil 7), each of which has six different layers, have been combined with three types of frame buildings (G+1, G+4 and G+9). Each model is analysed using the same procedure as mentioned in Chapter 3.

4.2. PROBLEM FORMULATION

In the present study an investigation has been made to find the effect of dynamic SSI due to variation of thickness of soft soil layer in different depth. Seven types of soils (Soil 1 to Soil 7) have been used in this study and each type of soil is an assembly of six different layers. For Soil 2 to Soil 6 there exists a soft soil layer of depth 5m at different depth. However, for soil 6 a thin soil layer of 2m thickness exist at intermediate level. All the soil layers are considered homogeneous in nature. The properties of all the soils used for developing the models have been presented in Table 4.2.1. to Table 4.2.7. Further, to determine the effects of various structural properties on

dynamic SSI phenomenon, three frame buildings-G+1, G+4 and G+9, have been considered. The shapes and properties of the buildings along with their components are identical to that of the buildings used in Chapter 3.

Table 4.2.1. PROPERTIES OF SOIL 1

Depth from Ground Level (m)		Mass Density (ρ) in kg/m^3	Young's Modulus (E) in N/m^2	Poisson's Ratio (ν)	Shear Wave Velocity (V_S) in m/s
From	To				
0	5	1500	9.7×10^7	0.43	150
5	10	1950	3.3×10^8	0.35	250
10	15	1980	4.8×10^8	0.34	300
15	20	2000	6.5×10^8	0.32	350
20	25	2100	1.11×10^9	0.3	450
25	30	2300	1.99×10^9	0.2	600

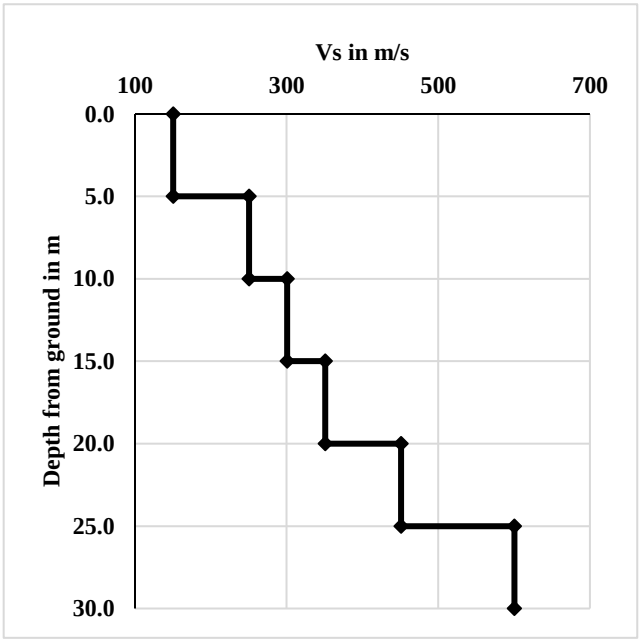

Table 4.2.2. PROPERTIES OF SOIL 2

Depth from Ground Level (m)		Mass Density (ρ) in kg/m^3	Young's Modulus (E) in N/m^2	Poisson's Ratio (ν)	Shear Wave Velocity (V_S) in m/s
From	To				
0	5	1750	1.96×10^8	0.4	200
5	10	1500	9.7×10^7	0.43	150
10	15	1980	4.8×10^8	0.34	300
15	20	2000	6.5×10^8	0.32	350
20	25	2100	1.11×10^9	0.3	450
25	30	2300	1.99×10^9	0.2	600

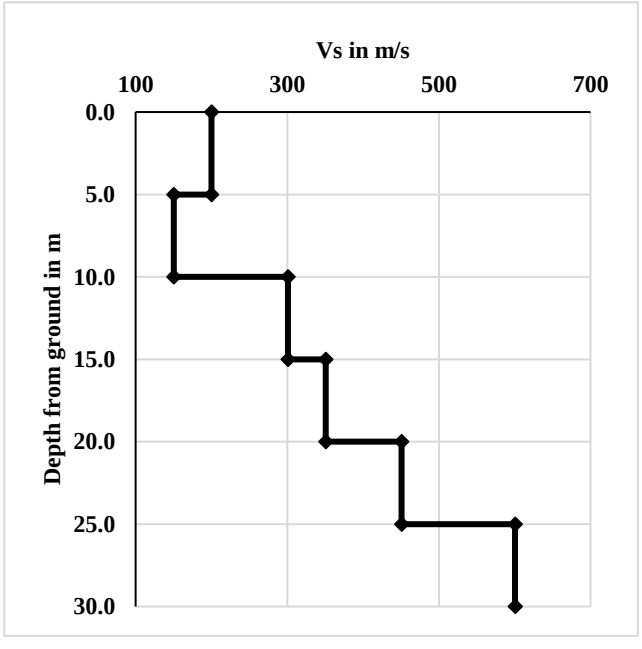

Table 4.2.3. PROPERTIES OF SOIL 3

Depth from Ground Level (m)		Mass Density (ρ) in kg/m^3	Young's Modulus (E) in N/m^2	Poisson's Ratio (ν)	Shear Wave Velocity (Vs) in m/s
From	To				
0	5	1750	1.96×10^8	0.4	200
5	10	1950	3.3×10^8	0.35	250
10	15	1500	9.7×10^7	0.43	150
15	20	2000	6.5×10^8	0.32	350
20	25	2100	1.11×10^9	0.3	450
25	30	2300	1.99×10^9	0.2	600

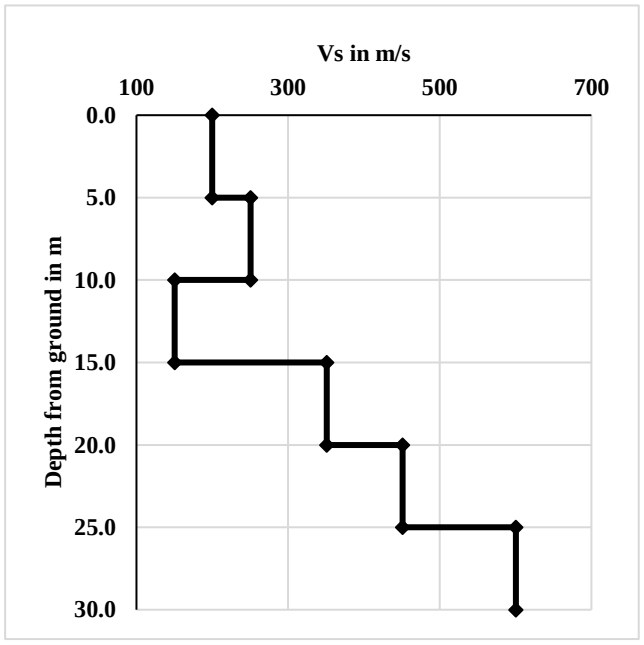

Table 4.2.4. PROPERTIES OF SOIL 4

Depth from Ground Level (m)		Mass Density (ρ) in kg/m^3	Young's Modulus (E) in N/m^2	Poisson's Ratio (ν)	Shear Wave Velocity (Vs) in m/s
From	To				
0	5	1750	1.96×10^8	0.4	200
5	10	1950	3.3×10^8	0.35	250
10	15	1980	4.8×10^8	0.34	300
15	20	1500	9.7×10^7	0.43	150
20	25	2100	1.11×10^9	0.3	450
25	30	2300	1.99×10^9	0.2	600

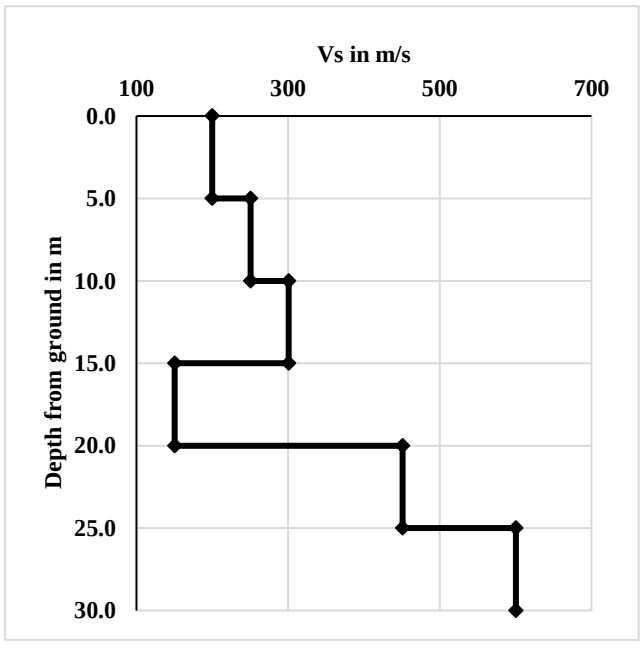

Table 4.2.5. PROPERTIES OF SOIL 5

Depth from Ground Level (m)		Mass Density (ρ) in kg/m^3	Young's Modulus (E) in N/m^2	Poisson's Ratio (ν)	Shear Wave Velocity (Vs) in m/s
From	To				
0	5	1750	1.96×10^8	0.4	200
5	10	1950	3.3×10^8	0.35	250
10	15	1980	4.8×10^8	0.34	300
15	20	2000	6.5×10^8	0.32	350
20	25	1500	9.7×10^7	0.43	150
25	30	2300	1.99×10^9	0.2	600

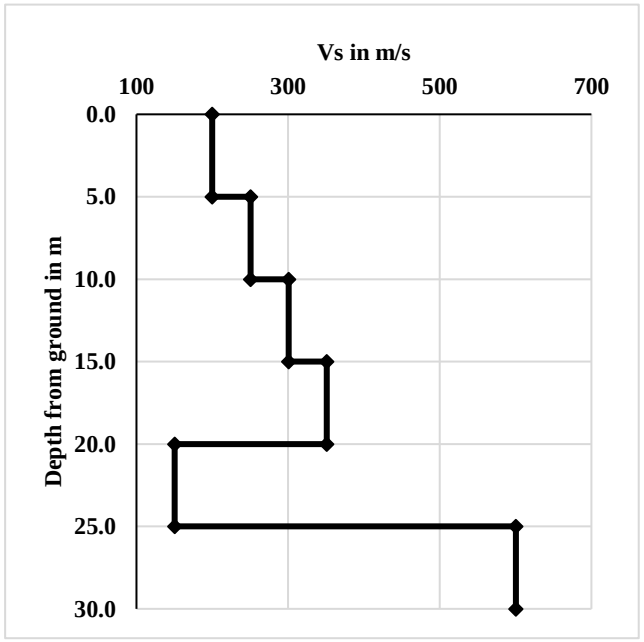

Table 4.2.6. PROPERTIES OF SOIL 6

Depth from Ground Level (m)		Mass Density (ρ) in kg/m^3	Young's Modulus (E) in N/m^2	Poisson's Ratio (ν)	Shear Wave Velocity (Vs) in m/s
From	To				
0	5	1750	1.96×10^8	0.4	200
5	10	1950	3.3×10^8	0.35	250
10	15	1980	4.8×10^8	0.34	300
15	20	2000	6.5×10^8	0.32	350
20	25	2100	1.11×10^9	0.3	450
25	30	1500	9.7×10^7	0.43	150

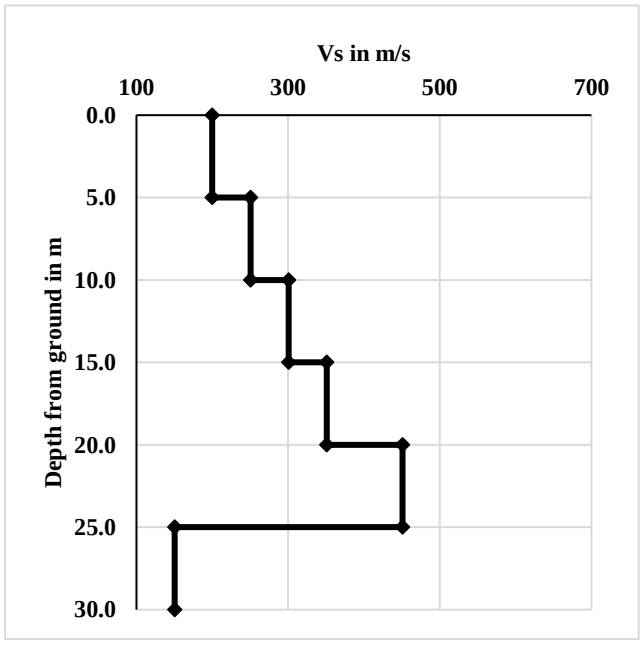

Table 4.2.7. PROPERTIES OF SOIL 7

Depth from Ground Level (m)		Mass Density (ρ) in kg/m^3	Young's Modulus (E) in N/m^2	Poisson's Ratio (v)	Shear Wave Velocity (Vs) in m/s
From	To				
0	5	1750	1.96×10^8	0.4	200
5	10	1950	3.3×10^8	0.35	250
10	12.5	1500	9.7×10^7	0.43	150
12.5	20	2000	6.5×10^8	0.32	350
20	25	2100	1.11×10^9	0.3	450
25	30	2300	1.99×10^9	0.2	600

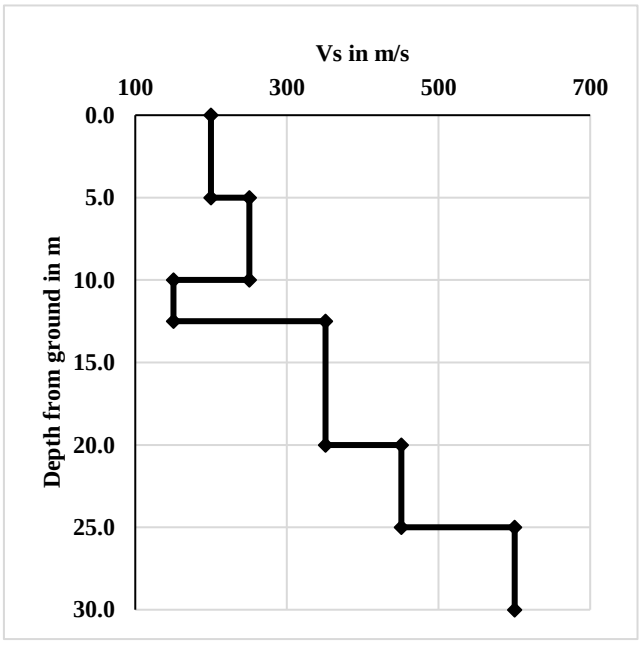

4.3. MODELLING THE PROBLEM

The procedure for modelling a general SSI problem using Abaqus software has been discussed briefly in Chapter 3. However, to model the problem stated in this chapter, eleven parts (Infinite Soil, Soil Layer 1, Soil Layer 2, Soil Layer 3, Soil Layer 4, Soil Layer 5, Soil Layer 6, Soil Tetrahedron, Footing, Column and Beam) are used. The nodes present on the interface of two adjacent soil layers have been merged to develop the entire layered soil base. Rest of the model is kept similar to the model used for analysing frame structures resting on uniform soil in Chapter 3. The analysis procedure followed in this chapter is also same as in the previous chapter. However, the meshing details of the elements used along with their properties have been tabulated in Table 4.3.1. In order to incorporate the effect of damping in the soil-structure models, Rayleigh damping coefficients are computed and assigned to every model following the procedure demonstrated in Chapter 3. For calculating Rayleigh damping coefficients, first and fifth mode frequencies are taken into account. In all cases, damping ratio value is taken as 0.05. Rayleigh damping coefficients for all the models along with their first and fifth mode frequencies are presented in Table 4.3.2.

Table 4.3.1. PROPERTIES OF THE ELEMENTS USED IN ABAQUS

Name of the Part	Cross-sectional Area	Depth or Length of the Part	Element Size for Meshing	No. of Nodes in Each Element	Type of Element
Infinite Soil	2.5 m × 2.5 m	N/A	2.5 m × 2.5 m × Infinite Length	8	Linear Hexahedron (Type CIN3D8)
Soil Layer 1 (Surrounded by the Infinite Soil)	32.5 m × 32.5 m	5 m	2.5 m × 2.5 m × 2.5 m	8	Linear Hexahedron (Type C3D8)
Soil Layer 2 (Surrounded by the Infinite Soil)	32.5 m × 32.5 m	5 m	2.5 m × 2.5 m × 2.5 m	8	Linear Hexahedron (Type C3D8)
Soil Layer 3 (Surrounded by the Infinite Soil)	32.5 m × 32.5 m	5 m (2.5 m for Soil 7 only)	2.5 m × 2.5 m × 2.5 m	8	Linear Hexahedron (Type C3D8)
Soil Layer 4 (Surrounded by the Infinite Soil)	32.5 m × 32.5 m	5 m (7.5 m for Soil 7 only)	2.5 m × 2.5 m × 2.5 m	8	Linear Hexahedron (Type C3D8)
Soil Layer 5 (Surrounded by the Infinite Soil)	32.5 m × 32.5 m	5 m	2.5 m × 2.5 m × 2.5 m	8	Linear Hexahedron (Type C3D8)
Soil Layer 6 (Surrounded by the Infinite Soil)	32.5 m × 32.5 m	5 m	2.5 m × 2.5 m × 2.5 m	8	Linear Hexahedron (Type C3D8)
Soil Tetrahedron (Embedded in the Soil Layer 1)	22.5 m × 22.5 m	5 m	N/A	4	Linear Tetrahedron (Type C3D4)
Footing (Embedded in the Soil Tetrahedron)	17.5 m × 17.5 m	2.5 m	0.625 m × 0.625 m × 0.625 m	8	Linear Hexahedron (Type C3D8)

Name of the Part		Cross-sectional Area	Depth or Length of the Part	Element Size for Meshing	No. of Nodes in Each Element	Type of Element
Column (Each column is placed on a Footing)	For G+1 Building	300 mm × 300 mm	3 m	0.6 m	2	Linear Line (Type B31)
	For G+4 Building	400 mm × 400 mm				
	For G+9 Building	500 mm × 500 mm				
Beam (Each beam is placed on two Columns)	For G+1 Building	250 mm × 300 mm	5 m	1 m	2	Linear Line (Type B31)
	For G+4 Building	250 mm × 400 mm				
	For G+9 Building	300 mm × 500 mm				

In order to incorporate the effect of damping in the soil-structure models, Rayleigh damping coefficients are computed and assigned to every model following the procedure demonstrated in Chapter 3. For calculating Rayleigh damping coefficients, first and fifth mode frequencies are taken into account. In all cases, damping ratio value is taken as 0.05. Rayleigh damping coefficients for all the models along with their first and fifth mode frequencies are presented in Table 4.3.2.

Table 4.3.2. RAYLEIGH DAMPING COEFFICIENTS OF MATERIALS FOR DIFFERENT SOIL-STRUCTURE COMBINATIONS

SOIL TYPE	STRUCTURE TYPE	FREQUENCY OF 1ST MODE (cps)	FREQUENCY OF 5TH MODE (cps)	DAMPING RATIO (ξ)	RAYLEIGH DAMPING COEFFICIENTS	
					α	β
Soil 1	**G+1**	2.5098	3.1471	0.05	0.877305849	0.002813466
	G+4	1.3781	2.5616	0.05	0.563000478	0.004039773
	G+9	0.73144	2.3864	0.05	0.351761246	0.005104654
Soil 2	**G+1**	2.2372	3.1387	0.05	0.820697867	0.002960526
	G+4	1.3738	2.2825	0.05	0.53885553	0.004352896
	G+9	0.73001	2.2449	0.05	0.346124105	0.005349908
Soil 3	**G+1**	1.9012	3.1246	0.05	0.742671743	0.003166758
	G+4	1.3683	1.9403	0.05	0.504180232	0.004810341
	G+9	0.73004	1.9178	0.05	0.33222943	0.006010746
Soil 4	**G+1**	1.6616	3.1145	0.05	0.68080271	0.00333232
	G+4	1.3571	1.7066	0.05	0.474982078	0.005194861
	G+9	0.7295	1.6773	0.05	0.319430152	0.00661272
Soil 5	**G+1**	1.4595	3.1012	0.05	0.623565727	0.003489704
	G+4	1.3251	1.5639	0.05	0.450702493	0.005508998
	G+9	0.72834	1.475	0.05	0.306354689	0.007223349
Soil 6	**G+1**	1.2928	3.0716	0.05	0.571677795	0.003646663
	G+4	1.2436	1.5467	0.05	0.433127509	0.005703865
	G+9	0.72687	1.3086	0.05	0.293615395	0.007819076
Soil 7	**G+1**	2.2121	3.1347	0.05	0.814866884	0.002976639
	G+4	1.377	2.2494	0.05	0.536666879	0.004388786
	G+9	0.73188	2.2216	0.05	0.345900811	0.005388726

4.4. INPUT MOTIONS AND THEIR PROPERTIES

The input motions used for analysing the models are identical to the motions used in Chapter 3. Various properties of those seismic excitations, such as acceleration time-history, acceleration response spectra and FFT, have already been presented in that chapter.

4.5. FUNDAMENTAL FREQUENCIES OF SOIL MEDIA

Following the procedure discussed in Chapter 3, fundamental frequency and amplification at fundamental frequency values are calculated for each type of soil, which have been shown in Table 4.5.1. It is to be mentioned that the amplification factor of a soil does not depend on the type of seismic excitation. Further, the amplification factor and fundamental frequency of Soil 1 are minimum among all types of soils. Moreover, Soil 6 has the highest amplification factor, while Soil 2 has the largest fundamental frequency value.

Table 4.5.1. AMPLIFICATION FACTORS OF VARIOUS SOILS UNDER DIFFERENT EARTHQUAKES

Type of Soil	Amplification Factor	Fundamental Frequency (cps)
Soil 1	1.01	15
Soil 2	1.33	24.88
Soil 3	1.53	18.88
Soil 4	2.18	21.25
Soil 5	2.94	23
Soil 6	3.78	20.63
Soil 7	1.7	16.13

4.6. DISPLACEMENT TIME-HISTORIES OF ROOF AND BASE RESPONSES

After analysing all the developed models using Abaqus software, the displacement time- histories of both roof and base responses are plotted for every case which are presented in Figure 4.6.1 to Figure 4.6.84. The graphs clearly reveal that the base responses change only due to the variation

in soil properties. In other words, change in building type does not alter the base response, if all other parameters are kept unchanged. On the contrary, the roof responses increase with the increment of the height of the buildings. For buildings located on Soil 1, Soil 2 and Soil 7, roof responses are nearly same. This statement also holds good for base responses. Moreover, in case of these three types of soils, roof responses of the buildings are the largest among all types of soils. It is also to be mentioned that the roof and base responses under the action of a near-field earthquake are smaller than the far-field one. This may be due to the presence of low frequency seismic wave in far-field earthquake.

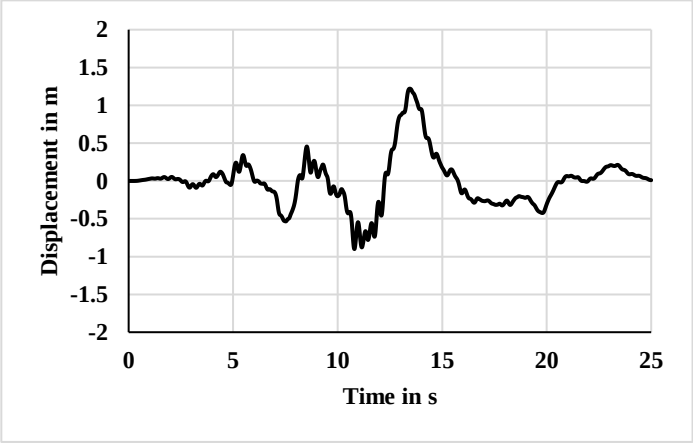

Figure 4.6.1. Displacement time-history for Roof of G+1 building on Soil 1 under Loma prieta earthquake

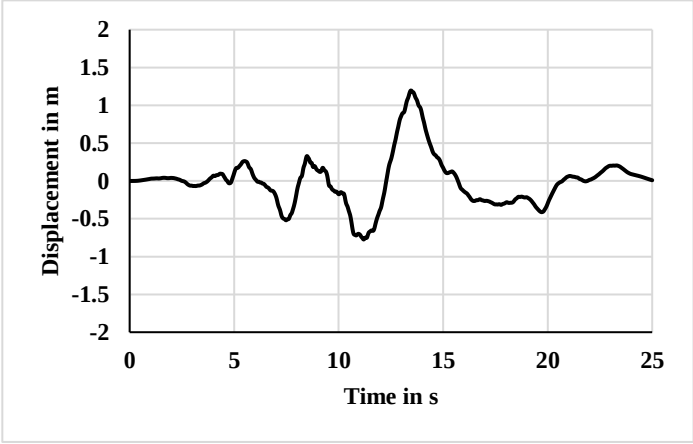

Figure 4.6.2. Displacement time-history for Base of G+1 building on Soil 1 under Loma prieta earthquake

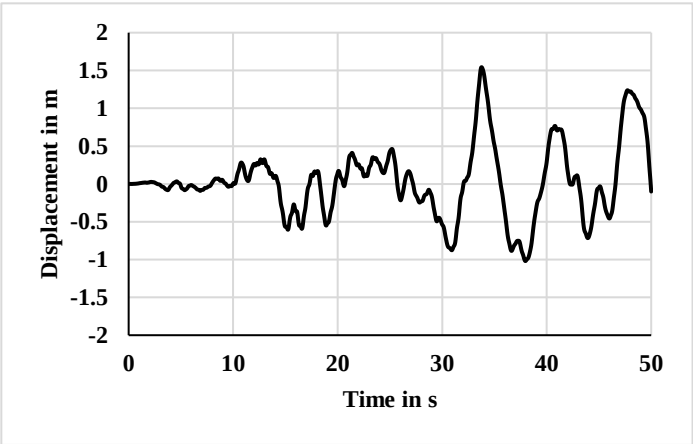

Figure 4.6.3. Displacement time-history for Roof of G+1 building on Soil 1 under Denali earthquake

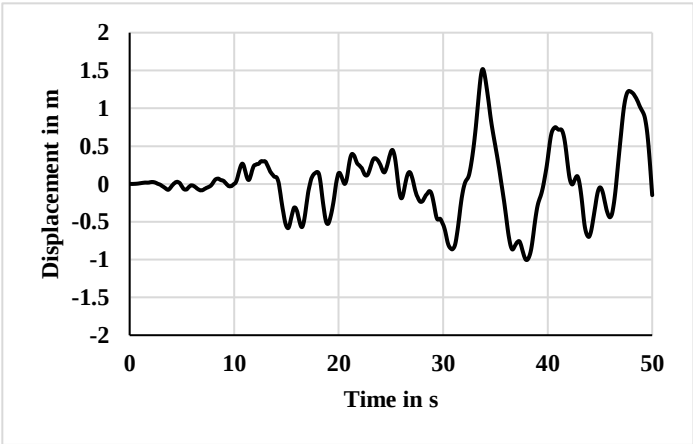

Figure 4.6.4. Displacement time-history for Base of G+1 building on Soil 1 under Denali earthquake

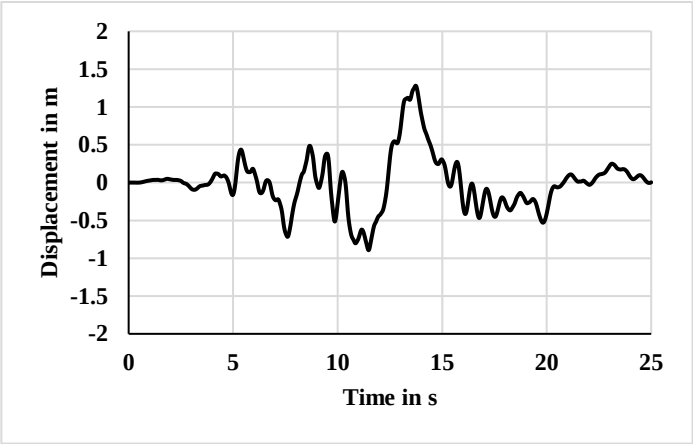

Figure 4.6.5. Displacement time-history for Roof of G+4 building on Soil 1 under Loma prieta earthquake

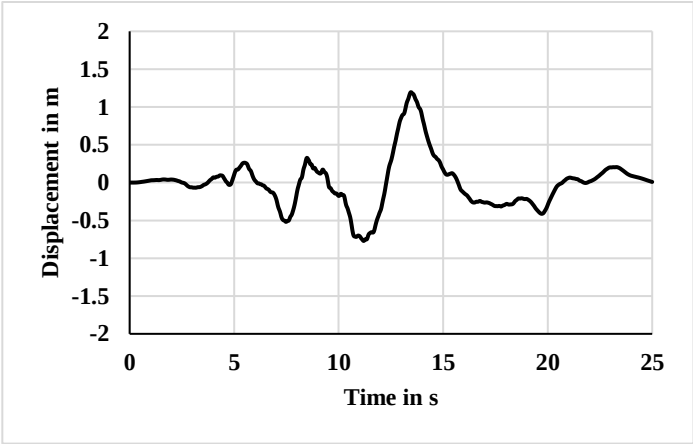

Figure 4.6.6. Displacement time-history for Base of G+4 building on Soil 1 under Loma prieta earthquake

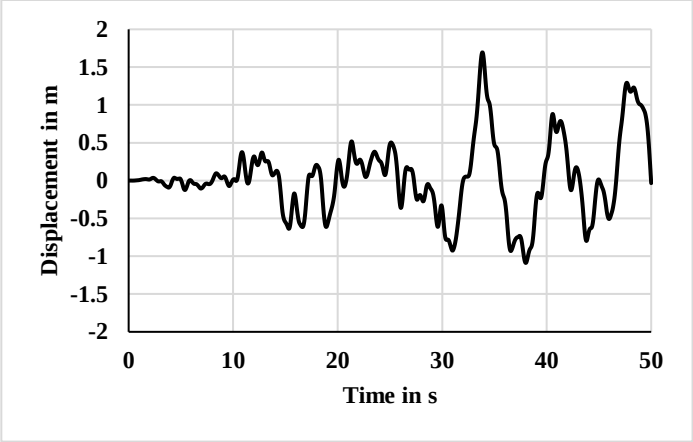

Figure 4.6.7. Displacement time-history for Roof of G+4 building on Soil 1 under Denali earthquake

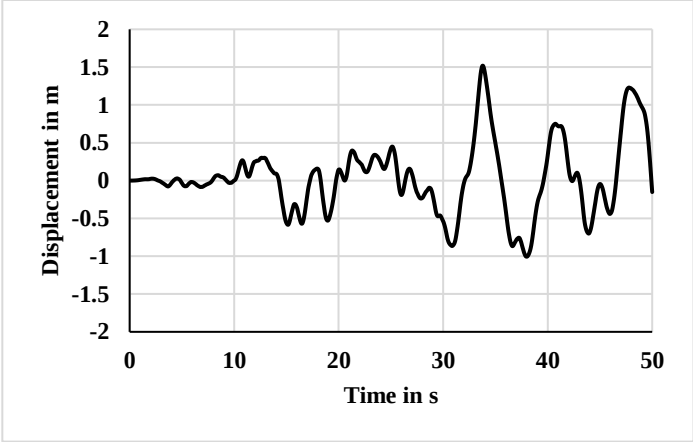

Figure 4.6.8. Displacement time-history for Base of G+4 building on Soil 1 under Denali earthquake

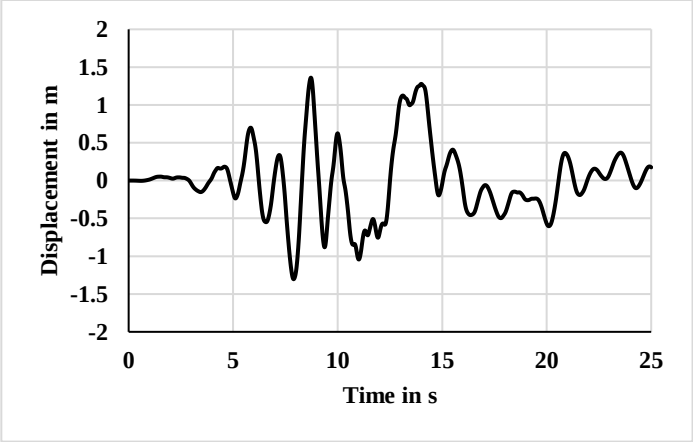

Figure 4.6.9. Displacement time-history for Roof of G+9 building on Soil 1 under Loma prieta earthquake

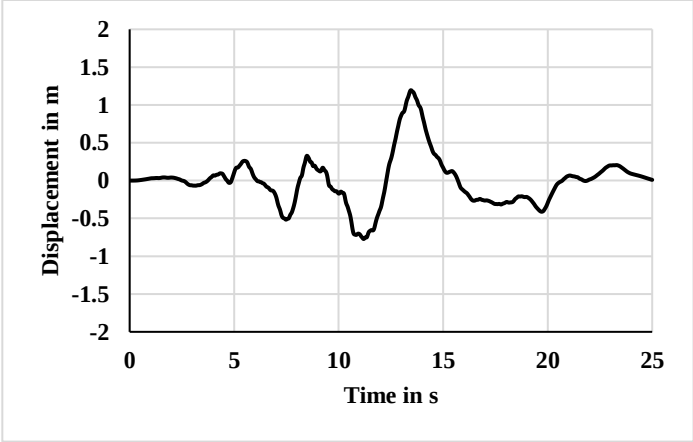

Figure 4.6.10. Displacement time-history for Base of G+9 building on Soil 1 under Loma prieta earthquake

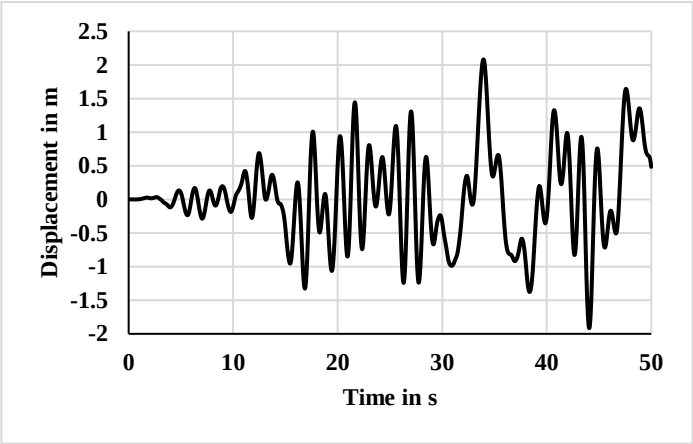

Figure 4.6.11. Displacement time-history for Roof of G+9 building on Soil 1 under Denali earthquake

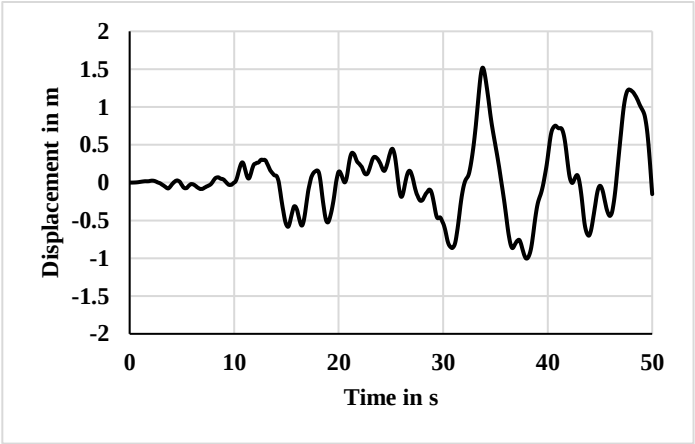

Figure 4.6.12. Displacement time-history for Base of G+9 building on Soil 1 under Denali earthquake

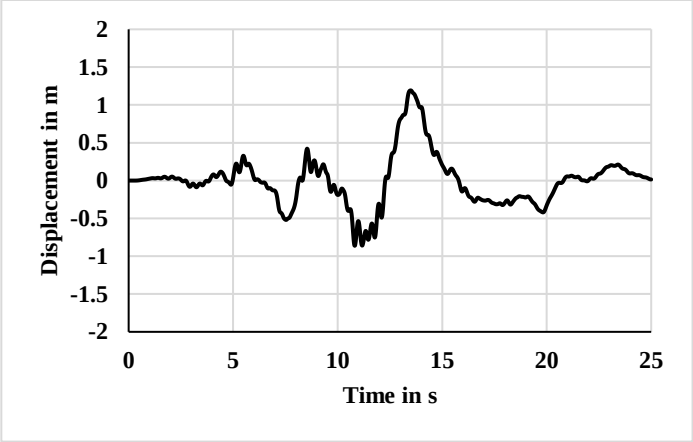

Figure 4.6.13. Displacement time-history for Roof of G+1 building on Soil 2 under Loma prieta earthquake

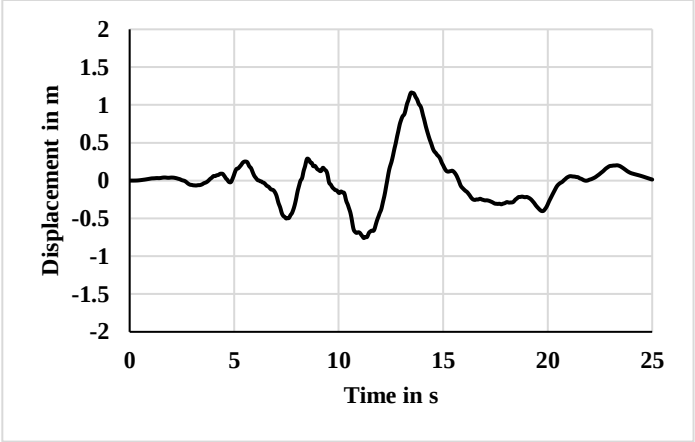

Figure 4.6.14. Displacement time-history for Base of G+1 building on Soil 2 under Loma prieta earthquake

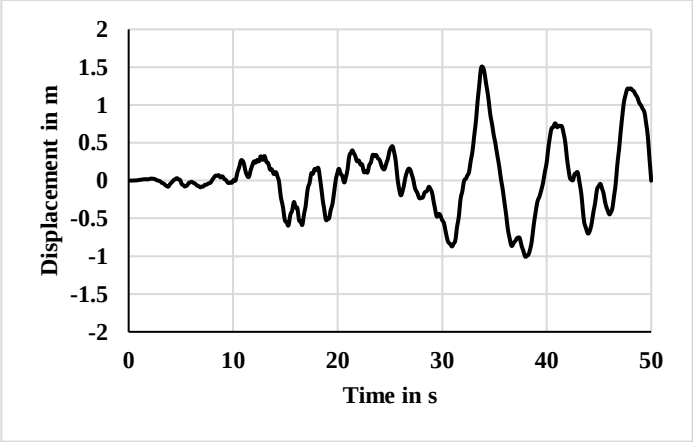

Figure 4.6.15. Displacement time-history for Roof of G+1 building on Soil 2 under Denali earthquake

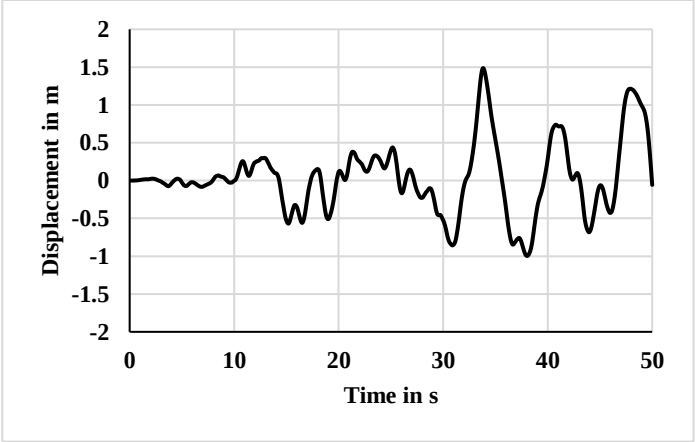

Figure 4.6.16. Displacement time-history for Base of G+1 building on Soil 2 under Denali earthquake

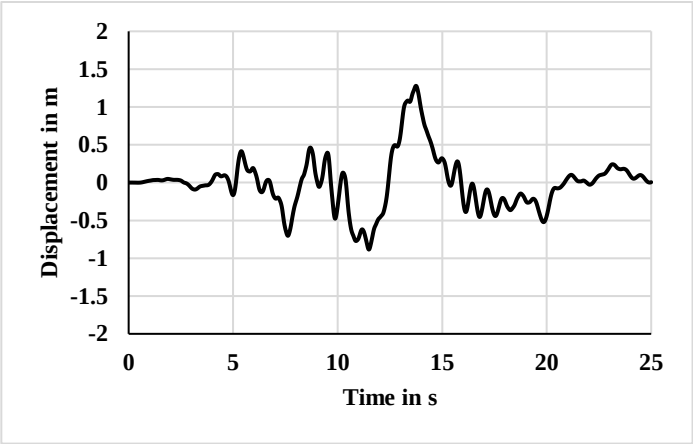

Figure 4.6.17. Displacement time-history for Roof of G+4 building on Soil 2 under Loma prieta earthquake

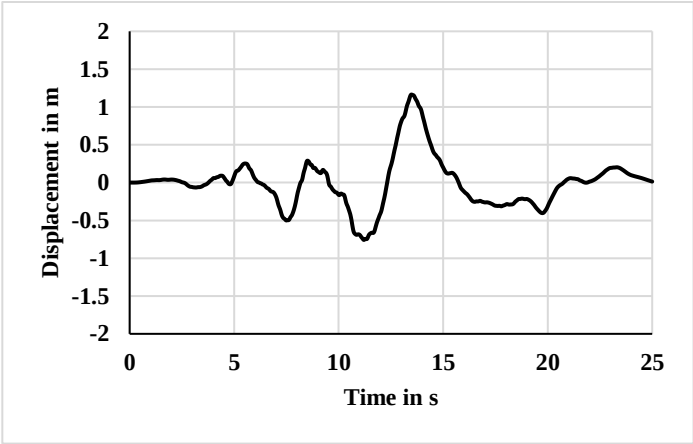

Figure 4.6.18. Displacement time-history for Base of G+4 building on Soil 2 under Loma prieta earthquake

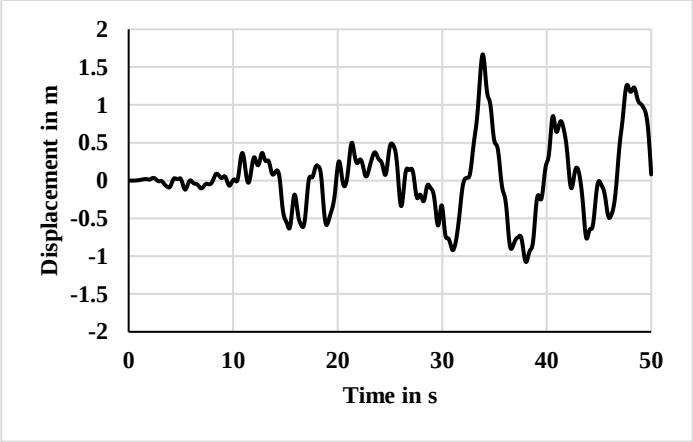

Figure 4.6.19. Displacement time-history for Roof of G+4 building on Soil 2 under Denali earthquake

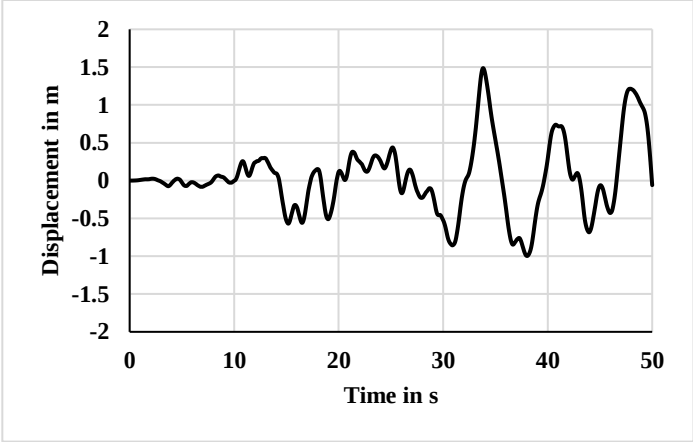

Figure 4.6.20. Displacement time-history for Base of G+4 building on Soil 2 under Denali earthquake

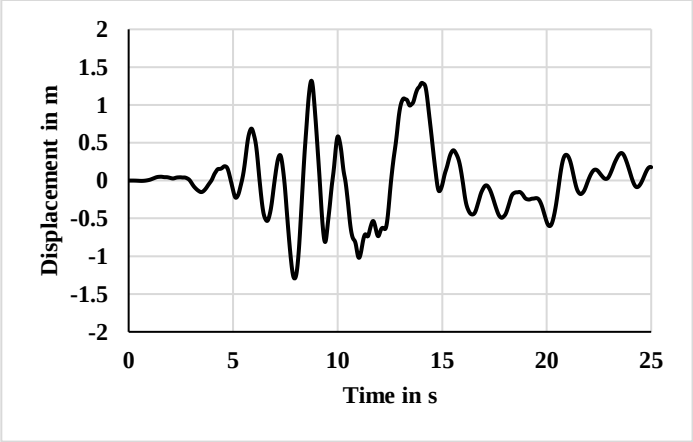

Figure 4.6.21. Displacement time-history for Roof of G+9 building on Soil 2 under Loma prieta earthquake

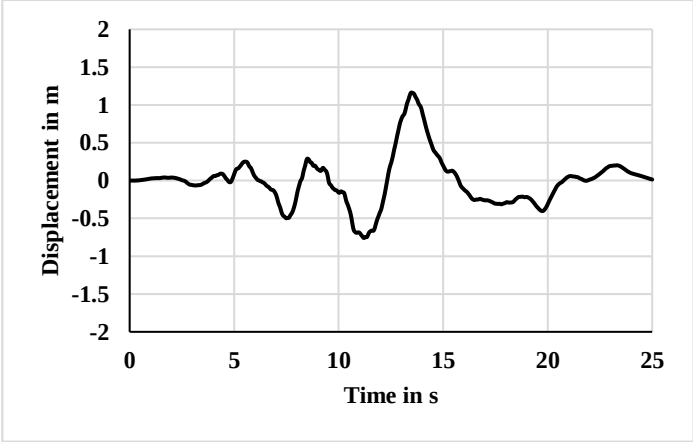

Figure 4.6.22. Displacement time-history for Base of G+9 building on Soil 2 under Loma prieta earthquake

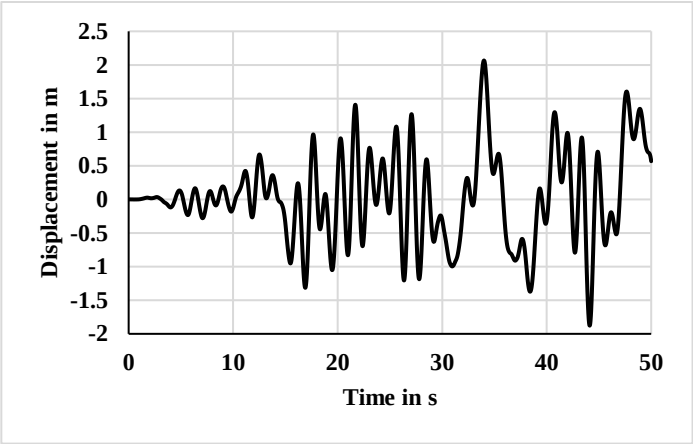

Figure 4.6.23. Displacement time-history for Roof of G+9 building on Soil 2 under Denali earthquake

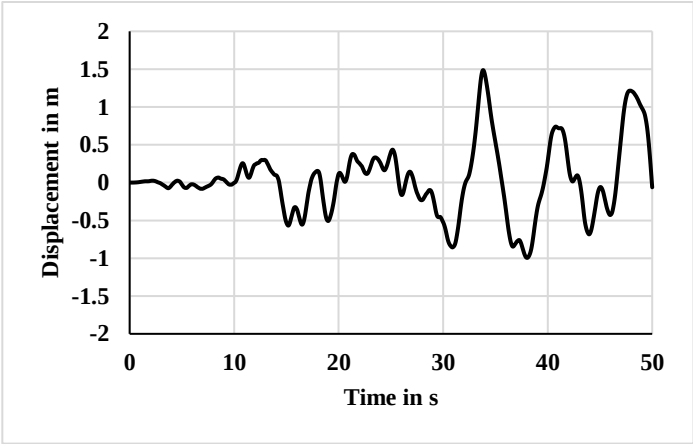

Figure 4.6.24. Displacement time-history for Base of G+9 building on Soil 2 under Denali earthquake

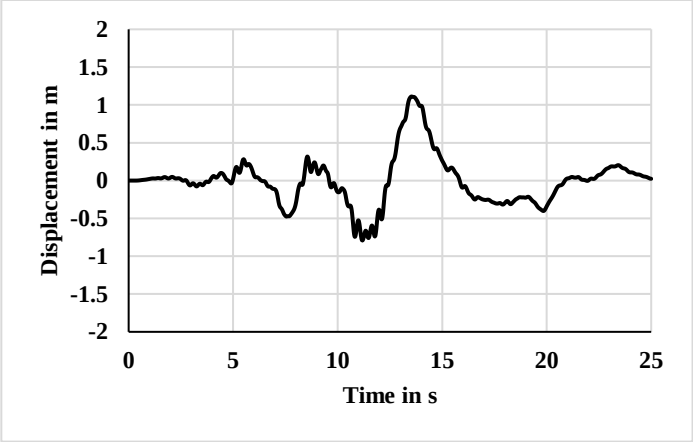

Figure 4.6.25. Displacement time-history for Roof of G+1 building on Soil 3 under Loma prieta earthquake

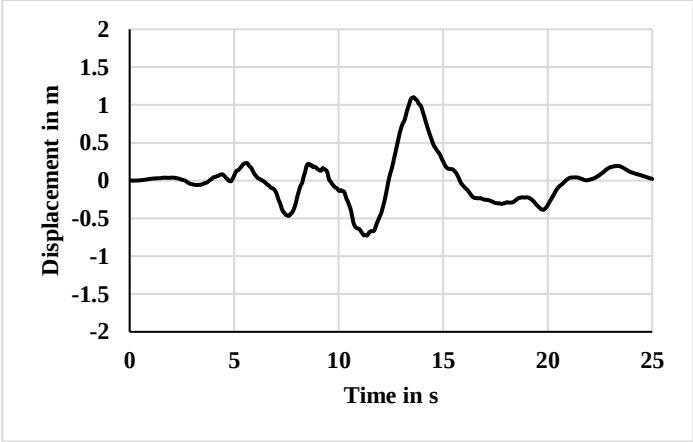

Figure 4.6.26. Displacement time-history for Base of G+1 building on Soil 3 under Loma prieta earthquake

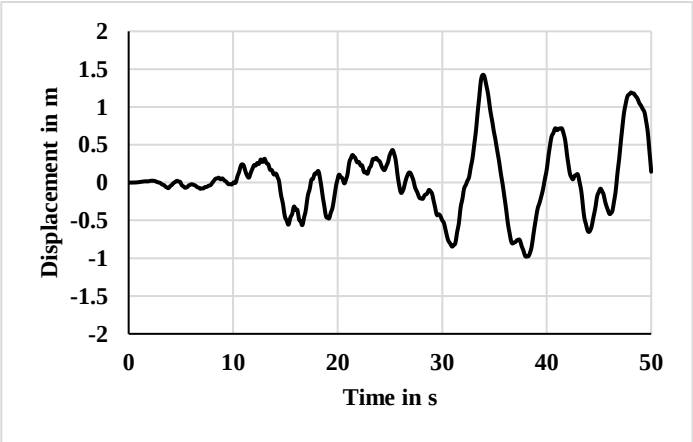

Figure 4.6.27. Displacement time-history for Roof of G+1 building on Soil 3 under Denali earthquake

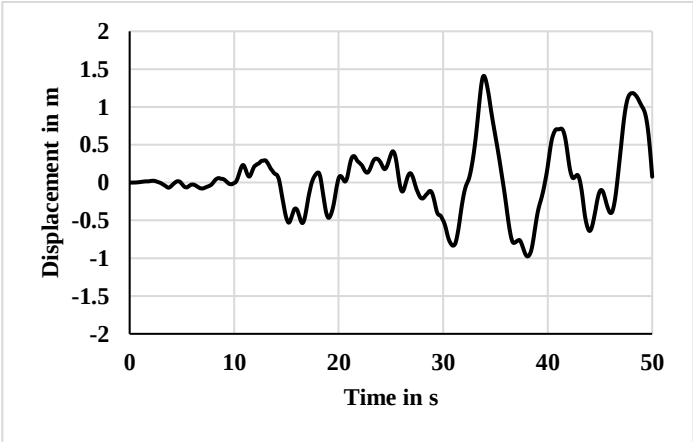

Figure 4.6.28. Displacement time-history for Base of G+1 building on Soil 3 under Denali earthquake

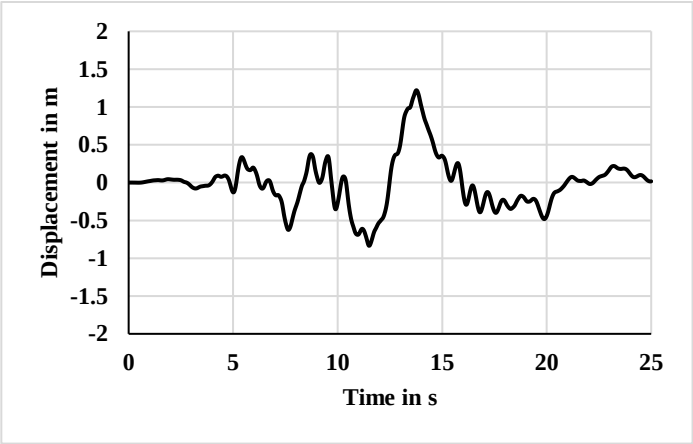

Figure 4.6.29. Displacement time-history for Roof of G+4 building on Soil 3 under Loma prieta earthquake

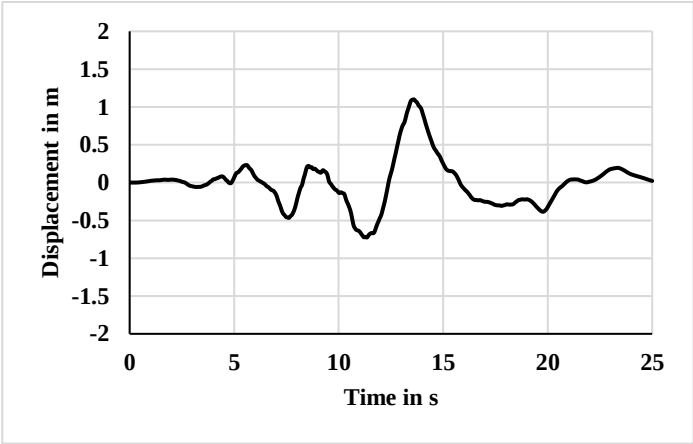

Figure 4.6.30. Displacement time-history for Base of G+4 building on Soil 3 under Loma prieta earthquake

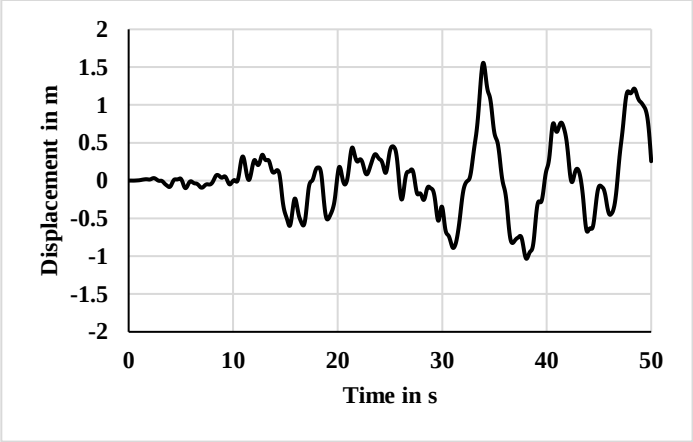

Figure 4.6.31. Displacement time-history for Roof of G+4 building on Soil 3 under Denali earthquake

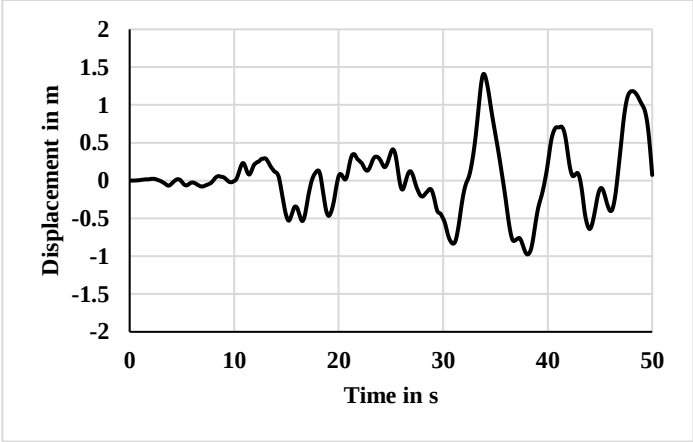

Figure 4.6.32. Displacement time-history for Base of G+4 building on Soil 3 under Denali earthquake

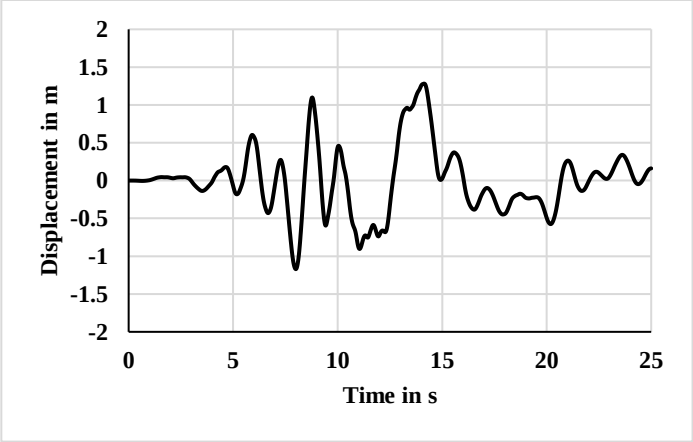

Figure 4.6.33. Displacement time-history for Roof of G+9 building on Soil 3 under Loma prieta earthquake

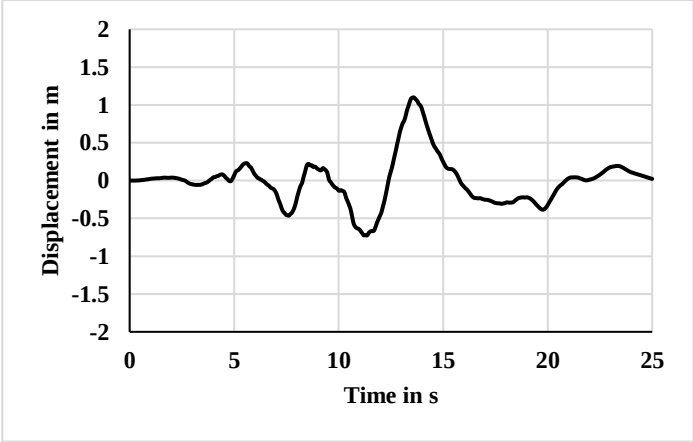

Figure 4.6.34. Displacement time-history for Base of G+9 building on Soil 3 under Loma prieta earthquake

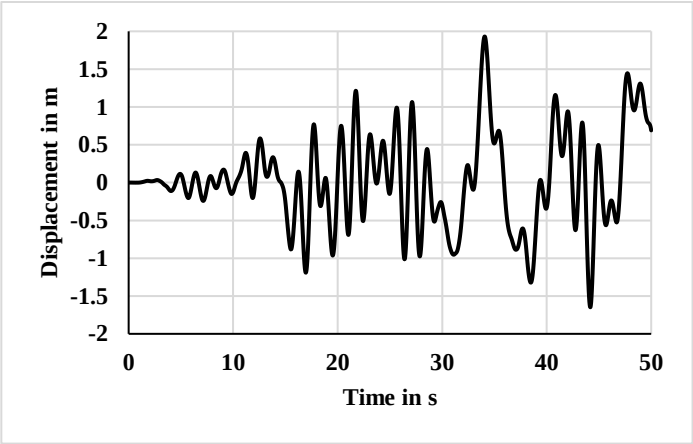

Figure 4.6.35. Displacement time-history for Roof of G+9 building on Soil 3 under Denali earthquake

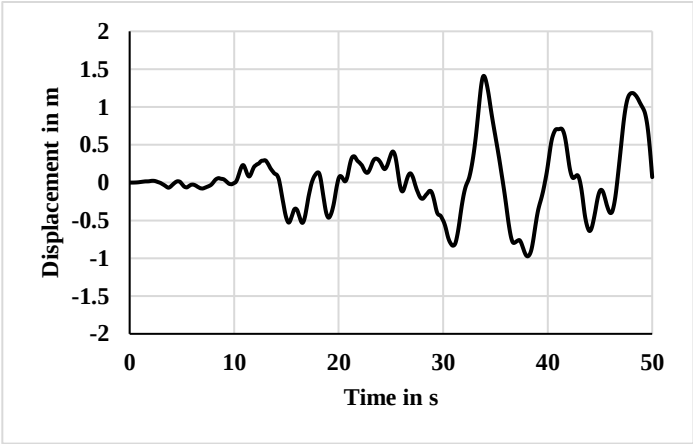

Figure 4.6.36. Displacement time-history for Base of G+9 building on Soil 3 under Denali earthquake

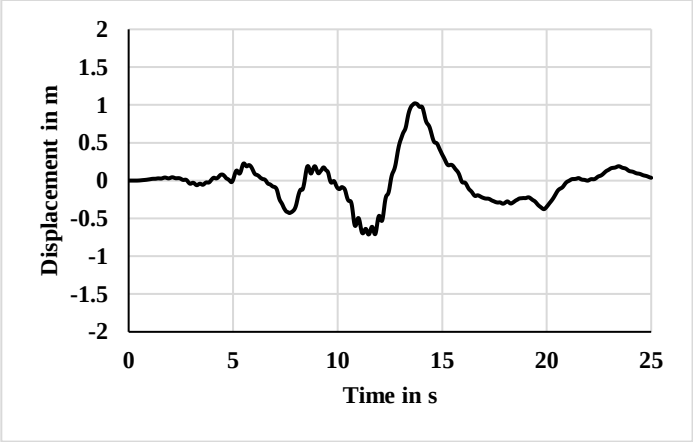

Figure 4.6.37. Displacement time-history for Roof of G+1 building on Soil 4 under Loma prieta earthquake

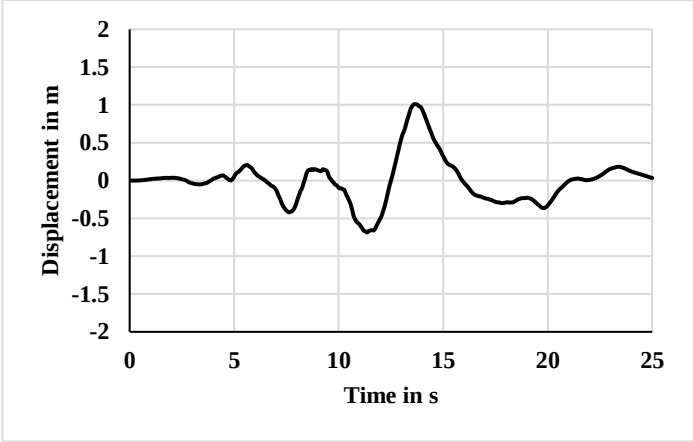

Figure 4.6.38. Displacement time-history for Base of G+1 building on Soil 4 under Loma prieta earthquake

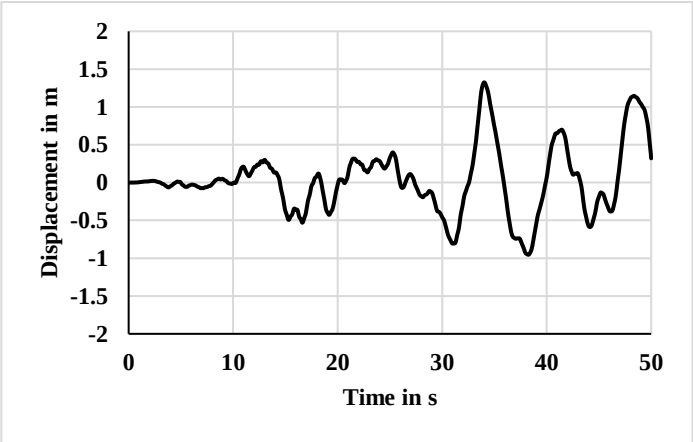

Figure 4.6.39. Displacement time-history for Roof of G+1 building on Soil 4 under Denali earthquake

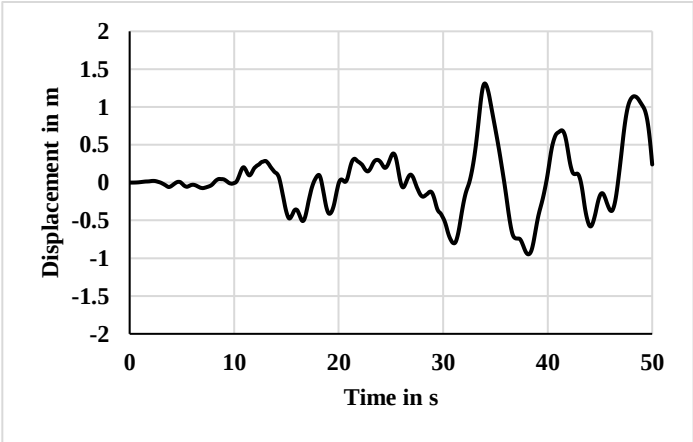

Figure 4.6.40. Displacement time-history for Base of G+1 building on Soil 4 under Denali earthquake

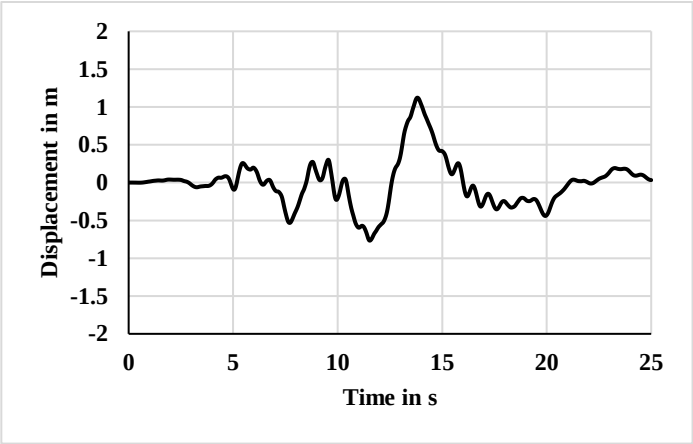

Figure 4.6.41. Displacement time-history for Roof of G+4 building on Soil 4 under Loma prieta earthquake

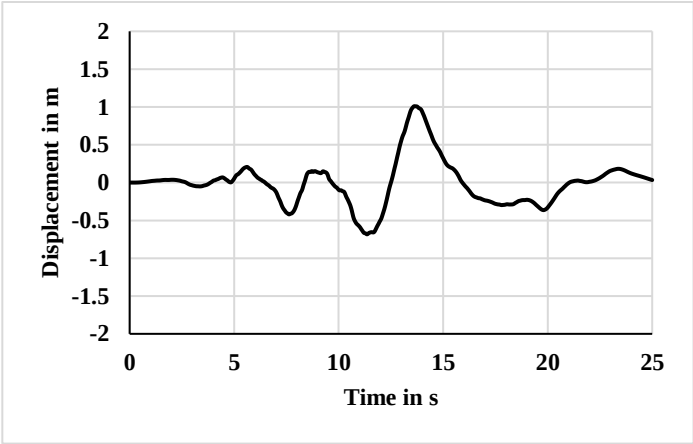

Figure 4.6.42. Displacement time-history for Base of G+4 building on Soil 4 under Loma prieta earthquake

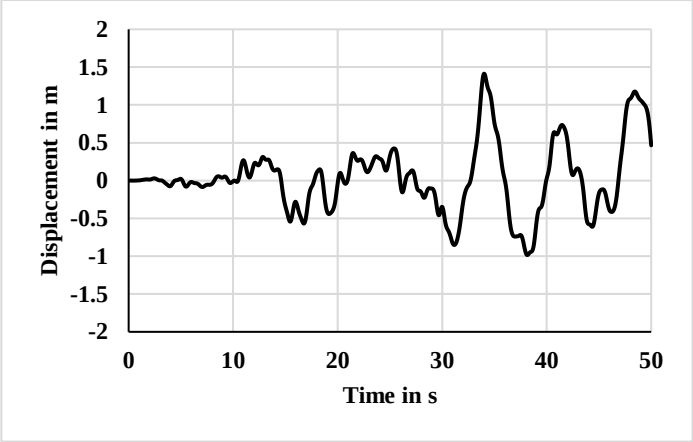

Figure 4.6.43. Displacement time-history for Roof of G+4 building on Soil 4 under Denali earthquake

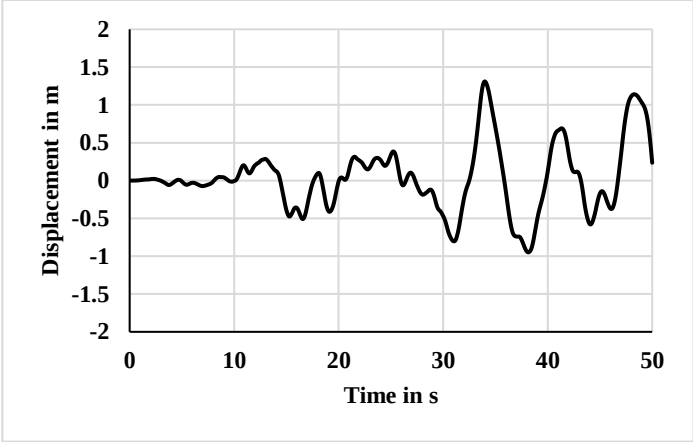

Figure 4.6.44. Displacement time-history for Base of G+4 building on Soil 4 under Denali earthquake

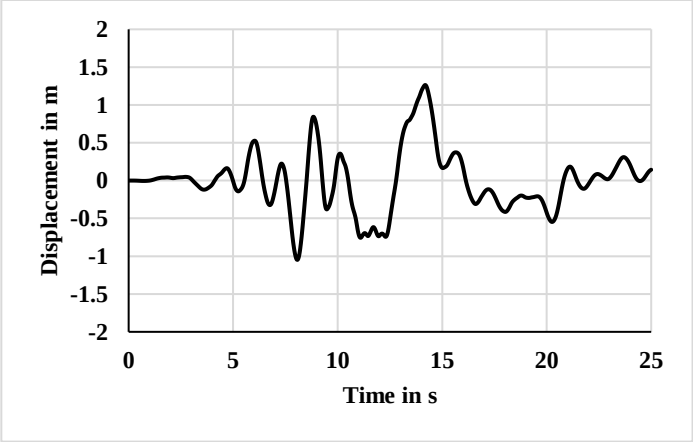

Figure 4.6.45. Displacement time-history for Roof of G+9 building on Soil 4 under Loma prieta earthquake

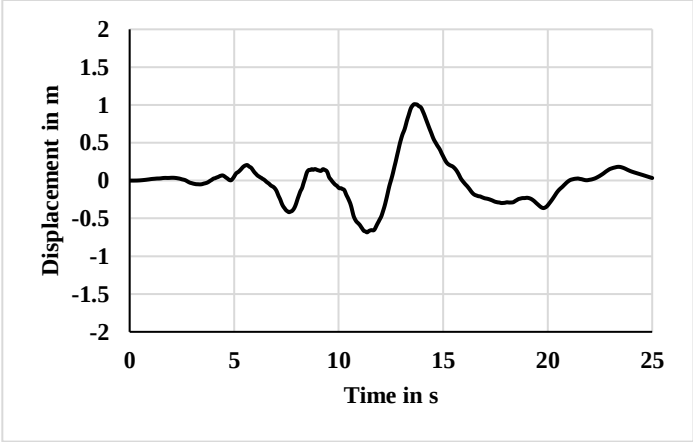

Figure 4.6.46. Displacement time-history for Base of G+9 building on Soil 4 under Loma prieta earthquake

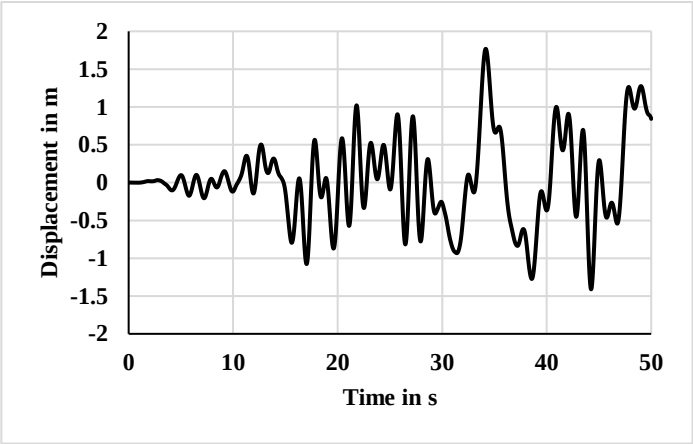

Figure 4.6.47. Displacement time-history for Roof of G+9 building on Soil 4 under Denali earthquake

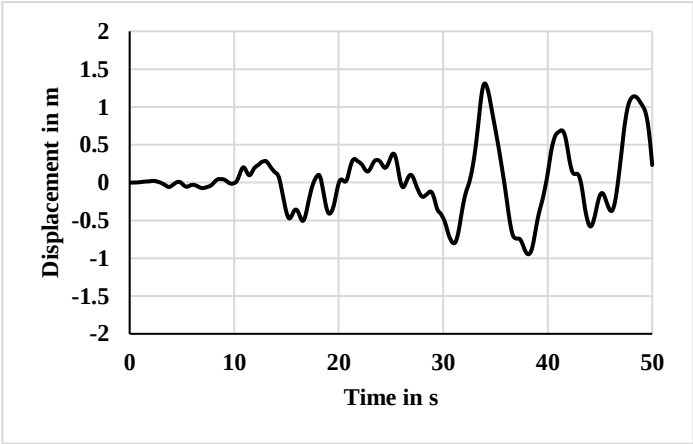

Figure 4.6.48. Displacement time-history for Base of G+9 building on Soil 4 under Denali earthquake

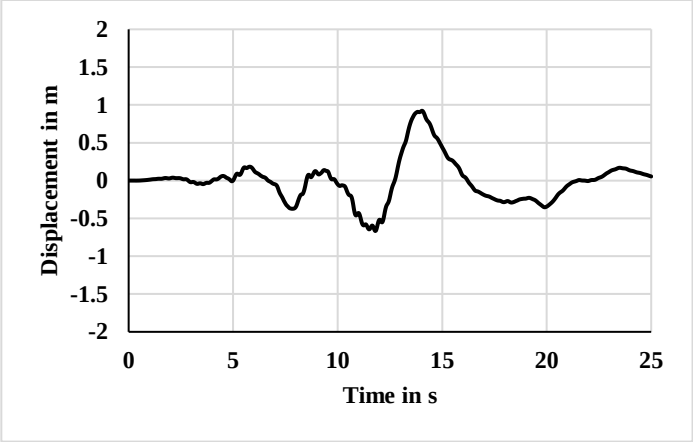

Figure 4.6.49. Displacement time-history for Roof of G+1 building on Soil 5 under Loma prieta earthquake

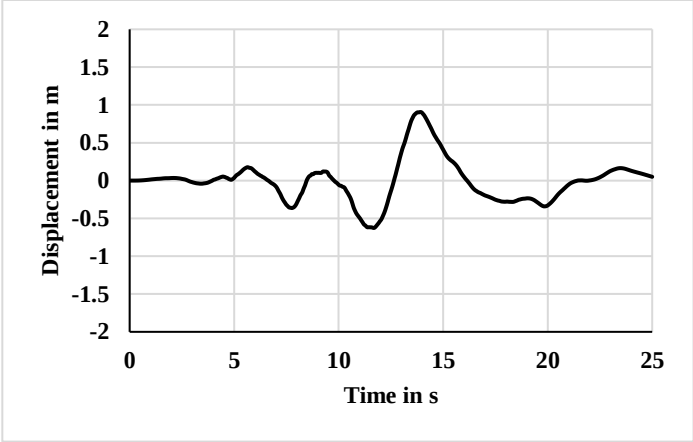

Figure 4.6.50. Displacement time-history for Base of G+1 building on Soil 5 under Loma prieta earthquake

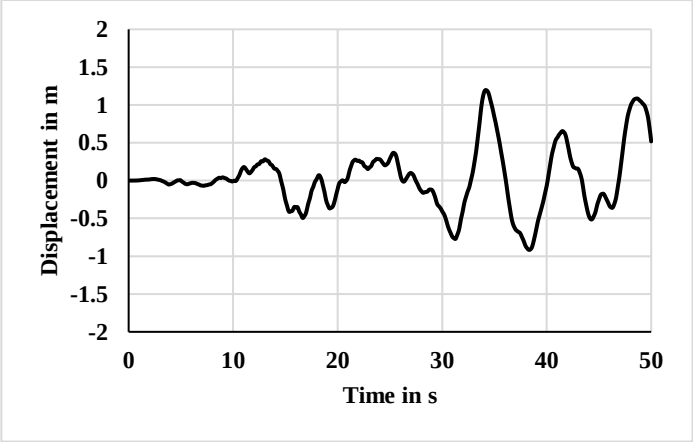

Figure 4.6.51. Displacement time-history for Roof of G+1 building on Soil 5 under Denali earthquake

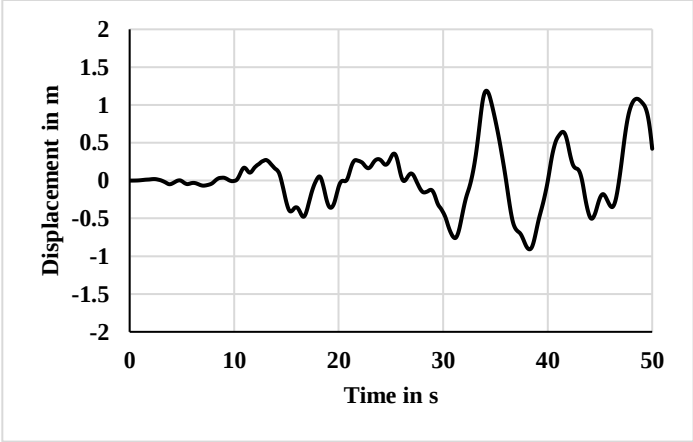

Figure 4.6.52. Displacement time-history for Base of G+1 building on Soil 5 under Denali earthquake

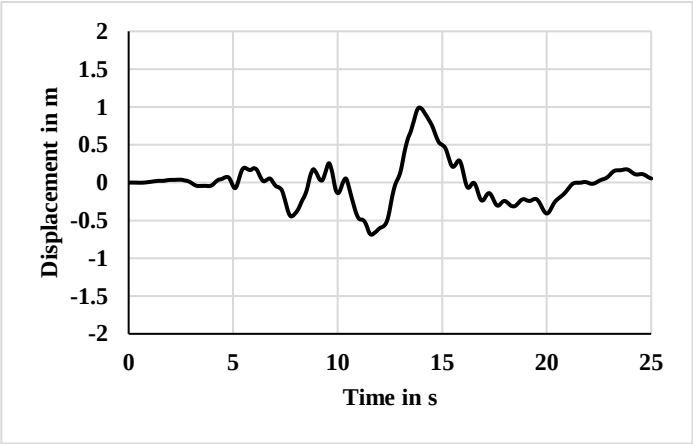

Figure 4.6.53. Displacement time-history for Roof of G+4 building on Soil 5 under Loma prieta earthquake

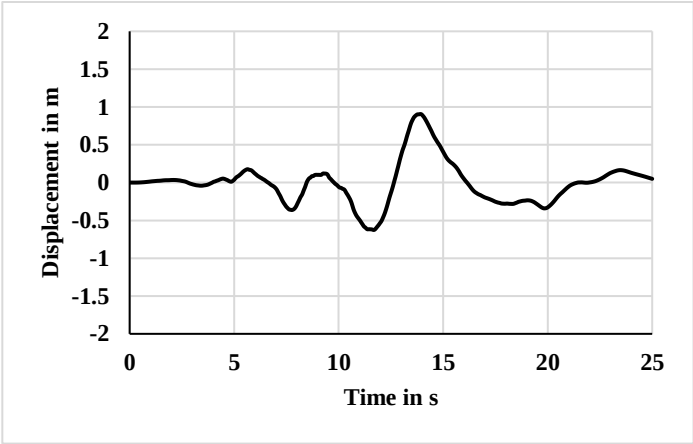

Figure 4.6.54. Displacement time-history for Base of G+4 building on Soil 5 under Loma prieta earthquake

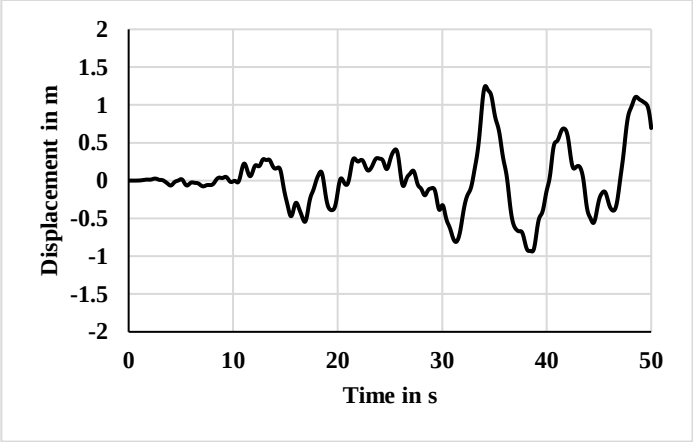

Figure 4.6.55. Displacement time-history for Roof of G+4 building on Soil 5 under Denali earthquake

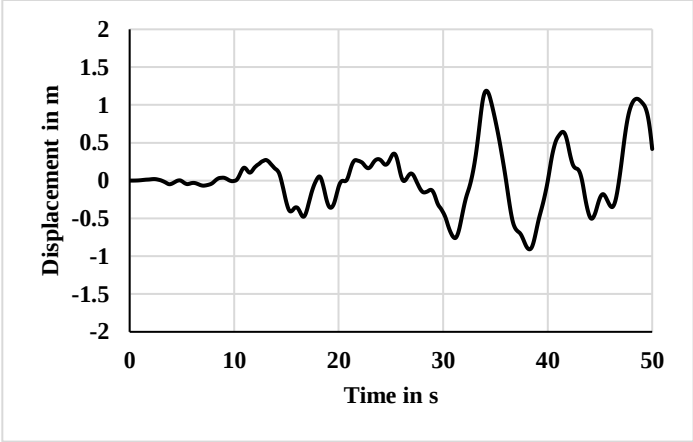

Figure 4.6.56. Displacement time-history for Base of G+4 building on Soil 5 under Denali earthquake

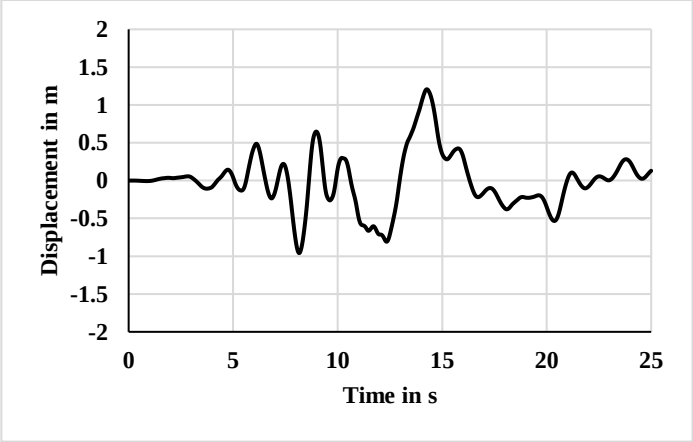

Figure 4.6.57. Displacement time-history for Roof of G+9 building on Soil 5 under Loma prieta earthquake

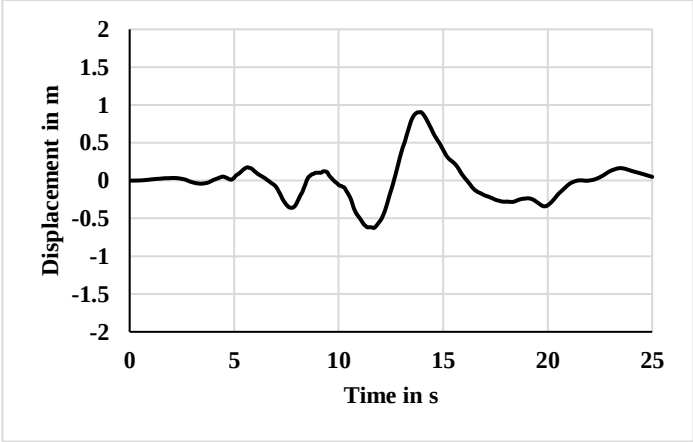

Figure 4.6.58. Displacement time-history for Base of G+9 building on Soil 5 under Loma prieta earthquake

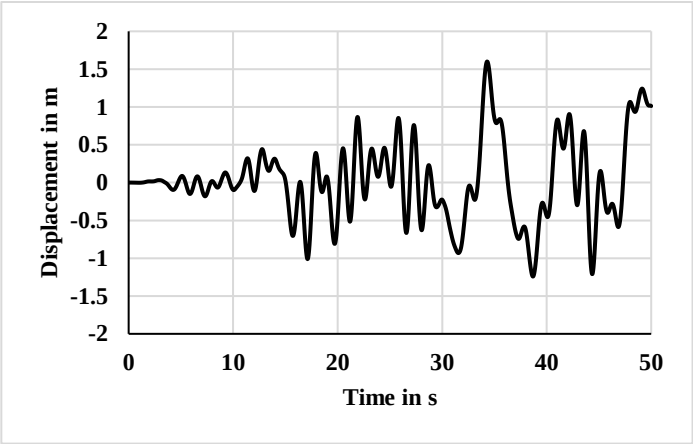

Figure 4.6.59. Displacement time-history for Roof of G+9 building on Soil 5 under Denali earthquake

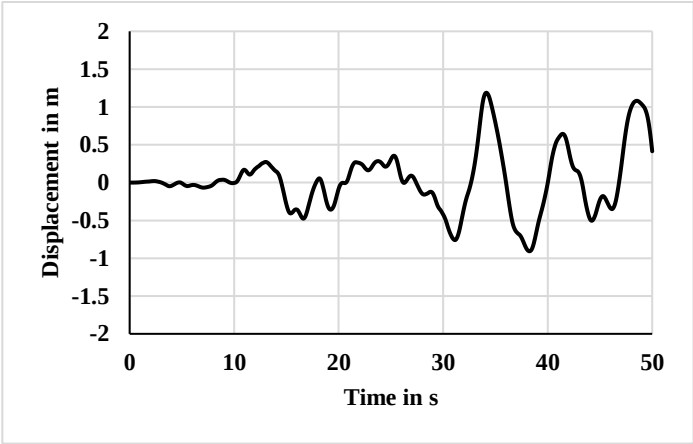

Figure 4.6.60. Displacement time-history for Base of G+9 building on Soil 5 under Denali earthquake

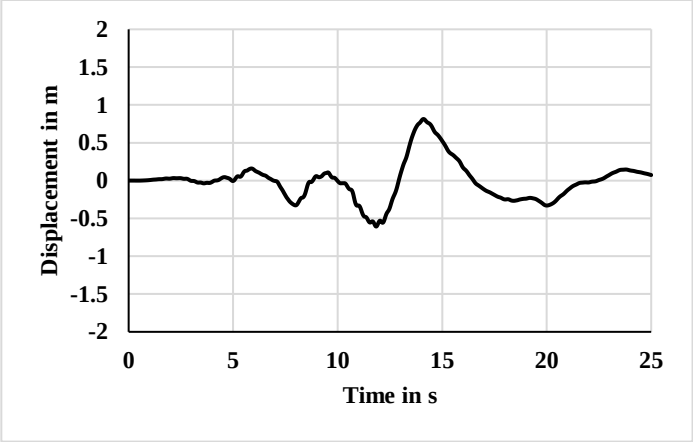

Figure 4.6.61. Displacement time-history for Roof of G+1 building on Soil 6 under Loma prieta earthquake

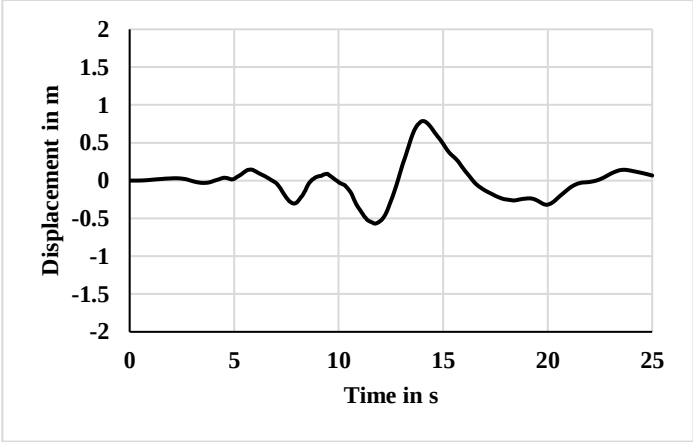

Figure 4.6.62. Displacement time-history for Base of G+1 building on Soil 6 under Loma prieta earthquake

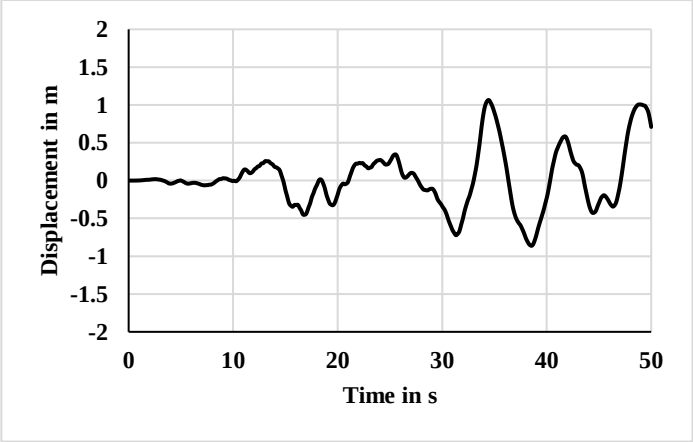

Figure 4.6.63. Displacement time-history for Roof of G+1 building on Soil 6 under Denali earthquake

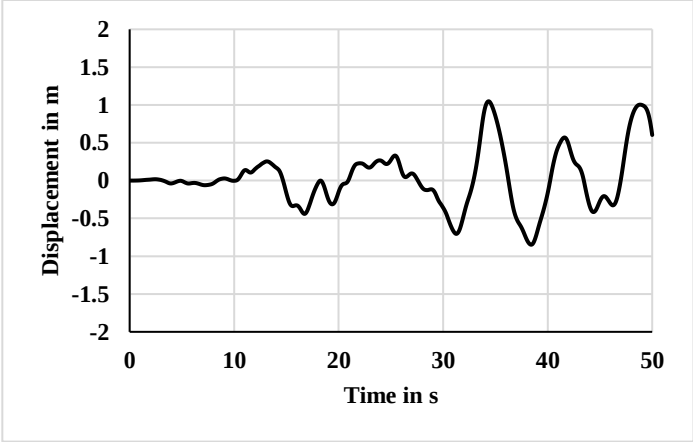

Figure 4.6.64. Displacement time-history for Base of G+1 building on Soil 6 under Denali earthquake

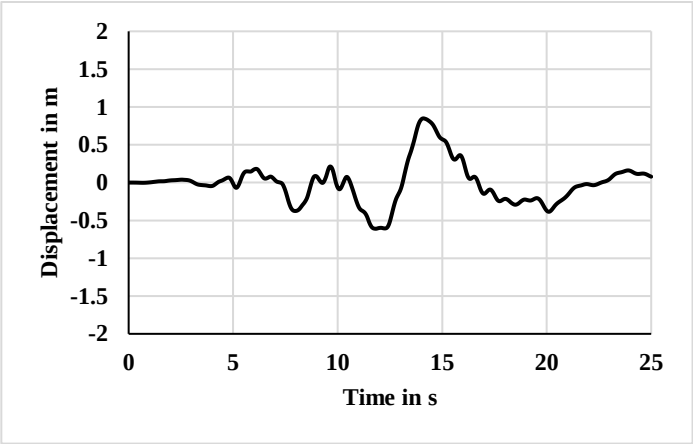

Figure 4.6.65. Displacement time-history for Roof of G+4 building on Soil 6 under Loma prieta earthquake

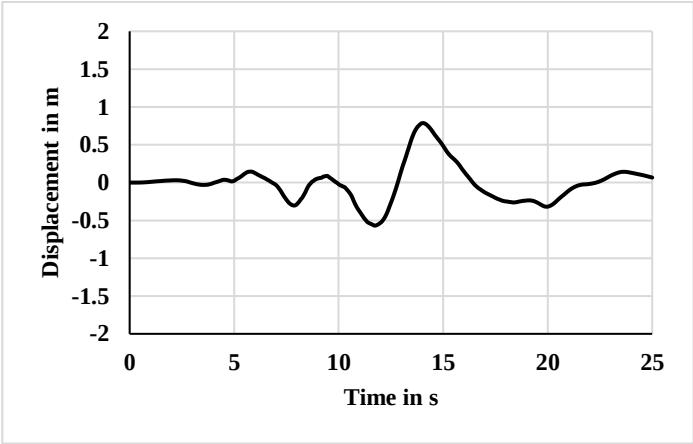

Figure 4.6.66. Displacement time-history for Base of G+4 building on Soil 6 under Loma prieta earthquake

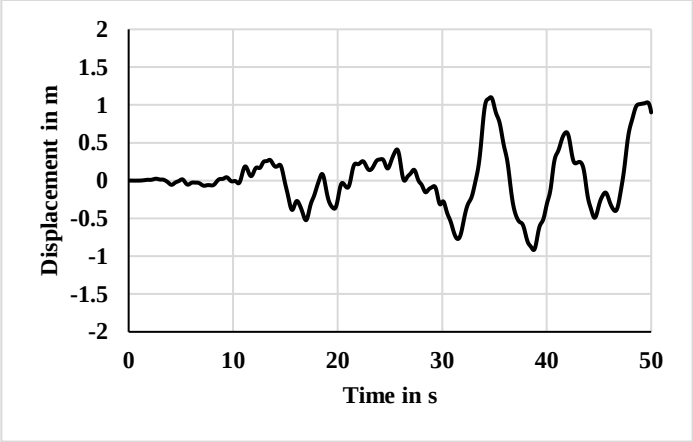

Figure 4.6.67. Displacement time-history for Roof of G+4 building on Soil 6 under Denali earthquake

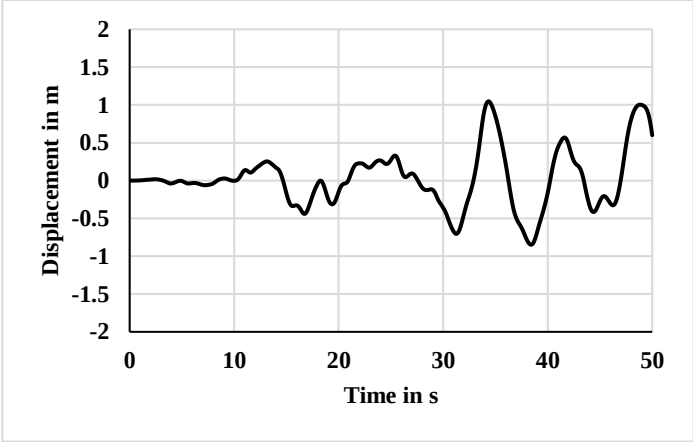

Figure 4.6.68. Displacement time-history for Base of G+4 building on Soil 6 under Denali earthquake

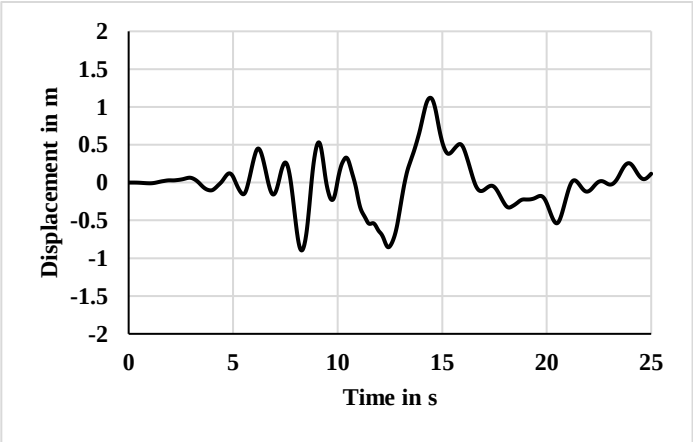

Figure 4.6.69. Displacement time-history for Roof of G+9 building on Soil 6 under Loma prieta earthquake

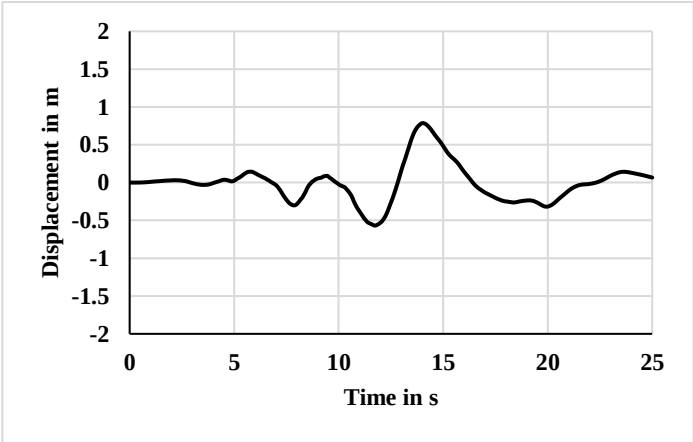

Figure 4.6.70. Displacement time-history for Base of G+9 building on Soil 6 under Loma prieta earthquake

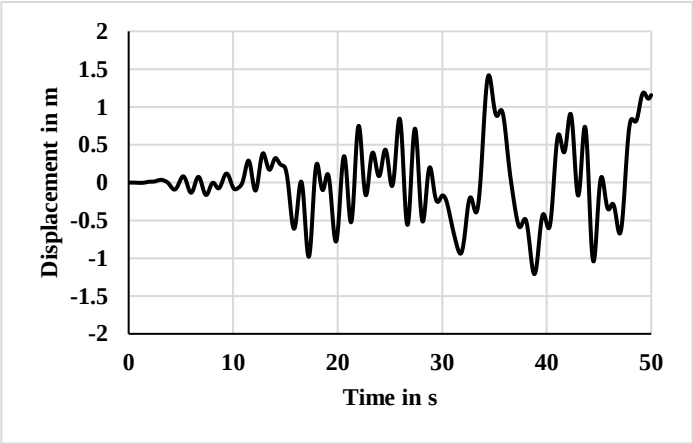

Figure 4.6.71. Displacement time-history for Roof of G+9 building on Soil 6 under Denali earthquake

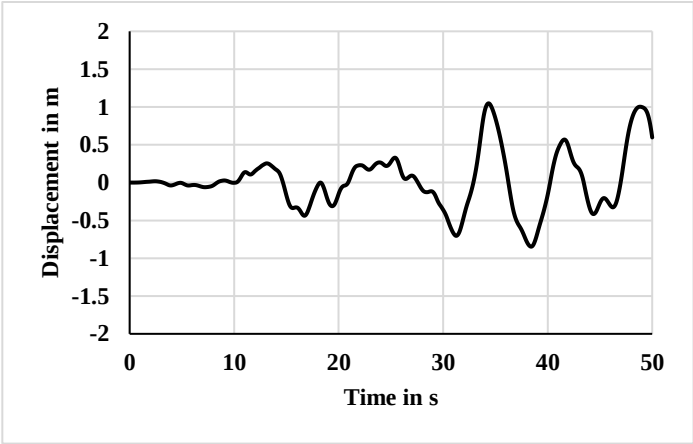

Figure 4.6.72. Displacement time-history for Base of G+9 building on Soil 6 under Denali earthquake

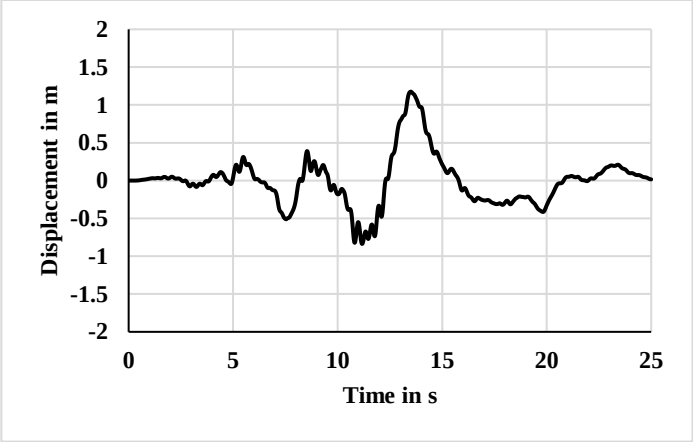

Figure 4.6.73. Displacement time-history for Roof of G+1 building on Soil 7 under Loma prieta earthquake

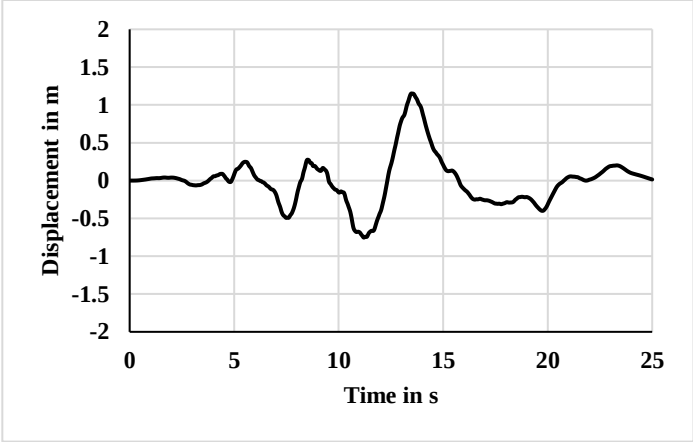

Figure 4.6.74. Displacement time-history for Base of G+1 building on Soil 7 under Loma prieta earthquake

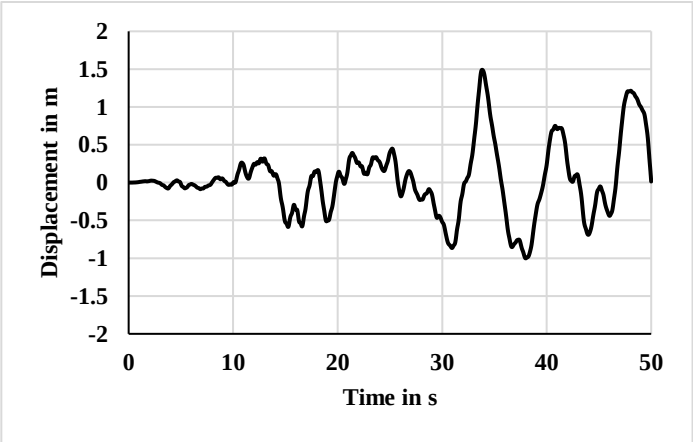

Figure 4.6.75. Displacement time-history for Roof of G+1 building on Soil 7 under Denali earthquake

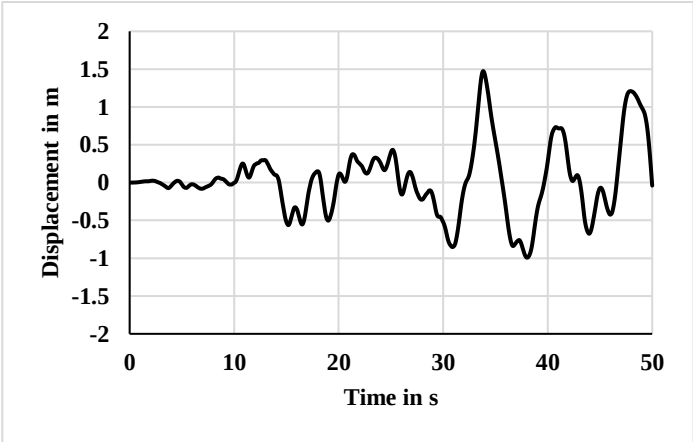

Figure 4.6.76. Displacement time-history for Base of G+1 building on Soil 7 under Denali earthquake

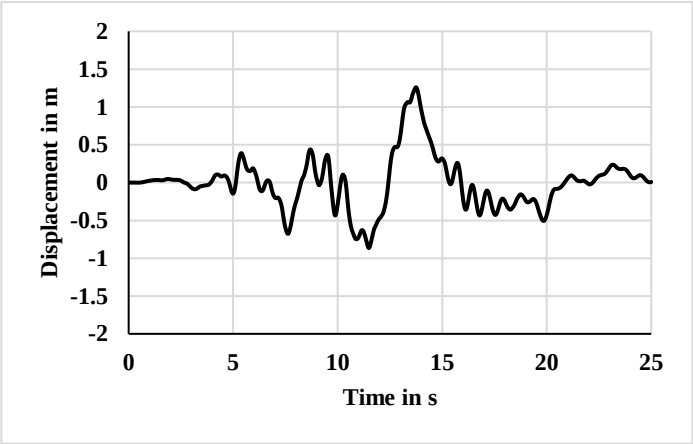

Figure 4.6.77. Displacement time-history for Roof of G+4 building on Soil 7 under Loma prieta earthquake

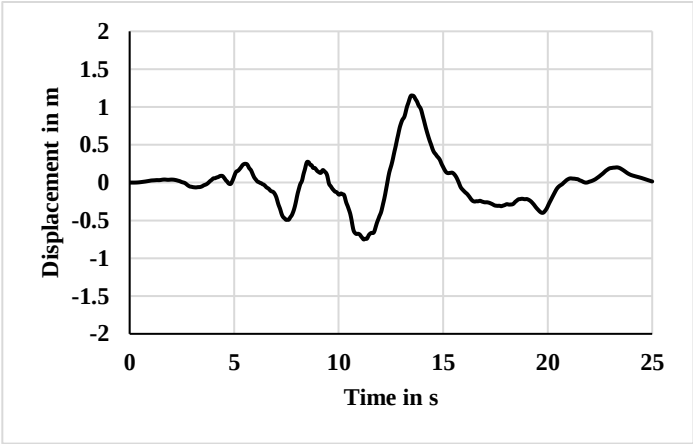

Figure 4.6.78. Displacement time-history for Base of G+4 building on Soil 7 under Loma prieta earthquake

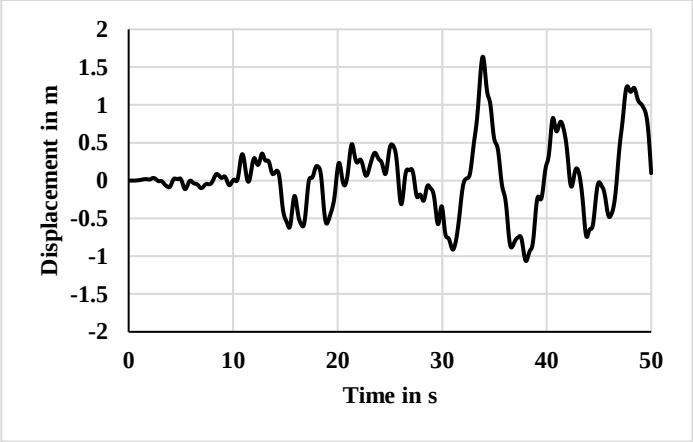

Figure 4.6.79. Displacement time-history for Roof of G+4 building on Soil 7 under Denali earthquake

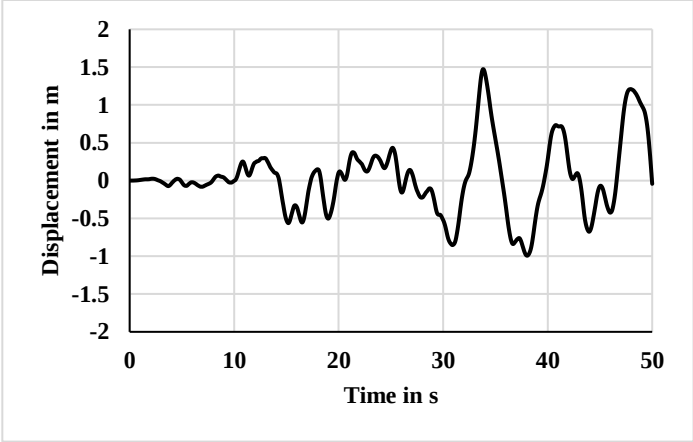

Figure 4.6.80. Displacement time-history for Base of G+4 building on Soil 7 under Denali earthquake

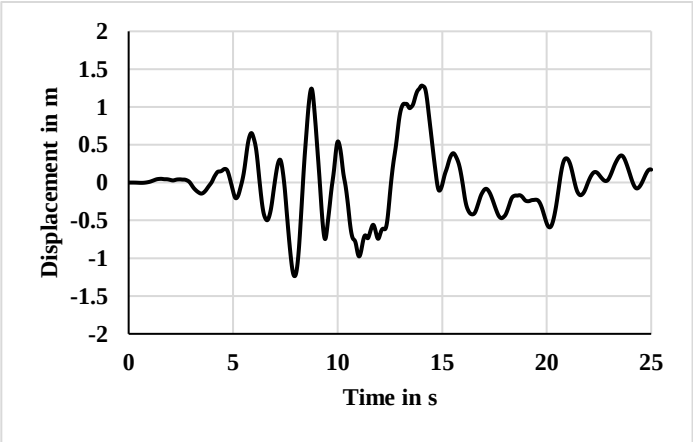

Figure 4.6.81. Displacement time-history for Roof of G+9 building on Soil 7 under Loma prieta earthquake

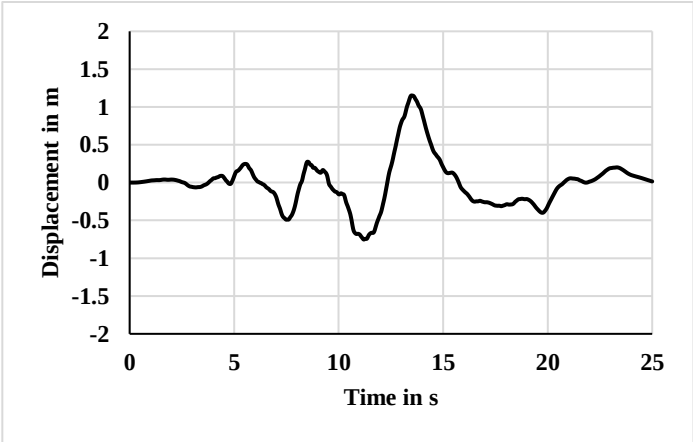

Figure 4.6.82. Displacement time-history for Base of G+9 building on Soil 7 under Loma prieta earthquake

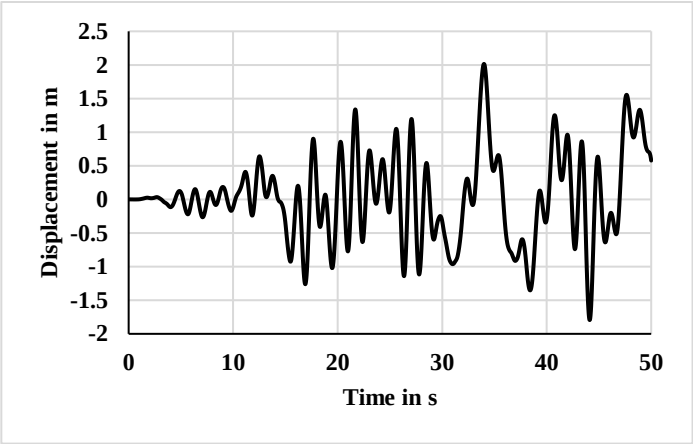

Figure 4.6.83. Displacement time-history for Roof of G+9 building on Soil 7 under Denali earthquake

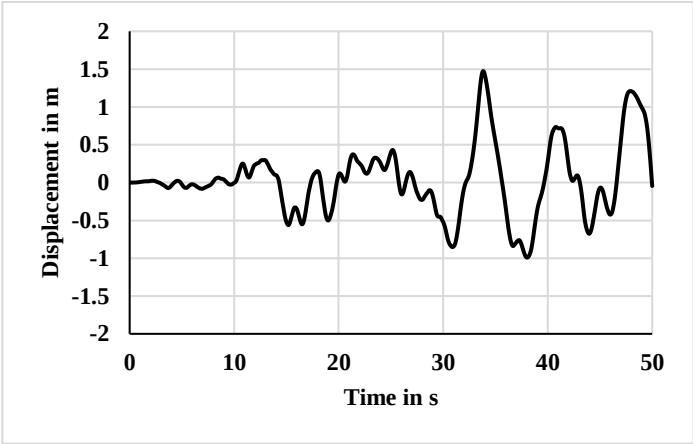

Figure 4.6.84. Displacement time-history for Base of G+9 building on Soil 7 under Denali earthquake

4.7. MAXIMUM DISPLACEMENT PROFILES

The maximum displacement profiles for all the buildings, plotted as described in Chapter 3, have been presented in Figure 4.7.1. to Figure 4.7.42. The figures clearly reveal that irrespective of the type of soil and structure, when any soil-structure system is subjected to a far-field earthquake like Denali earthquake, the shape of the maximum displacement profile is concave upward. Further, under Denali earthquake, maximum displacements of the floors always increase monotonically with their heights. This may be presence of only low frequency seismic wave in far field earthquake. However, under the action of a near-field earthquake, such as, Loma prieta earthquake, the shape of the maximum displacement profile of a building purely depends upon the type of soil and structure and thus cannot be predicted. Moreover, when subjected to Loma prieta earthquake, in some cases (e.g. G+4 building on Soil 1 Soil 2 and Soil 7; G+9 building on Soil 1, Soil 2, Soil 3, Soil 4 and Soil 7), the maximum displacements of the floors first decreases and then increases with the increment of height. This may be due to presence of seismic wave of all frequency content.

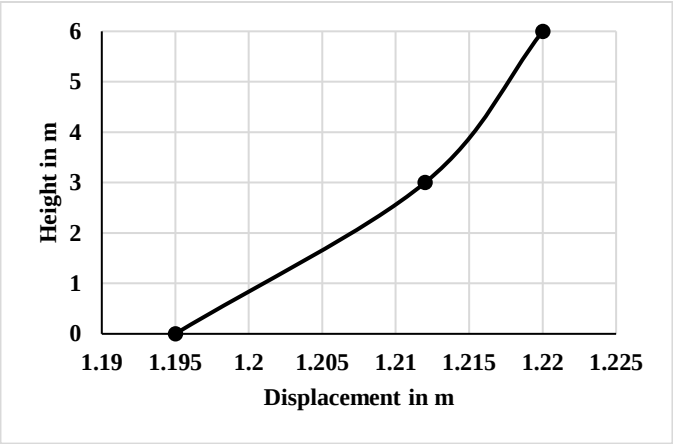

Figure 4.7.1. Maximum displacements of different floors of G+1 building on Soil 1 under Loma prieta earthquake

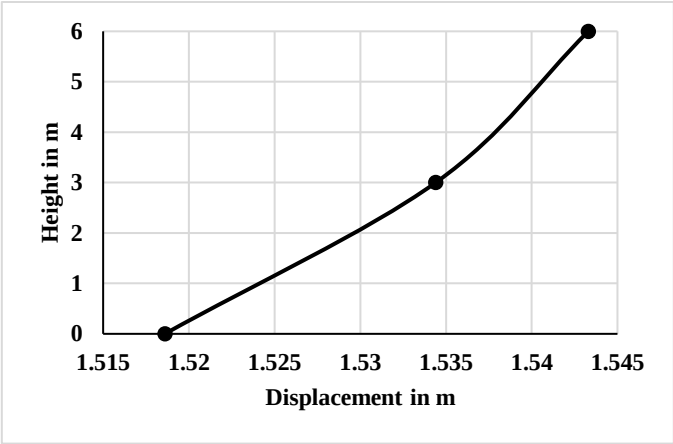

Figure 4.7.2. Maximum displacements of different floors of G+1 building on Soil 1 under Denali earthquake

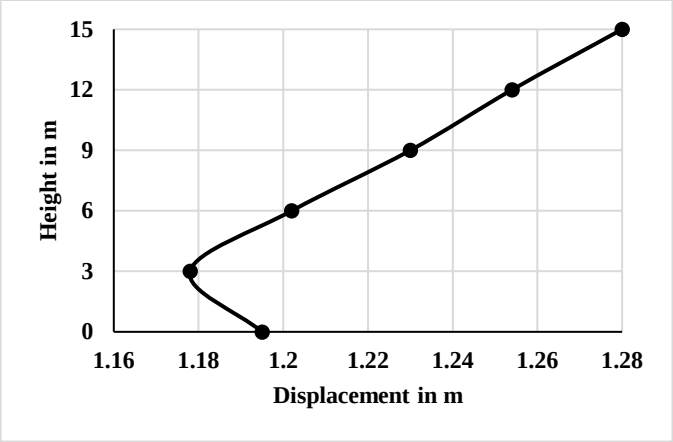

Figure 4.7.3. Maximum displacements of different floors of G+4 building on Soil 1 under Loma prieta earthquake

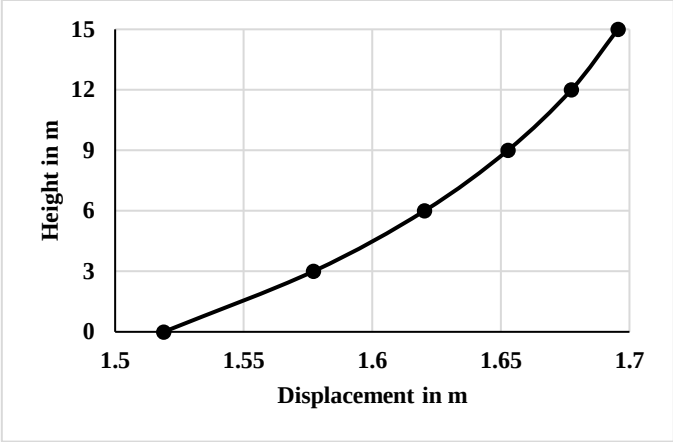

Figure 4.7.4. Maximum displacements of different floors of G+4 building on Soil 1 under Denali earthquake

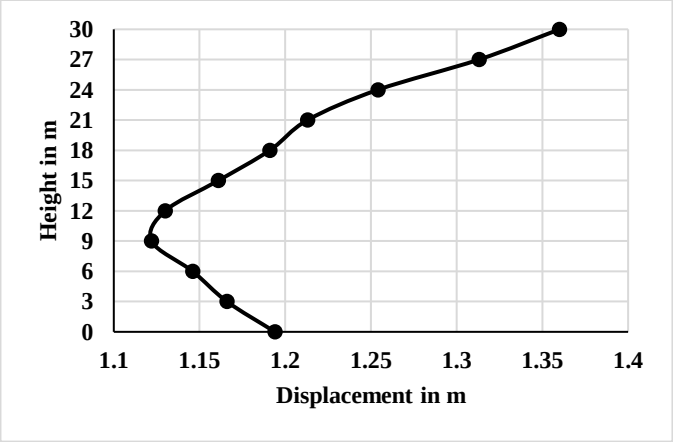

Figure 4.7.5. Maximum displacements of different floors of G+9 building on Soil 1 under Loma prieta earthquake

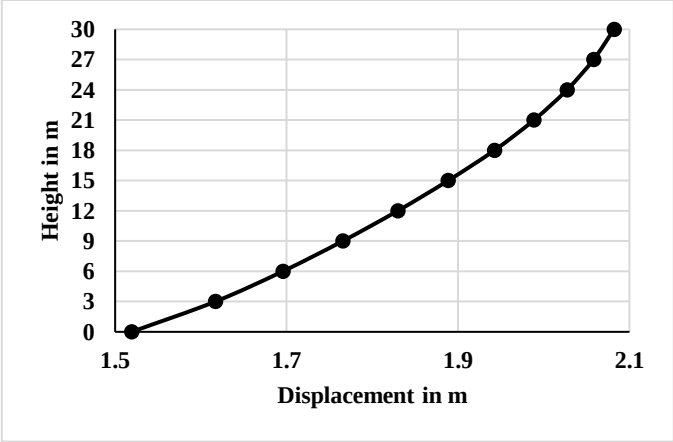

Figure 4.7.6. Maximum displacements of different floors of G+9 building on Soil 1 under Denali earthquake

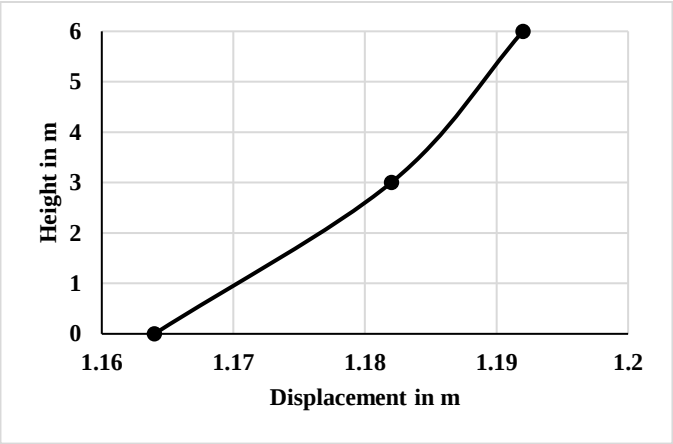

Figure 4.7.7. Maximum displacements of different floors of G+1 building on Soil 2 under Loma prieta earthquake

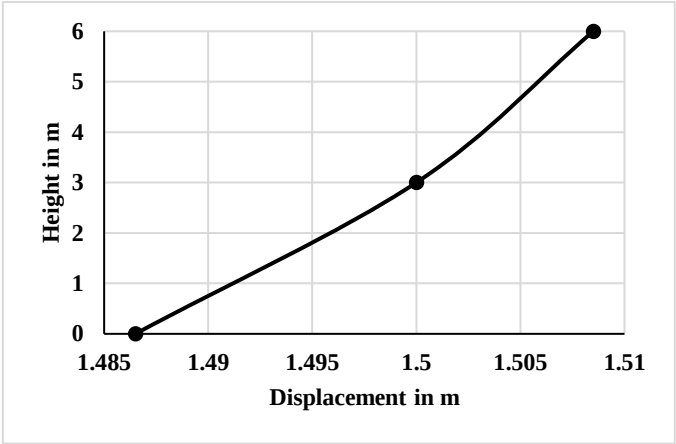

Figure 4.7.8. Maximum displacements of different floors of G+1 building on Soil 2 under Denali earthquake

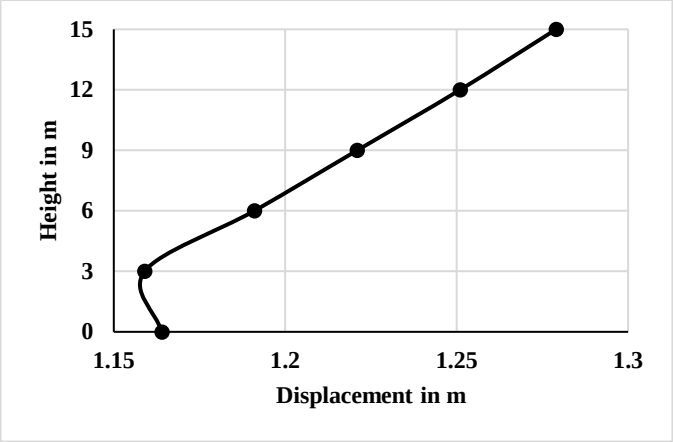

Figure 4.7.9. Maximum displacements of different floors of G+4 building on Soil 2 under Loma prieta earthquake

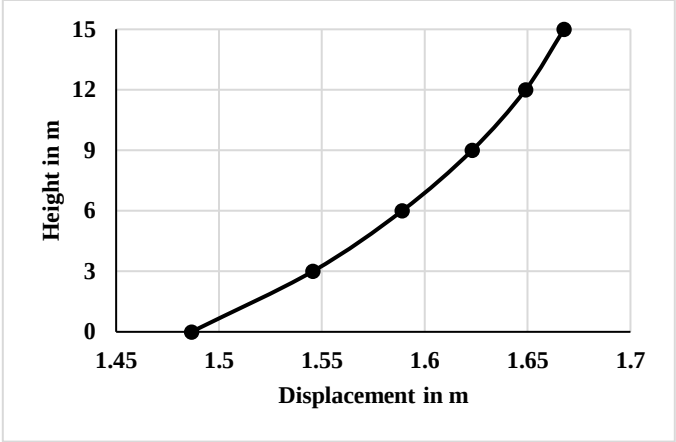

Figure 4.7.10. Maximum displacements of different floors of G+4 building on Soil 2 under Denali earthquake

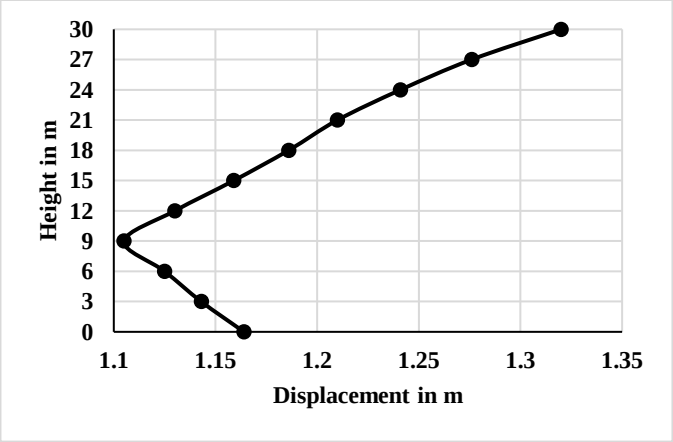

Figure 4.7.11. Maximum displacements of different floors of G+9 building on Soil 2 under Loma prieta earthquake

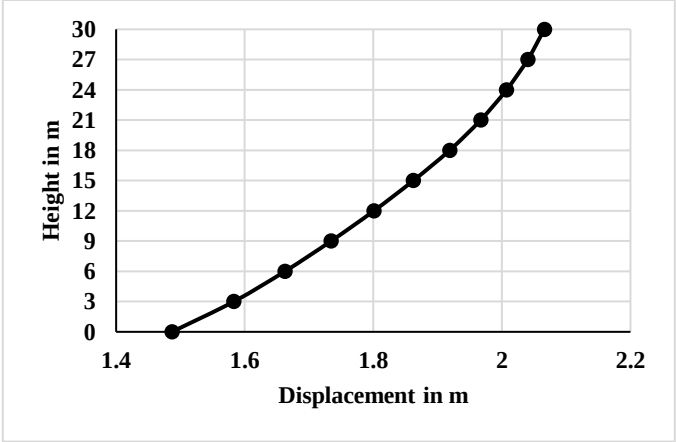

Figure 4.7.12. Maximum displacements of different floors of G+9 building on Soil 2 under Denali earthquake

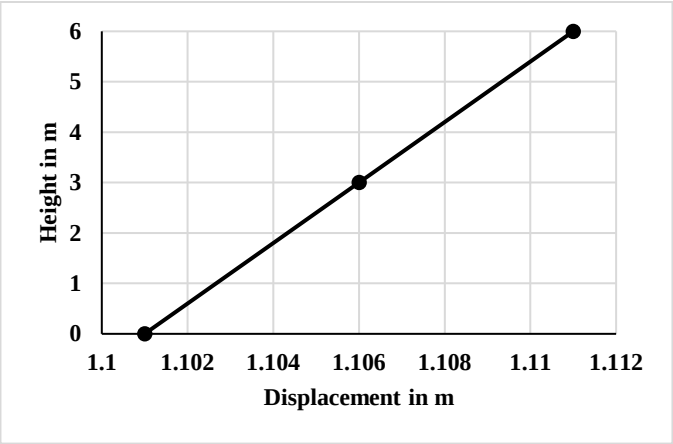

Figure 4.7.13. Maximum displacements of different floors of G+1 building on Soil 3 under Loma prieta earthquake

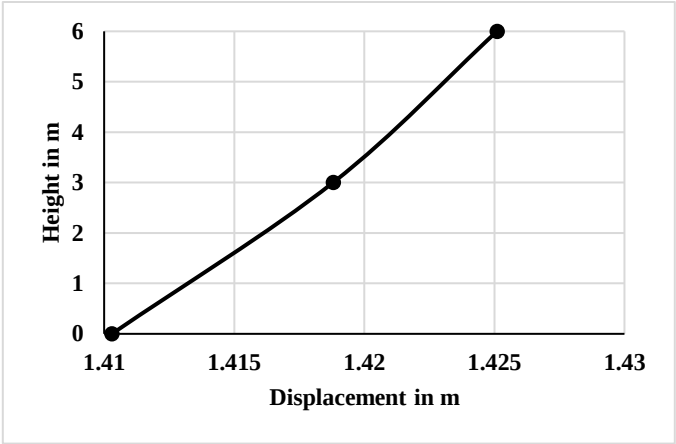

Figure 4.7.14. Maximum displacements of different floors of G+1 building on Soil 3 under Denali earthquake

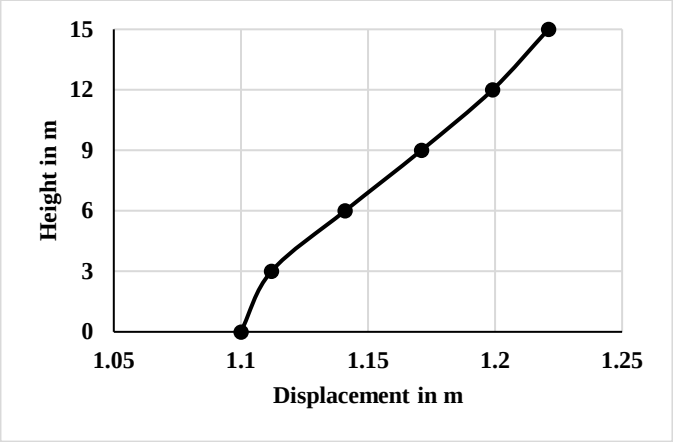

Figure 4.7.15. Maximum displacements of different floors of G+4 building on Soil 3 under Loma prieta earthquake

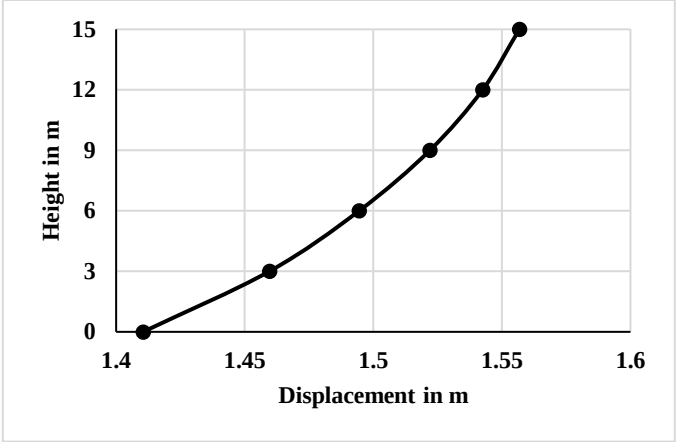

Figure 4.7.16. Maximum displacements of different floors of G+4 building on Soil 3 under Denali earthquake

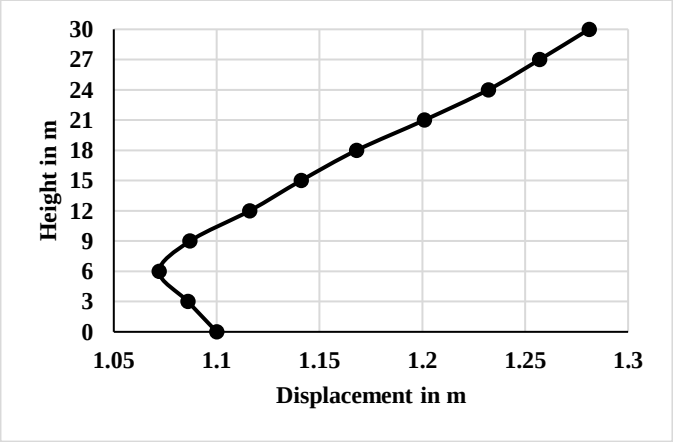

Figure 4.7.17. Maximum displacements of different floors of G+9 building on Soil 3 under Loma prieta earthquake

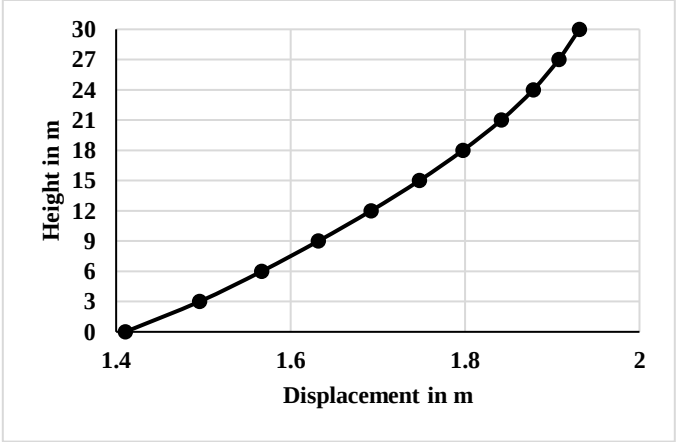

Figure 4.7.18. Maximum displacements of different floors of G+9 building on Soil 3 under Denali earthquake

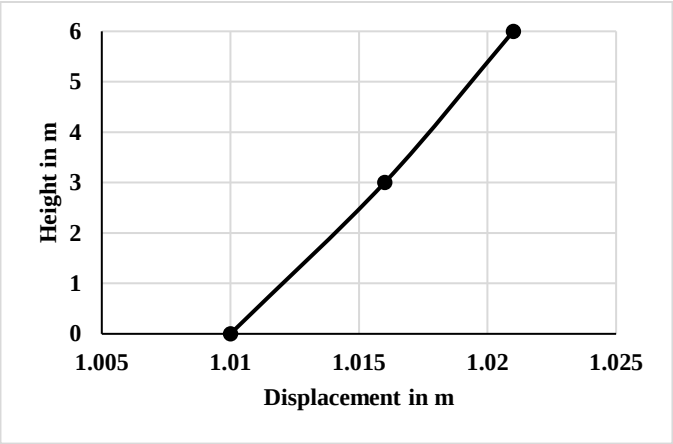

Figure 4.7.19. Maximum displacements of different floors of G+1 building on Soil 4 under Loma prieta earthquake

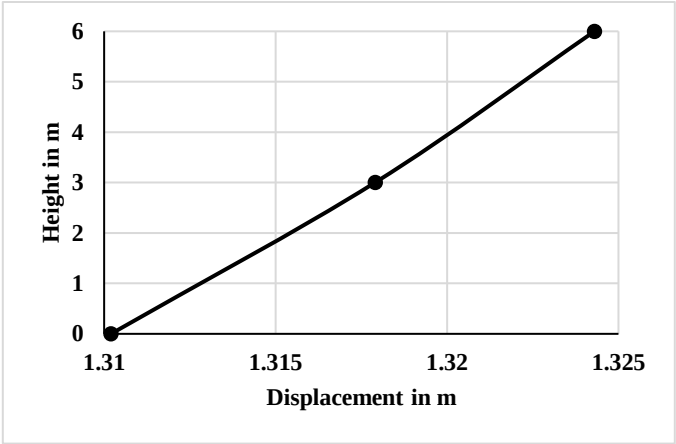

Figure 4.7.20. Maximum displacements of different floors of G+1 building on Soil 4 under Denali earthquake

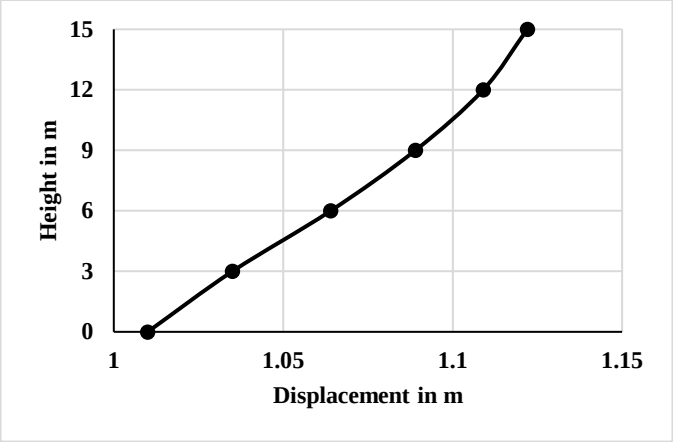

Figure 4.7.21. Maximum displacements of different floors of G+4 building on Soil 4 under Loma prieta earthquake

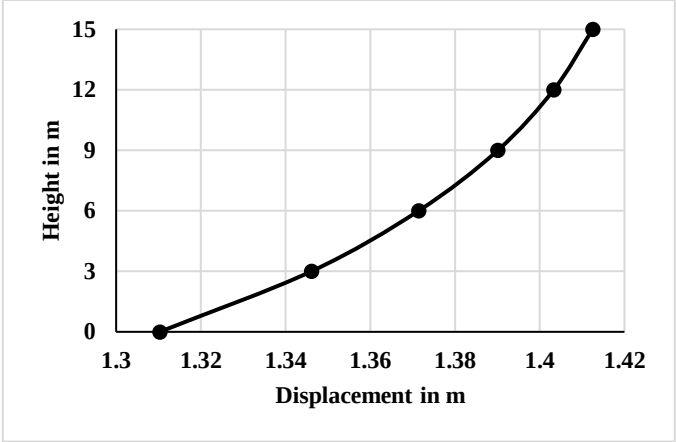

Figure 4.7.22. Maximum displacements of different floors of G+4 building on Soil 4 under Denali earthquake

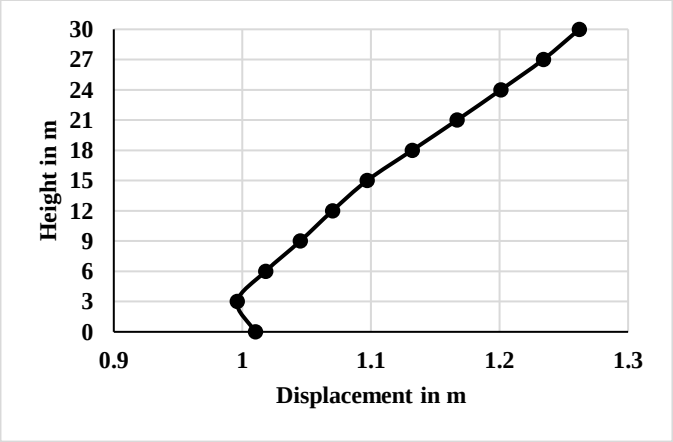

Figure 4.7.23. Maximum displacements of different floors of G+9 building on Soil 4 under Loma prieta earthquake

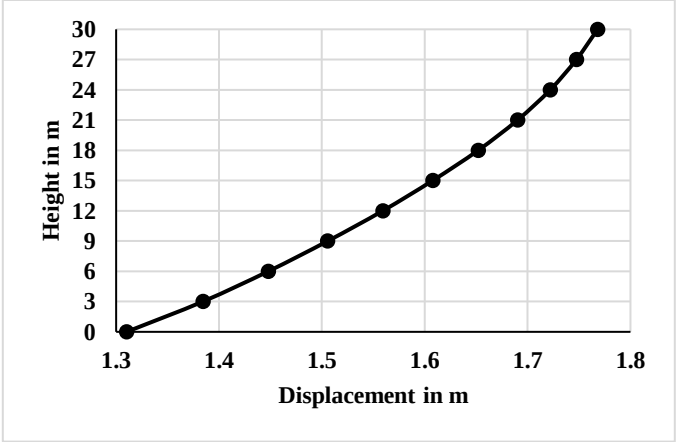

Figure 4.7.24. Maximum displacements of different floors of G+9 building on Soil 4 under Denali earthquake

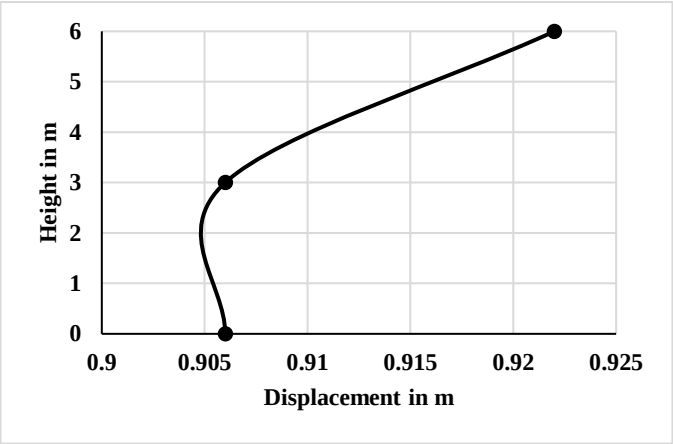

Figure 4.7.25. Maximum displacements of different floors of G+1 building on Soil 5 under Loma prieta earthquake

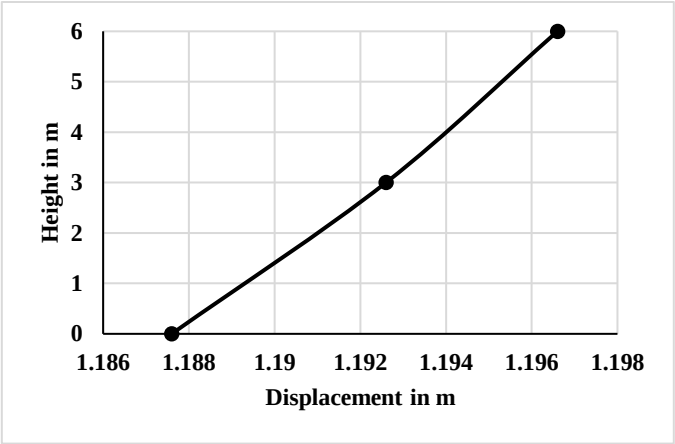

Figure 4.7.26. Maximum displacements of different floors of G+1 building on Soil 5 under Denali earthquake

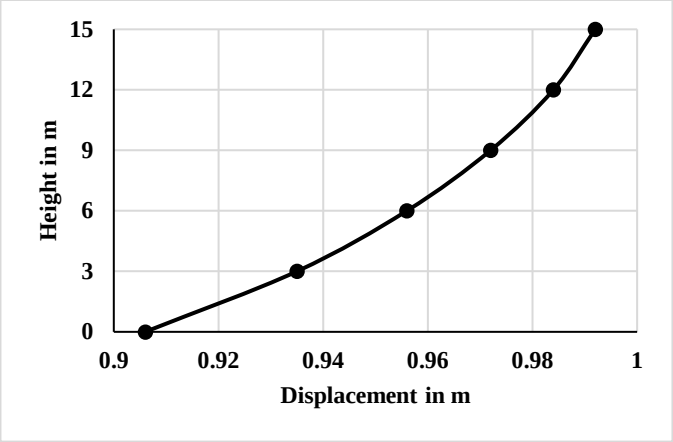

Figure 4.7.27. Maximum displacements of different floors of G+4 building on Soil 5 under Loma prieta earthquake

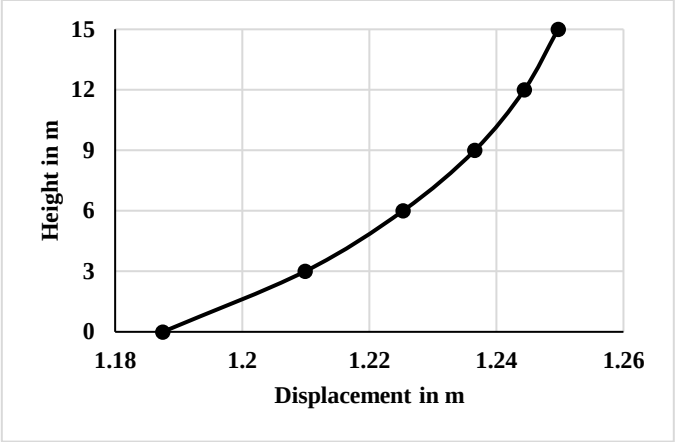

Figure 4.7.28. Maximum displacements of different floors of G+4 building on Soil 5 under Denali earthquake

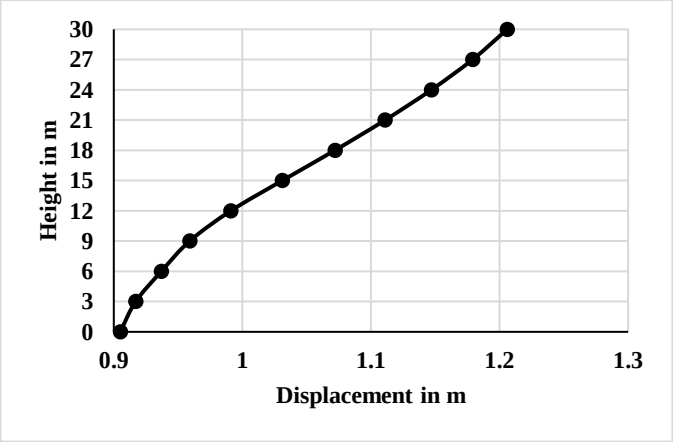

Figure 4.7.29. Maximum displacements of different floors of G+9 building on Soil 5 under Loma prieta earthquake

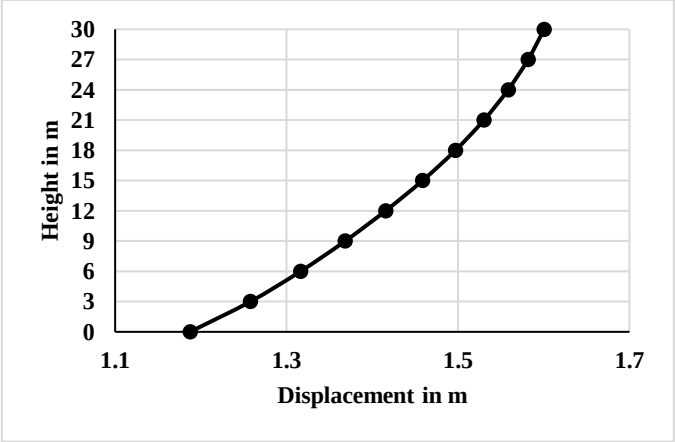

Figure 4.7.30. Maximum displacements of different floors of G+9 building on Soil 5 under Denali earthquake

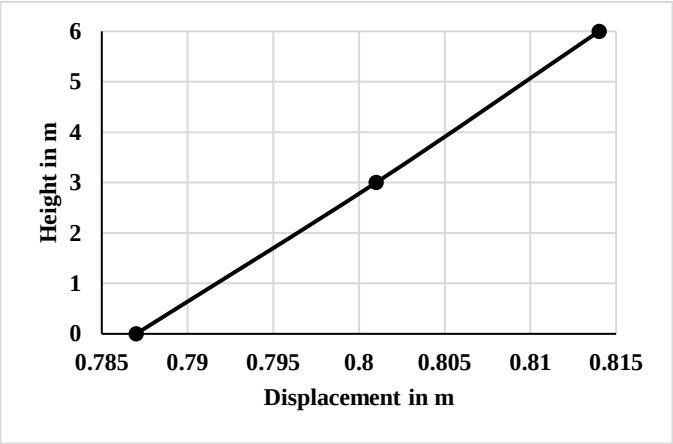

Figure 4.7.31. Maximum displacements of different floors of G+1 building on Soil 6 under Loma prieta earthquake

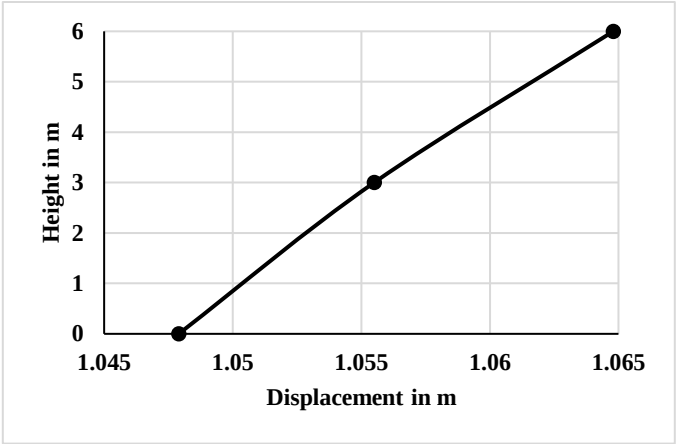

Figure 4.7.32. Maximum displacements of different floors of G+1 building on Soil 6 under Denali earthquake

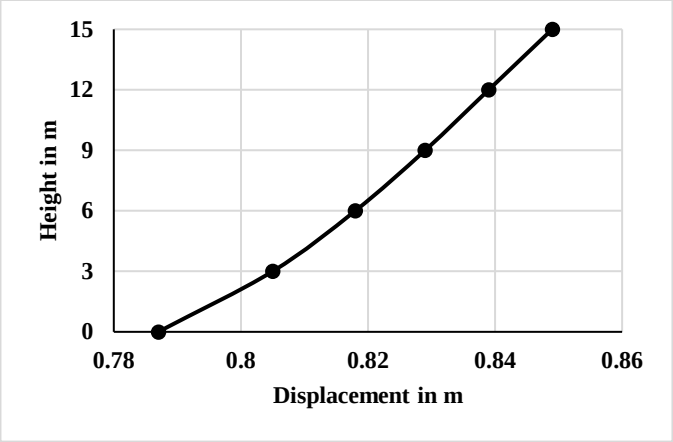

Figure 4.7.33. Maximum displacements of different floors of G+4 building on Soil 6 under Loma prieta earthquake

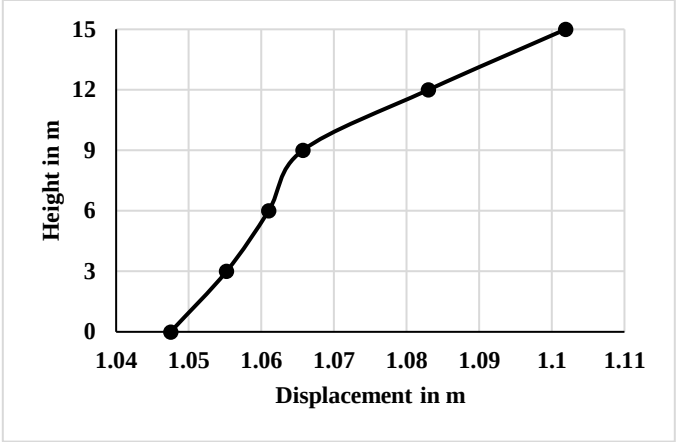

Figure 4.7.34. Maximum displacements of different floors of G+4 building on Soil 6 under Denali earthquake

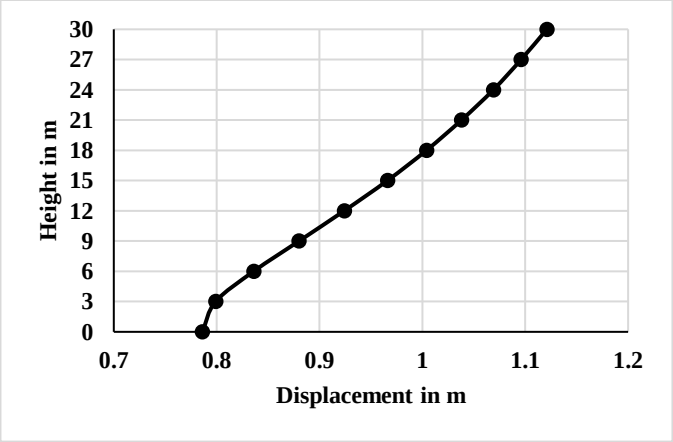

Figure 4.7.35. Maximum displacements of different floors of G+9 building on Soil 6 under Loma prieta earthquake

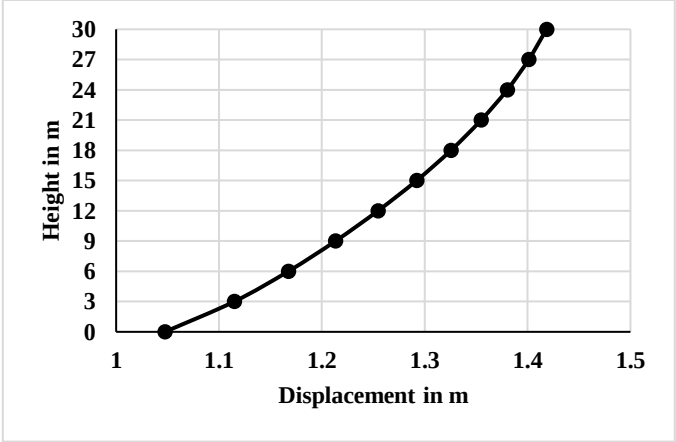

Figure 4.7.36. Maximum displacements of different floors of G+9 building on Soil 6 under Denali earthquake

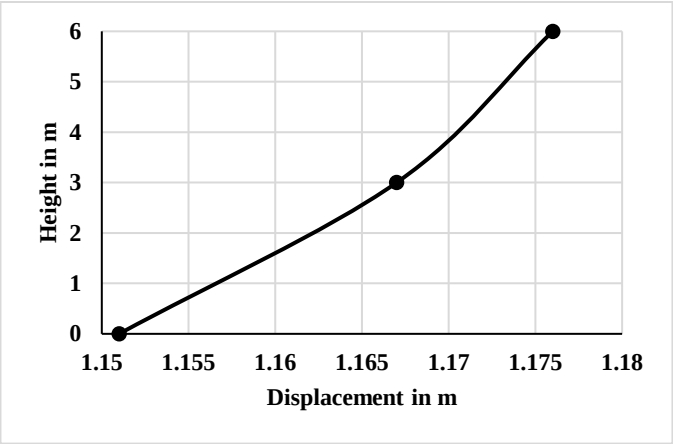

Figure 4.7.37. Maximum displacements of different floors of G+1 building on Soil 7 under Loma prieta earthquake

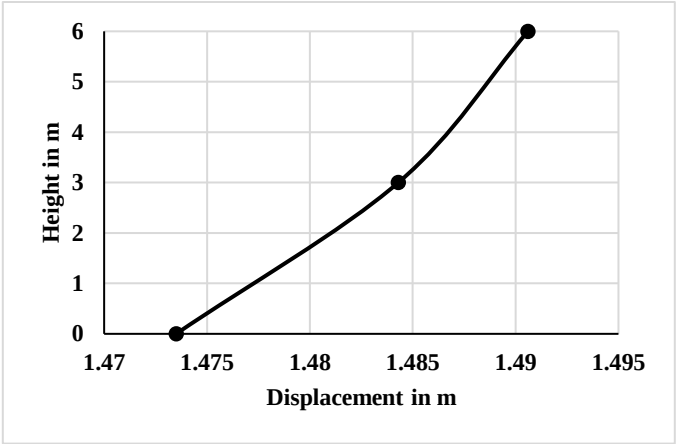

Figure 4.7.38. Maximum displacements of different floors of G+1 building on Soil 7 under Denali earthquake

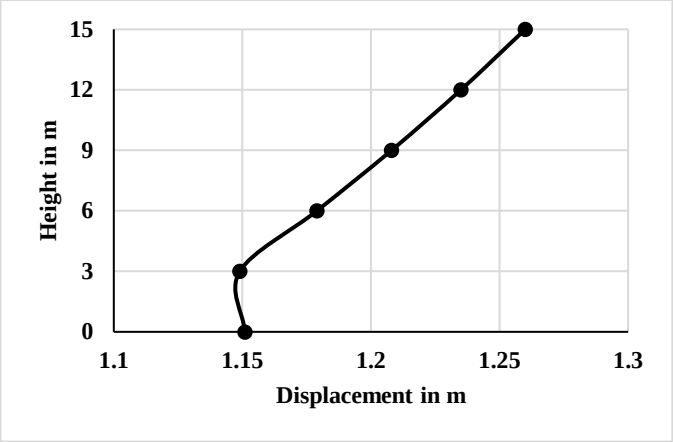

Figure 4.7.39. Maximum displacements of different floors of G+4 building on Soil 7 under Loma prieta earthquake

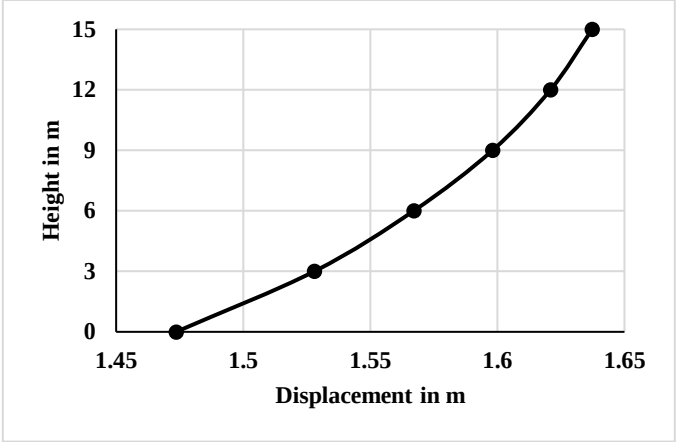

Figure 4.7.40. Maximum displacements of different floors of G+4 building on Soil 7 under Denali earthquake

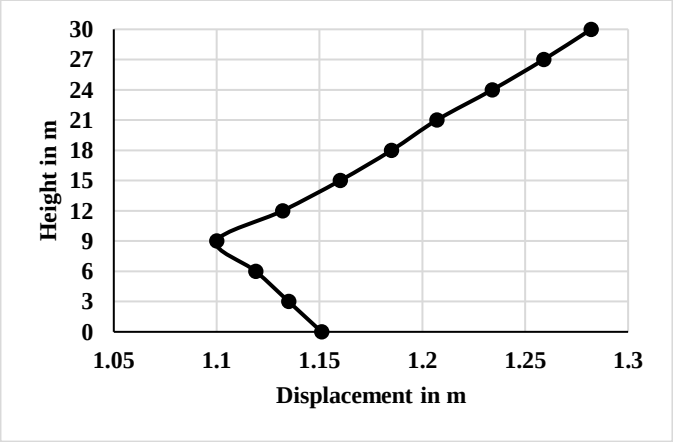

Figure 4.7.41. Maximum displacements of different floors of G+9 building on Soil 7 under Loma prieta earthquake

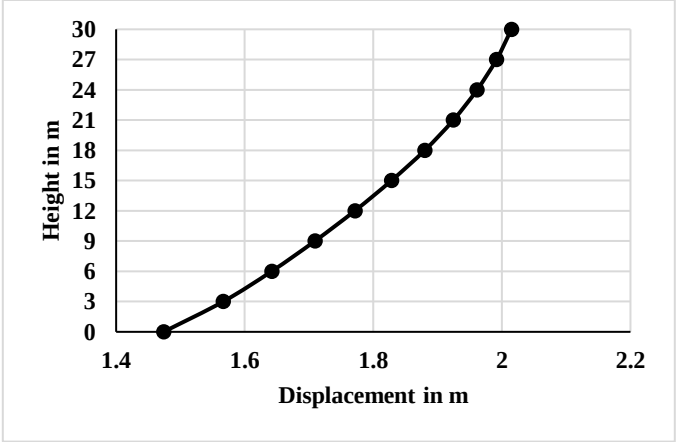

Figure 4.7.42. Maximum displacements of different floors of G+9 building on Soil 7 under Denali earthquake

4.8. FRAGILITY CURVES

In the present study PSDMs and fragility curves have been plotted following the 2000 SAC/FEMA method[35] as discussed in Chapter 3. The developed PSDMs along with the fragility curves are presented in Figure 4.8.1. to Figure 4.8.84. Several conclusions can be drawn after observing the PSDMs and fragility curves of the frame buildings located on layered soil. For all the models, the generated PSDMs are actually straight lines passing through the origin. It is to be noted that under the action of a particular earthquake, the probability of exceedance of CP is the minimum and that of Indian Codal Limit is the maximum. Generally, if the soil type and seismic excitation remain unchanged, the probability of exceeding a particular limit state is the largest for a G+9 building and smallest for a G+1 building. However, when located on Soil 5 and Soil 6, and subjected to a near-field earthquake, a G+4 building has the least probability of exceeding for any limit state. On the contrary, if a near-field earthquake acts on Soil 7, or a far-field earthquake acts on Soil 6 and Soil 7, the highest probability of exceedance is observed in case of G+4 building. Generally, under the action of a near-field earthquake, the limit state exceedance probability is more compared to the far-field earthquake. Exceptionally, when a G+1 building rests on Soil 1, Soil 3 and Soil 4, the probability of exceeding a particular limit state under the far-field earthquake exceeds that under a near-field earthquake.

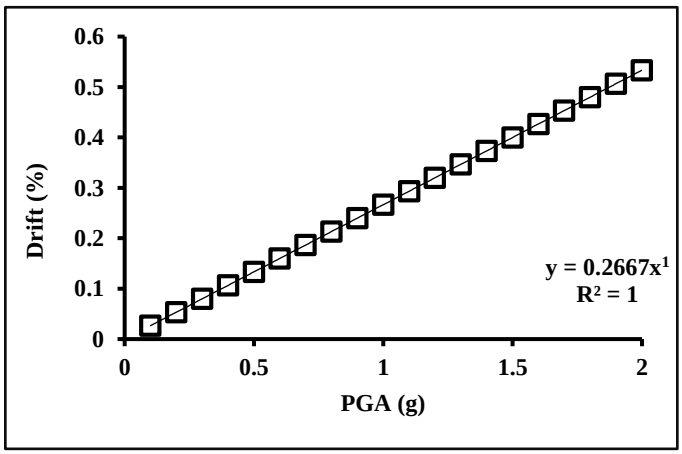

Figure 4.8.1. PSDM for roof of G+1 building on Soil 1 under Loma prieta earthquake

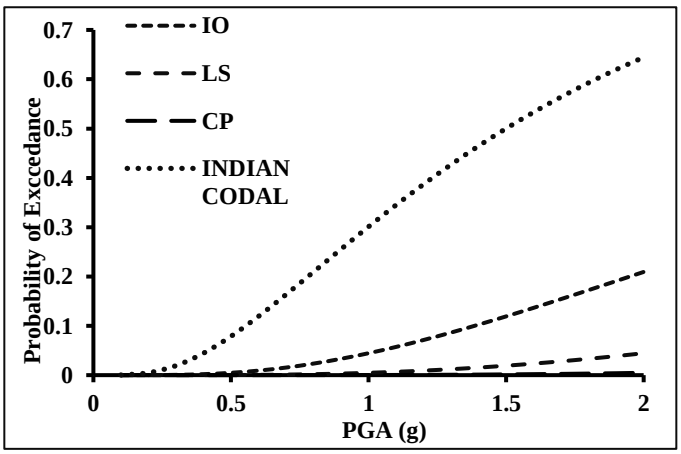

Figure 4.8.2. Fragility curves for roof of G+1 building on Soil 1 under Loma prieta earthquake

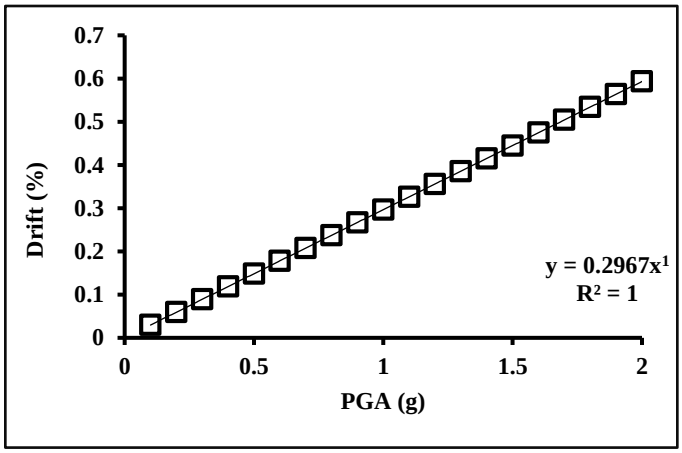

Figure 4.8.3. PSDM for roof of G+1 building on Soil 1 under Denali earthquake

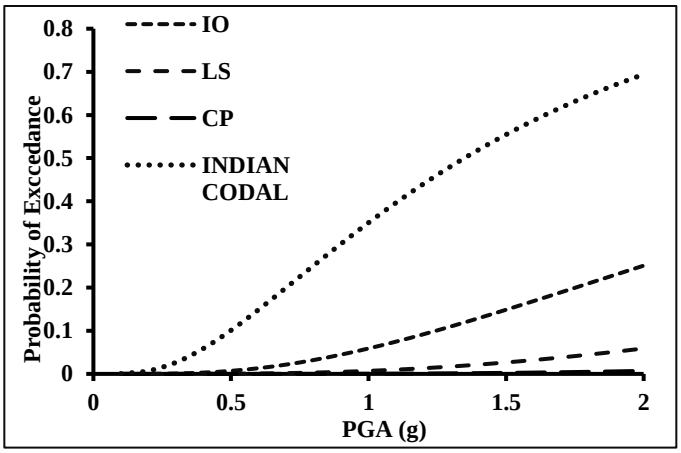

Figure 4.8.4. Fragility curves for roof of G+1 building on Soil 1 under Denali earthquake

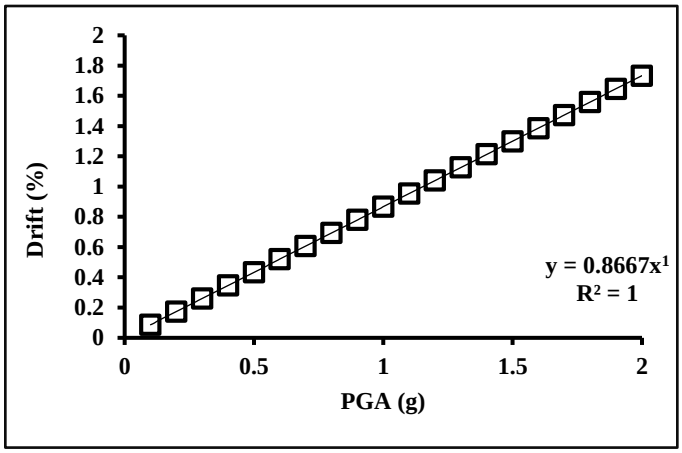

Figure 4.8.5. PSDM for roof of G+4 building on Soil 1 under Loma prieta earthquake

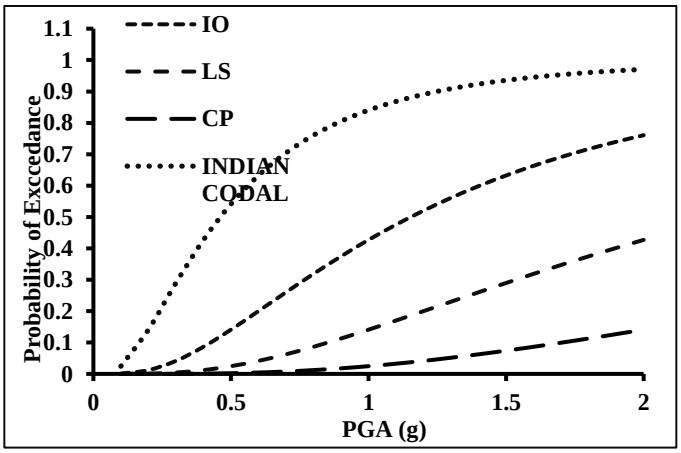

Figure 4.8.6. Fragility curves for roof of G+4 building on Soil 1 under Loma prieta earthquake

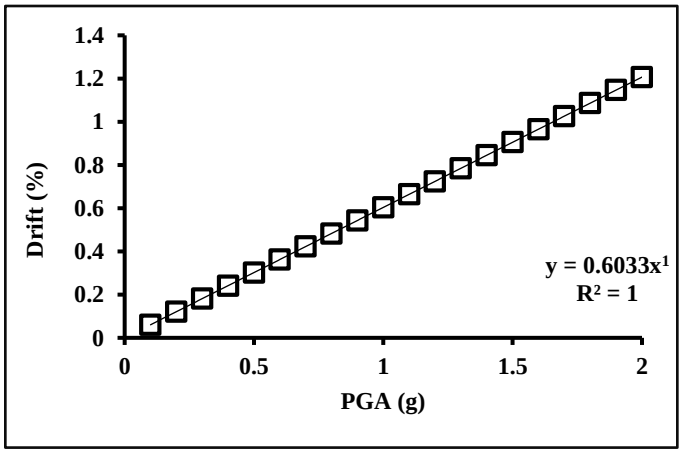

Figure 4.8.7. PSDM for roof of G+4 building on Soil 1 under Denali earthquake

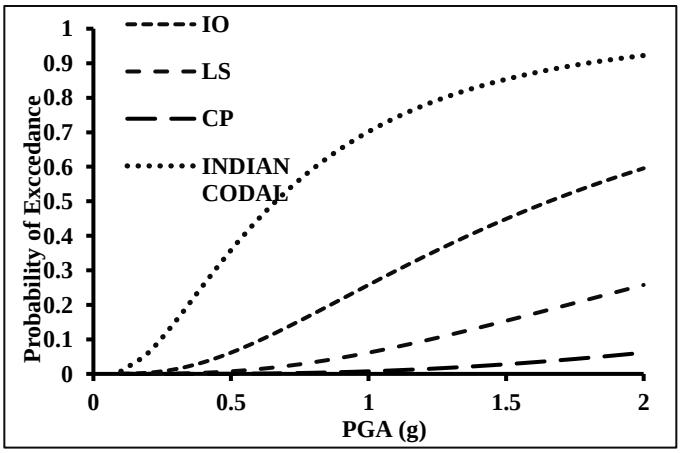

Figure 4.8.8. Fragility curves for roof of G+4 building on Soil 1 under Denali earthquake

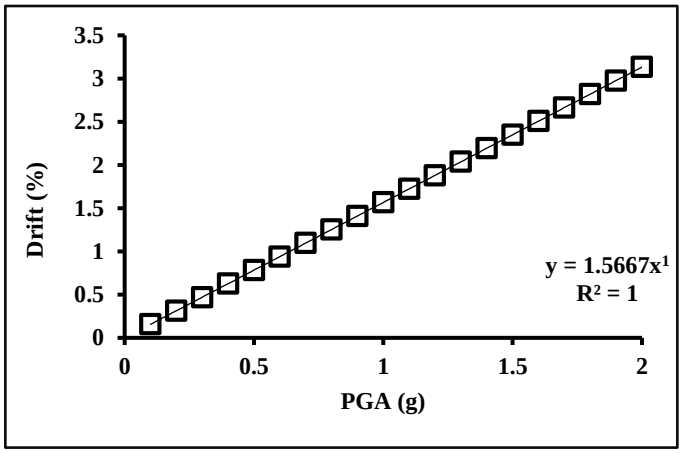

Figure 4.8.9. PSDM for roof of G+9 building on Soil 1 under Loma prieta earthquake

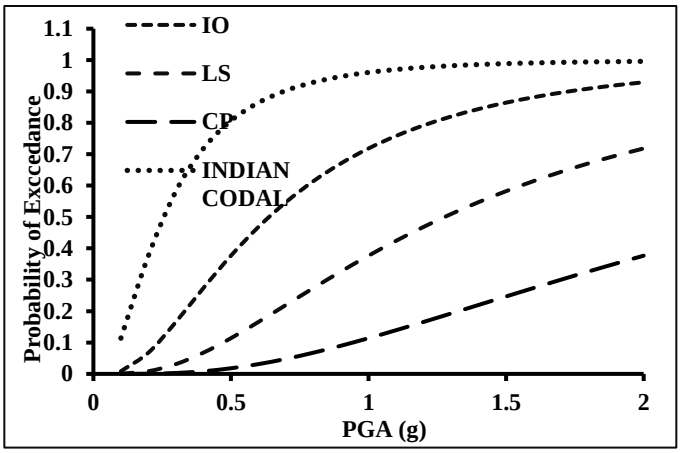

Figure 4.8.10. Fragility curves for roof of G+9 building on Soil 1 under Loma prieta earthquake

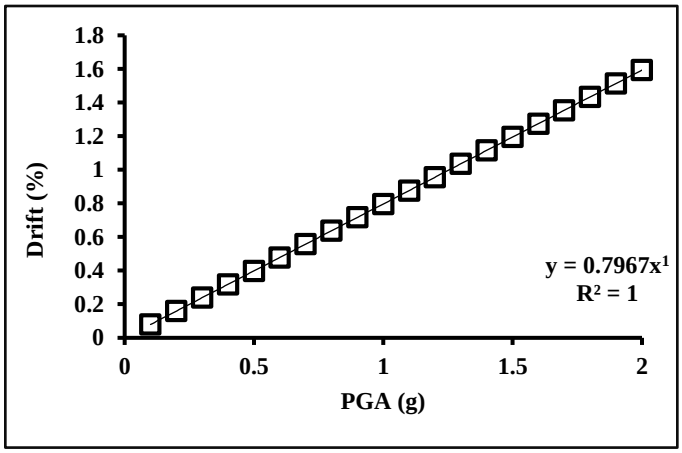

Figure 4.8.11. PSDM for roof of G+9 building on Soil 1 under Denali earthquake

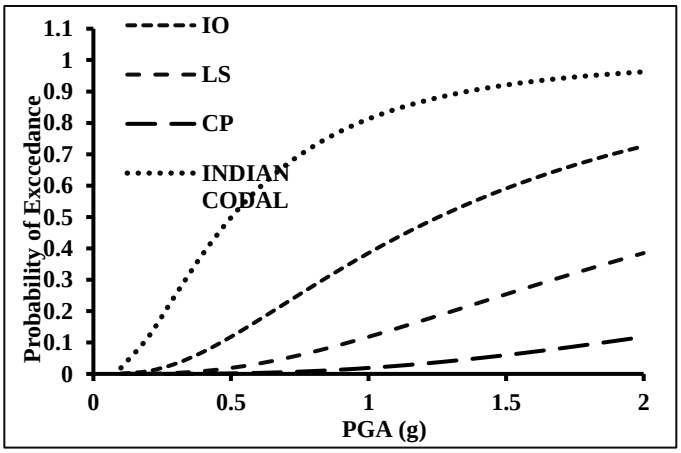

Figure 4.8.12. Fragility curves for roof of G+9 building on Soil 1 under Denali earthquake

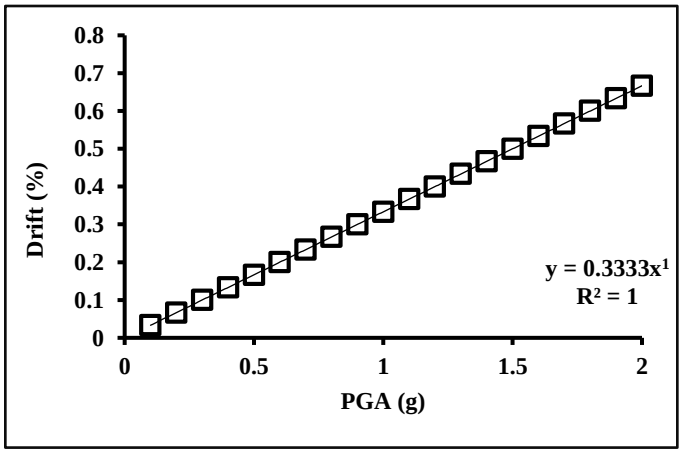

Figure 4.8.13. PSDM for roof of G+1 building on Soil 2 under Loma prieta earthquake

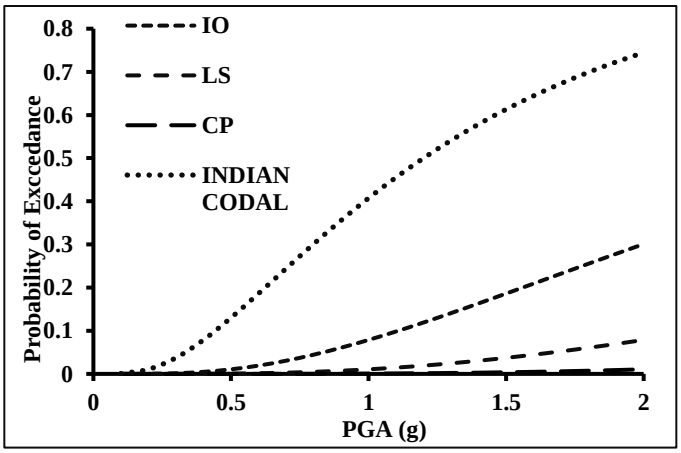

Figure 4.8.14. Fragility curves for roof of G+1 building on Soil 2 under Loma prieta earthquake

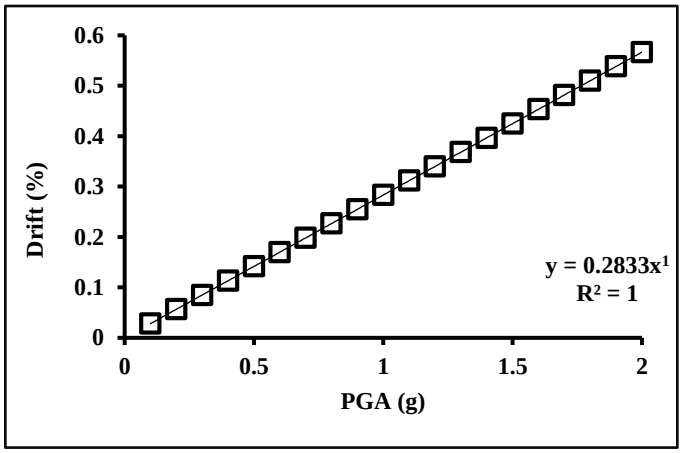

Figure 4.8.15. PSDM for roof of G+1 building on Soil 2 under Denali earthquake

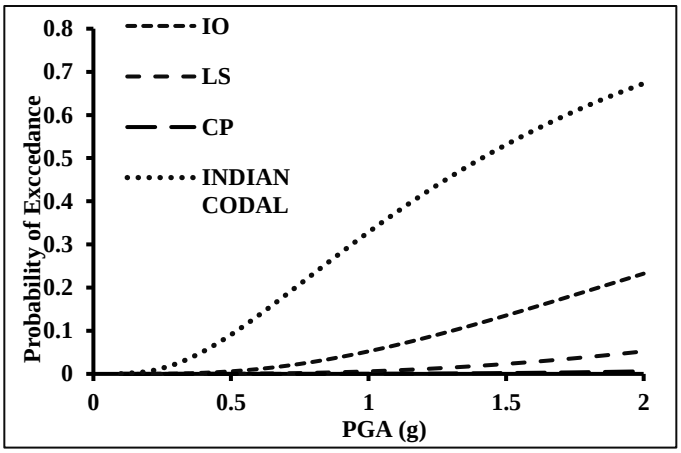

Figure 4.8.16. Fragility curves for roof of G+1 building on Soil 2 under Denali earthquake

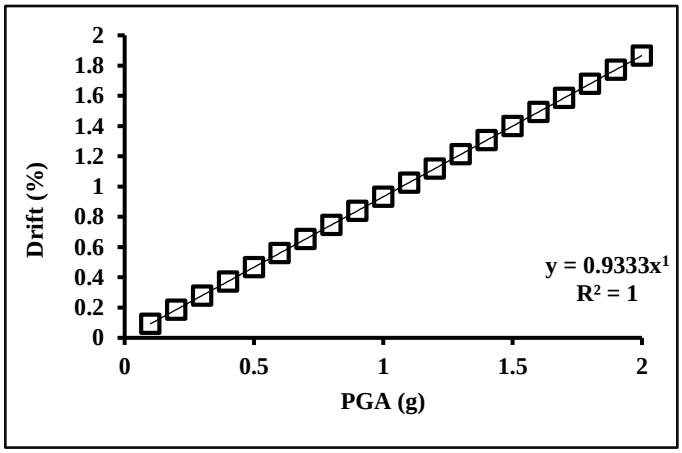

Figure 4.8.17. PSDM for roof of G+4 building on Soil 2 under Loma prieta earthquake

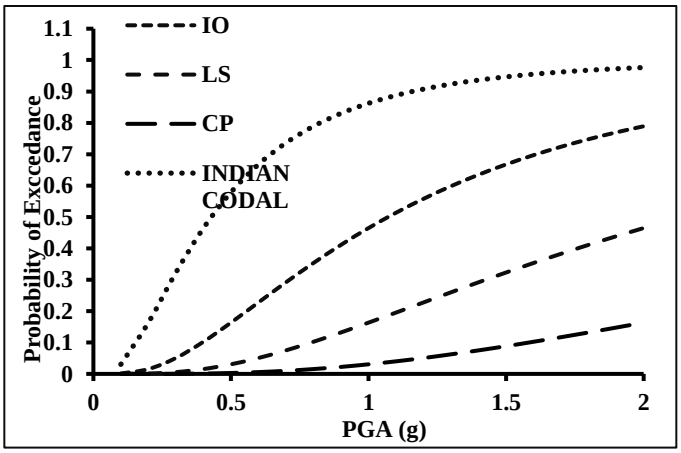

Figure 4.8.18. Fragility curves for roof of G+4 building on Soil 2 under Loma prieta earthquake

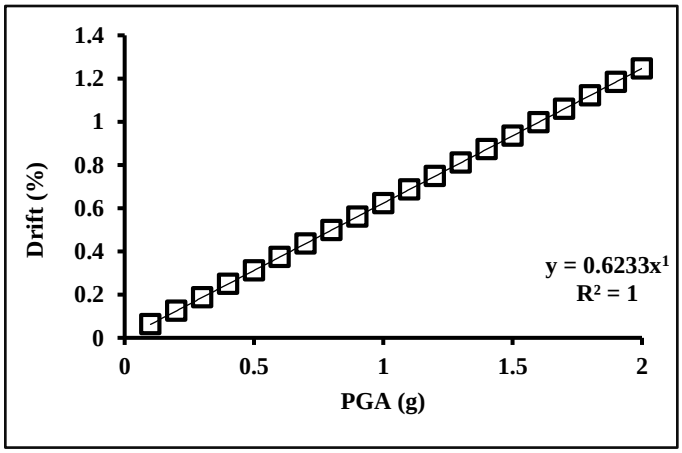

Figure 4.8.19. PSDM for roof of G+4 building on Soil 2 under Denali earthquake

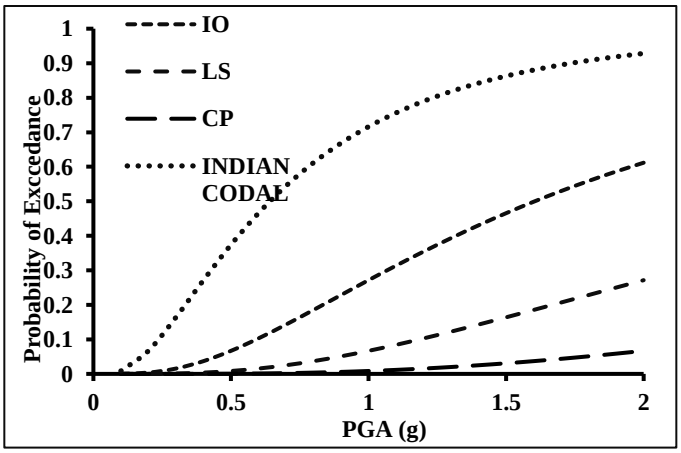

Figure 4.8.20. Fragility curves for roof of G+4 building on Soil 2 under Denali earthquake

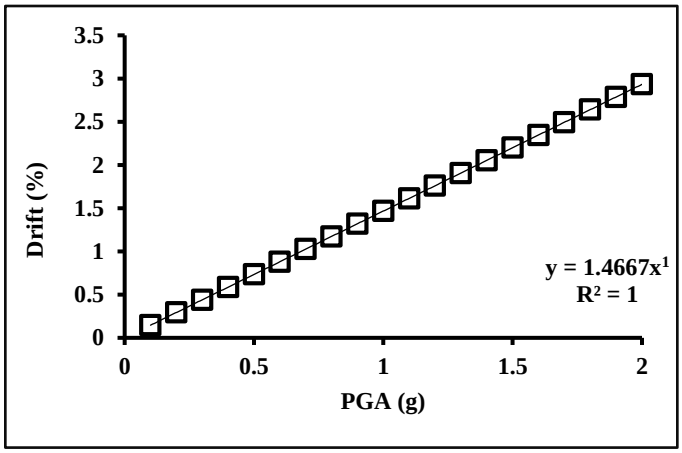

Figure 4.8.21. PSDM for roof of G+9 building on Soil 2 under Loma prieta earthquake

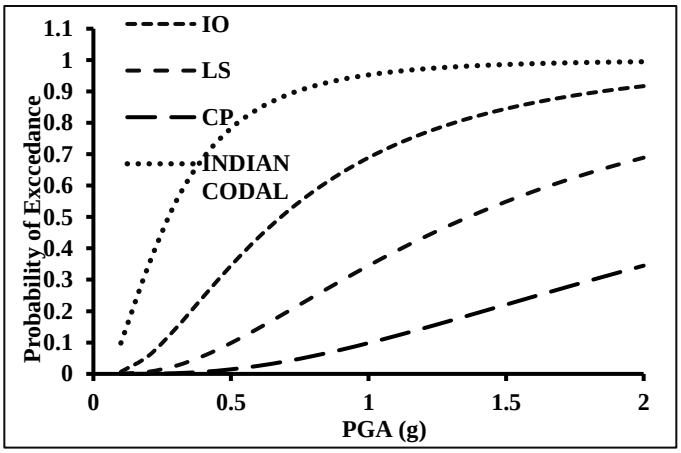

Figure 4.8.22. Fragility curves for roof of G+9 building on Soil 2 under Loma prieta earthquake

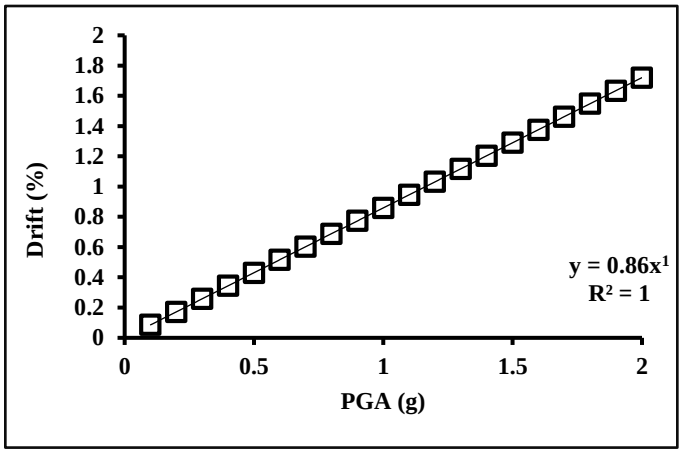

Figure 4.8.23. PSDM for roof of G+9 building on Soil 2 under Denali earthquake

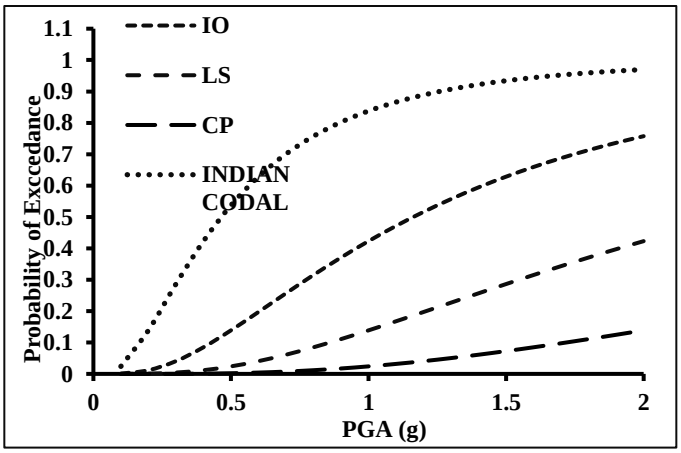

Figure 4.8.24. Fragility curves for roof of G+9 building on Soil 2 under Denali earthquake

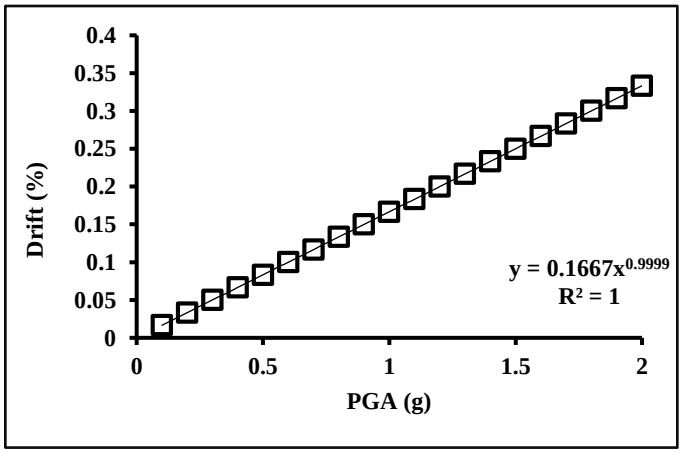

Figure 4.8.25. PSDM for roof of G+1 building on Soil 3 under Loma prieta earthquake

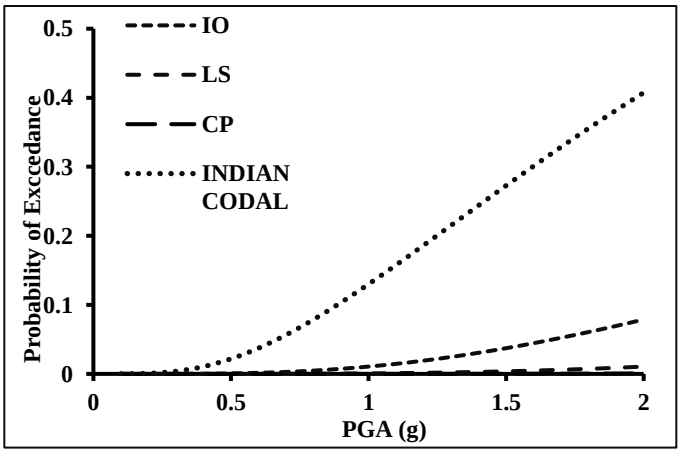

Figure 4.8.26. Fragility curves for roof of G+1 building on Soil 3 under Loma prieta earthquake

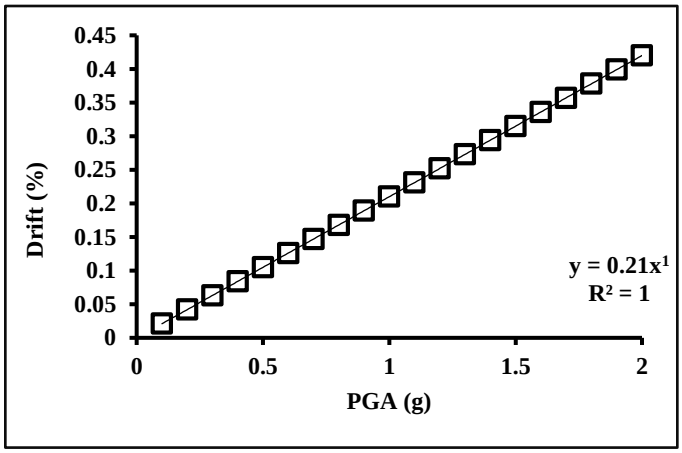

Figure 4.8.27. PSDM for roof of G+1 building on Soil 3 under Denali earthquake

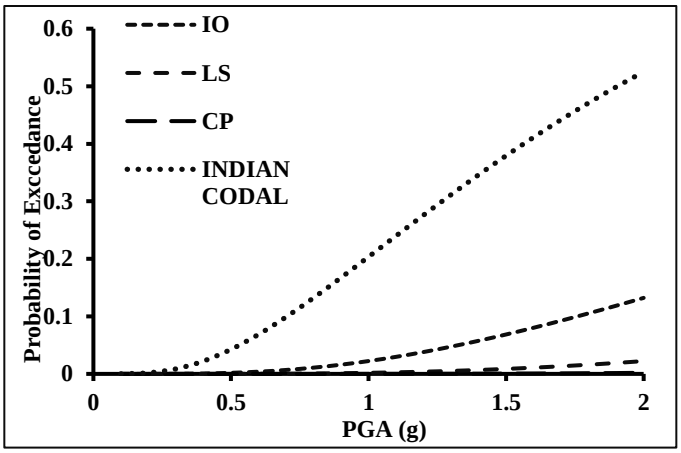

Figure 4.8.28. Fragility curves for roof of G+1 building on Soil 3 under Denali earthquake

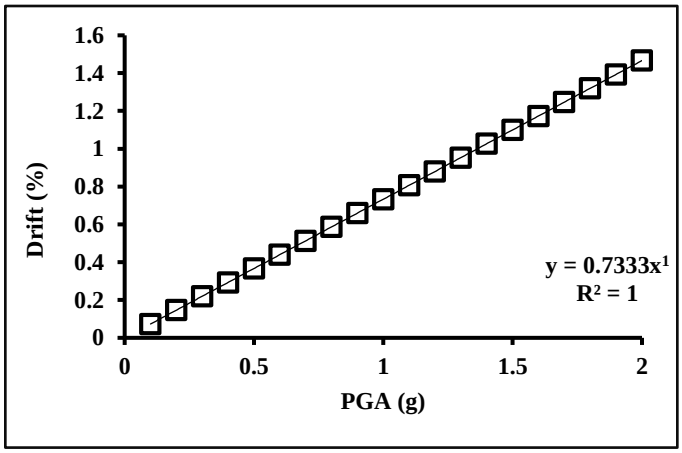

Figure 4.8.29. PSDM for roof of G+4 building on Soil 3 under Loma prieta earthquake

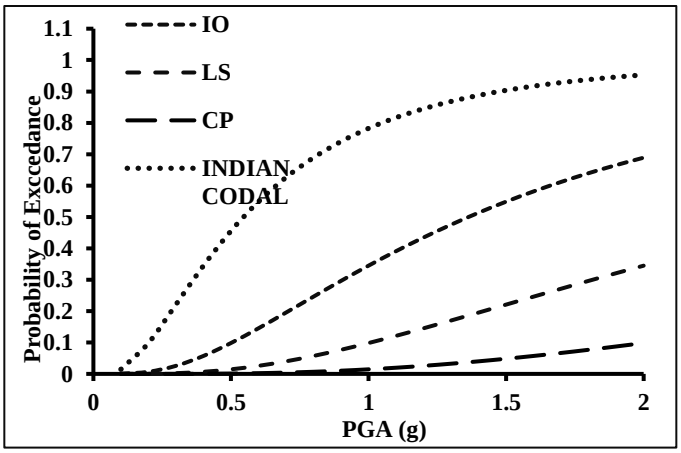

Figure 4.8.30. Fragility curves for roof of G+4 building on Soil 3 under Loma prieta earthquake

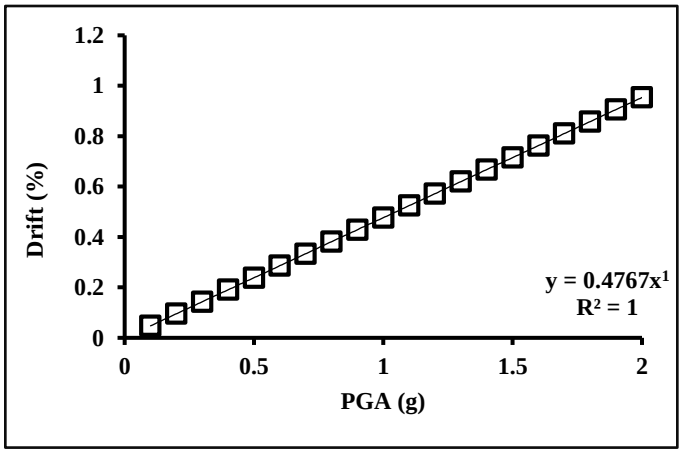

Figure 4.8.31. PSDM for roof of G+4 building on Soil 3 under Denali earthquake

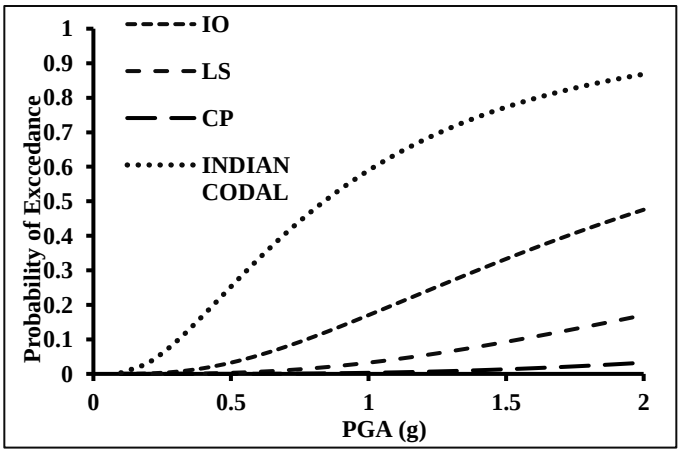

Figure 4.8.32. Fragility curves for roof of G+4 building on Soil 3 under Denali earthquake

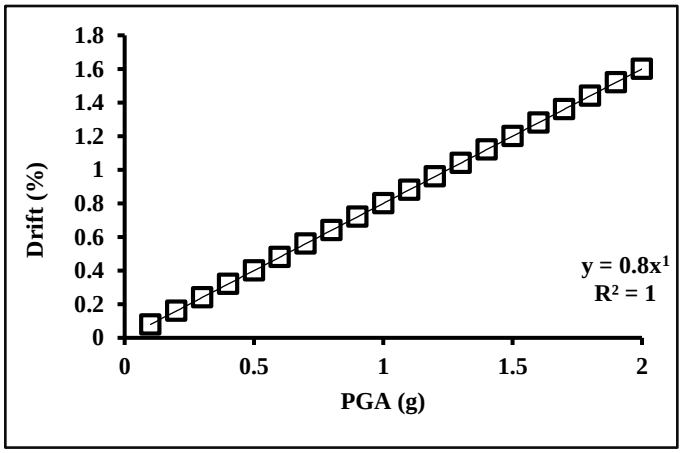

Figure 4.8.33. PSDM for roof of G+9 building on Soil 3 under Loma prieta earthquake

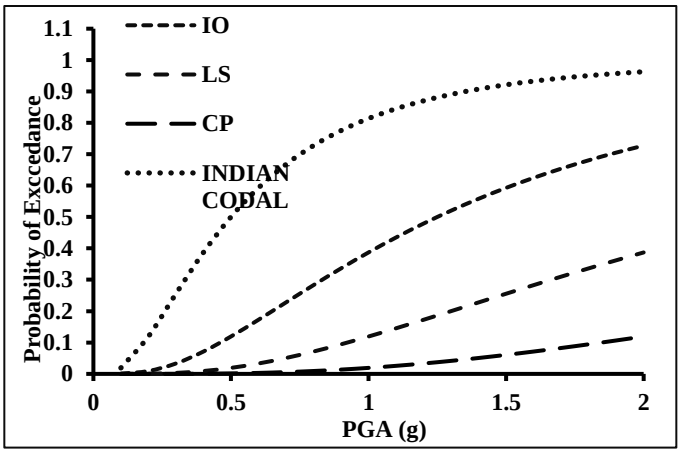

Figure 4.8.34. Fragility curves for roof of G+9 building on Soil 3 under Loma prieta earthquake

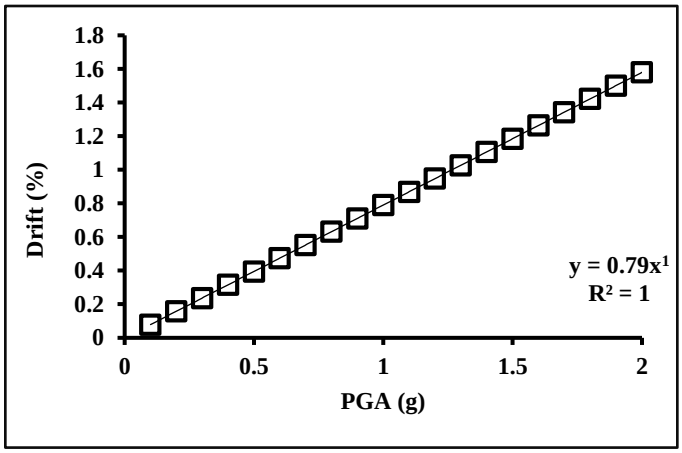

Figure 4.8.35. PSDM for roof of G+9 building on Soil 3 under Denali earthquake

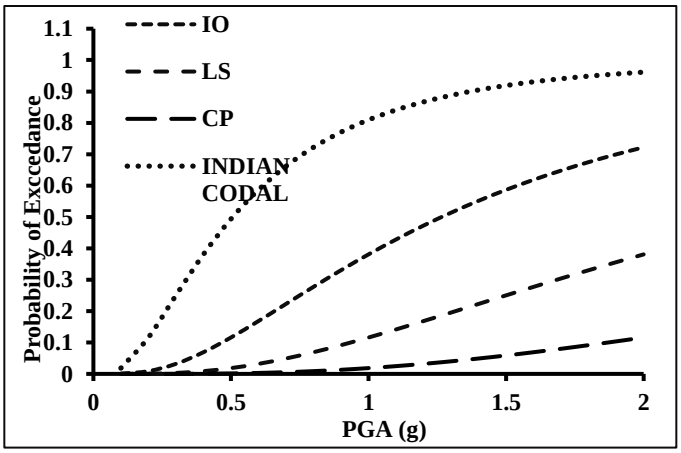

Figure 4.8.36. Fragility curves for roof of G+9 building on Soil 3 under Denali earthquake

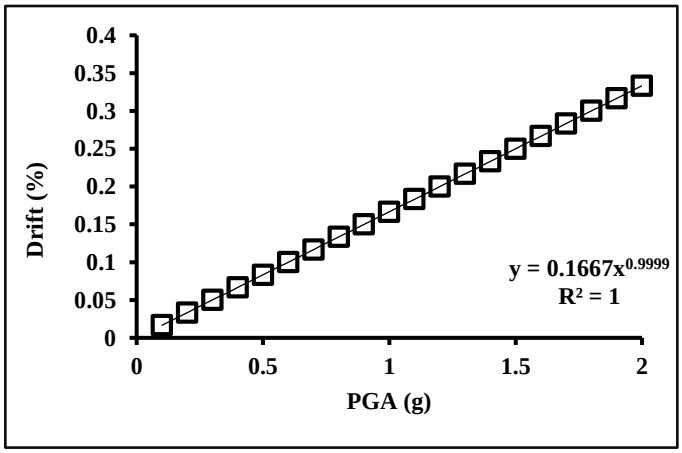

Figure 4.8.37. PSDM for roof of G+1 building on Soil 4 under Loma prieta earthquake

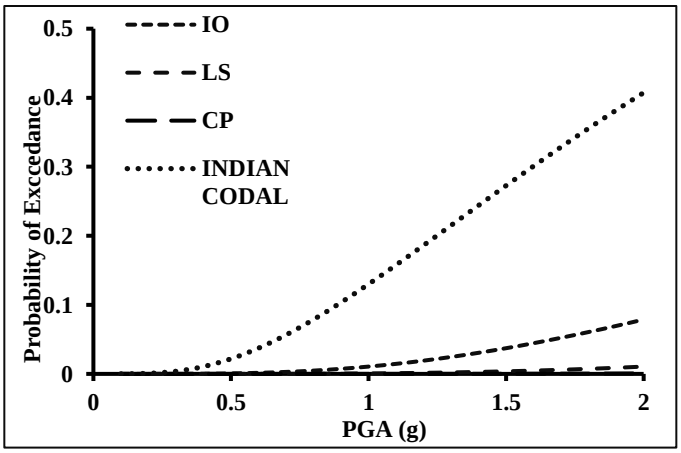

Figure 4.8.38. Fragility curves for roof of G+1 building on Soil 4 under Loma prieta earthquake

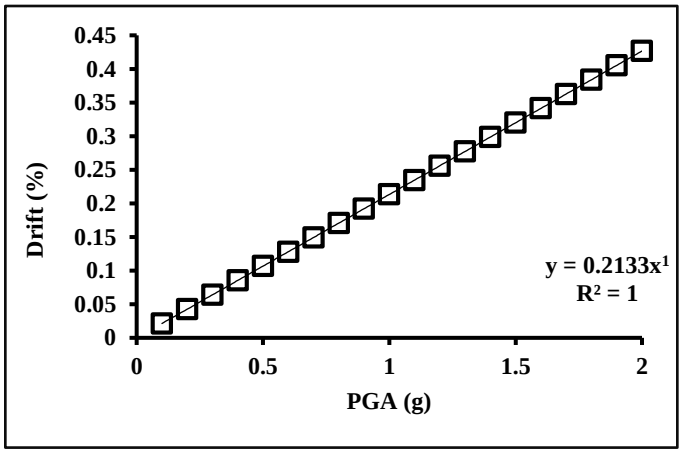

Figure 4.8.39. PSDM for roof of G+1 building on Soil 4 under Denali earthquake

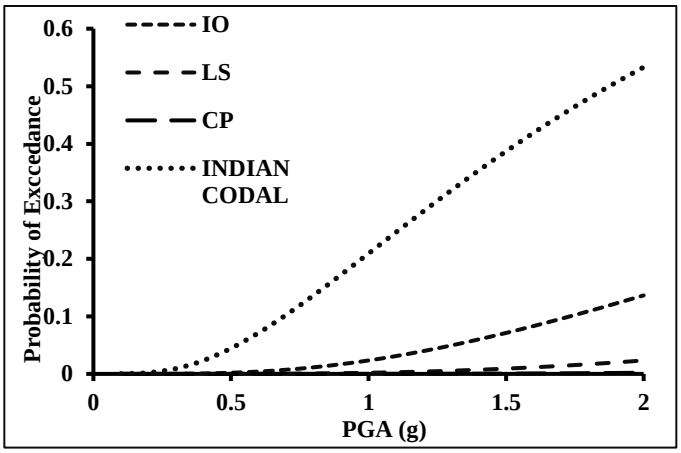

Figure 4.8.40. Fragility curves for roof of G+1 building on Soil 4 under Denali earthquake

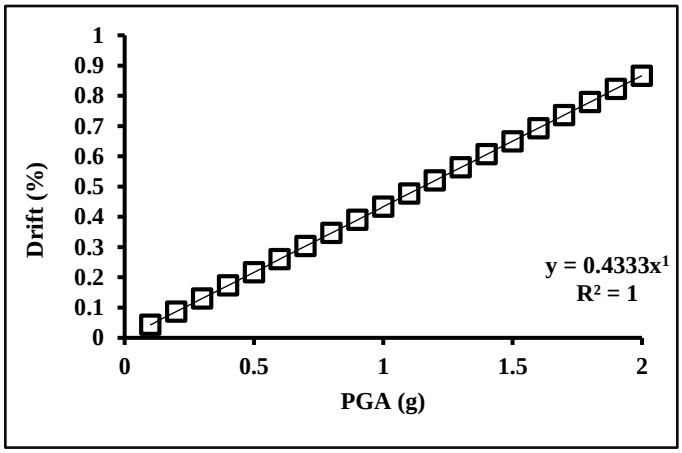

Figure 4.8.41. PSDM for roof of G+4 building on Soil 4 under Loma prieta earthquake

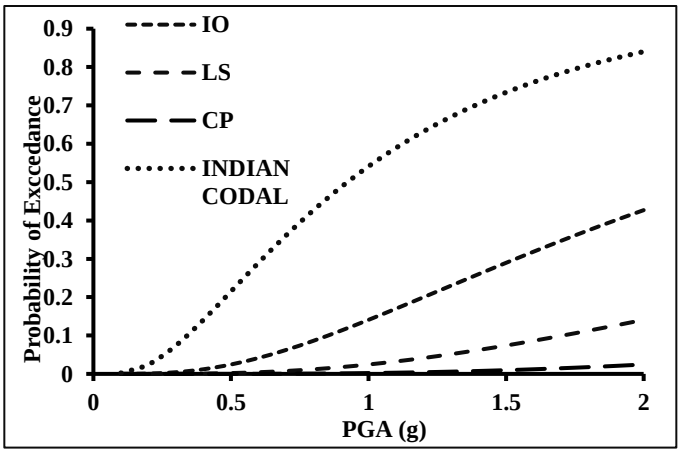

Figure 4.8.42. Fragility curves for roof of G+4 building on Soil 4 under Loma prieta earthquake

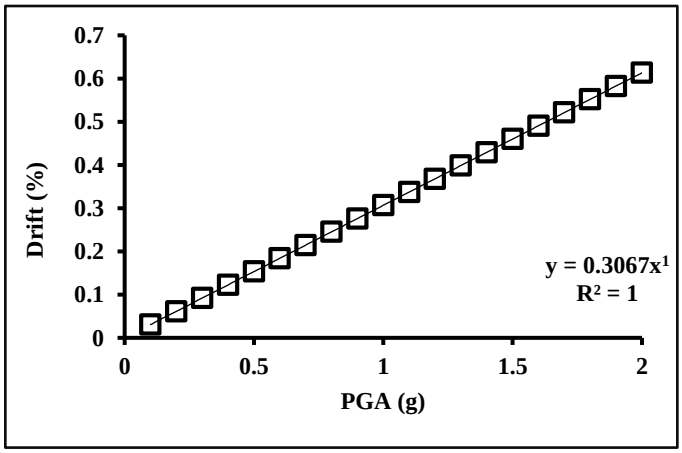

Figure 4.8.43. PSDM for roof of G+4 building on Soil 4 under Denali earthquake

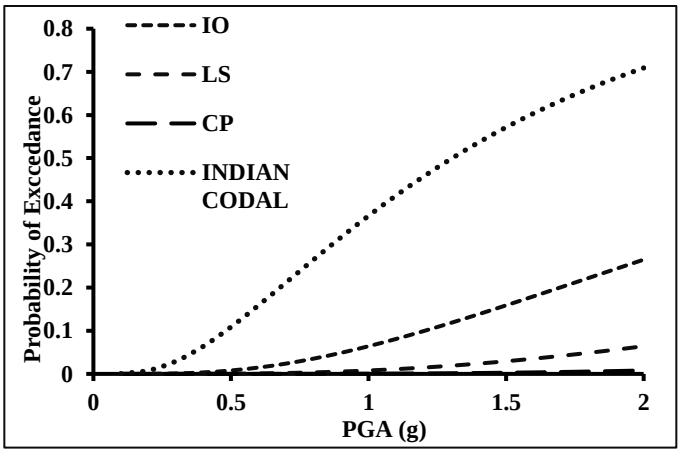

Figure 4.8.44. Fragility curves for roof of G+4 building on Soil 4 under Denali earthquake

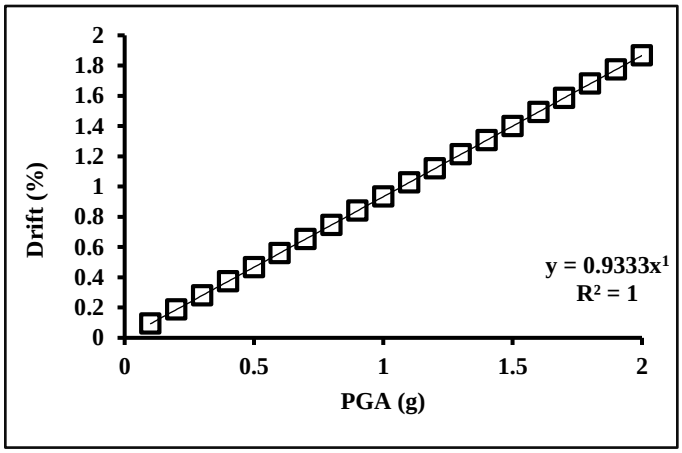

Figure 4.8.45. PSDM for roof of G+9 building on Soil 4 under Loma prieta earthquake

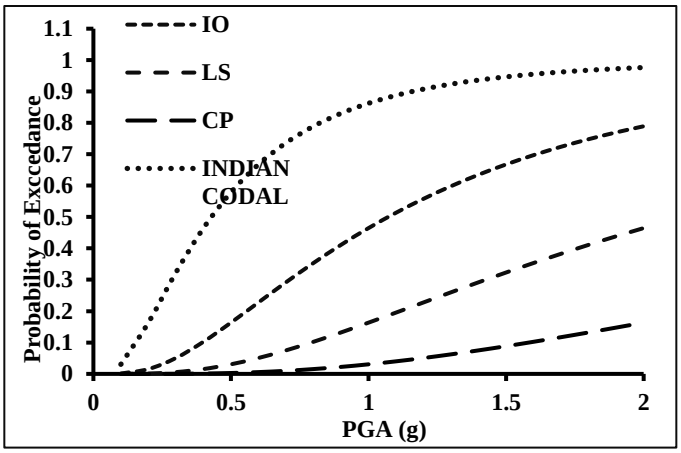

Figure 4.8.46. Fragility curves for roof of G+9 building on Soil 4 under Loma prieta earthquake

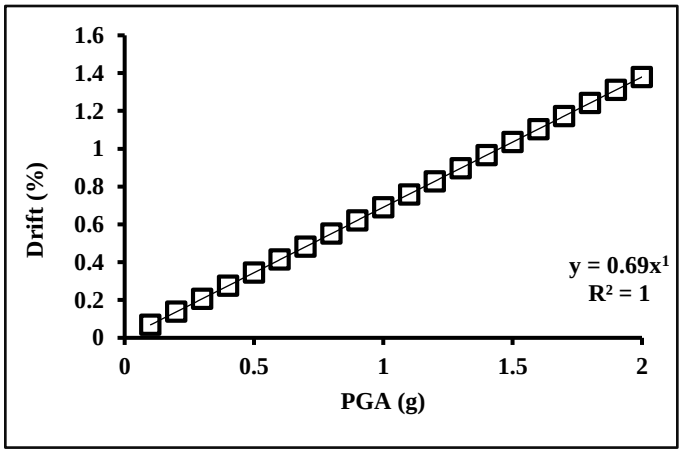

Figure 4.8.47. PSDM for roof of G+9 building on Soil 4 under Denali earthquake

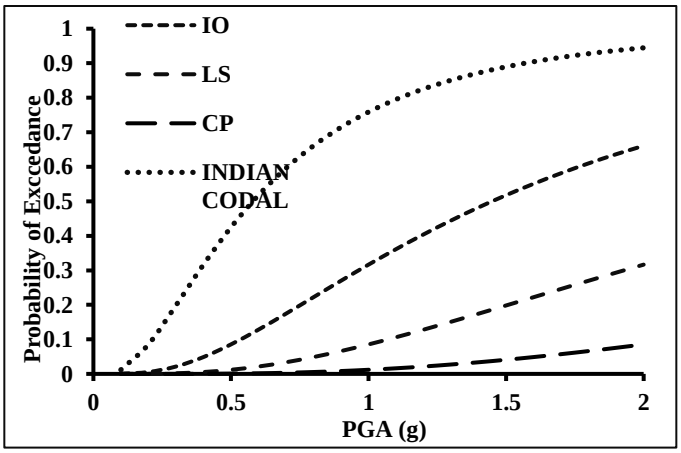

Figure 4.8.48. Fragility curves for roof of G+9 building on Soil 4 under Denali earthquake

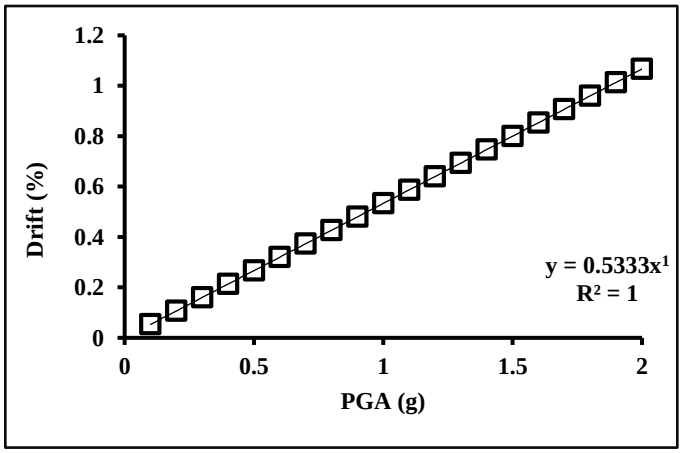

Figure 4.8.49. PSDM for roof of G+1 building on Soil 5 under Loma prieta earthquake

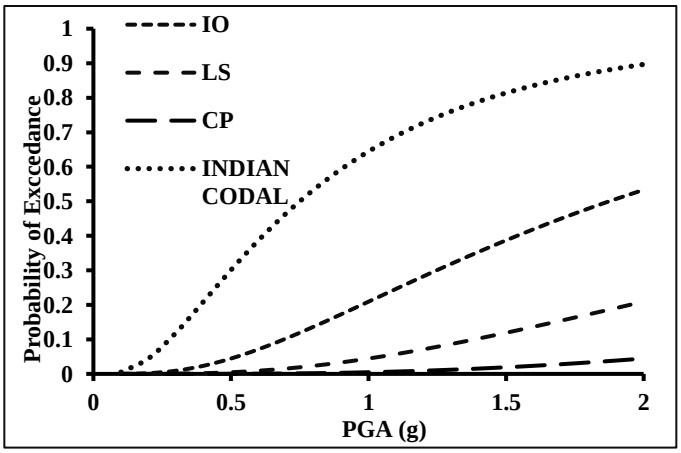

Figure 4.8.50. Fragility curves for roof of G+1 building on Soil 5 under Loma prieta earthquake

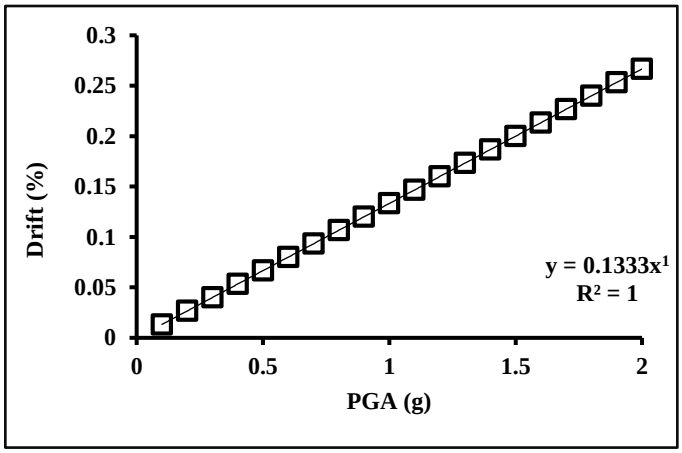

Figure 4.8.51. PSDM for roof of G+1 building on Soil 5 under Denali earthquake

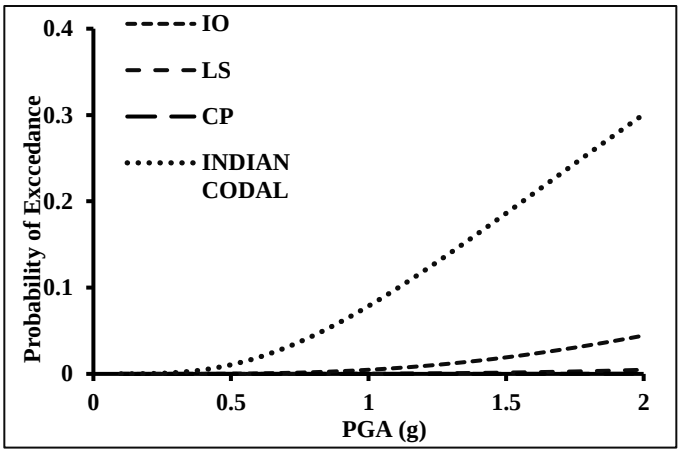

Figure 4.8.52. Fragility curves for roof of G+1 building on Soil 5 under Denali earthquake

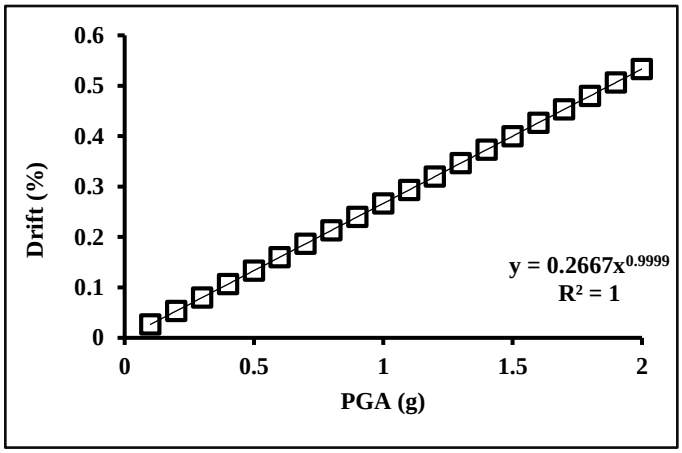

Figure 4.8.53. PSDM for roof of G+4 building on Soil 5 under Loma prieta earthquake

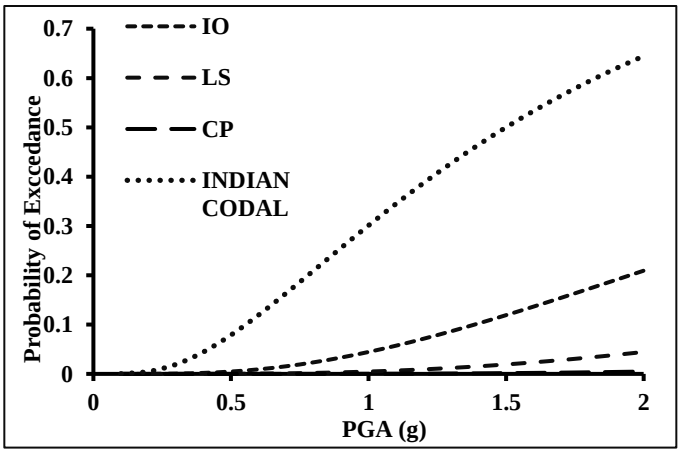

Figure 4.8.54. Fragility curves for roof of G+4 building on Soil 5 under Loma prieta earthquake

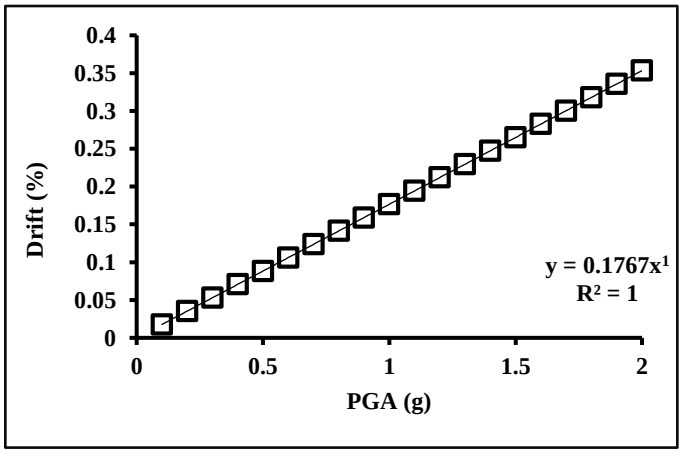

Figure 4.8.55. PSDM for roof of G+4 building on Soil 5 under Denali earthquake

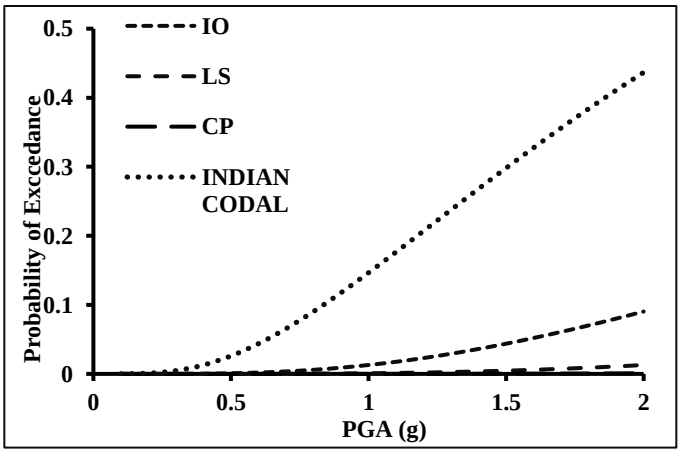

Figure 4.8.56. Fragility curves for roof of G+4 building on Soil 5 under Denali earthquake

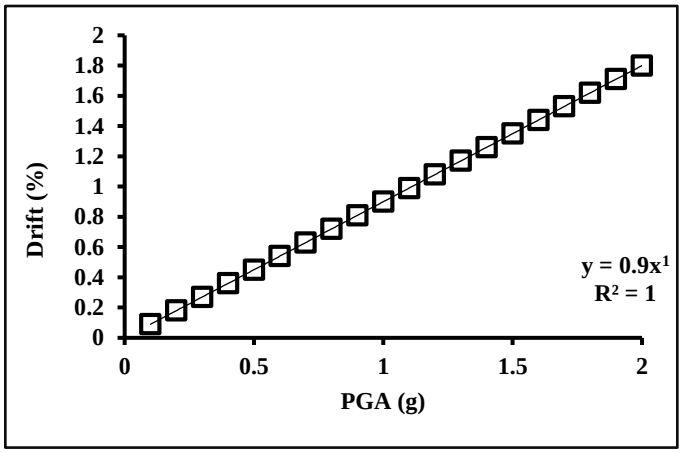

Figure 4.8.57. PSDM for roof of G+9 building on Soil 5 under Loma prieta earthquake

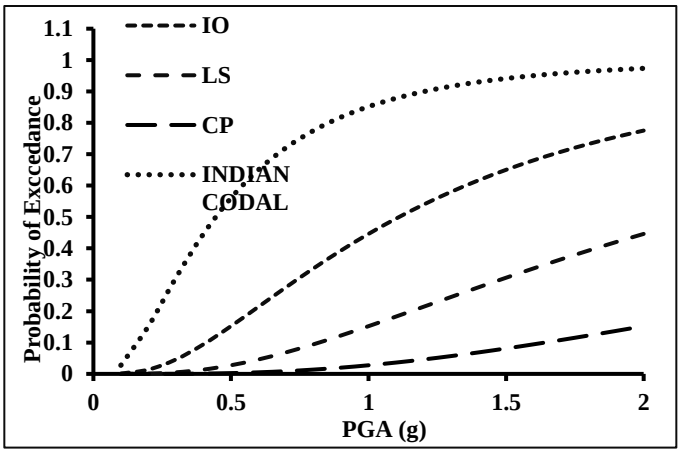

Figure 4.8.58. Fragility curves for roof of G+9 building on Soil 5 under Loma prieta earthquake

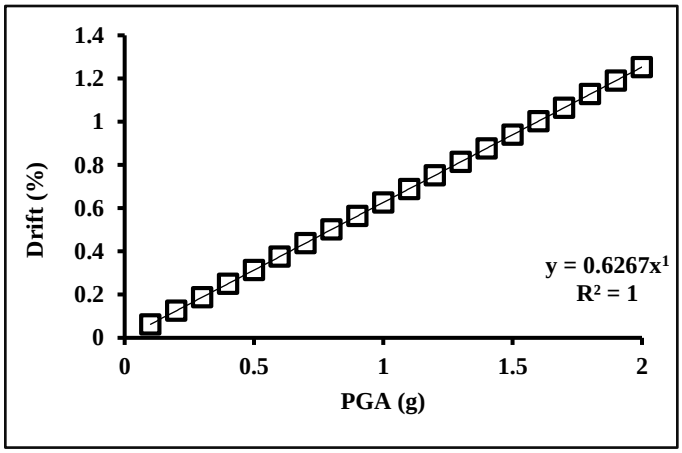

Figure 4.8.59. PSDM for roof of G+9 building on Soil 5 under Denali earthquake

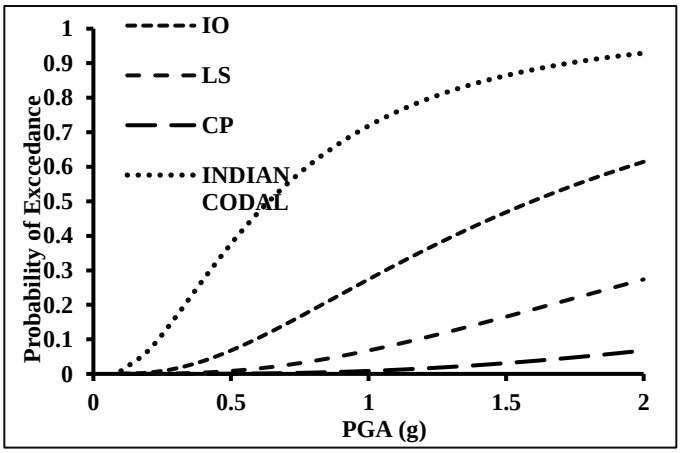

Figure 4.8.60. Fragility curves for roof of G+9 building on Soil 5 under Denali earthquake

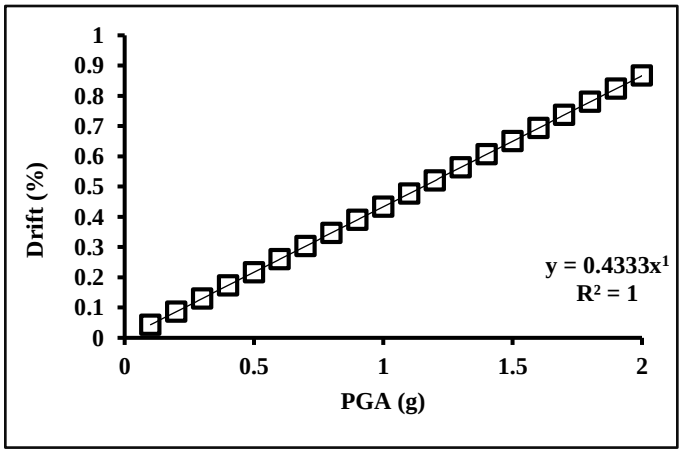

Figure 4.8.61. PSDM for roof of G+1 building on Soil 6 under Loma prieta earthquake

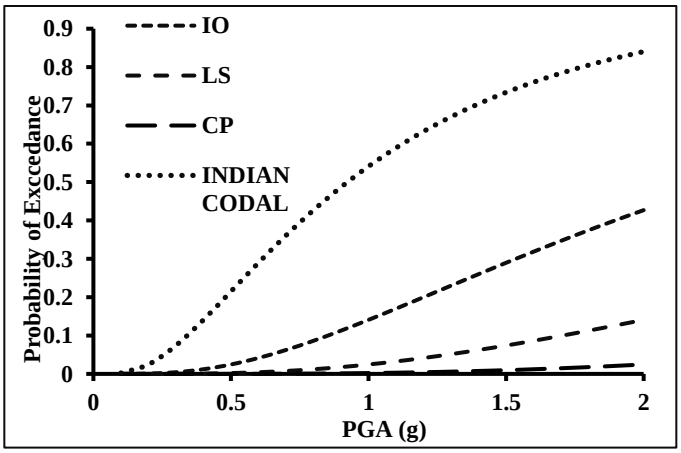

Figure 4.8.62. Fragility curves for roof of G+1 building on Soil 6 under Loma prieta earthquake

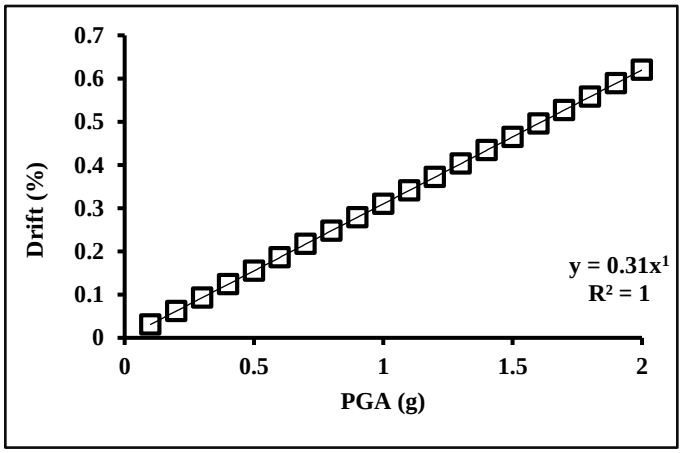

Figure 4.8.63. PSDM for roof of G+1 building on Soil 6 under Denali earthquake

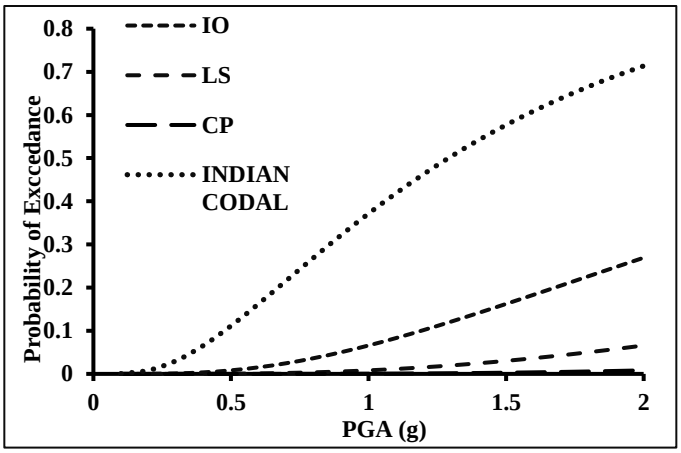

Figure 4.8.64. Fragility curves for roof of G+1 building on Soil 6 under Denali earthquake

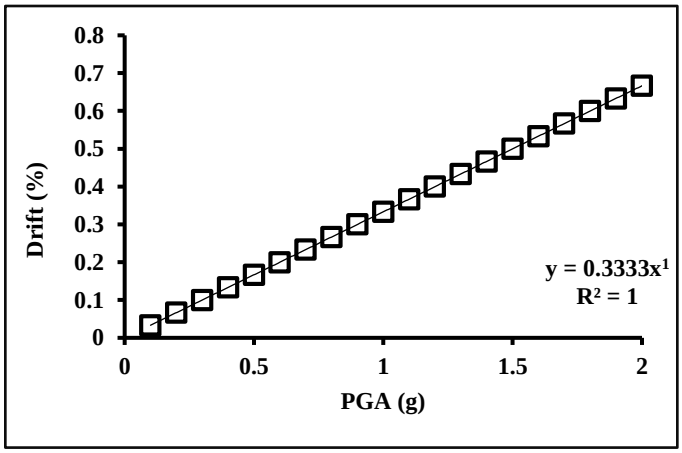

Figure 4.8.65. PSDM for roof of G+4 building on Soil 6 under Loma prieta earthquake

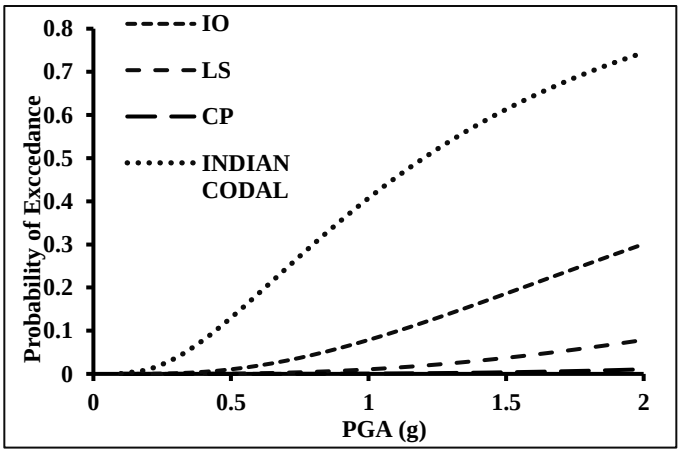

Figure 4.8.66. Fragility curves for roof of G+4 building on Soil 6 under Loma prieta earthquake

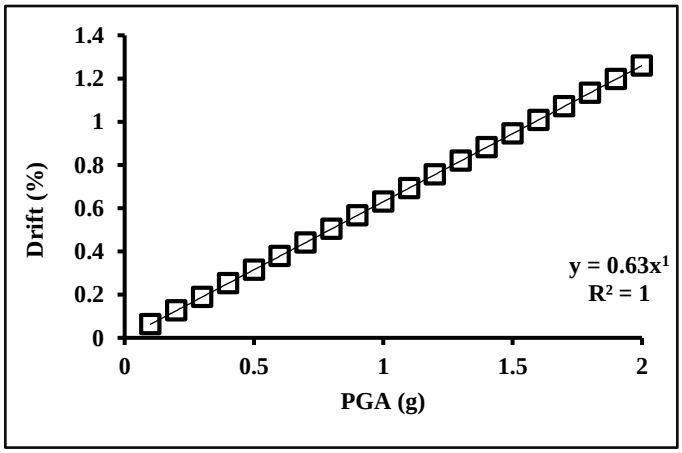

Figure 4.8.67. PSDM for roof of G+4 building on Soil 6 under Denali earthquake

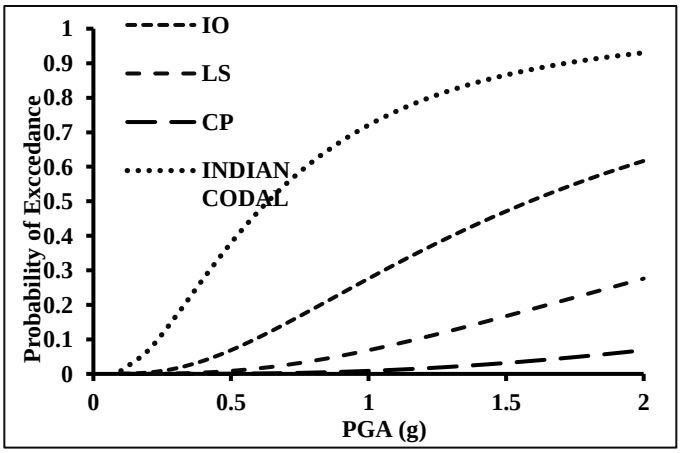

Figure 4.8.68. Fragility curves for roof of G+4 building on Soil 6 under Denali earthquake

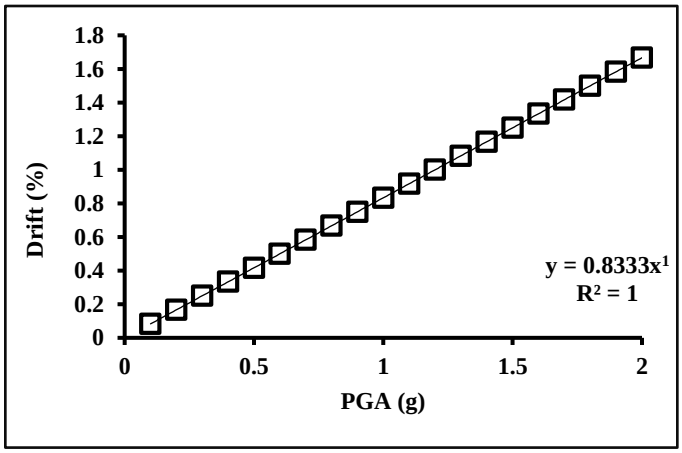

Figure 4.8.69. PSDM for roof of G+9 building on Soil 6 under Loma prieta earthquake

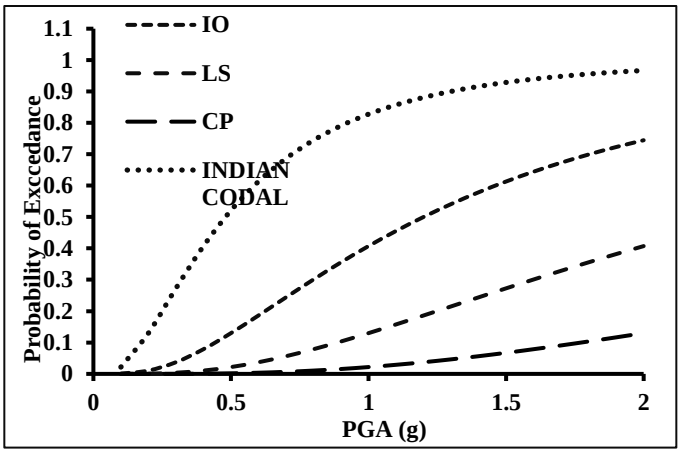

Figure 4.8.70. Fragility curves for roof of G+9 building on Soil 6 under Loma prieta earthquake

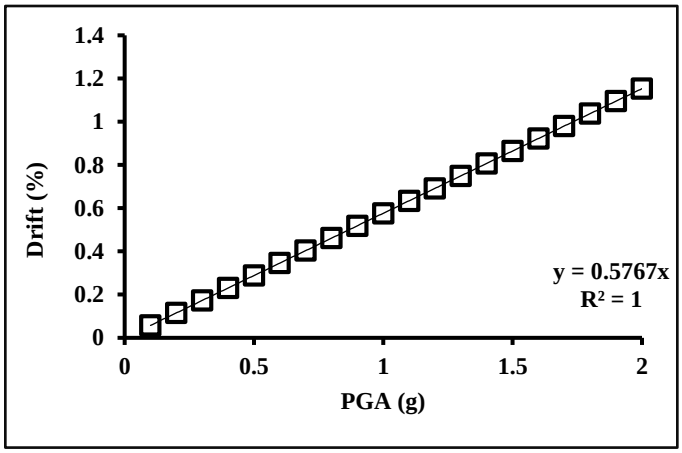

Figure 4.8.71. PSDM for roof of G+9 building on Soil 6 under Denali earthquake

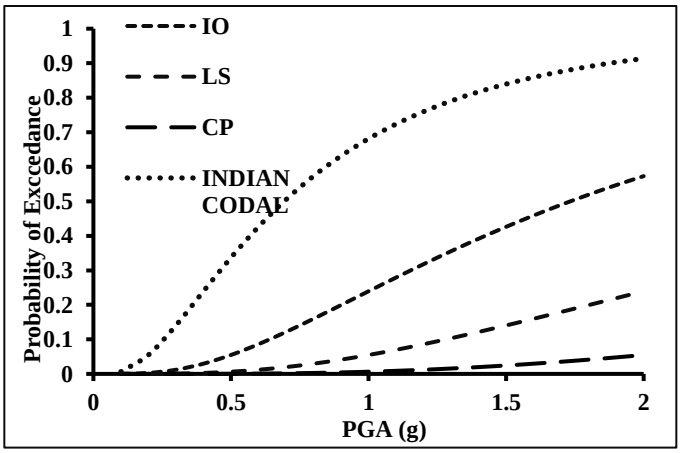

Figure 4.8.72. Fragility curves for roof of G+9 building on Soil 6 under Denali earthquake

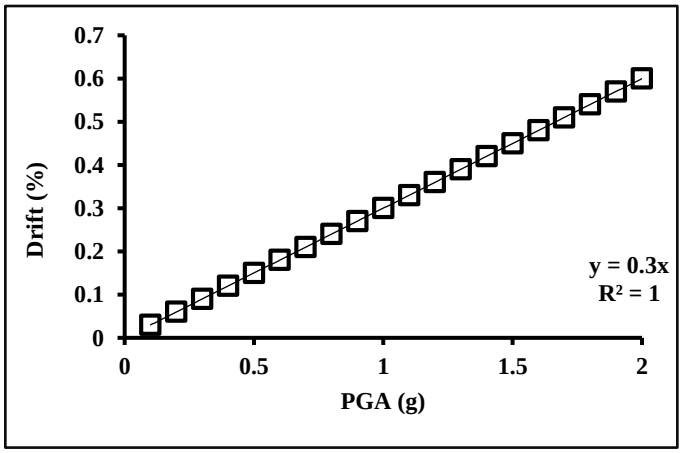

Figure 4.8.73. PSDM for roof of G+1 building on Soil 7 under Loma prieta earthquake

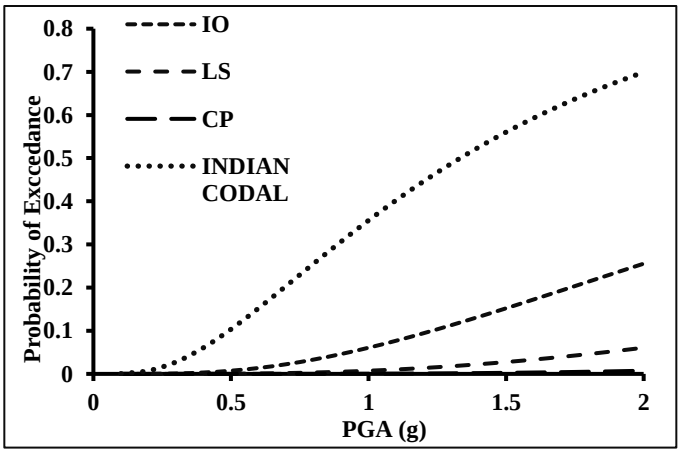

Figure 4.8.74. Fragility curves for roof of G+1 building on Soil 7 under Loma prieta earthquake

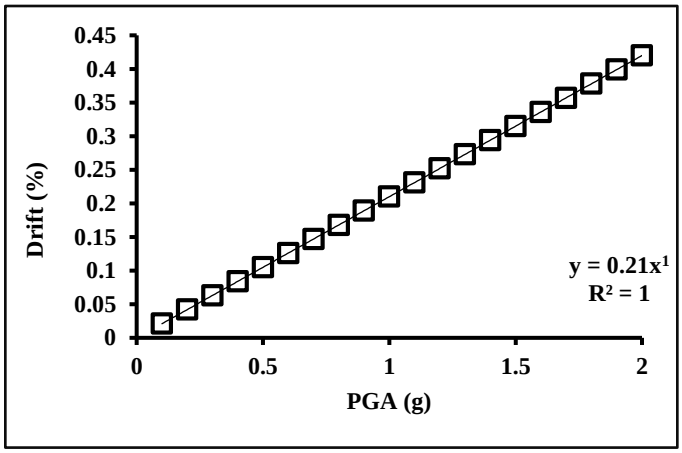

Figure 4.8.75. PSDM for roof of G+1 building on Soil 7 under Denali earthquake

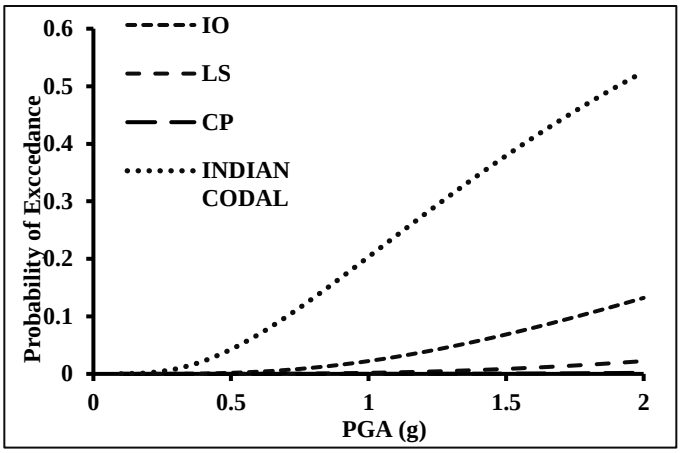

Figure 4.8.76. Fragility curves for roof of G+1 building on Soil 7 under Denali earthquake

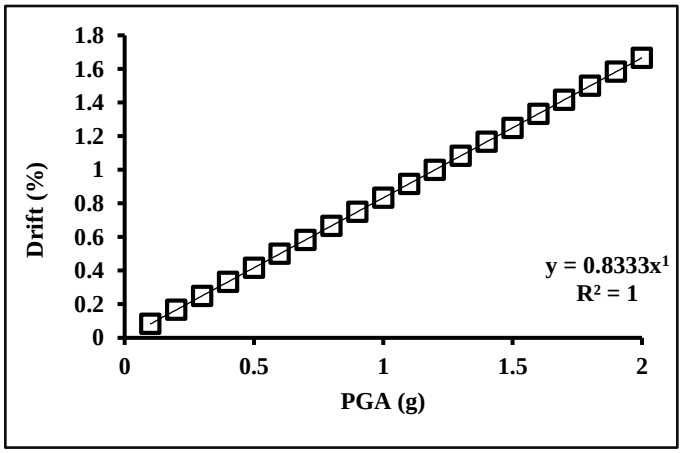

Figure 4.8.77. PSDM for roof of G+4 building on Soil 7 under Loma prieta earthquake

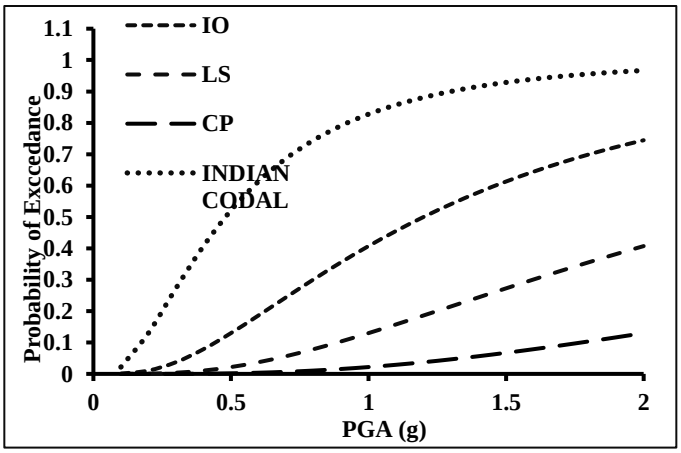

Figure 4.8.78. Fragility curves for roof of G+4 building on Soil 7 under Loma prieta earthquake

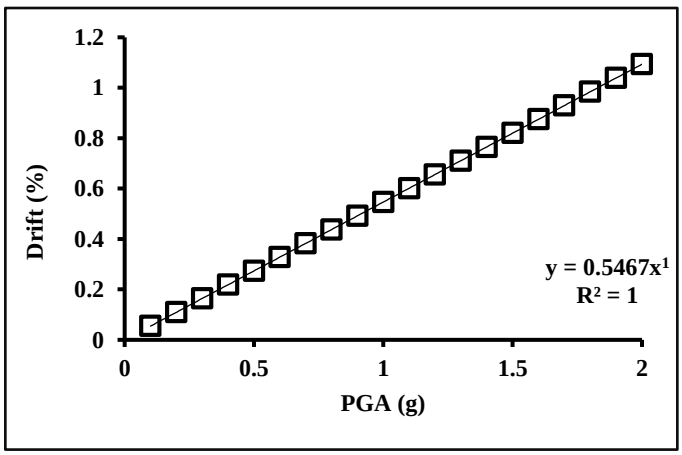

Figure 4.8.79. PSDM for roof of G+4 building on Soil 7 under Denali earthquake

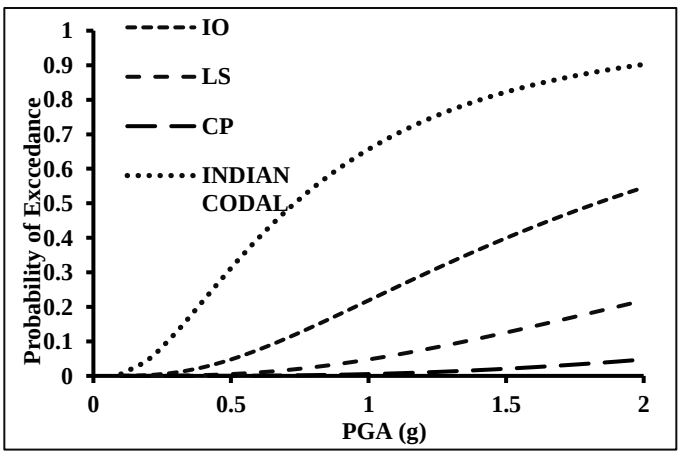

Figure 4.8.80. Fragility curves for roof of G+4 building on Soil 7 under Denali earthquake

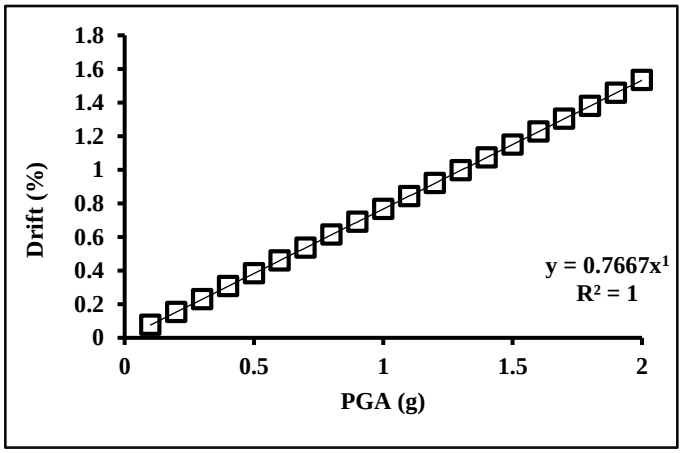

Figure 4.8.81. PSDM for roof of G+9 building on Soil 7 under Loma prieta earthquake

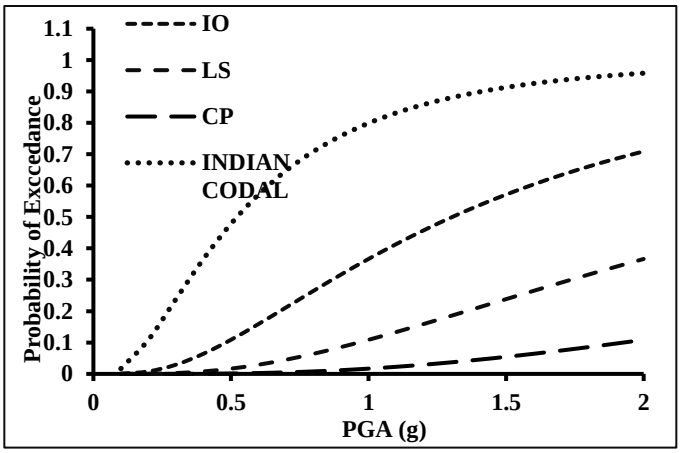

Figure 4.8.82. Fragility curves for roof of G+9 building on Soil 7 under Loma prieta earthquake

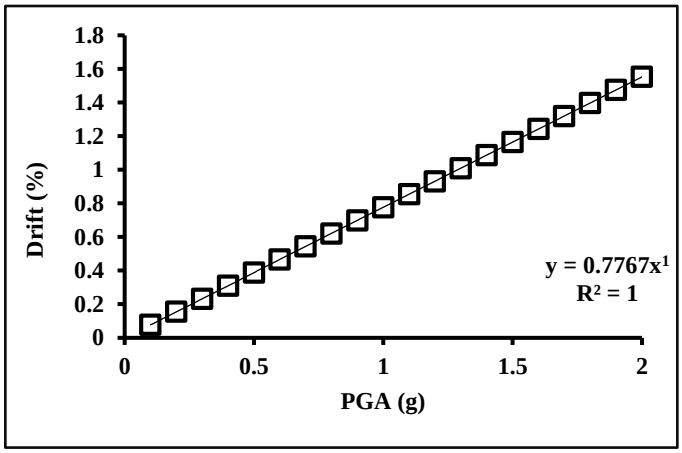

Figure 4.8.83. PSDM for roof of G+9 building on Soil 7 under Denali earthquake

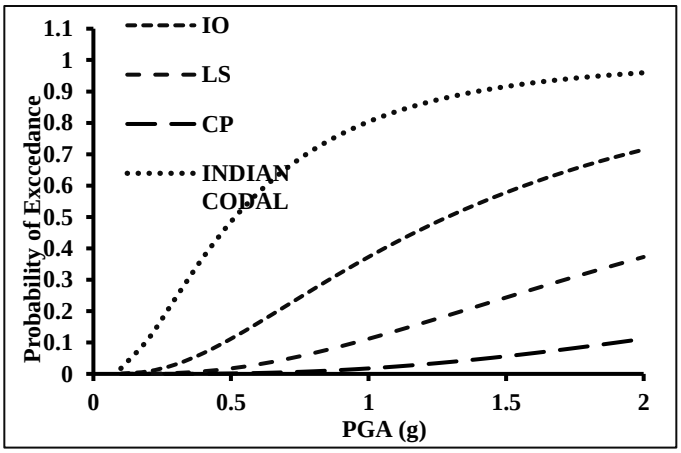

Figure 4.8.84. Fragility curves for roof of G+9 building on Soil 7 under Denali earthquake

Chapter-5: RELIABILITY BASED ANALYSIS

5.1. GENERAL

The fragility curves indicate the probability of exceedance of a particular performance level for a soil-structure system if the system is subjected to a seismic excitation of predefined intensity (in terms of PGA). However, to assess the risk of any soil-structure system, these fragility curves should be combined with the seismic hazard curve, which corroborates the probability of occurrence of an earthquake having more than certain intensity at a particular location of interest. Reliability is a measure of safety of a building frame, which can be expressed by a statistical parameter named 'Reliability Index'. This Reliability Index can be obtained by subtracting the probability of failure of a structure from unity. Risk of any frame can be expressed using the probability of exceedance of a particular performance level such as IO, LS, CP and limitation given by IS 1893 (Part I):2002[45] along with the probability of occurrence of an earthquake having more than a specified intensity. In this chapter, reliability indices for all the aforementioned models have been presented graphically using the seismic hazard curve for Saltlake area under the action of Loma prieta and Denali earthquakes.

5.2. SEISMIC HAZARD CURVE

Seismic hazard is defined as the probability of occurrence of an earthquake in a particular geographic area, within a specified window of time, and with ground motion intensity exceeding a given threshold. A hazard curve depicts the variation of probability of exceedance of an earthquake with respect to maximum seismic intensities (mainly in terms of PGA). In the present study, seismic hazard curve for the Saltlake area proposed by Nath et al. (2012)[60] has been used to obtain the reliability curves for G+1, G+4 and G+9 frame buildings constructed on uniform as well as layered soils and subjected to near-field and far-field earthquakes. The seismic hazard curve for the Saltlake area, given by, used for analysis is shown below in Figure 5.2.1.

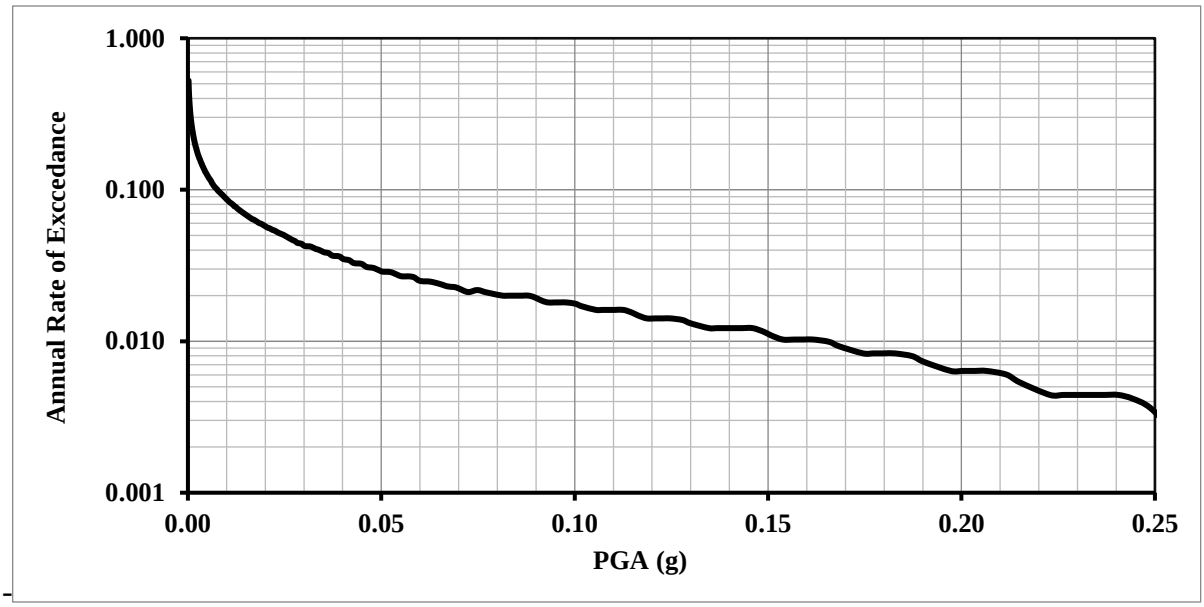

Figure 5.2.1. Seismic hazard curve for Saltlake area (Nath, 2012)[60]

5.3. RELIABILITY CURVES AND THEIR FORMULATIONS

The reliability is the probability that a structure will perform its intended function during a specified time period under the considered operating conditions. Mathematically, it can be expressed as

$$\boldsymbol{Reliabilty = 1 - Probability\ of\ Failure} \qquad \textbf{...5.3.1.}$$

The probability of failure at a specific performance level can be obtained by convolving the fragility curve $F_R(x)$ with the derivative of the seismic hazard curve $G_A(x)$. This conditional probability is sometimes assumed to follow a lognormal probability distribution[61]. Mathematically, it can be expressed using equation 5.3.2.

$$\mathbf{P[LS] = \int F_R(x) \frac{dG_A(x)}{dx} dx} \qquad \textbf{...5.3.2.}$$

The fragility-hazard interface, as illustrated by Ellingwood (2001)[49], has been presented in Figure 5.3.1.

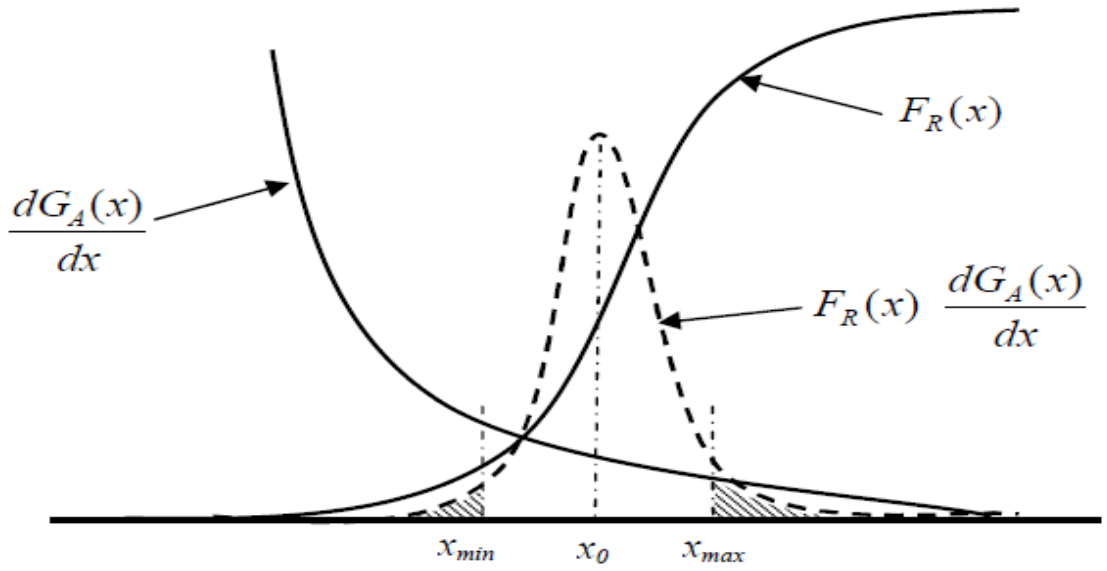

Figure 5.3.1. Fragility-hazard interface (Ellingwood, 2001)[49]

In this figure, $F_R(x)$ and $\frac{dG_A(x)}{dx}$ are the two parameters from which probability distribution P[LS] is established. In order to determine the performance of every soil-structure system, reliability index (RI) has been computed which is a direct measure of the safety margin. Hassofer and Lind (1974)[62] defined RI (β_{pf}) as the shortest distance between the origin and the Limit State Function (LSF) in a standard normal variable space. RI (β_{pf}) corresponding to a specific probability of failure at a certain performance limit can be found from equation 5.3.3.

$$\boldsymbol{\beta_{pf} = -\emptyset^{-1}(\mathbf{P[LS]})} \qquad \textbf{...5.3.3.}$$

where, $\emptyset$ () represents the standard normal distribution.

In Figure 5.3.2., the shaded area indicates the probability of failure. This figure clearly reveals that the Reliability Index (β_{pf}) is the shortest distance from the origin to the limit state function (LSF) in a standard normal variable space. The steps to be followed for plotting the reliability curves have been illustrated graphically in Figure 5.3.3.

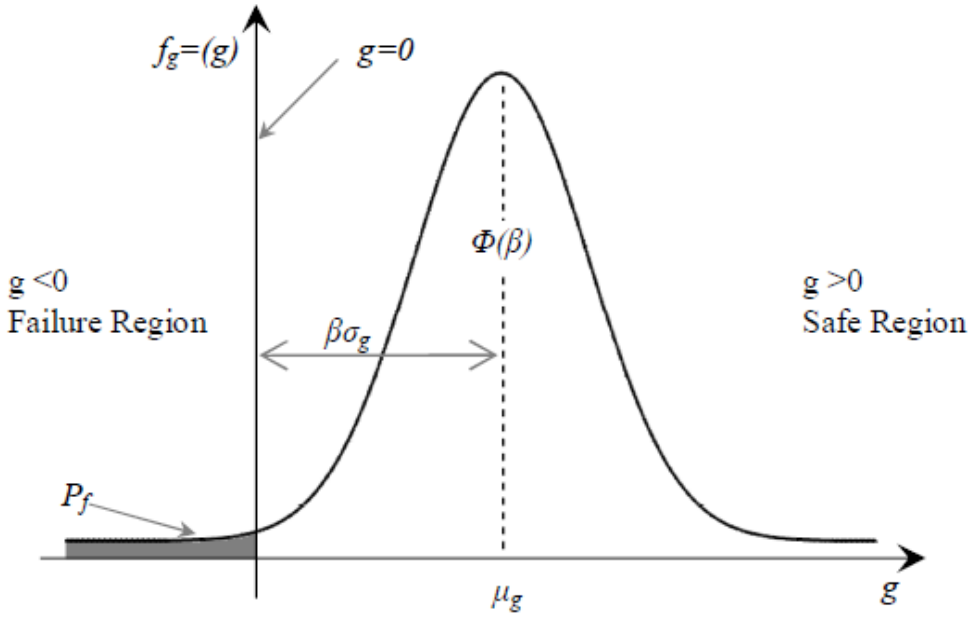

Figure 5.3.2. . Probability Density for Limit-state (Ellingwood, 2001)

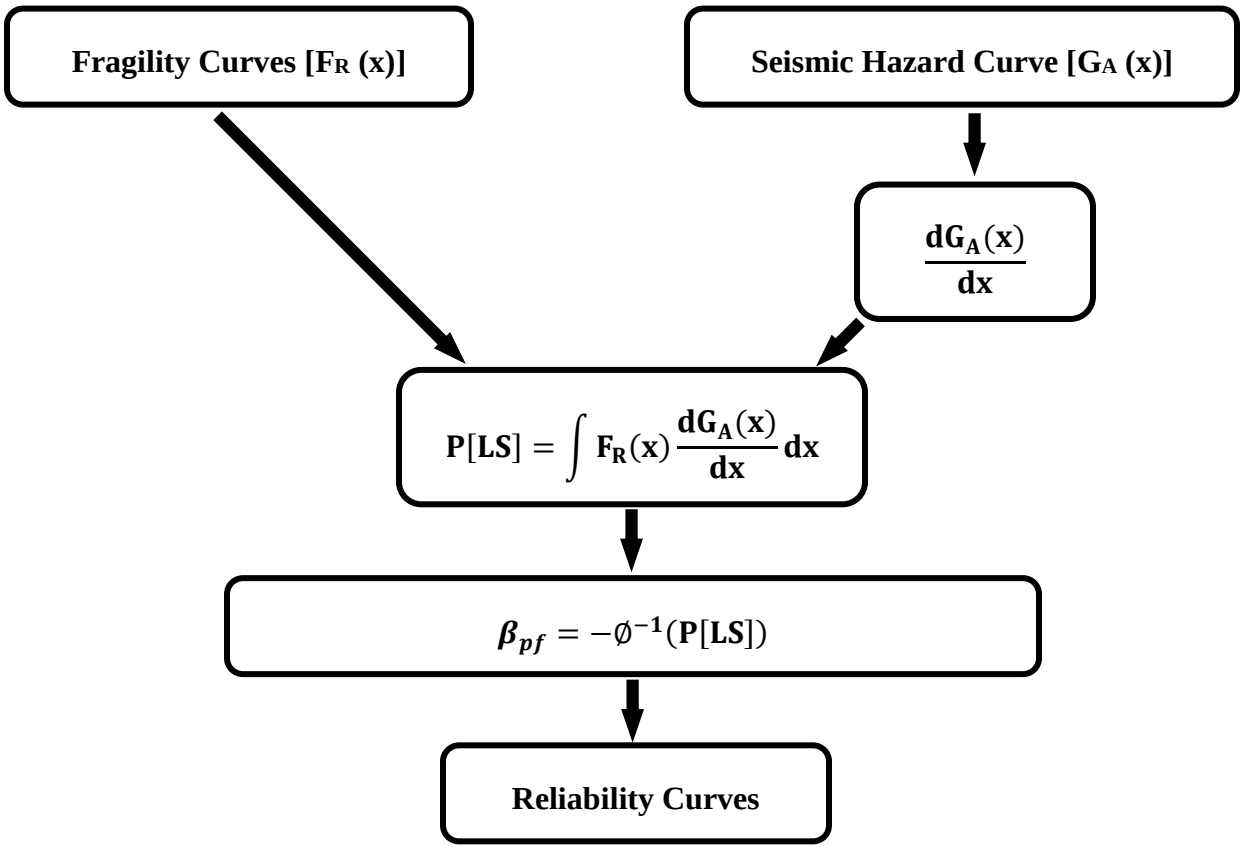

Figure 5.3.3. Flow chart for plotting reliability curves

In this study, total 60 reliability curves have been generated for G+1, G+4 and G+9 frame buildings located on three types of uniform soils (Hard, Medium and Soft) and seven types of layered soils (Soil 1 to Soil 7) in the Saltlake area which are subjected to a near-field (Loma prieta) and a far-field (Denali) seismic excitation. These curves are displayed in Figure 5.3.4. to Figure. 5.3.63.

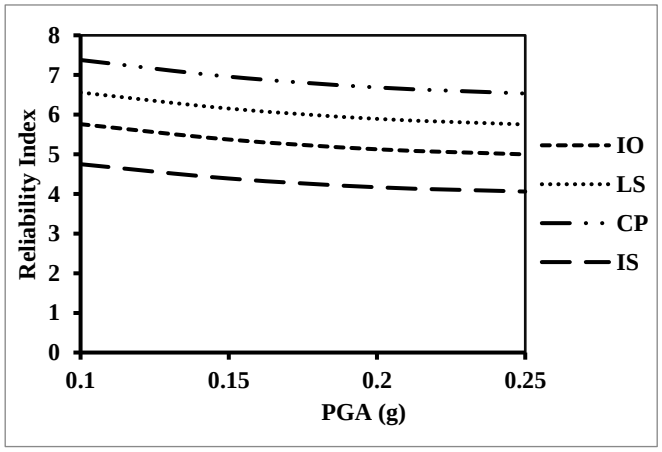

Figure 5.3.4. Reliability Index for roof of G+1 building on hard soil under Loma prieta earthquake at Saltlake

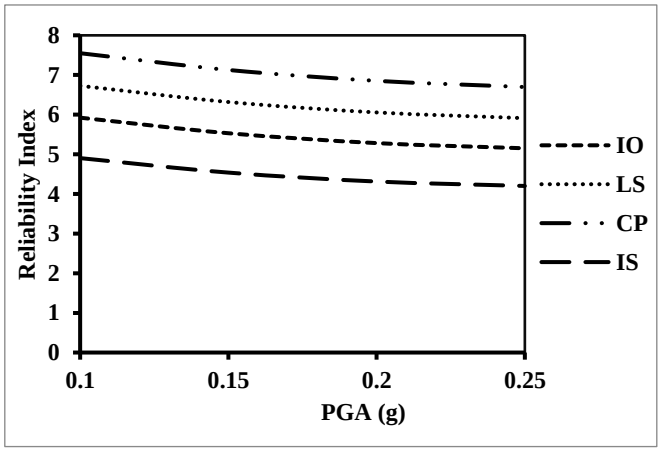

Figure 5.3.5. Reliability Index for roof of G+1 building on hard soil under Denali earthquake at Saltlake

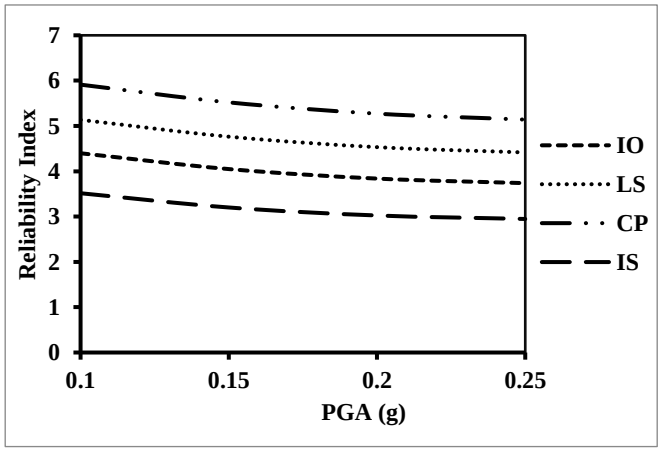

Figure 5.3.6. Reliability Index for roof of G+4 building on hard soil under Loma prieta earthquake at Saltlake

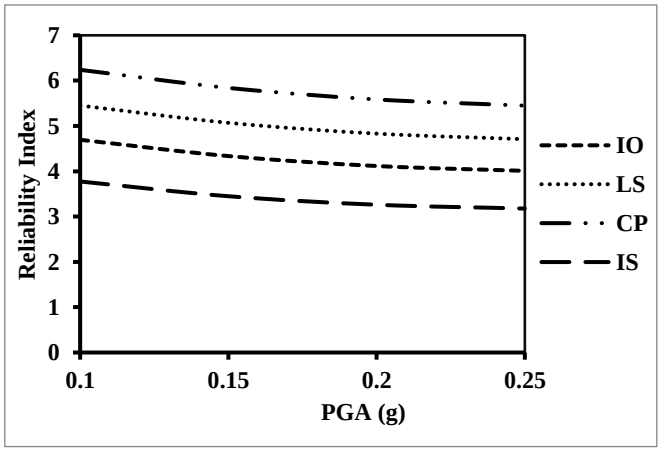

Figure 5.3.7. Reliability Index for roof of G+4 building on hard soil under Denali earthquake at Saltlake

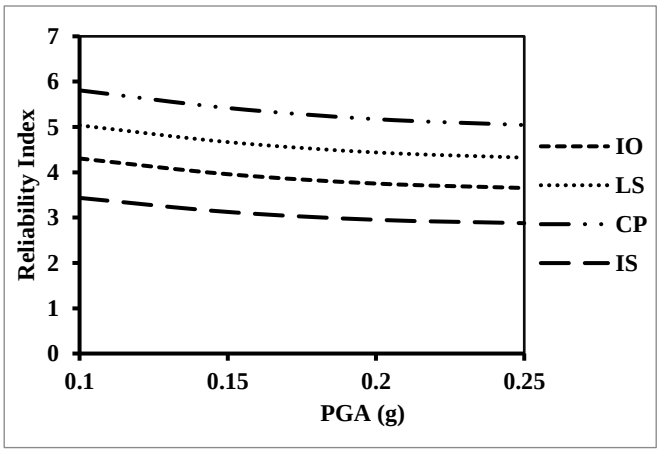

Figure 5.3.8. Reliability Index for roof of G+9 building on hard soil under Loma prieta earthquake at Saltlake

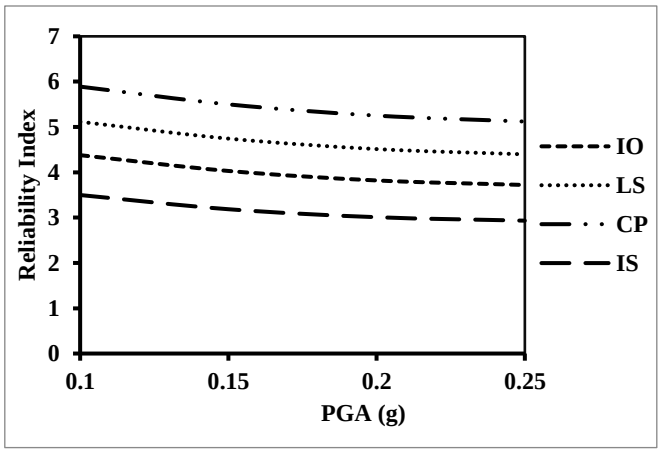

Figure 5.3.9. Reliability Index for roof of G+9 building on hard soil under Denali earthquake at Saltlake

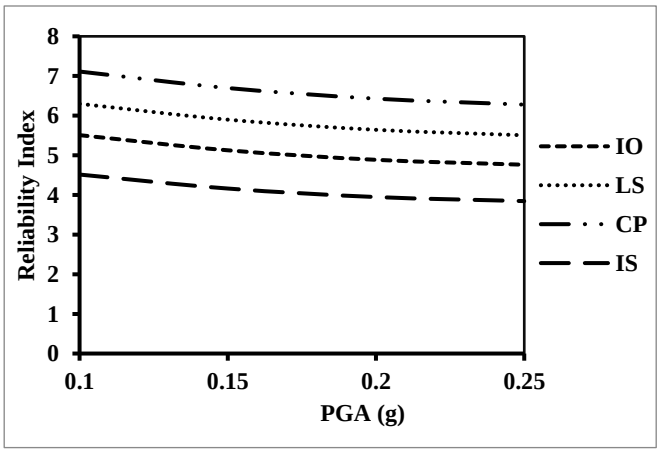

Figure 5.3.10. Reliability Index for roof of G+1 building on medium soil under Loma prieta earthquake at Saltlake

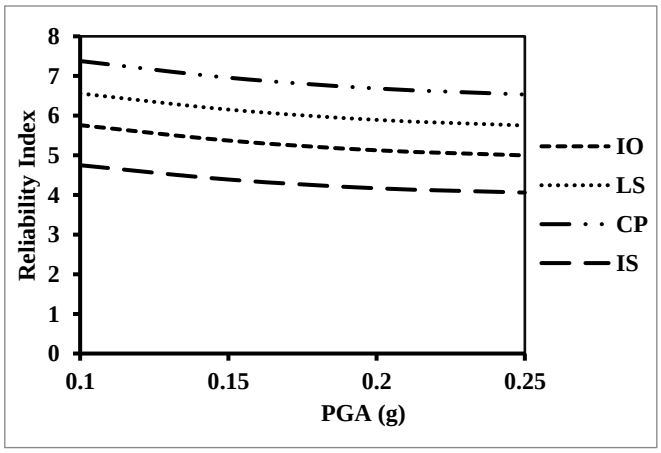

Figure 5.3.11. Reliability Index for roof of G+1 building on medium soil under Denali earthquake at Saltlake

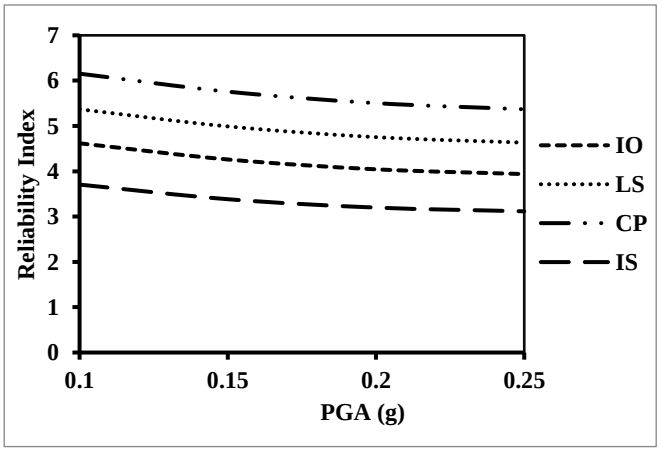

Figure 5.3.12. Reliability Index for roof of G+4 building on medium soil under Loma prieta earthquake at Saltlake

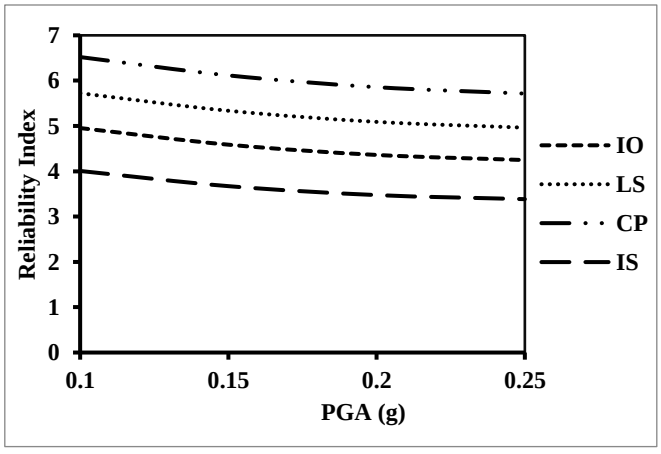

Figure 5.3.13. Reliability Index for roof of G+4 building on medium soil under Denali earthquake at Saltlake

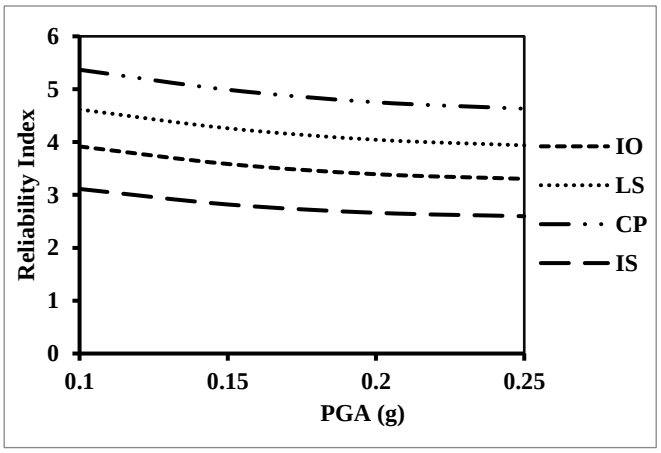

Figure 5.3.14. Reliability Index for roof of G+9 building on medium soil under Loma prieta earthquake at Saltlake

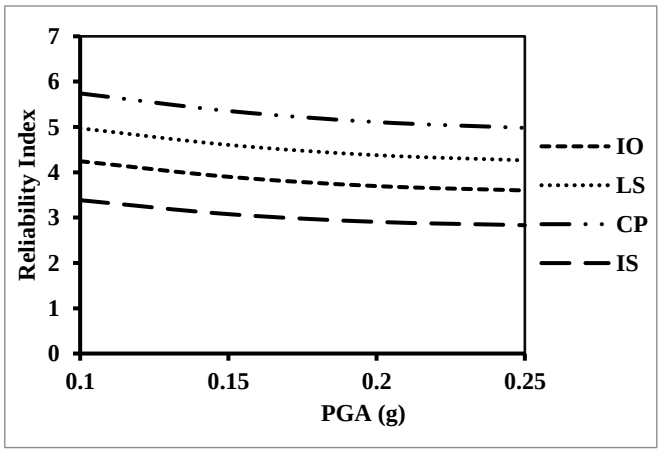

Figure 5.3.15. Reliability Index for roof of G+9 building on medium soil under Denali earthquake at Saltlake

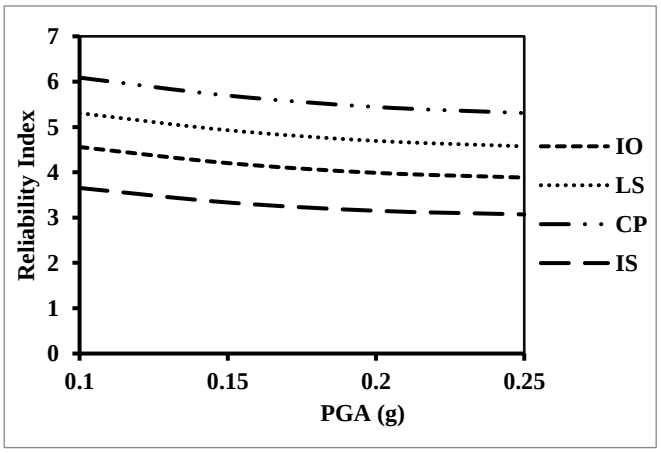

Figure 5.3.16. Reliability Index for roof of G+1 building on soft soil under Loma prieta earthquake at Saltlake

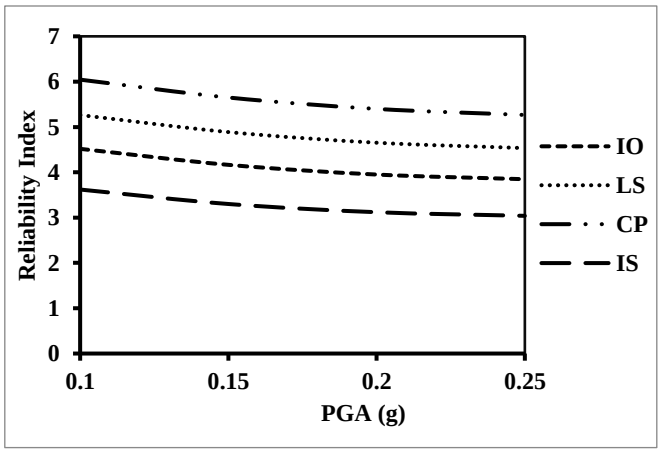

Figure 5.3.17. Reliability Index for roof of G+1 building on soft soil under Denali earthquake at Saltlake

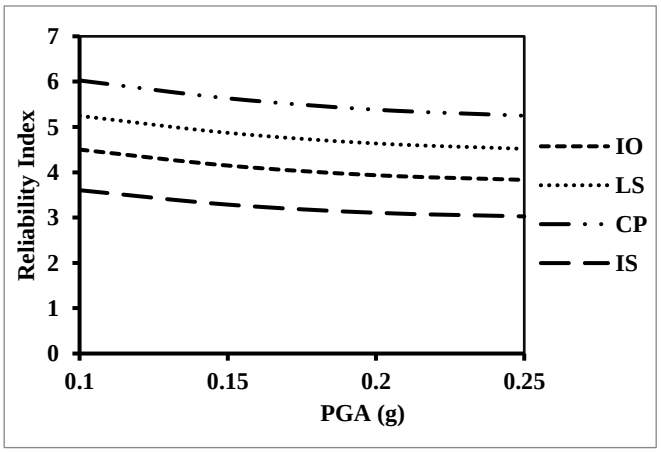

Figure 5.3.18. Reliability Index for roof of G+4 building on soft soil under Loma prieta earthquake at Saltlake

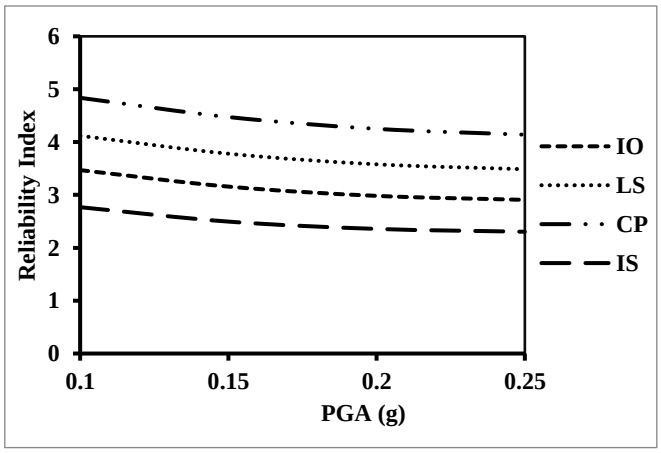

Figure 5.3.19. Reliability Index for roof of G+4 building on soft soil under Denali earthquake at Saltlake

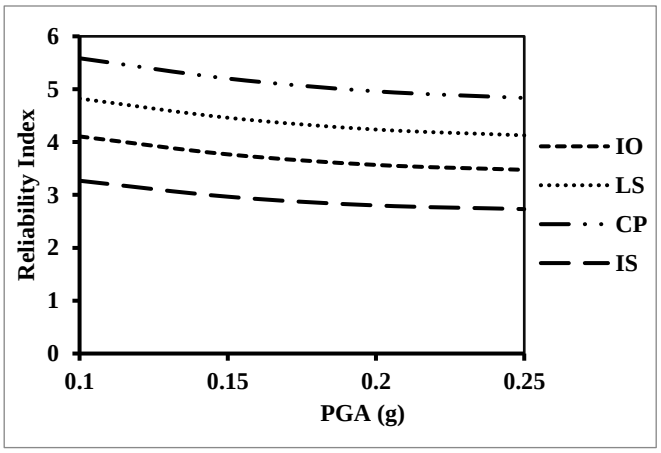

Figure 5.3.20. Reliability Index for roof of G+9 building on soft soil under Loma prieta earthquake at Saltlake

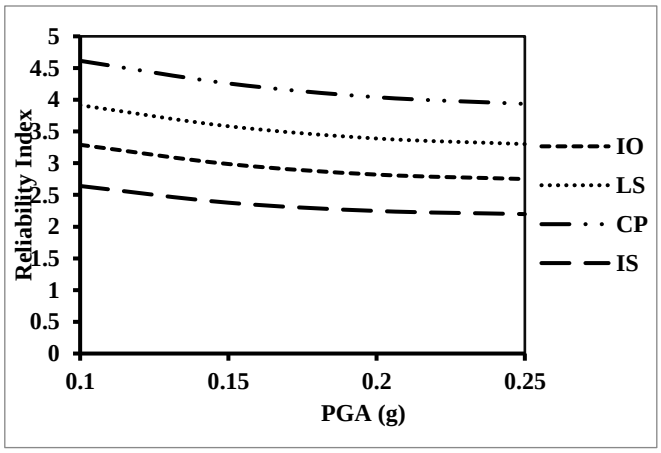

Figure 5.3.21. Reliability Index for roof of G+9 building on soft soil under Denali earthquake at Saltlake

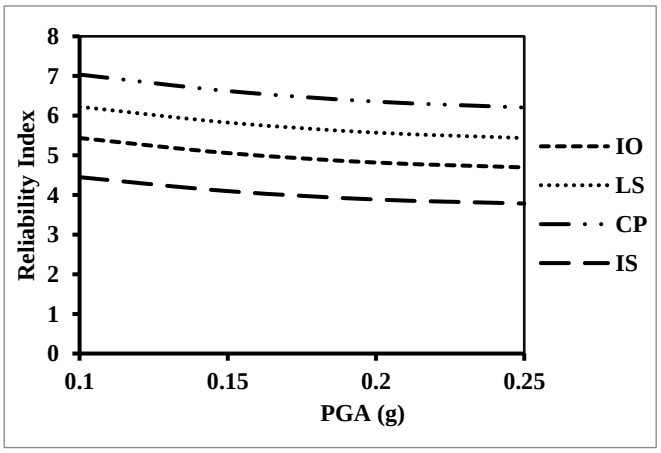

Figure 5.3.22. Reliability Index for roof of G+1 building Soil 1 under Loma prieta earthquake at Saltlake

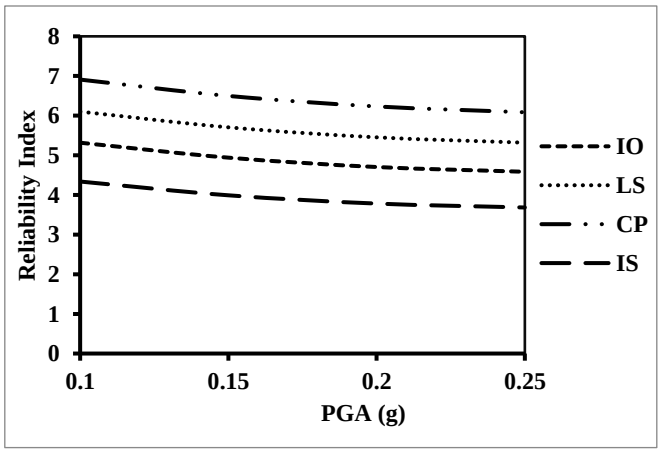

Figure 5.3.23. Reliability Index for roof of G+1 building Soil 1 under Denali earthquake at Saltlake

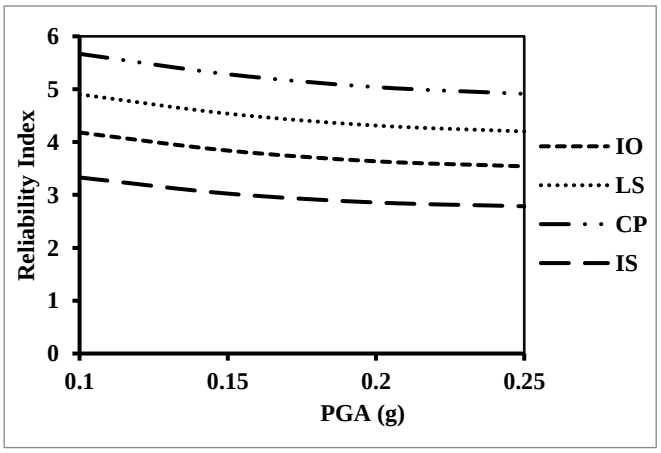

Figure 5.3.24. Reliability Index for roof of G+4 building on Soil 1 under Loma prieta earthquake at Saltlake

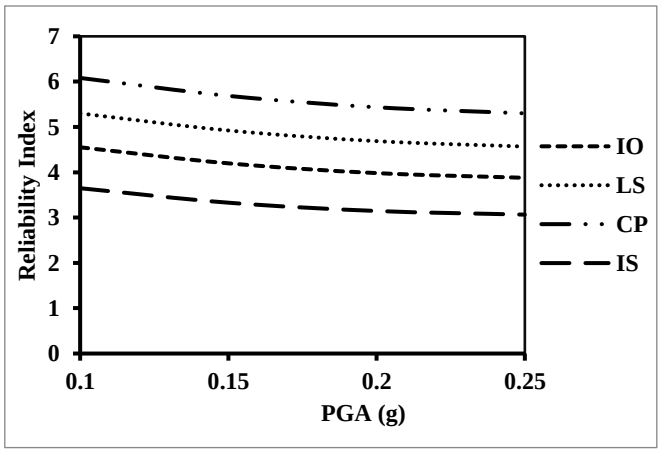

Figure 5.3.25. Reliability Index for roof of G+4 building on Soil 1 under Denali earthquake at Saltlake

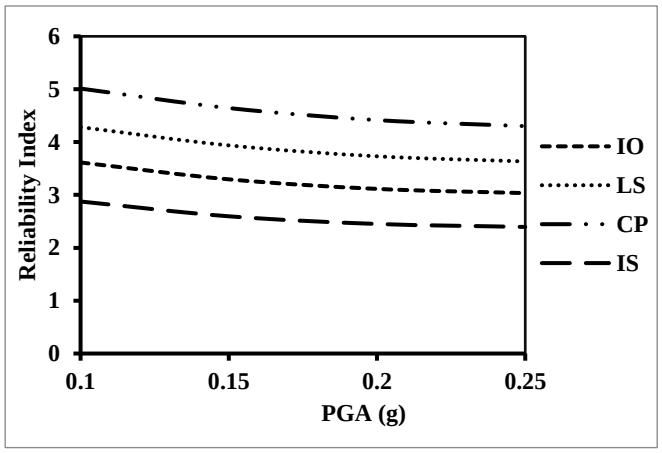

Figure 5.3.26. Reliability Index for roof of G+9 building on Soil 1 under Loma prieta earthquake at Saltlake

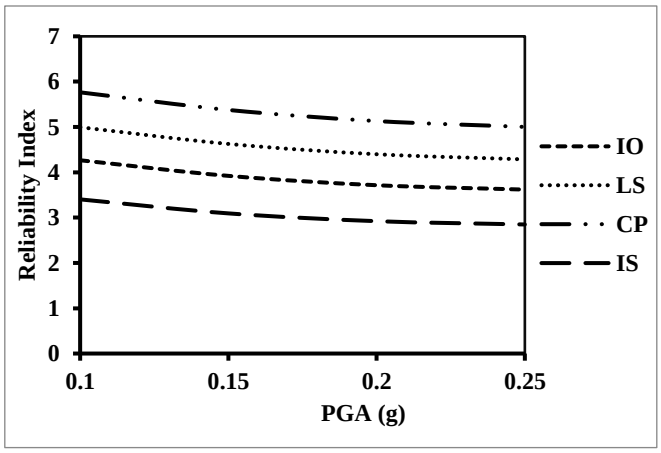

Figure 5.3.27. Reliability Index for roof of G+9 building on Soil 1 under Denali earthquake at Saltlake

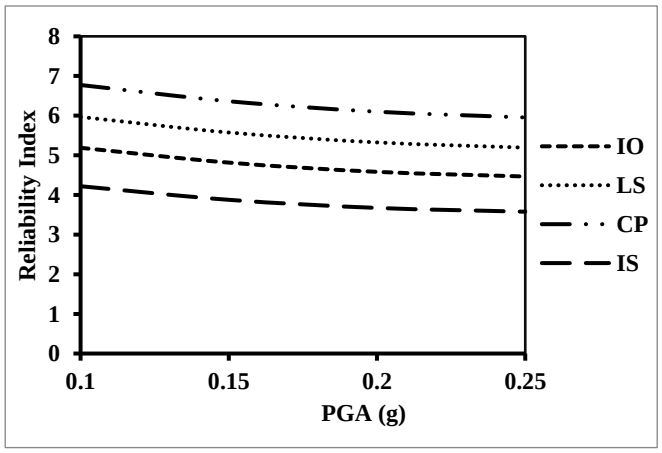

Figure 5.3.28. Reliability Index for roof of G+1 building Soil 2 under Loma prieta earthquake at Saltlake

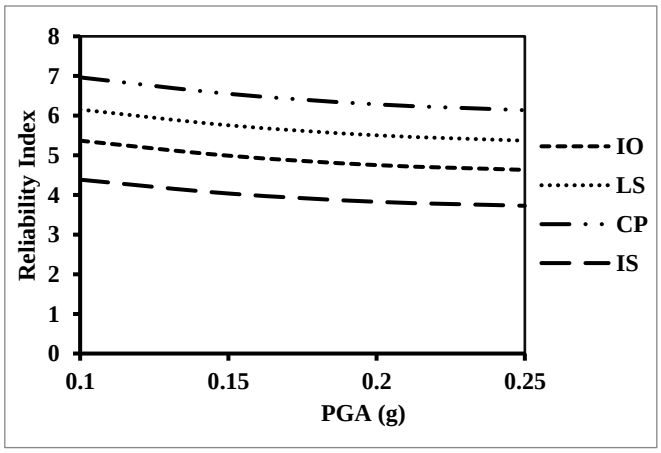

Figure 5.3.29. Reliability Index for roof of G+1 building Soil 2 under Denali earthquake at Saltlake

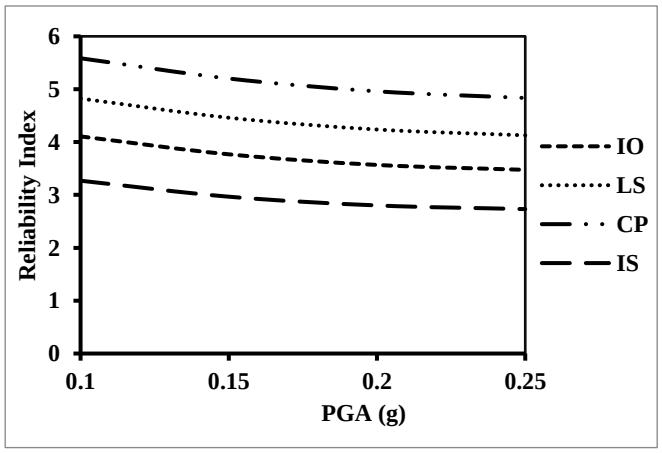

Figure 5.3.30. Reliability Index for roof of G+4 building on Soil 2 under Loma prieta earthquake at Saltlake

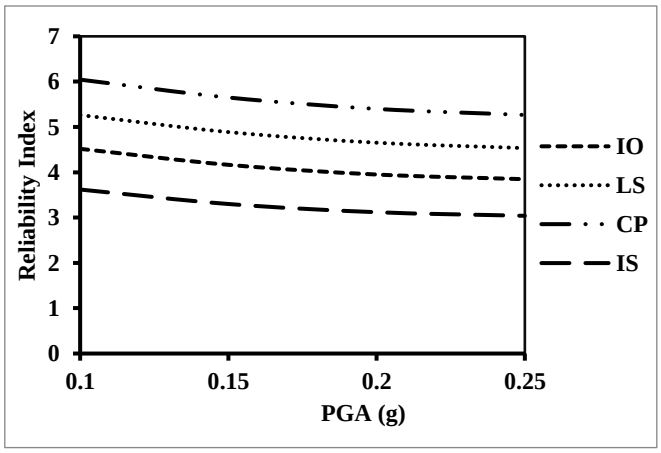

Figure 5.3.31. Reliability Index for roof of G+4 building on Soil 2 under Denali earthquake at Saltlake

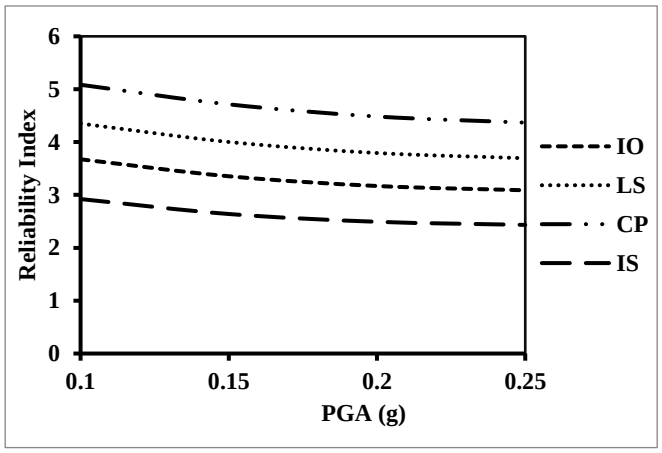

Figure 5.3.32. Reliability Index for roof of G+9 building on Soil 2 under Loma prieta earthquake at Saltlake

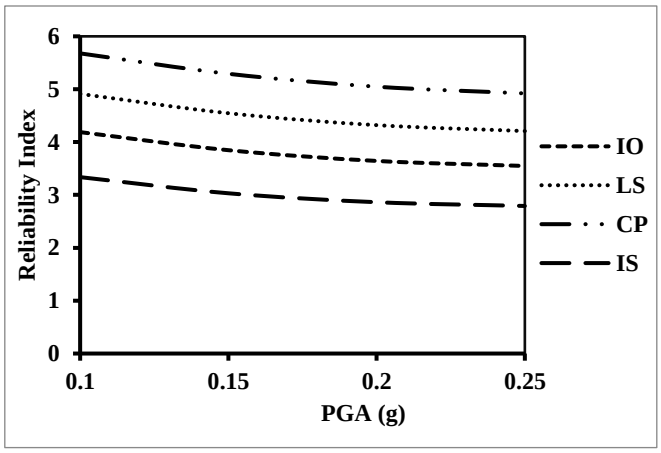

Figure 5.3.33. Reliability Index for roof of G+9 building on Soil 2 under Denali earthquake at Saltlake

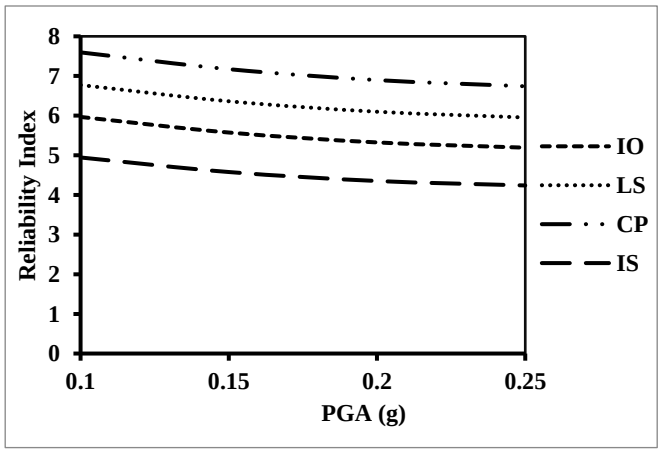

Figure 5.3.34. Reliability Index for roof of G+1 building Soil 3 under Loma prieta earthquake at Saltlake

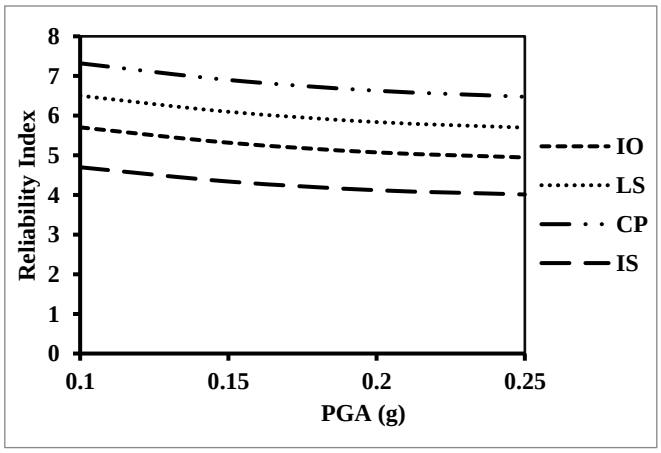

Figure 5.3.35. Reliability Index for roof of G+1 building Soil 3 under Denali earthquake at Saltlake

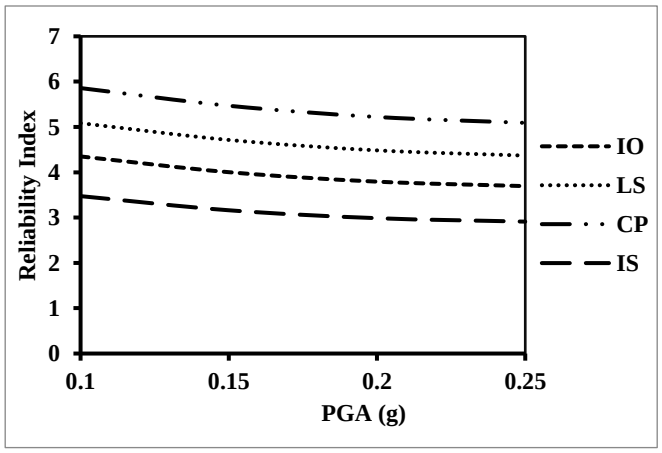

Figure 5.3.36. Reliability Index for roof of G+4 building on Soil 3 under Loma prieta earthquake at Saltlake

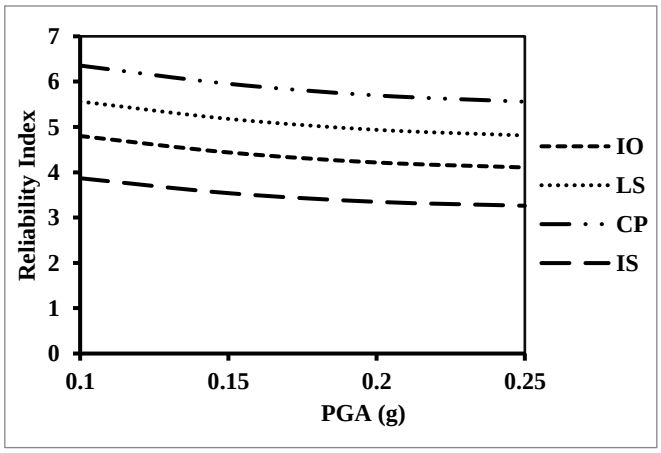

Figure 5.3.37. Reliability Index for roof of G+4 building on Soil 3 under Denali earthquake at Saltlake

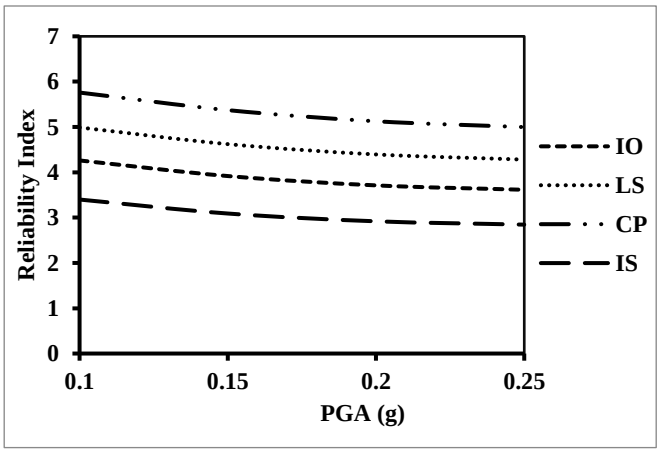

Figure 5.3.38. Reliability Index for roof of G+9 building on Soil 3 under Loma prieta earthquake at Saltlake

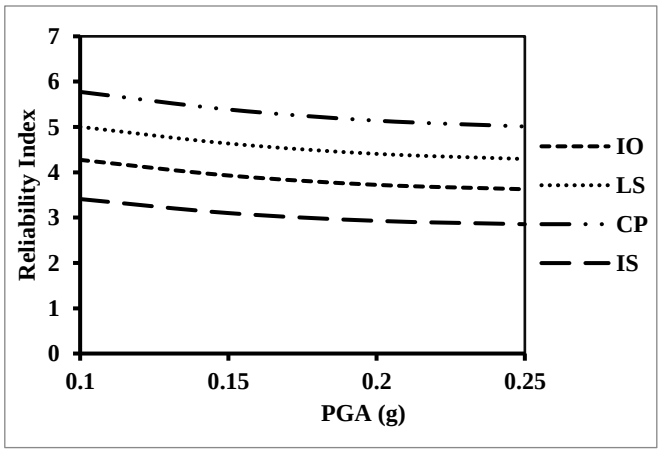

Figure 5.3.39. Reliability Index for roof of G+9 building on Soil 3 under Denali earthquake at Saltlake

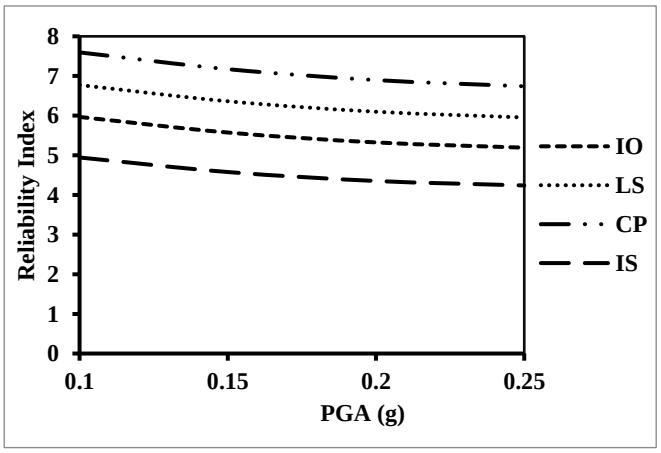

Figure 5.3.40. Reliability Index for roof of G+1 building Soil 4 under Loma prieta earthquake at Saltlake

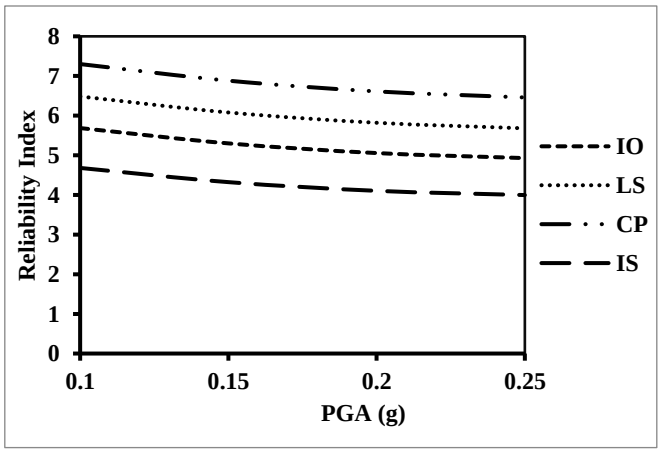

Figure 5.3.41. Reliability Index for roof of G+1 building Soil 4 under Denali earthquake at Saltlake

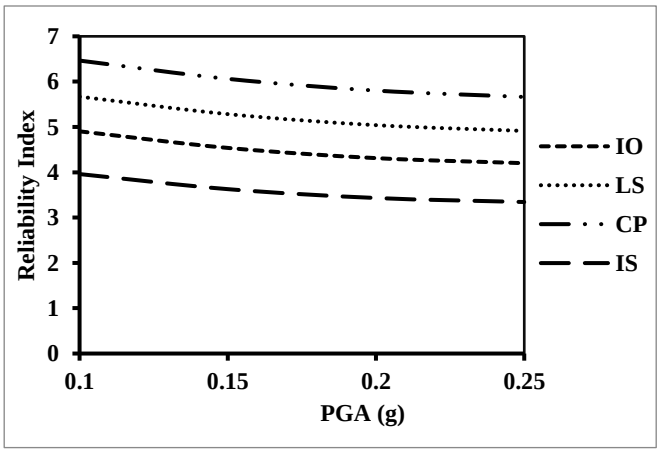

Figure 5.3.42. Reliability Index for roof of G+4 building on Soil 4 under Loma prieta earthquake at Saltlake

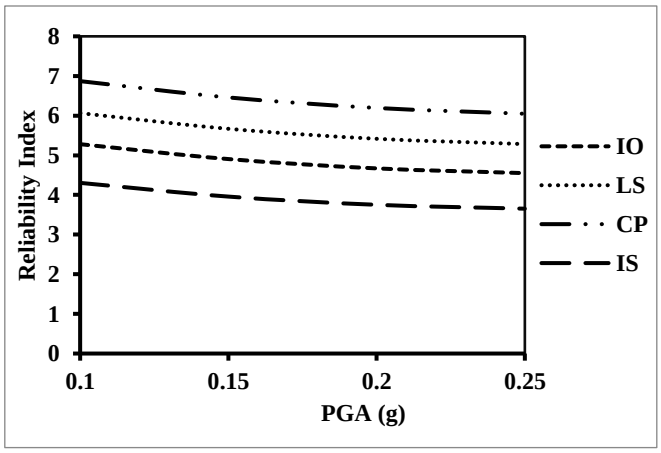

Figure 5.3.43. Reliability Index for roof of G+4 building on Soil 4 under Denali earthquake at Saltlake

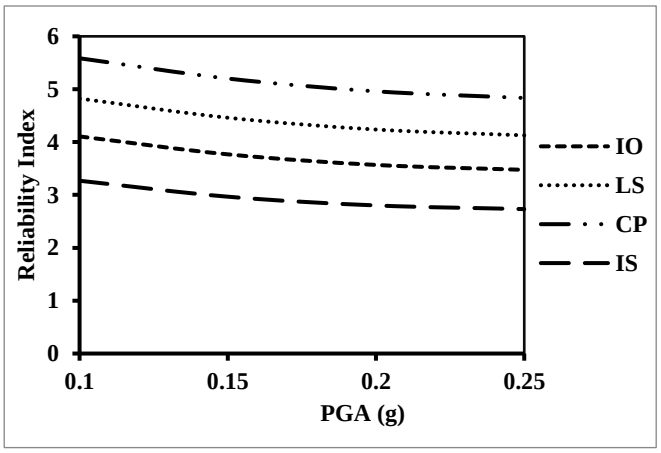

Figure 5.3.44. Reliability Index for roof of G+9 building on Soil 4 under Loma prieta earthquake at Saltlake

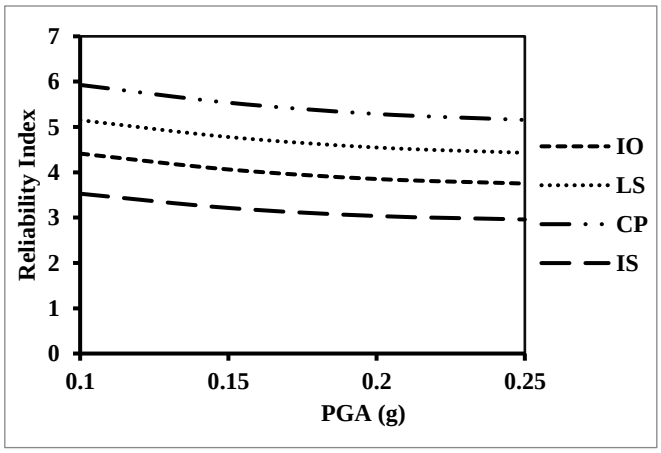

Figure 5.3.45. Reliability Index for roof of G+9 building on Soil 4 under Denali earthquake at Saltlake

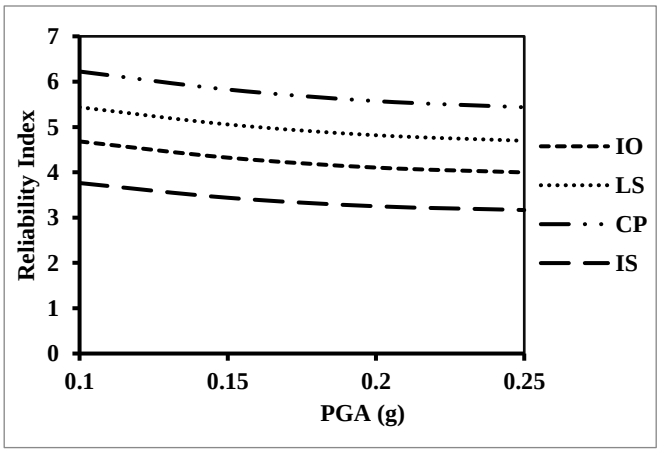

Figure 5.3.46. Reliability Index for roof of G+1 building Soil 5 under Loma prieta earthquake at Saltlake

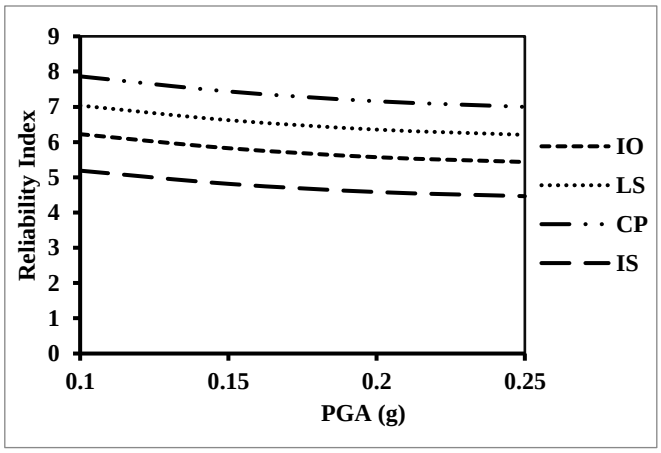

Figure 5.3.47. Reliability Index for roof of G+1 building Soil 5 under Denali earthquake at Saltlake

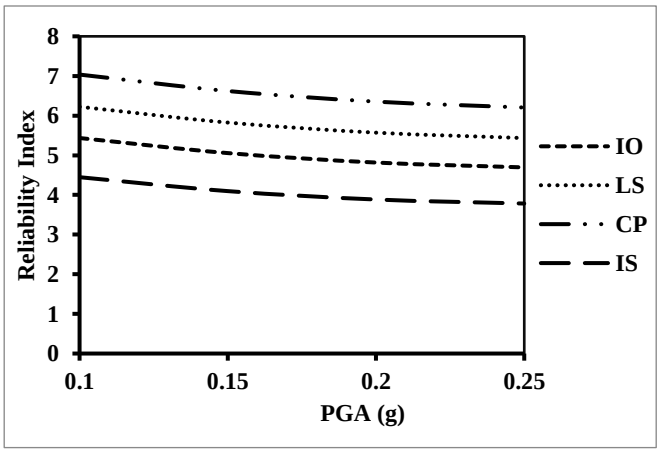

Figure 5.3.48. Reliability Index for roof of G+4 building on Soil 5 under Loma prieta earthquake at Saltlake

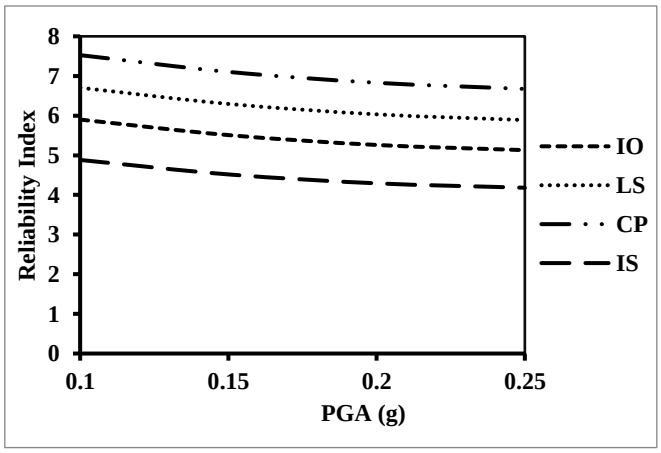

Figure 5.3.49. Reliability Index for roof of G+4 building on Soil 5 under Denali earthquake at Saltlake

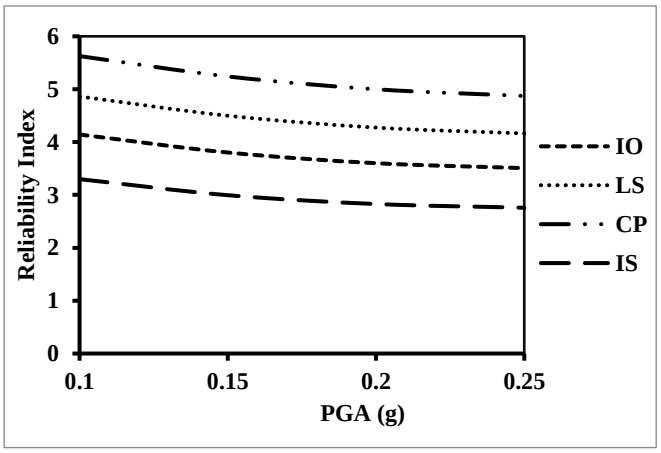

Figure 5.3.50. Reliability Index for roof of G+9 building on Soil 5 under Loma prieta earthquake at Saltlake

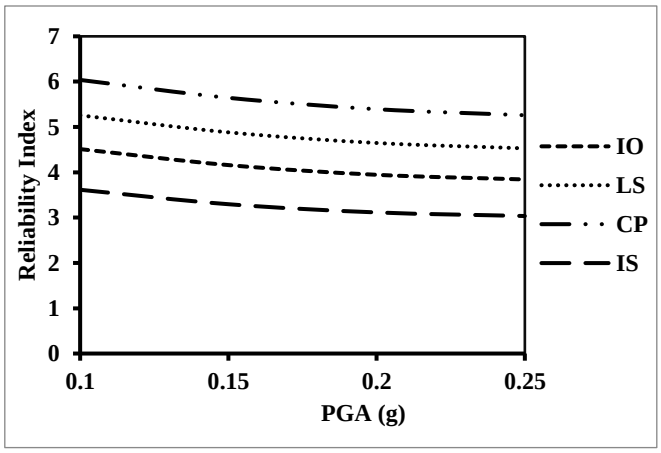

Figure 5.3.51. Reliability Index for roof of G+9 building on Soil 5 under Denali earthquake at Saltlake

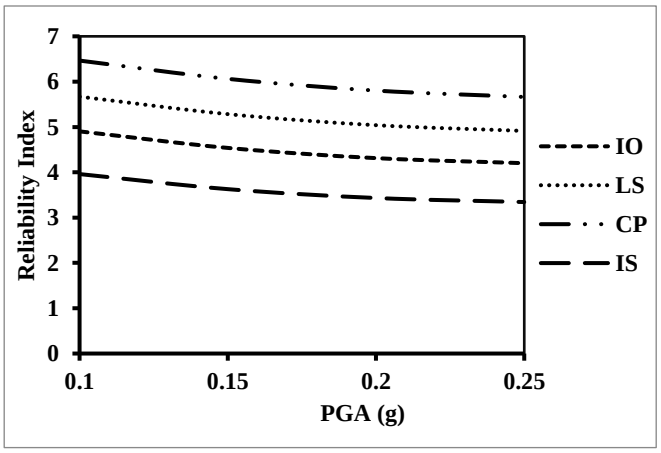

Figure 5.3.52. Reliability Index for roof of G+1 building Soil 6 under Loma prieta earthquake at Saltlake

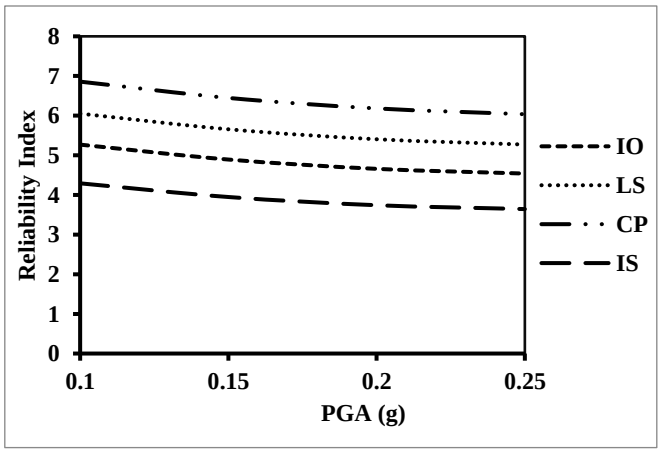

Figure 5.3.53. Reliability Index for roof of G+1 building Soil 6 under Denali earthquake at Saltlake

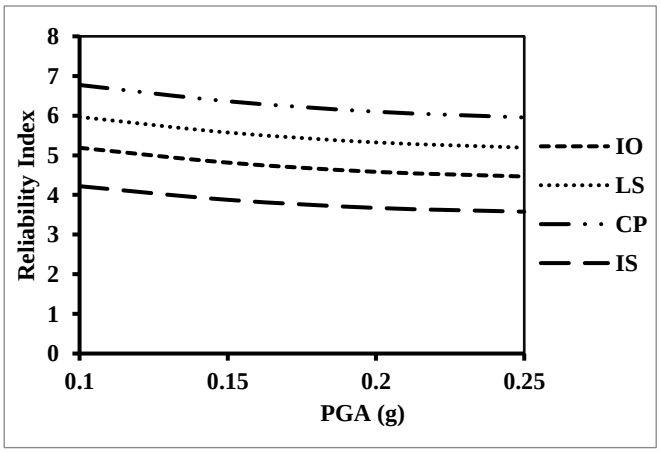

Figure 5.3.54. Reliability Index for roof of G+4 building on Soil 6 under Loma prieta earthquake at Saltlake

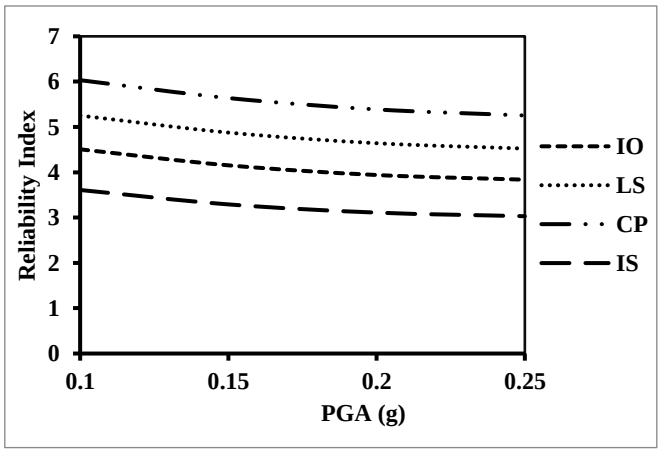

Figure 5.3.55. Reliability Index for roof of G+4 building on Soil 6 under Denali earthquake at Saltlake

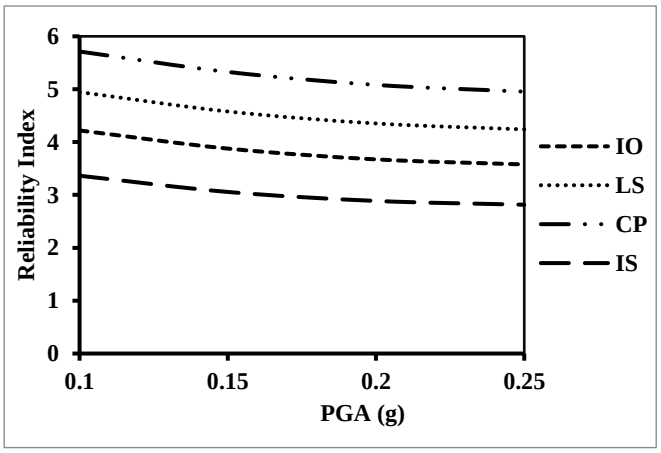

Figure 5.3.56. Reliability Index for roof of G+9 building on Soil 6 under Loma prieta earthquake at Saltlake

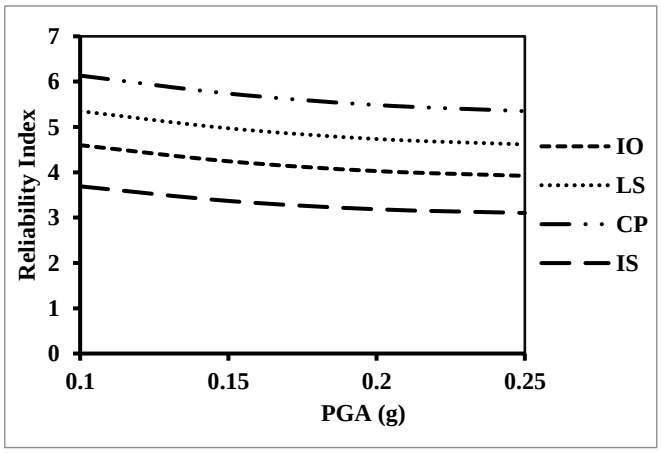

Figure 5.3.57. Reliability Index for roof of G+9 building on Soil 6 under Denali earthquake at Saltlake

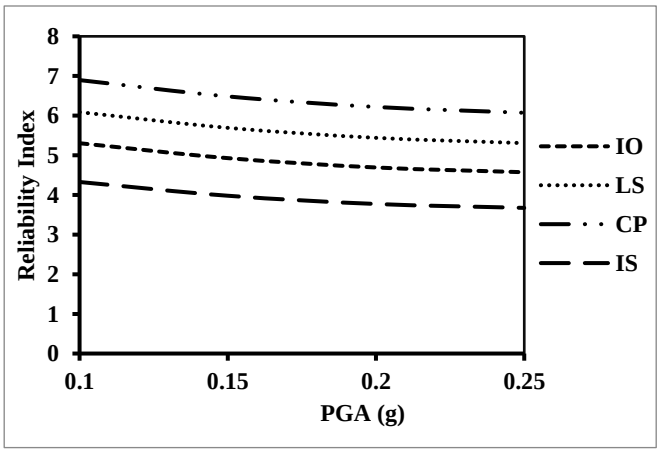

Figure 5.3.58. Reliability Index for roof of G+1 building Soil 7 under Loma prieta earthquake at Saltlake

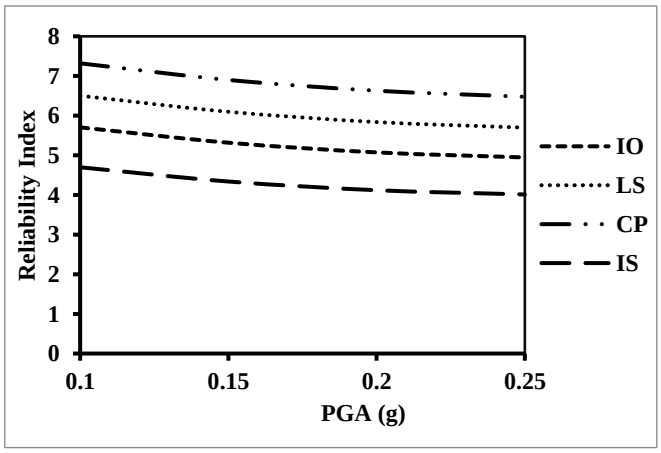

Figure 5.3.59. Reliability Index for roof of G+1 building Soil 7 under Denali earthquake at Saltlake

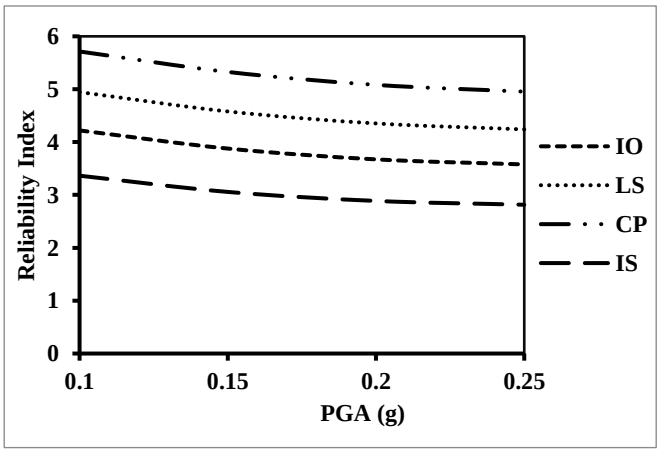

Figure 5.3.60. Reliability Index for roof of G+4 building on Soil 7 under Loma prieta earthquake at Saltlake

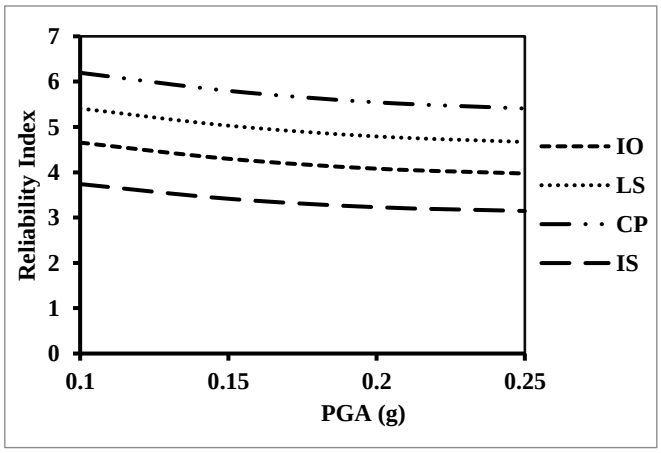

Figure 5.3.61. Reliability Index for roof of G+4 building on Soil 7 under Denali earthquake at Saltlake

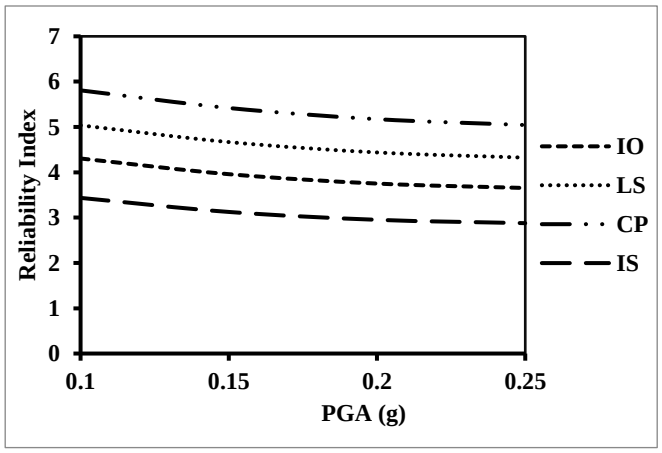

Figure 5.3.62. Reliability Index for roof of G+9 building on Soil 7 under Loma prieta earthquake at Saltlake

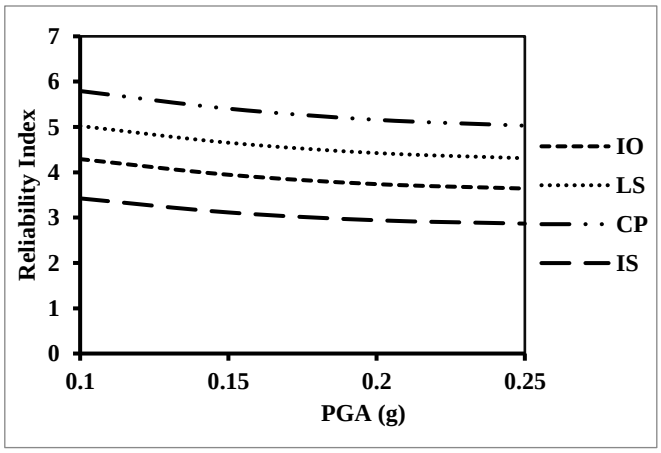

Figure 5.3.63. Reliability Index for roof of G+9 building on Soil 7 under Denali earthquake at Saltlake

5.4. DISCUSSION ON RELIABILITY CUVRES

After analysing reliability curves of frame buildings situated on uniform soil some important observations have been made. Firstly, for a specific type of soil and under a particular seismic excitation, the RI value of a G+1 building is always maximum and that of a G+9 building is always minimum among all the other cases. Further, when a G+1 building is subjected to a particular earthquake, it has the most RI value when it is situated on hard soil. On the other hand, it has the least RI value when it is located on soft soil. However, under the action of a particular seismic excitation, a G+4 building has the highest RI value when it is situated in the medium soil. It is also to be noted that in case a building is situated on hard or medium soil, RI of the soil-structure system is more when it is subjected to a far-field earthquake like Denali earthquake. On the other hand, if the building rests on soft soil, the RI value of the soil-structure system will be greater under near-field earthquake like Loma prieta earthquake.

Now from the reliability curves of the frame buildings resting on layered soil, the following conclusions may be drawn. Generally, the RI value of a G+1 building is the largest and that of a G+9 building is the smallest when soil type and seismic excitation remains unaltered. However, only when a near-field earthquake motion is subjected to Soil 5 and Soil 6, G+4 building has the highest RI value. Further, if a near-field earthquake is subjected to Soil 7 and a far-field earthquake is subjected to Soil 6 and Soil 7, G+4 building has the lowest RI value. Generally, under the influence of a far-field earthquake RI of a soil-structure system is more than the RI of that system

under the action of a near-field earthquake. Moreover, when a G+1 building situated in Soil 1, Soil 3 and Soil 4, the RI due to near-field earthquake exceeds the RI due to far-field earthquake.

Chapter-6: CONCLUDING REMARKS

6.1. GENERAL

It is a well-determined fact that dynamic soil structure- interaction (SSI) effect plays an important role on seismic response of structure. In the present study, an investigation has been carried out to understand the SSI effect on frame buildings constructed over both uniform and layered soils by nonlinear dynamic analysis using three-dimensional finite element modelling (FEM). For uniform soil, three types of soils (Hard, Medium and Soft) and while for layered soil seven types of layered soils (Soil 1 to Soil 7), each of which has six different layers, are taken for the present analysis. It is to be mentioned that for all the soil profiles fundamental frequency and amplification at fundamental frequency have been determined at frequency domain. Three types of buildings (G+1, G+4 and G+9) are subjected to Loma Prieta (1989) earthquake motion as near-field and Denali (2002) earthquake as far-field seismic excitation under the above mentioned soil condition. By the present analysis horizontal displacements and percentage drifts of all the storeys are computed and thus fragility curves for each storey are developed. Further on the basis of the fragility curve and seismic hazard curve of Saltlake, Kolkata region reliability index have also been evaluated for different soil-structure combinations.

6.2. MAJOR FINDINGS

The major conclusions made from the study are:

1. For any type of soil and under a specific seismic excitation, the probability of exceedance of a certain limit state in case of a G+1 building is always minimum and that of a G+9 building is always maximum among all the cases.
2. When a building is subjected to an earthquake motion situated on hard soil, it has the least probability of exceeding a limit state. On the contrary, it has the largest probability of exceeding a limit state when located on soft soil.
3. In case a building is located on hard or medium soil, the probability of exceedance of a specific limit state for that soil-structure system is more when it is subjected to a near-field earthquake.

On the other hand, if the building rests on soft soil, the probability of exceedance value of the soil-structure system will be greater under the influence of far-field earthquake.

4. Irrespective of the type of soil and structure, when any soil-structure system is subjected to a far-field earthquake, the shape of the maximum displacement profile is concave upward. This may be presence of only low frequency seismic wave in far field earthquake. However, under the action of a near-field earthquake, the shape of the maximum displacement profile of a building purely depends upon the type of soil and structure and thus cannot be predicted. This may be due to presence of seismic wave of all frequency content.
5. If the soil type and seismic excitation remain unchanged, the probability of exceeding a particular limit state is the largest for a G+9 building and smallest for a G+1 building.
6. Generally, under the action of a near-field earthquake, the limit state exceedance probability is more compared to the far-field earthquake.
7. For a specific type of soil and under a particular seismic excitation, the RI value of a G+1 building is always maximum and that of a G+9 building is always minimum among all the other cases.
8. While a G+1 building situated on hard soil is subjected to a particular earthquake, has the most RI value. However, it has the least RI value when it is located on soft soil. Moreover, under the action of a particular seismic excitation, a G+4 building has the highest RI value when it is situated in the medium soil.
9. In case a building is situated on hard or medium soil, RI of the soil-structure system is more when it is subjected to a far-field earthquake. On the other hand, if the building rests on soft soil, the RI value of the soil-structure system will be greater under near-field earthquake.
10. However, only when a near-field earthquake motion is subjected to Soil 5 and Soil 6, G+4 building has the highest RI value.
11. If a near-field earthquake is subjected to Soil 7 and a far-field earthquake is subjected to Soil 6 and Soil 7, G+4 building has the lowest RI value.
12. Under the influence of a far-field earthquake RI of a soil-structure system is more than the RI of that system under the action of a near-field earthquake.

6.3. LIMITATIONS OF PRESENT WORK

The limitations of present study are as follows:

1. Development of fragility curve by Monte Carlo method has not been carried out.
2. Irregular and real buildings should be analysed.
3. Effect of concrete reinforcement should be incorporated in the study.
4. Present study has been carried out considering the SSI of shallow foundation only.

6.4. FUTURE SCOPES

1. Fragility and RI may be developed under two directional seismic motions.
2. Efficient seismic fragility analysis in the meta-model based framework by efficient Monte Carlo Simulation can be performed.
3. Effect of reinforcement should be taken into account. However, it needs a high configuration computer.
4. Present study has been conducted considering SSI effect of shallow foundation. However, pile soil interaction should also be conducted.

REFERENCES

[1] L. Zeevaert, "Seismosoil Dynamics of Foundations in Mexico City Earthquake, September 19,1985," *J. Geotech. Eng.*, vol. 117, no. 3, pp. 376–428, 1991.

[2] H. B. Seed, M. P. Romo, J. I. Sun, A. Jaime, and J. Lysmer, "The Mexico Earthquake of September 19,1985- Relationships Between Soil Conditions and Earthquake Ground Motions," *Earthq. Spectra*, vol. 4, no. 4, pp. 687–729, 1988.

[3] R. Dobry *et al.*, "New Site Coefficients and Site Classification System Used in Recent Building Seismic Code Provisions," *Earthq. Spectra*, vol. 16, no. 1, pp. 41–67, 2000.

[4] M. Celebi, "Topographical and Geological Amplification: Case studies and Engineering Implifications," *Struct. Saf.*, vol. 10, no. 1–3, pp. 199–217, 1991.

[5] P. M. Davis, "Northridge Earthquake Damage Caused By Geologic Focusing of Seismic Waves," *Science.*, vol. 289, no. 5485, pp. 1746–1750, 2000.

[6] S. L. Kramer, *Geotechnical Earthquake Engineering*. New York: Prentice-Hall, Inc., 1996.

[7] M. K. Jafari, M. R. Ghayamghamian, M. Davoodi, M. Kamalian, and A. SohrabiBidar, "Site Effects of the 2003 Bam, Iran Earthquake," *Earthq. Spectra*, vol. 21, no. S1, pp. 125–136, 2005.

[8] J. P. Narayan, M. L. Sharma, and A. Kumar, "A Seismological Report on the 26 January 2001 Bhuj, India Earthquake," *Seismol. Res. Lett.*, vol. 73, no. 3, pp. 343–355, 2002.

[9] L. Govindaraju, G. L. Ramana, C. HanumanthaRao, and T. G. Sitharam, "Site-specific Ground Response Analysis," *Curr. Sci.*, vol. 87, no. 10, pp. 1354–1362, 2004.

[10] J. P. Stewart, S. Chiou, J. Bray, R. Graves, P. Somerville, and N. Abrahamson, "Ground Motion Evaluation Procedures for Performance-based Design, Report No-9," 2001.

[11] M. Corigliano, "Seismic Response of Deep Tunnels in Near-Fault Conditions," Politecnico di Torino, Italy, 2007.

[12] P. Somerville, N. Smith, R. Graves, and N. Abrahamson, "Modification of Empirical

Strong Ground Motion Attenuation Relations to Include the Amplitude and Duration Effects of Rupture Directivity," *Seismol. Soc. Lett.*, vol. 68, no. 1, pp. 180–203, 1997.

[13] B. A. Bolt, *Earthquakes*. W.H. Freeman and Company, New York, 1993.

[14] R. Tuladhar, T. Maki, and H. Mutsuyoshi, "Cyclic behavior of laterally loaded concrete piles embedded into cohesive soil," *Earthq. Eng. Struct. Dyn.*, vol. 37, no. 1, pp. 43–59, 2008.

[15] J. P. Wolf, *Dynamic Soil-Structure Interaction*. Englewood Cliffs, New Jersey: Prentice-Hall, Inc., 1985.

[16] *IS 1893 (Part-1) : 2016, Criteria for Earthquake Resistant Design of Structures - General Provisions and Buildings*. New Delhi.

[17] T. K. Datta, *Sesimic Analysis of Structures*. John Wiley & Sons (Asia) Pte Ltd., 2010.

[18] R. W. Clough and J. Penzien, *Dynamics of Structures*, 2nd ed. New York: McGraw Hill, Inc., 1993.

[19] NPTEL, "Seismic Soil-Structure Interaction." [Online]. Available: https://nptel.ac.in/courses/105101004/downloads/06 Chapter.pdf.

[20] J. P. Stewart, G. L. Fenves, and R. B. Seed, "Seismic Soil-Structure Interaction in Buildings: Analytical aspects," *J. Geotech. Geoenvironmental Eng.*, vol. 125, no. 1, 1999.

[21] J. A. García, "Soil Structure Interaction in the Analysis and Seismic Design of Reinforced Concrete Frame Buildings," in *The 14th World Conference on Earthquake Engineering*, 2008.

[22] A. P. Karthika and V. Gayathri, "Literature Review on Effect of Soil Structure Interaction on Dynamic Behaviour of Buildings," *Int. Res. J. Eng. Technol.*, vol. 5, no. 4, pp. 2522–2525, 2018.

[23] N. Anand, C. Mightraj, and G. Prince Arulraj, "Seismic Behaviour of RCC Shear Wall Under Different Soil Conditions," in *Indian Geotechnical Conference - 2010, GEOtrendz*, 2010.

[24] H. Matinmanesh and M. S. Asheghabadi, "Seismic Analysis on Soil-Structure Interaction of Buildings over Sandy Soil," in *The Twelfth East Asia-Pacific Conference on Structural*

Engineering and Construction, 2011.

[25] A. D. Pandey, P. Kumar, and S. Sharma, "Seismic Soil-Structure Interaction of Buildings on Hill Slopes," *Int. J. Civ. Struct. Eng.*, vol. 2, no. 2, pp. 535–546, 2011.

[26] R. M. J. Priyanka, N. Anand, and S. Justin, "Studies on Soil Structure Interaction of Multi Storeyed Buildings with Rigid and Flexible Foundation," *Int. J. Emerg. Technol. Adv. Eng.*, vol. 2, no. 12, pp. 111–118, 2012.

[27] M. N. Kuladeepu, G. Narayana, and B. K. Narendra, "Soil Structure Interaction Effect on Dynamic Behavior of 3D Building Frames with Raft Footing," *Int. J. Res. Eng. Technol.*, vol. 4, no. 7, pp. 87–91, 2015.

[28] M. V. Gaikwad, R. B. Ghogare, and S. M. Vageesha, "Finite Element Analysis of Frame with Soil Structure Interaction," *Int. J. Res. Eng. Technol.*, vol. 4, no. 1, pp. 91–95, 2015.

[29] M. A. Ghannad, "Effects of Soil-Structure Interaction on Respponse of Structures Subjected to Near-Fault Earthquake Records," in *Seismic Engineering Conference Commemorating the 1908 Messina and Reggio Calabria Earthquake*, 2008.

[30] J. Zhang and Y. Tang, "Dimensional Analysis of Linear Soil-Foundation-Structure System Subjected to Near- Fault Ground Motions," in *Structure Congress 2008*, 2008.

[31] Z. Azharhoosh and G. R. Amiri, "Elastic Response of Soil-Structure Systems Subjected to Near-Fault Rupture Directivity Pulses," in *Proceedings of the GeoShanghai International Conference*, 2010.

[32] G. Minasidis, G. D. Hatzigeorgiou, and D. E. Beskos, "SSI in Steel Frames Subjected to Near-Fault Earthquakes," *Soil Dyn. Earthq. Eng.*, vol. 66, pp. 56–68, 2014.

[33] F. Gelagoti, R. Kourkoulis, I. Anastasopoulos, and G. Gazetas, "Rocking-isolated Frame Structures: Margins of Safety against Toppling Collapse and Simplified Design Approach," *Soil Dyn. Earthq. Eng.*, vol. 32, pp. 87–102, 2012.

[34] M. Davoodi, M. Sadjadi, P. Goljahani, and M. Kamalian, "Effects of Near-Field and Far-Field Earthquakes on Seismc Response of SDOF System Considering Soil Structure Interaction," in *15th World Conference on Earthquake Engineering*, 2012.

[35] American Society of Civil Engineers, *FEMA 356, NEHRP Guidelines for Prestandard*

and Commentary for the Seismic Rehabilitation of Buildings. Washington, D.C., 2000.

[36] C. A. Cornell, F. Jalayer, R. O. Hamburger, and D. A. Foutch, "The Probabilistic Basis for the 2000 SAC/FEMA Steel Moment Frame Guidelines," *J. Struct. Eng.*, vol. 128, no. 4, pp. 526–533, 2002.

[37] O. C. Celik and B. R. Ellingwood, "Seismic Fragilities for Non-ductile Reinforced Concrete Frames – Role of Aleatoric and Epistemic Uncertainties," *Struct. Saf.*, vol. 32, no. 1, pp. 1–12, 2010.

[38] *ATC-58, Seismic Performance Assessment of Buildings*, vol. 1. California, 2012.

[39] D. C. H. Pragalath, A. Bhosale, P. R. Davis, and P. Sarkar, "Multiplication Factor for Open Ground Storey Buildings – A Reliability Based Evaluation," *Earthq. Eng. Eng. Vib.*, vol. 15, no. 2, pp. 283–295, 2016.

[40] A. Singhal and A. S. Kiremidjian, "Method for Probabilistic Evaluation of Seismic Structural Damage," *J. Struct. Eng.*, vol. 122, no. 12, pp. 1459–1467, 1996.

[41] K. M. Mosalam, G. Ayala, R. N. White, and C. Roth, "Seismic Fragility of LRC Frames with and without Masonry Infill Walls," *J. Earthq. Eng.*, vol. 1, no. 4, pp. 693–720, 1997.

[42] E. M. Guneyisi and G. Altay, "Seismic Fragility Assessment of Effectiveness of Viscous Dampers in R/C Buildings under Scenario Earthquakes," *Struct. Saf.*, vol. 30, no. 5, pp. 461–480, 2008.

[43] S. V. Borele, "Damage Assessment of Structural System Using Fragility Curves," *J. Civ. Eng. Environ. Technol.*, vol. 2, pp. 72–76, 2015.

[44] *IS 456 : 2000, Plain and Renforced Concrete - Code of Practice*. New Delhi.

[45] *IS 1893 (Part-1) : 2002, Criteria for Earthquake Resistant Design of Structures - General Provisions and Buildings*. New Delhi.

[46] U. Y. Vazurkar and D. J. Chaudhari, "Development of Fragility Curves for RC Buildings," *Int. J. Eng. Res.*, vol. 5, pp. 591–594, 2016.

[47] *ATC-40, Seismic Evaluation and Retrofit of Concrete Buildings*, vol. 1. California, 1996.

[48] K. R. Collins, Y. K. Wen, and D. A. Foutch, "Dual-level Seismic Design: A Reliability

Based Methodology," *Earthq. Eng. Struct. Dyn.*, vol. 25, no. 12, pp. 1433–1467, 1996.

[49] B. R. Ellingwood, "Earthquake Risk Assessment of Building Structures," *Reliab. Eng. Syst. Saf.*, vol. 74, no. 3, pp. 251–262, 2001.

[50] Y. K. Wen, "Reliability and Performance-Based Design," *Struct. Saf.*, vol. 23, pp. 407–428, 2001.

[51] J. A. Hunter *et al.*, "Surface and Downhole Shear Wave Seismic Methods for Thick Soil Site Investigations," *Soil Dyn. Earthq. Eng.*, vol. 22, no. 9–12, pp. 931–941, 2002.

[52] R. Sarkar, D. K. Paul, and L. Stempniewski, "Influence of Reservoir and Foundation on the Nonlinear Dynamic Response of Concrete Gravity Dams," *ISET J. Earthq. Technol. Pap. No. 490*, vol. 44, no. 2, pp. 377–389, 2007.

[53] J. Lee and G. L. Fenves, "Plastic-Damage Model for Cyclic Loading of Concrete Structures," *J. Eng. Mech.*, vol. 124, no. 8, pp. 892–900, 1998.

[54] J. Lubliner, J. Oliver, S. Oller, and E. Onate, "A Plastic-Damage Model for Concrete," *Int. J. Solids Struct.*, vol. 25, no. 3, pp. 229–326, 1989.

[55] I. Chowdhury and S. Dasgupta, "Computation of Rayleigh Damping Coefficients for Large Systems," *Electron. J. Geotech. Eng.*, vol. 8C, 2003.

[56] J. P. Narayan, "Study of Basin-edge Effects on the Ground Motion Characteristics Using 2.5-D Modeling," *Pure Appl. Geophys.*, vol. 162, no. 2, pp. 273–289, 2005.

[57] J. P. Narayan and S. P. Singh, "Effects of Soil Layering on the Characteristics of Basin-edge Induced Surface Waves and Differential Ground Motion," *J. Earthq. Eng.*, vol. 10, pp. 595–616, 2006.

[58] J. P. Narayan, "Effects of Impedance Contrast and Soil Thickness on the Basin Transduced Rayleigh Waves and Associated Differential Ground Motion," *Pure Appl. Geophys.*, vol. 167, pp. 1485–1510, 2010.

[59] J. P. Narayan, "Effects of P-wave and S-wave Impedance Contrast on the Characteristics of Basin Transduced Rayleigh Waves," *Pure Appl. Geophys.*, 2011.

[60] S. K. Nath, M. D. Adhikari, S. K. Maiti, N. Devaraj, N. Srivastava, and L. D. Mohapatra, "Earthquake Scenario in West Bengal with Emphasis on Seismic Hazard Microzonation

of the City of Kolkata," *J. Dep. Geol. Geophys. Indian Inst. Technol. Kharagpur, West Bengal, India*, 2012.

[61] J. Song and B. R. Ellingwood, "Seismic Reliability of Special Moment Steel Frames with Welded Connections: I and II," *J. Struct. Eng.*, vol. 125, no. 4, pp. 357–372, 1999.

[62] A. M. Hasofer and N. Lind, "An Exact and Invariant First Order Reliability Format," *J. Eng. Mech.*, vol. 100, no. 1, 1974.